UNIVERSITÄT PADERBORN
Die Universität der Informationsgesellschaft

On the Optimal Control of Mechanical Systems
–
Hybrid Control Strategies and Hybrid Dynamics

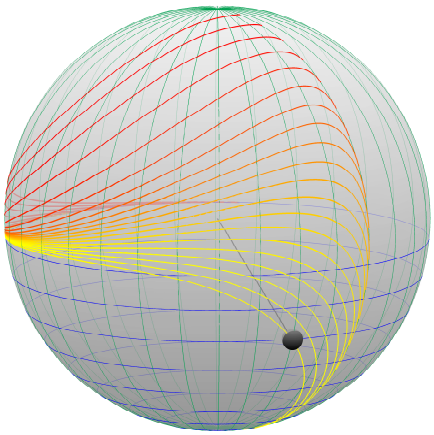

Von der Fakultät für Elektrotechnik, Informatik und Mathematik der Universität Paderborn zur Erlangung des akademischen Grades Doktor der Naturwissenschaften (Dr. rer. nat.) genehmigte Dissertation von

Kathrin Flaßkamp

Paderborn 2013

Gutachter: Jun.-Prof. Dr. Sina Ober-Blöbaum
Prof. Dr. Michael Dellnitz
Prof. Dr. Todd D. Murphey

Tag der mündlichen Prüfung: 20. Dezember 2013

I regarded as quite useless the reading of large treatises of pure analysis: too large a number of methods pass at once before the eyes. It is in the works of application that one must study them; one judges their utility there and appraises the manner of making use of them.

Joseph Louis Lagrange (1736–1813), Italian-French astronomer and mathematician. Quotation as reported by J. F. Maurice in Moniteur Universel (1814). In W. F. Bynum, Roy Porter (Eds.): Oxford Dictionary of Scientific Quotations, Oxford University Press, 2012

Acknowledgements

First of all, I would like to express my deepest gratitude to Jun.-Prof. Dr. Sina Ober-Blöbaum for her constant support and advice, for introducing me to the interesting field of optimal control and geometric mechanics, to many exciting open questions therein and to its vivid, international research community. I also thank her for giving me the freedom to follow my own ideas, for the numerous extensive and helpful discussions, also late in the evening or over long distances, and finally and foremost, for supervising this thesis.

I am grateful to Prof. Dr. Michael Dellnitz who has risen my interest in dynamical systems and related topics already during my studies and who later gave me the opportunity to work at the Chair of Applied Mathematics. I deeply appreciate his impressive enthusiasm, the motivation he passes on and the rousing manner of thinking about mathematics as well as his participation in my development in the last years.

Then, I would like to thank Prof. Dr. Ansgar Trächtler for getting me enthusiastic about control theory as an interdisciplinary field of research at first, during my studies, and, in particular, for his interest in novel mathematical methods for control engineering, which raised my wish for balancing "theory" and "application" in my own work.

Special thanks also to Prof. Dr. Todd Murphey from the Northwestern University (Evanston, Illinois) who even intensified my interest in optimal control and geometric mechanics throughout our collaboration and especially during my visit at his lab in June 2012. I appreciated the stimulating discussions with himself and his group and the friendly atmosphere in his lab.

I gratefully acknowledge the financial support I have received within the Collaborative Research Center SFB 614, "Self-optimizing concepts and structures in mechanical engineering" and highly appreciated the interdisciplinary research within this project. Especially, I would like to thank my colleagues Christian Heinzemann, Martin Krüger, Tobias Meyer, Dr. Claudia Priesterjahn, Peter Reinold, Dr. Ing. Christoph Romaus, Tobias Schneider, Christoph Schulte, Albert Seifried, Dominik Steenken, and Julia Timmermann for the productive and enjoyable collaboration.

Many thanks go to my – partly former – colleagues at the University of Paderborn for many enlightening and fruitful discussions, their helpful advices and valuable support, distracting moments once in a while, and their kindness; all of which contributed a lot in making the last years an experience I would not have wanted to miss. Namely, I would like to thank Dr. Alessandro Dell'Aere, Dr. Mirko Hessel-von Molo, Dr. Stefan Klus, Dr. Anna-Lena Meyer, Sebastian Peitz, Dr. Marcus Post, Dr. Robert Preis, Maik Ringkamp, Stefan Sertl, Bianca Thiere and Dr. Katrin Witting from the Chair of Applied Mathematics and Dr. Alexander Schmeding and Beate Kossak, formerly at the Institute of Mathematics. In particular, I am grateful

to Dr. Sebastian Hage-Packhäuser, Christian Horenkamp and Robert Timmermann for the patience for all my questions, our helpful exchange of tips and tricks, the mutual proof-reading of our manuscripts and the constant encouragement and grown friendship until the end of this thesis and, hopefully, far beyond.

In the transient area between professional to private live, I have to mention Martin Krüger and Julia and Robert Timmermann with whom I share a great number of happy memories dating back to the beginning of our jointly studies in "Technomathematik", which probably induced our several collaborations in recent years and, intertwined with all that, a lasting friendship since many years – thank you!

Finally, I would like to express my sincere gratitude to my family. I deeply appreciate the love and steady encouragement of my parents Maria and Thomas, their unlimited trust in me and their support of all my decisions in life. Many thanks also to my brother Martin and my sister Hannah, not only for proof-reading and technical advices, but mainly for the love and companionship throughout the years. I am very thankful to Tobias, my partner in live and personal engineer to contact for technical questions in research as well as in every day life. However, Tobi, foremost I thank you for your love and support, your imperturbably belief in me, and for keeping a balance in my life.

Abstract

Optimal control problems for mechanical systems manifoldly arise in the fields of engineering and natural sciences, for instance, in robotics, biomechanics, automotive systems, or in space mission design. Here, the aim is to influence the system's dynamical behavior via its control inputs such that a given problem is optimally solved. In complex technical systems, mechanical subsystems interact with electronic components and logic devices for information processing, such that an adequate modeling leads to *hybrid dynamical systems*. Hybrid control strategies provide a range of new possibilities for the design and the numerical computation of optimal control laws and, at the same time, a number of interesting open questions in the analysis, control, and optimization of hybrid dynamical systems arise.

This thesis is devoted to two main aspects in this field: structure exploiting motion planning and optimal control of hybrid mechanical systems. The first part focuses on an optimal control method termed *motion planning with motion primitives*, which is based on exploiting inherent dynamical structures of the system, namely *symmetry* and *(un)stable invariant manifolds*. Symmetry in the context of mechanical systems occurs in form of invariances which in turn give rise to symmetry induced motions. This is linked to the classical symmetry reduction theory in geometric mechanics. Motion primitives represent the equivalence classes with respect to this symmetry; they are short pieces of trajectories, which can then be concatenated to sequences in various ways in order to solve a given control problem.

In many applications, *energy efficiency* plays a major role in the control design. To compute sequences with minimal control effort, in the methodology which has been developed in this work, the uncontrolled, i.e. natural dynamics are searched for (un)stable invariant manifolds of equilibrium points. Then, motion primitives along these (un)stable manifolds can be combined with other pieces into an energy efficient sequence. The corresponding (hybrid) control trajectory is characterized by switches between controlled and uncontrolled phases. In case of several objectives, the controlled motion primitives can be generated from multiobjective optimal control problems.

In the second part of this thesis, the optimal control method DMOC (Discrete Mechanics and Optimal Control) is extended to hybrid mechanical systems. In order to derive the hybrid equations of motions, a hybrid variational principle is developed in continuous time and for discrete time, as well. Then, an optimal control problem for a hybrid mechanical system can be addressed by a two layer approach that combines DMOC with other state-of-the-art optimization methods. As an important subproblem, switching time optimization for discretized dynamical systems is studied. Finally, the motion planning method is brought into the hybrid optimal control setting. Throughout the thesis, the methods and concepts are illustrated and evaluated by academic examples or real-world applications.

Zusammenfassung

In den Ingenieur- und Naturwissenschaften treten häufig Optimalsteuerungsprobleme für mechanische Systeme auf, beispielsweise in der Robotik, der Biomechanik, in Fahrzeugsystemen oder im Design von Weltraummissionen. Das jeweilige Ziel ist, das dynamische Verhalten des Systems mittels seiner Steuerungseingänge so zu beeinflussen, dass eine gegebene Aufgabe optimal erfüllt wird. In komplexen technischen Systemen stehen mechanische Systeme jedoch in Interaktion mit elektronischen Komponenten und Logik-Bauteilen zur Informationsverarbeitung. Daher führt eine adäquate Modellierung zu *hybriden dynamischen Systemen.* Hybride Steuerungsstrategien eröffnen neue Möglichkeiten für das Design und die Berechnung von Steuer- oder Regelgesetzen; gleichzeitig ergeben sich eine Vielzahl offener Fragestellungen in der Analyse, Steuerung, Regelung und Optimierung von hybriden dynamischen Systemen.

Diese Arbeit ist zwei Aspekten in diesem Forschungsgebiet gewidmet, einem strukturausnutzenden "Motion Planning" sowie der Optimalsteuerung hybrider mechanischer Systeme. Im ersten Teil liegt der Fokus auf einer Optimalsteuerungsmethode, die *"Motion Planning"* mit *"Motion Primitives"* genannt wird. Sie basiert darauf, inhärente, dynamische Systemstrukturen auszunutzen, zum einen *Symmetrie* und zum anderen *(in)stabile invariante Mannigfaltigkeiten.* Symmetrie tritt im Kontext mechanischer Systeme in Form von Invarianzen auf, die wiederum symmetrieinduzierte Bewegungen ermöglichen. Dies wird in Bezug zur klassischen Symmetriereduktion in der geometrischen Mechanik gesetzt. "Motion Primitives" bilden Repräsentanten der entsprechenden Äquivalenzklasse zu einer Symmetrie. Sie sind kurze Trajektorienstücke, die in verschiedener Weise zu Sequenzen gereiht werden können, um ein gegebenes Steuerungsproblem zu lösen.

In vielen Anwendungen spielt *Energieeffizienz* eine primäre Rolle im Steuerungsdesign. Um Sequenzen, die minimalen Steuerungsaufwand benötigen, zu berechnen, wird in dieser Arbeit eine Methodologie entwickelt, in der die ungesteuerte, d.h. natürliche Dynamik nach (in)varianten Mannigfaltigkeiten von Gleichgewichtspunkten durchsucht wird. Dann können "Motion Primitives" entlang dieser (in)stabilen Mannigfaltigkeiten mit anderen Stücken zu einer energieeffizienten Sequenz kombiniert werden. Die entsprechende (hybride) Steuerungstrajektorie zeichnet sich durch wechselnde gesteuerte und ungesteuerte Abschnitte aus. Falls mehrere Optimierungsziele vorliegen, können gesteuerte "Motion Primitives" aus Mehrzieloptimalsteuerungsproblemen erzeugt werden.

Im zweiten Teil der Arbeit wird die Optimalsteuerungsmethode DMOC ("Discrete Mechanics and Optimal Control") auf hybride mechanische Systeme erweitert. Um hybride Bewegungsgleichungen herzuleiten, wird ein hybrides Variationsproblem in kontinuierlicher und diskreter Zeit entwickelt. Ein Optimalsteuerungsproblem für ein hybrides mechanisches System kann dann mittels eines Zwei-Ebenen-Ansatzes

gelöst werden, der DMOC mit weiteren modernen Optimierungsmethoden kombiniert. Als ein wichtiges Teilproblem werden Umschaltzeitpunktsoptimierungsprobleme für diskretisierte dynamische Systeme untersucht. Schließlich wird die "Motion Planning"-Methode auf hybride Optimalsteuerungsprobleme erweitert. Die im Laufe dieser Arbeit entwickelten Methoden und Konzepte werden an verschiedenen akademischen Beispielen oder realen Anwendungen illustriert und evaluiert.

Contents

CHAPTER 1

Introduction

In nature as well as in man-made products, *dynamical systems* – systems with a state that changes over time – can be found everywhere. In order to understand and analyze them, to simulate and predict their behavior into the future, and, eventually, to design optimized dynamical systems, *modeling* plays an important role in engineering and the natural sciences. For the application of formal optimization techniques, mathematical models of the dynamic behavior are essential; for this reason, the term "dynamical system" is often used synonymously to denote the model and the real system. By model-based optimization methods, optimal values of the free design parameters can be determined. If the parameters are control inputs which can be defined as functions of time and the task is to optimally steer the system into a desired final state, we speak of *optimal control*.

The *mechanics* of modern technical systems are classically modeled by continuous time ordinary differential equations. However, their embedded electronics and digital control units, for instance, give rise to effects which are typically modeled by discrete events. This leads to the concept of *hybrid systems* which are characterized by interacting continuous time and discrete time dynamics.

Simulations as well as optimization for complex technical system models are only realizable by *efficient numerical techniques*. These methods have to provide highly accurate approximations of the real solutions in minimal computation time. To meet these challenges, this thesis is devoted to the development of methods which *exploit inherent dynamical system structures*. More concretely, for the computation of optimal control maneuvers, motions of the natural, i.e. uncontrolled or simply controlled, mechanical system can be beneficially used. They become part of *hybrid control sequences* in which phases of no control or of simple control and phases with short controlled maneuvers are concatenated in order to optimally solve a given control problem. Natural dynamics play a crucial role for the computation of *energy efficient control strategies*, in particular. For hybrid systems, an optimal control

policy consists of optimal controls for the continuous time dynamics together with *optimized discrete events* in between the continuous parts.

In the following, the classes of systems and the types of methods which are considered in this work are introduced and embedded into their scientific surroundings. The structure of this thesis together with a short summary of the contributions in each chapter is described afterwards.

From Classical Mechanics to Hybrid Mechanical Systems

A controlled dynamical system is described by a set of *states*, denoted by x, and by a vector field $\mathcal{F}$ that defines the temporal evolution depending on the current state and the *controls* u. An *evolution* of the dynamical system for a fixed control function $u(t)$ is given by the solution $x(t)$ of the ordinary differential equation $\dot{x}(t) = \frac{d}{dt}x(t) = \mathcal{F}(x(t), u(t))$, with $x(0) = x^0$ denoting the initial state at time zero.

Variational Principles The differential equations to model the dynamics of mechanical systems, i.e. their motions in space, can be derived by a variational approach in a differential geometric setting. The state of a mechanical system consists of the configurations, i.e. the positions of each body of the system, denoted by q, together with the corresponding velocities $\dot{q}$. Hamilton's variational principle of least action is based on the system's Lagrangian L, which defines the behavior of the conservative *natural system* by its different types of energy. A system's motion between two configurations, say $q(0) = q^0$ and $q(T) = q^T$, is a critical point of the *action integral*,

$$\delta \int_0^T L(q(t), \dot{q}(t))\, dt = 0.$$

The underlying idea of this approach to classical mechanics is that the minimization of the action is an intrinsic objective of nature. Thus, the motion of a free, i.e. unforced, mechanical system is the one which extremizes the action integral. Lagrangian forces that act on a mechanical system, e.g. dissipative forces due to friction or external control forces, influence its dynamic behavior. The *Lagrange-d'Alembert principle* takes this into account by extending the variational equation by a virtual work term leading to the identity

$$\delta \int_0^T L(q(t), \dot{q}(t))\, dt + \int_0^T f(q(t), \dot{q}(t), u(t)) \cdot \delta q\, dt = 0.$$

This is equivalent to the *forced Euler-Lagrange equations*,

$$\frac{d}{dt}\frac{\partial L}{\partial \dot{q}} - \frac{\partial L}{\partial q} = f(q(t), \dot{q}(t), u(t)).$$

These second order differential equations can be usually transformed into first order equations of the general form $\dot{x} = \mathcal{F}(x, u)$ with states $x = (q, \dot{q})$.

Integrators The study of mechanical systems from the perspective of differential geometry has a long history (cf. [AM87, MR99], for instance). However, *geometric mechanics* is still an active field of research, in particular with regard to simulation schemes and optimal control problems (cf. e.g. [MW01, Blo03, BL04, OJM11]). Solving forced Euler-Lagrange equations analytically becomes impossible for complex systems with nonlinear dynamics. Thus, the solutions $x(t)$ have to be approximated numerically by means of an *integration scheme*. The explicit Euler integrator for an uncontrolled system, for instance, iteratively defines the discrete sequence of states by $x_{k+1} = x_k + h\mathcal{F}(x_k)$ starting at $x_0 = x(0)$ and for a step size h. Implicit integrators, on the contrary, provide an implicit equation for the next node x_{k+1}. The accuracy of the integration scheme, in general, depends on its order (cf. [HLW06]). However, the class of *geometric integrators*, exactly preserves certain system properties regardless of the order of integration. A class of these integrators can be derived from a discretization of the variational principle for mechanical systems and they are therefore also called *variational integrators* or *symplectic integrators*. To this aim, the action integral between neighboring points q_k and q_{k+1}, each a time step h apart, is approximated by the *discrete Lagrangian* L_d for some quadrature rule applied to the integral, i.e.

$$L_d(q_k, q_{k+1}, h) \approx \int_{kh}^{(k+1)h} L(q(t), \dot{q}(t))\, dt.$$

Together with a discretization of the virtual work, discrete variations lead to the *discrete forced Euler-Lagrange equations*,

$$D_2 L_d(q_{k-1}, q_k) + D_1 L_d(q_k, q_{k+1}) + f_{k-1}^+ + f_k^- = 0.$$

Here, D_i $(i = 1, 2)$ is the derivative w.r.t. the i-th argument and f_{k-1}^+, f_k^- approximate the Lagrangian forces depending, in particular, on discretized controls. This approach to the development of symplectic integrators goes back to Veselov, cf. [Ves88, MV91, WM97, MPS98].

Hybrid Mechanics The reasons for the occurrence of discrete events interrupting the continuous evolution of mechanical systems are diverse: impacts because of collisions between rigid bodies or interactions with the ground, structural changes in the environment (e.g. different road surfaces for a driving car), varying coupling structures of dynamical systems (e.g. a switch from an open to a closed kinematic chain of industrial robots), an instantaneous drop of mass (e.g. for rockets or satel-

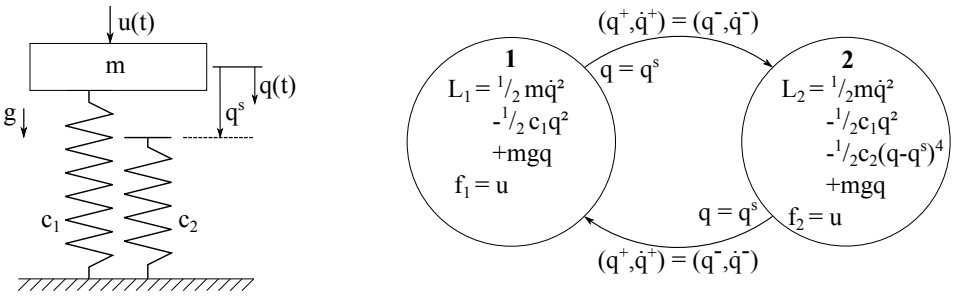

Figure 1.1: Hybrid automaton for a hybrid oscillator: the Lagrangian and thus, the dynamics, depend on the position of the mass. For $q \leq q^s$, only the linear spring is loaded, while for $q \geq q^s$ both springs are tensioned. The state is kept constant at the discrete events, i.e. the switches between the discrete states.

lite launchers), simplified subsystem models (e.g. nonlinear friction models idealized by switching linear or nonlinear dampers), a switch in the internal control unit (e.g. between different closed-loop controllers), a change in the communication network of interacting mechanical systems and so forth. In some cases, the dynamics before and after the switch are not the same. The different types of dynamics have to be modeled by different Lagrangian and Lagrangian forces together with switching rules, leading to *hybrid mechanical systems*. The switching conditions may be time-dependent or state-dependent and define an instantaneous reset of the elsewise continuous configurations and velocities. Simulation or optimization of mechanical systems with impacts have been studied from the variational point of view, e.g. in [FMOW03, AS06, PAM07, BL07a, PM11, SM12, LHK+12, KL13].

A general modeling framework for hybrid systems is given by *hybrid automata* (cf. [LJS+03, SJSL05]), in which the discrete dynamics are represented by a graph structure. The different Lagrangian are attached to the vertices of this graph such that a transition from one vertex to another corresponds to a discrete event. In some works on impact mechanics, e.g. [AS06, PAM07], the hybrid automaton definition is specified to Lagrangian systems. However, to the best of the author's knowledge, there has not been a generalization of hybrid automata to arbitrary hybrid Lagrangian systems, as it is developed in this thesis. While Lagrangian systems with impacts are hybrid systems with a single discrete state, i.e. only one type of continuous time dynamics, general hybrid Lagrangian systems may have multiple discrete states with different types of continuous time dynamics, as it is shown for the hybrid oscillator in Figure 1.1.

Optimal Control and Motion Planning

Optimal control theory goes back to the work of Pontryagin on necessary optimality conditions in the last century. Its roots, however, are attributed to Bernoulli's work on the Brachistochrone problem dating more than 300 years ago (see the historical perspective from Sussmann and Willems in [SW97], for instance). To this day, it is an important field of research, based on the central question of how to force a system into a desired behavior in an optimal way. A typical problem formulation is as follows: which path of the dynamical system's states, forced by an admissible control trajectory, minimizes a given cost functional? Formally, an optimal control problem for a mechanical system is stated as

$$\min_{q,u} J(q,u) = \int_0^T C(q(t), \dot{q}(t), u(t))\, dt,$$

subject to the state $(q, \dot{q})(t)$ being a solution of the forced Euler-Lagrange equations with control $u(t)$, boundary conditions $(q, \dot{q})(0) = (q^0, \dot{q}^0)$, $(q, \dot{q})(T) = (q^T, \dot{q}^T)$, and, possibly, further constraints on the path of the controls or states. The Pontryagin maximum principle provides necessary conditions for optimal control and state trajectories in terms of a boundary value problem for the states and additional adjoint differential equations. Thus, analytical solutions can be hardly found for systems with nonlinear dynamics and therefore, solutions have to be approximated numerically.

Numerical Methods State of the art numerical methods can be divided into two classes (for an overview, cf. e.g. [BBB$^+$01]). Indirect methods apply the Pontryagin maximum principle to obtain a system of necessary optimality conditions and then solve these boundary value problems by numerical techniques, e.g. shooting or collocation methods. In contrast, direct methods (cf. [Bet98]) begin with a discretization of the dynamics which transforms the optimal control problem into a high-dimensional, nonlinear, constrained optimization problem. Highly developed nonlinear programming methods, such as SQP (sequential quadratic programming, cf. e.g. [GJL$^+$00]) methods can then be applied. The discretization of the dynamics is obtained by applying an integration scheme to the differential equation. For mechanical systems, the method DMOC (*Discrete Mechanics and Optimal Control*, cf. [OJM11]) is based on variational integrators, i.e. the forced Euler-Lagrange equations of the original optimal control problem are replaced by the discrete forced Euler-Lagrange equations.

In real world applications, optimal control problems appear in many different areas of research in engineering and natural sciences, e.g. power systems, aerodynamics and space mission design, biomedicine, robotics, or automotive engineering.

The method of using discrete mechanics for optimal control problems has been successfully applied to optimal control problems in space mission design (cf. [JMO06, DOP+09, MOM12]), for a helicopter (cf. [Kob08]), a double pendulum on a cart (cf. [TKOT11]), for gaited bipeds and marionettes (cf. [PAM07, Joh12]), and in biomechanics (cf. [KM05, OT09, ML13]).

In many applications, there arise multiple objectives which have to be simultaneously optimized. This leads to *multiobjective optimal control problems*, which can be solved by combinations of optimal control methods and multiobjective optimization techniques (cf. [Ehr05] for an overview). The discretization of the dynamics, as used in direct methods, leads to high-dimensional multiobjective optimization problems. Efficient methods for these classes of problems are scalarization methods, e.g. reference point techniques as proposed in [LHDV10] and in [ORZ12].

However, finding optimal solutions for larger systems with complicated, in particular nonlinear, dynamics is still a challenging task for state of the art methods since the nonlinear optimization techniques are of local nature only. That is, sophisticated initial guesses are indispensable in order to guarantee that the computed local optima are globally efficient – or at least close to the normally unknown global optimum. One approach to overcome this limitations is to combine the local optimization with global methods from planning, as it is shortly described in the following. Alternatively, or in combination with this, methods for the generation of sophisticated initial guesses have to be developed. This is described in more detail below.

Motion Planning The growing interest in mechatronic systems, which consist of mechanical subsystems with embedded electronics and digital control units, has led to multidisciplinary research on control issues for this class of systems. The influence from the field of artificial intelligence has brought discrete *planning* techniques into novel combinations with classical control methods (for continuous time models). This gave rise to the term *motion planning* for discrete planning methods that (in contrast to classical planning methods) consider the dynamic motions of the systems as constraints for the planning problem (cf. [LaV06]). Thus, in this interpretation, *optimal motion plans* are identical to solutions of optimal control problems. *Motion planning with motion primitives* fits into the category of such hybrid motion planning approaches. The methodology has been developed by Frazzoli et al. in [FDF99, FDF00, Fra01, FB02, Fra03, FDF05]. Its underlying idea is a quantization of the continuous state space by an abstraction to a finite number of representative motions, called *motion primitives*. Thereby, the search for an optimal control maneuver in the infinite-dimensional state space is limited to a search for an optimal sequence of motion primitives. These motion primitives are stored in a so called *motion planning library*. Global search methods, such as probabilistic roadmap methods (cf. e.g. [CLH+05, LaV06, Kob08]) can be applied to this library. However, the

superior feature of the motion planning with primitives approach is the exploitation of inherent symmetry properties of the dynamical systems. This will be discussed in the third part of this introduction.

Hybrid Control Systems Optimal control for hybrid systems consists not only of the computation of optimal control trajectories for the continuous parts of the hybrid system but it also includes the optimization of the switching sequence and the switching times for its discrete states. Necessary optimality conditions for hybrid optimal control problems have been derived in [Sus99a, SC07, AAR10], for instance, as hybrid extensions of the Pontryagin maximum principle. Again, numerical methods play an important role in solving hybrid optimal control problems. Due to the discrete modes, in general, mixed-integer optimization problems have to be solved in the optimal control of hybrid systems. Here, various methods have been developed, e.g. a combination of direct optimal control methods with branch and bound techniques ([BGH$^+$02]), a general relaxation of the mode sequence (cf. [CM11] and [CM13] for projection based optimization) or the node insertion technique proposed in [GVK$^+$10]. Several approaches are based on a problem splitting such that a hierarchical problem is obtained which can be addressed by appropriate methods on each level (cf. [XA02b, XA02a, PAM07, GVK$^+$10]).

This thesis essentially focuses on two aspects of hybrid optimal control: firstly, a two layer formulation for hybrid optimal control problems and secondly, switching time optimization for discretized switched systems. The two layer formulation (which does not include integer optimization) allows to apply the direct optimal control method DMOC to the continuous control problems and standard nonlinear optimization methods to the switching time problem. Insofar, the approach resembles the algorithms in [XA02b, PAM07] and also the decentralized DMOC approach presented in [JMO06]. Beyond this, we consider multiobjective optimization problems for the switching times. Since the switching times form a low dimensional optimization space, in comparison to the discretized state and control space for the continuous parts of the hybrid system, the global optimization methods of GAIO (*Global Analysis of Invariant Objects*) for multiobjective optimization problems can be applied (cf. [DSH05, Sch04, SWOD13]).

However, efficient nonlinear optimization techniques are based on gradient information. In this thesis, we study adjoint based optimization methods for the subclass of *switched systems* which consists of a family of vector fields defining the continuous time dynamics together with a prescribed switching sequence and switching times that can be optimized with respect to a given cost function. *Switching time optimization* is well studied, cf. [CM11, EWD03, AA04, EWA06, SDEL09, XA02a, XA04, JM11, KT12], for instance. Nevertheless, the influence of the integration method on switched system optimization is typically not considered in the literature, for some

rare exceptions we refer to [XA02b], [SDEL09] or [ST10]. In [ST10], hybrid system simulators, which generate time-discretized hybrid systems, have been studied w.r.t. stability and convergence to the solutions of the original time-continuous hybrid system, but not w.r.t. switching time optimization. To the best of the author's knowledge, switching time optimization in a discretized setting, obtained from a numerical integration of the dynamics, has not been studied so far. Our analysis of the discretized setting reveals that differentiability properties are not fully inherited from the original continuous time optimization problem. More precisely, the nondifferentiable points of the cost function can be exactly characterized for general systems dependent on the time grid of the integration scheme. Thus, the discretized switching time optimization problem falls into the category of nonsmooth optimization problems, for which a considerable machinery exists (cf. e.g. [Cla83, Lem89, LO12]).

Exploiting Inherent Dynamical System Properties

The underlying idea of the optimal control method for mechanical systems, which is developed in this thesis, is to exploit inherent, i.e. natural properties of the dynamical system, namely

- *symmetry*, in terms of invariances of the system's dynamics, which allow the reusability of control maneuvers,
- *trim primitives*, which are relative equilibria of the constantly controlled system and thus, form motion primitives with special features, and
- *stable and unstable manifolds* of invariant objects of the uncontrolled system for energy optimal control maneuvers.

Symmetry Many dynamical systems, and mechanical systems, in particular, exhibit symmetries. In this work, we focus on continuous symmetries that can be described by the action of a Lie group. For mechanical systems, symmetry is characterized by an invariance of the Lagrangian with respect to the Lie group action which corresponds, for example, to a translation or a rotation of the system. Due to symmetry, *equivalent trajectories* exist, namely trajectories which can be transformed into each other via a shift by the symmetry action. Symmetry in mechanical systems is well studied from the perspective of differential geometry, cf. [AM87, MR99, Blo03, BL04].

In control design, symmetry can be beneficially exploited. A solution trajectory that has been designed for one specific situation, for example a highly dynamic turn maneuver for a helicopter, may be suitable in many other situations as well, because it does not explicitly depend on the absolute position in space. A sketch of two equivalent maneuvers for the controlled spherical pendulum is depicted in Figure 1.2.

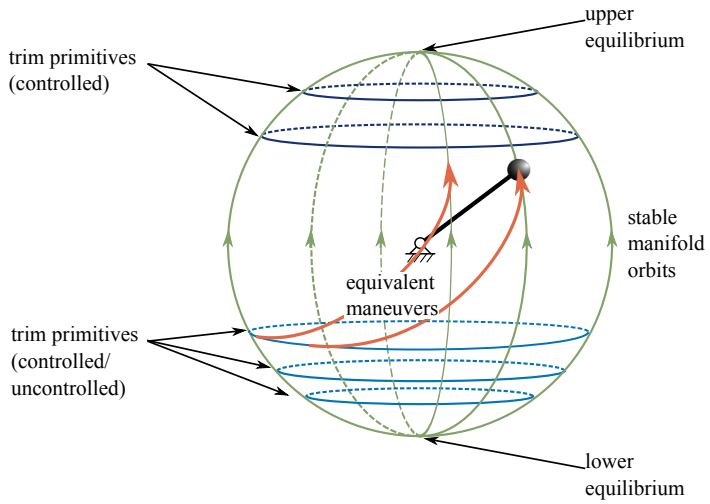

Figure 1.2: Motion primitives of the controlled spherical pendulum: equivalent maneuvers due to the rotational symmetry of the system, trim primitives as horizontal rotations with constant rotational velocity (in the lower hemisphere, trim primitives with zero control, i.e. classical relative equilibria, exist; in the upper hemisphere, a constant vertical control is necessary for trim primitives), and orbits on the (un)stable manifolds, which are purely vertical motions.

This is one of the underlying ideas of the motion planning with primitives approach of Frazzoli, Daleh and Feron (cf. [FDF05]). Here, equivalent control maneuvers are represented by an *equivalence class*, the motion primitive. A motion plan then consists of a sequence of motion primitives with some primitives being extraordinary simple, as we will explain below. According to [FDF05], this resembles the intuitive way in which human pilots steer helicopters, that is by recurrent simple steering modes with short intermediate control maneuvers.

Trim Primitives Continuous symmetries in mechanical systems correspond to the conservation of momenta and to the existence of motions that are solely induced by the symmetry action and are therefore called *relative equilibria*. For Hamiltonian and Lagrangian systems, relative equilibria can be determined by symmetry reduction procedures (see e.g. [MR99, MRS00, Mar93]). Whereas relative equilibria and symmetry reduction for Hamiltonian systems have been comprehensively studied for several decades (see e.g. the textbooks [MR99, Mar93] and for more recent works, e.g. [BL07b, RWL02]), reduction procedures directly on Lagrangian systems have gained less attention (cf. [MS93]).

Frazzoli extends the concept of relative equilibria to general controlled dynamical

systems by the definition of *trim primitives*. These are solutions of the systems with constant controls and state trajectories generated by the symmetry action. For mechanical systems, trim primitives are motions with constant body fixed velocities (cf. [Fra03]). As motion primitives, they have the special property that they can be solely defined by the constant velocity (more precisely, the symmetry's Lie algebra element) together with the constant control value. The corresponding trajectory is simply time parametrized and thus, trim primitives can be stored in the motion planning library without fixing their duration. This leads to more freedom in the sequencing of motion primitives and provides good controllability properties for this motion planning method (cf. e.g. [FDF05]).

In this thesis, we study trim primitives for mechanical systems in the geometric mechanics setting and extend the definition of a relative equilibrium and the related symmetry reduction method to controlled mechanical systems, such that a controlled relative equilibrium coincides with the definition of a trim primitive. As an illustrative example, the trim primitives of a simple spherical pendulum are shown in Figure 1.2.

Stable and Unstable Manifolds In the control of mechanical, electrical or mechatronic systems, minimizing the energetic effort is often of particular importance. In space mission design, for example, reducing the fuel consumption is essential for long term transitions and in the control of walking robots, reducing the energetic effort improves their range of operation or allows a smaller onboard energy supply which is beneficial for their dynamics. Obviously, trajectories of the natural, i.e. uncontrolled dynamics that are free of cost, should be used whenever the planning scenario allows for it. However, even the natural dynamics of nonlinear systems are typically quite complicated such that an analysis, by analytical and/or numerical means, is necessary to identify promising candidates of natural motion. Since, in general, there is no purely uncontrolled solution to a control problem, the uncontrolled motions have to be combined with controlled maneuvers to solution sequences.

Research in astrodynamics and space mission design showed that the invariant stable and unstable manifolds serve as such candidates. Since the studies of orbit structures in celestial mechanics performed in [Con68, McG69], invariant manifolds have been exploited in this spirit for a variety of space mission trajectories for the energy efficient transport between different planets and their nearby orbits (see e.g. [GKL$^+$04, KLMR01] among numerous others). This concept has been extended in such a way that (un)stable manifolds of several different systems are used as partial orbits that are concatenated into a hybrid solution trajectory by appropriately controlled maneuvers (see e.g. [DOP$^+$09] or [KLMR00], and related works of these authors).

(Un)stable manifolds belong to critical objects, such as equilibrium points or pe-

riodic orbits, and nearby, they are tangent to the eigenspaces of the system's linearization. For a hyperbolic spectrum (i.e. no purely imaginary eigenvalues), the stable manifold consists of all points in state space that tend to the critical object under the system's flow; points of the unstable manifold show the same behavior in backward time (cf. [GH83] for a reference on general dynamical system's theory or [AM87] for a focus on Hamiltonian and Lagrangian systems). A variety of numerical approximation methods for (un)stable manifolds has been developed in the last decades, for an overview, we refer to [KOD+05] and the references therein. For the numerical examples of this thesis, we use the set-oriented method GAIO (cf. [DFJ01, DJ02, DSH05]).

In this work, a framework for the sequencing of manifold orbits and controlled maneuvers is developed by an extension of the motion planning with motion primitives approach of [FDF05]. For the controlled maneuvers, optimal control problems with specific boundary conditions are formulated such that sequences of motion primitives can be build which connect orbits on manifolds with trim primitives and vice versa. Searching for the optimal motion plan then shows, which manifold orbits or which pieces of manifold orbits yield the optimal solution sequence. Numerical experiments are performed for spherical pendula models and, in similar fashion and including a validation on the test rig, for a planar double pendulum on a cart.

Contributions and Outline of this Thesis

In this thesis, optimal control problems for mechanical systems are studied. The focus lies on the development of new methods using hybrid control strategies and the applicability of the methods to hybrid dynamics. Parts of this thesis grew out of several preceding publications which are referred to at the beginning of the respective sections. For each of these publications, the author has given a substantial contribution.

In **Chapter 2**, an introduction to classical mechanics from the Lagrangian and the Hamiltonian viewpoint is given. Discrete forced Euler-Lagrange equations, which are used for the simulation or for the optimal control of mechanical systems, are derived via the discrete variational principle as in [MW01]. In the third part of this chapter, the concept of symmetry in mechanics is formally introduced. Symmetry presents itself as an invariance of the Lagrangian w.r.t. the symmetry's action and leads to momentum maps as conserved quantities for the system. We recall the classical Routh reduction and the generalized Lagrangian reduction method (cf. [MS93]). Symmetry gives rise to relative equilibria which are revealed by the reduction methods. A discussion of related concepts for symmetry reduction and a short transfer to symmetry in discrete mechanical systems complete the chapter.

Optimal control problems are introduced in **Chapter 3**. We summarize general problem formulations and the necessary optimality conditions given by the Pontryagin maximum principle from literature. State-of-the-art numerical solution techniques are discussed with a focus on direct methods. Then, the DMOC method (cf. [OJM11]) is introduced. This chapter ends with a technical application of DMOC. With substantial contribution of the author, the method has been used for the optimization of a switched reluctance drive test rig. To this aim, the (discrete) variational principle, classically used for purely mechanical systems, is applied to the electro-mechanical system. The obtained nonlinear constrained optimization problem is solved for an approximation of optimal current profiles that assure a static motor torque of the drive but minimize energetic losses. Resulting solutions outperform standard approaches in the control of switched reluctance drives when validated at the test rig.

One aim of this thesis is the exploitation of inherent dynamical properties of mechanical systems for the computation of energy efficient control sequences. Thus, in **Chapter 4**, this issue is selected to be studied separately beforehand. In a preliminary section, the definition of stable and unstable manifolds of invariant objects, e.g. equilibrium points, of dynamical systems are given from literature. Then, we present our approach for a computation of control strategies along (un)stable manifolds, which is later taken over to Chapter 5. Numerical experiments with this strategy are carried out for two planar double pendula examples. The results are discussed in comparison to ordinary optimal control techniques. The new approach provides better solutions, i.e. pendula swing-ups that require less energetic effort, for a great majority of problem instances given by varying boundary conditions and design parameters for the control sequence. Here, energy optimality combined with minimal transition time for the swing-ups is studied in the sense of a multiobjective optimal control problem. Also, provided that representative orbits on the (un)stable manifolds have been computed, the computational effort of the novel optimal control strategy is comparable to black-box optimizations, which do not require any information of the systems' natural dynamics.

The motion planning with primitives approach, presented in **Chapter 5**, formalizes the idea of hybrid control strategies based on inherent dynamical system properties. Its original framework, as introduced by Frazzoli et al., cf. [FDF05], is presented in the first two sections. Then, trim primitives are studied in the light of geometric mechanics, in particular with regard to symmetry reduction methods. Here, the classical definition of a relative equilibrium is extended to controlled potentials of the Lagrangian in order to give an approach for the computation of trim primitives of mechanical systems. As a new kind of motion primitive, which becomes

quite important for energy efficient motion plans, orbits on (un)stable manifolds are introduced. By means of defining extended maneuvers, they can be included in the maneuver automaton. As another extension of the original framework, Pareto-optimal control maneuvers are proposed. This generalization of optimal control maneuvers is highly relevant if a prioritization of objectives cannot yet be fixed in the design phase of the motion planning library. Optimal solution sequences are computed by a motion primitive search tree method which has been jointly developed in [FOK12]. The proposed extended motion planning approach is validated in three examples. For the spherical pendulum and the double spherical pendulum, the motion primitive sequences are used as initial guesses for a post optimization by DMOC and compared to black-box optimizations, similar to the comparisons taken in Chapter 4. In particular for the example of a double spherical pendulum, the sophisticated initial guesses are highly relevant for the computation of energy efficient solutions. In a third example, a two dimensional simple car, the variety of solution sequences for Pareto-optimal control maneuvers is illustrated.

In **Chapter 6**, optimal control problems for hybrid mechanical systems, the second main topic of this thesis, are considered. As a base point, a definition of a hybrid system as a hybrid automaton is given as it is typically used in the literature. We introduce a suitable concept of hybrid time which includes switching times and we define pairs of guard sets and reset maps for the discrete events that interrupt the continuous evolution of hybrid mechanical systems. Then, we concretize the general automaton's definition for hybrid mechanical systems. A hybrid variational principle is developed to derive hybrid Euler-Lagrange equations and discrete approximations from taking the analogue discrete variations. To this aim, an extension of the infinite dimensional path space is considered, on which variations in the configurations as well as in the switching times can be defined. The proof follows the ideas of [FMOW03] for mechanical systems with impacts, but goes beyond this setting by considering more general types of discrete events and Lagrangian systems under the influence of control forces.

In the following section, an approach for solving hybrid optimal control problems is considered. By an equivalent reformulation of the problem, two layers of optimization problems of different kinds arise. The lower layer consists of ordinary, infinite dimensional optimization problems for controlled mechanical systems and thus, can be efficiently solved by the DMOC method. In the upper layer, the (finite) optimization of the switching times and corresponding switching states remains, such that the overall hybrid optimal control problem can be comfortably solved by a combination of optimization tools for both layers.

The switching time optimization problem is studied individually from a theoretical point of view afterwards. It is shown that a time-discretization on a fixed time grid, but with an arbitrary integration scheme, leads to nondifferentiable points of the

corresponding discrete cost function, whenever the switching time parameter coincides with a grid point of the time discretization. Analogous to the original problem setting, which is well studied in the literature, adjoint equations can be derived for the discretized switching time optimization problem. However, the nondifferentiability has to be considered for the development of an adjoint based, nonsmooth optimization algorithm. The proposed algorithm is successfully tested for two academic examples and for the switched double pendulum application.

In **Chapter 7**, relations between motion planning with primitives, as presented in Chapter 5, and hybrid mechanical control systems, as studied in Chapter 6, are given. As the term "maneuver automaton" suggests, a motion planning library can be reformulated as a hybrid automaton. Furthermore, the two step procedure of firstly computing control maneuvers by solving optimal control problems and secondly finding an optimal sequence by a mixed combinatorial and switching time optimization problem is closely related to a two layer hybrid optimal control approach. The definition of trim primitives as symmetry induced motions of a mechanical system is generalized to hybrid mechanical systems and studied in an example scenario of motion planning for hybrid systems.

This thesis closes with concluding remarks on a summary of the results and a discussion of open problems and possible directions of future research in **Chapter 8**.

Three sections in the **Appendix** provide detailed information for optional reference during the reading of the main part. The first section sums up basic definitions and results from differential geometry as a background to geometric mechanics. In the second section, numerical methods, which are not in the focus of this thesis, but which have been applied in the various numerical examples, are shortly described. Finally, modeling details on the double pendulum models, which have been used in Chapter 4, are collected.

CHAPTER 2

Mechanical Systems

Mechanical systems have already been studied from the perspective of differential geometry for some decades; for an introduction and historical remarks, we refer to the classical textbooks [AM87] and [MR99]. However, *geometric mechanics* is still an active field of research, e.g. regarding optimal control problems, cf. [MW01, Blo03, BL04, Obe08, OJM11], for instance. Two main and different points of view have been developed in the study of mechanical systems: the *Lagrangian approach*, based on variational principles, and the *Hamiltonian approach*, based on energy observations. Under certain conditions, the resulting modeling equations are equivalent, but both techniques have their own advantages in special fields of application or provide different analysis techniques, e.g. for symmetry.

In Section 2.1, an introduction to the modeling concepts of Lagrange and Hamilton is given. Both of these approaches are based on descriptions in continuous time. We restrict ourselves to finite-dimensional systems, since infinite-dimensional systems as occuring in field theory are not in the scope of this thesis. In Section 2.2, the discrete variational approach for Lagrangian systems in discrete time that has been developed by Marsden and West [MW01] is presented. Discrete equations of motion are important for numerical purposes, such as system integrations or optimization tasks. In a short excursus we show how *mechanical integrators* fit into the category of symplectic integration schemes. In the continuous as well as in the discrete setting, we do not consider *Lagrangian* which explicitly depend on time; for a study of the corresponding non-autonomous systems we refer to [MW01], for instance. Finally, definitions of symmetry, related conservation properties, and an introduction to symmetry induced motions of mechanical systems, so-called *relative equilibria*, are given in Section 2.3 and illustrated by several examples. In the appendix, basic definitions of differential geometry are given (cf. Section A), to which we refer throughout this chapter.

2.1 Lagrangian and Hamiltonian Mechanics

Let Q be an n-dimensional configuration manifold (cf. Definition A.1) and for some final time $T \in \mathbb{R}^+$,

$$\mathcal{C}(Q) = \mathcal{C}([0,T], Q) = \{q : [0,T] \to Q \,|\, q \text{ is a } C^2 \text{ curve}\} \tag{2.1}$$

the *path space*, such that in local coordinates, $q(t) = (q_1(t), \ldots, q_n(t))$ is a time-dependent configuration of the mechanical system. The corresponding state space is then given by the tangent bundle TQ (Definition A.2) in the Lagrangian setting and by the cotangent bundle T^*Q (Definition A.5) in Hamiltonian mechanics.

2.1.1 Euler-Lagrange Equations

For the derivation of the Euler-Lagrange equations, we follow the formulation in [MW01] and [OJM11]. Assume that the mechanical system is described by a Lagrangian $L : TQ \to \mathbb{R}$. Typically, the Lagrangian L consists of the difference between the kinetic and potential energy, or it is even of the special structure $L(q, \dot{q}) = T(q, \dot{q}) - V(q) = \frac{1}{2}\dot{q}^T M(q)\dot{q} - V(q)$ with $M(q)$ being a symmetric, positive definite mass matrix, and $V(q)$ a potential function. $T(q, \dot{q})$ is sometimes also written as $T(q, \dot{q}) = \frac{1}{2}\|\dot{q}\|_q^2$ with $\|\cdot\|_q$ being the mass matrix induced norm on TQ and $\langle\langle \cdot, \cdot \rangle\rangle$ the corresponding metric.

Then, the *action map* $\mathfrak{S} : \mathcal{C} \to \mathbb{R}$ on the path space (Equation (2.1)) is defined as

$$\mathfrak{S}(q) = \int_0^T L(q(t), \dot{q}(t))dt. \tag{2.2}$$

Let $\pi_Q : TQ \to Q$ be the canonical projection of a tangent vector to its basis point on the configuration manifold. The tangent space $T_q\mathcal{C}(Q)$ of $\mathcal{C}(Q)$ at the point q is the set of C^2 maps $v_q : [0,T] \to TQ$ which are projected onto q, i.e. $\pi_Q \circ v_q = q$. We define the second-order submanifold of $T(TQ)$ to be

$$\ddot{Q} = \{w \in T(TQ) \,|\, T\pi_Q(w) = \pi_{TQ}(w)\} \subset T(TQ), \tag{2.3}$$

where $\pi_{TQ} : T(TQ) \to TQ$ is the corresponding natural projection on $T(TQ)$. Elements of $\ddot{Q}$ are those 4-tuples $((q, \dot{q}), (\dot{q}, \ddot{q})) \in T(TQ)$, which are second derivatives $d^2q/dt^2(0)$ of curves $q : \mathbb{R} \to Q$.

Theorem 2.1 (Hamilton's principle)**:** Given a C^k Lagrangian L, $k \geq 2$, there exists a unique C^{k-2} mapping $D_{EL}L : \ddot{Q} \to T^*Q$ and a unique C^{k-1} one-form Θ_L on TQ, such that for all variations $\delta q \in T_q\mathcal{C}(Q)$ of $q(t)$ (cf. Definition A.22) it holds for the

differential of the action

$$\mathbf{d}\mathfrak{S}(q)\cdot\delta q=\int_0^T D_{EL}L(\ddot{q})\cdot\delta q dt+\Theta_L(\dot{q})\cdot\hat{\delta}q\,|_0^T\,, \tag{2.4}$$

where

$$\hat{\delta}q(t)=\left(\left(q(t),\frac{\partial q}{\partial t}(t)\right),\left(\delta q(t),\frac{\partial\delta q}{\partial t}(t)\right)\right). \tag{2.5}$$

The mapping $D_{EL}L$ is called the *Euler-Lagrange map* and has the coordinate expression $(D_{EL}L)_i=\frac{\partial L}{\partial q^i}-\frac{d}{dt}\frac{\partial L}{\partial\dot{q}^i}$, and the one-form Θ_L is called the *Lagrangian one-form* and in coordinates is given by $\Theta_L=\frac{\partial L}{\partial\dot{q}^i}\mathbf{d}q^i$.

Proof. Computing the variation of the action map using integration by parts leads to (cf. e.g. [MW01])

$$\begin{aligned}\mathbf{d}\mathfrak{S}(q)\cdot\delta q&=\int_0^T\left[\frac{\partial L}{\partial q^i}\delta q^i+\frac{\partial L}{\partial\dot{q}^i}\frac{d}{dt}\delta q^i\right]dt\\&=\int_0^T\left[\frac{\partial L}{\partial q^i}-\frac{d}{dt}\frac{\partial L}{\partial\dot{q}^i}\right]\cdot\delta q^i dt+\left[\frac{\partial L}{\partial\dot{q}^i}\delta q^i\right]_0^T.\end{aligned} \tag{2.6}$$

The integrand can be identified as the Euler-Lagrange map and the second term as the Lagrangian one-form (cf. A.6 for the definition of differential forms). □

The *Lagrangian vector field* $X_L:TQ\to T(TQ)$ is a second-order vector field on TQ satisfying

$$D_{EL}L\circ X_L=0.$$

It is uniquely defined if L is regular (cf. [MW01]). Then, the existence of the flow of X_L, the so-called *Lagrangian flow* $F_L:TQ\times\mathbb{R}\to TQ$, is guaranteed. For a fixed time t, we write $F_L^t:TQ\to TQ$.

A curve $q\in\mathcal{C}(Q)$ is a solution of the Euler-Lagrange equations if the integral in Equation (2.6) vanishes for all variations $\delta q\in T_q\mathcal{C}(Q)$. This is equivalent to q satisfying the Euler-Lagrange equations

$$\frac{\partial L}{\partial q^i}(q,\dot{q})-\frac{d}{dt}\left(\frac{\partial L}{\partial\dot{q}^i}(q,\dot{q})\right)=0 \tag{2.7}$$

for all $t\in(0,T)$, i.e. $(q,\dot{q})$ is an integral curve of X_L (cf. Definition A.4).

Lagrangian flows are symplectic, i.e. $(F_L^T)^*(\Omega_L)=\Omega_L$ with $\Omega_L=\mathbf{d}\Theta_L$ being the Lagrangian symplectic form (recall that Θ_L is the Lagrangian one-form). The

coordinate expression is given by

$$\Omega_L(q,\dot{q}) = \frac{\partial^2 L}{\partial q^i \partial \dot{q}^j}\mathbf{d}q^i \wedge \mathbf{d}q^j + \frac{\partial^2 L}{\partial \dot{q}^i \partial \dot{q}^j}\mathbf{d}\dot{q}^i \wedge \mathbf{d}q^j.$$

2.1.2 External Forces

So far, neither the influence of exterior forces, such as friction, nor the effect of controls have been considered. This can be done by an extension of Lagrange's equations which results from the *Lagrange-d'Alembert principle*. Here, we mainly refer to [OJM11], where Lagrangian control forces are defined that combine Lagrangian forces and additional time-dependent control forces (extending the approach in [MR99] and [MW01], cf. [Obe08] for a discussion).

Let $U \subset \mathbb{R}^m$ be a control manifold and define the *control path space* to be

$$\mathcal{C}(U) = \mathcal{C}([0,T],U) = \{u : [0,T] \to U \mid u \in L^\infty\},$$

with the control parameter $u(t) \in U$ and L^∞ denoting the space of essentially bounded, measurable functions equipped with the essential supremum norm[1]. Then, a Lagrangian control force is defined as a map $f_L : TQ \times U \to T^*Q$, which is given in coordinates as

$$f_L : (q,\dot{q},u) \mapsto (q, f_L(q,\dot{q},u)).$$

It is assumed that f_L may also include configuration and velocity dependent forces, but not explicitly time-dependent forces. We can interpret a Lagrangian control force as a family of Lagrangian forces with fixed curves u. These are fiber-preserving maps (cf. Definition A.11) $f_L^u : TQ \to T^*Q$ over the identity id_Q, written in coordinates as $f_L^u : (q,\dot{q}) \mapsto (q, f_L^u(q,\dot{q}))$.

For a given control path $u \in \mathcal{C}(U)$, the Lagrange-d'Alembert principle seeks curves $q \in \mathcal{C}(Q)$ with fixed initial value $q(0)$ and fixed final value $q(T)$ (cf. Definition A.22) satisfying

$$\delta \int_0^T L(q(t),\dot{q}(t))\,dt + \int_0^T f_L(q(t),\dot{q}(t),u(t)) \cdot \delta q(t)\,dt = 0 \tag{2.8}$$

for all variations $\delta q \in T_q\mathcal{C}$. The second integral in (2.8) is defined as the *virtual work* acting on the mechanical system via the force f_L. Integration by parts, analogously to the proof of Theorem 2.1 yields as an equivalent formulation the forced Euler-

[1] By allowing controls to be in L^∞ we lose some regularity for the configurations, i.e. we then have curves $q \in C^{1,1}([0,T],Q)$, which is the space of all functions $q : [0,T] \to Q$ that are continuously differentiable on $(0,T)$ and for which the first derivative is Lipschitz continuous on $[0,T]$ (cf. [OJM11]).

Lagrange equations

$$\frac{\partial L}{\partial q}(q,\dot{q}) - \frac{d}{dt}\left(\frac{\partial L}{\partial \dot{q}}(q,\dot{q})\right) + f_L(q,\dot{q},u) = 0. \tag{2.9}$$

Equation (2.9) implicitly defines a family of *forced Lagrangian flows* $F_L^u : TQ \times [0,T] \to TQ$ for fixed curves $u \in \mathcal{C}$. The corresponding *forced Lagrangian vector fields* are then denoted by $X_L^u : TQ \to T(TQ)$.

2.1.3 Forced Hamiltonian Systems

This thesis focuses on the Lagrangian point of view and only rarely uses Hamilton equations, so we restrict ourselves to a short introduction into forced Hamiltonian systems based on [OJM11] and refer to [MR99, MW01, OJM11] for a detailed discussion.

The Hamiltonian is a function $H : T^*Q \to \mathbb{R}$ on the cotangent bundle T^*Q, on which we denote local coordinates by $q = (q^1, \dots, q^n)$ and $p = (p_1, \dots, p_n)$. For points $p_q \in T^*Q$ and $w_{p_q} \in T_{p_q}(T^*Q)$, we define the canonical one-form Θ on T^*Q by

$$\Theta(p_q) \cdot w_{p_q} = \langle p_q, T_{\pi_Q} \cdot w_{p_q} \rangle,$$

where $\pi_Q : T^*Q \to Q$ is the canonical projection and $T_{\pi_Q} : T(T^*Q) \to TQ$ its tangent map. Here, $\langle \cdot, \cdot \rangle$ denotes the natural pairing between vectors and covectors. The canonical two-form Ω on T^*Q is defined to be $\Omega = -\mathbf{d}\Theta$.

A Hamilton control force is a map $f_H : T^*Q \times U \to T^*Q$ defined by a family of fiber preserving maps $f_H^u : T^*Q \to T^*Q$ over the identity. For a given f_H and a fixed curve $u \in \mathcal{C}(U)$, the corresponding family of horizontal one-forms $f_H^{u'}$ on T^*Q is given by $(f_H^u)'(p_q) \cdot w_{p_q} = \langle f_H^u(p_q), T_{\pi_Q} \cdot w_{p_q} \rangle$. The forced Hamiltonian vector field X_H^u for a fixed curve u is defined by the equation

$$\mathbf{i}_{X_H^u}\Omega = \mathbf{d}H - (f_H^u)'$$

and in coordinates by

$$\begin{aligned} X_q^u(q,p) &= \frac{\partial H}{\partial p}(q,p) \\ X_p^u(q,p) &= -\frac{\partial H}{\partial q}(q,p) + f_H^u(q,p). \end{aligned}$$

This defines the forced Hamiltonian flow $F_H^u : T^*Q \times [0,T] \to T^*Q$ and the forced Hamiltonian vector field $X_H^u = (X_q^u, X_p^u)$ for fixed $u \in \mathcal{C}(U)$.

2.1.4 Legendre Transform

The following informal calculations for the unforced case show that, in many cases, the Euler-Lagrange equations are equivalent to Hamilton's equations (cf. [MR99, MW01]). Formally, their relation is given by the Legendre transform, which we introduce afterwards.

Define the Hamiltonian by $H(q,p) = \frac{\partial L}{\partial \dot{q}}(q,\dot{q}) \cdot \dot{q} - L(q,\dot{q}) = p \cdot \dot{q} - L(q,\dot{q})$ with the momentum $p = \frac{\partial L}{\partial \dot{q}}(q,\dot{q})$ and assume the Euler-Lagrange equations hold, then we compute

$$\begin{aligned}\frac{\partial H}{\partial q}(p,q) &= p \cdot \frac{\partial \dot{q}}{\partial q} - \frac{\partial L}{\partial q}(q,\dot{q}) - \frac{\partial L}{\partial \dot{q}}(q,\dot{q})\frac{\partial \dot{q}}{\partial q} \\ &= -\frac{\partial L}{\partial q}(q,\dot{q}) = -\frac{d}{dt}\frac{\partial L}{\partial \dot{q}}(q,\dot{q}) = -\dot{p}\end{aligned}$$

and

$$\frac{\partial H}{\partial p}(q,p) = \dot{q} + p \cdot \frac{\partial \dot{q}}{\partial p} - \frac{\partial L}{\partial \dot{q}}(q,\dot{q})\frac{\partial \dot{q}}{\partial p} = \dot{q},$$

which are the Hamilton's equations in coordinate expression.

The Legendre transform or fiber derivative $\mathbb{F}L : TQ \to T^*Q$ is defined by

$$\mathbb{F}L(v_q) \cdot w_q = \left.\frac{d}{d\epsilon}\right|_{\epsilon=0} L(v_q + \epsilon w_q), \quad \mathbb{F}L : (q,\dot{q}) \mapsto (q,p) = \left(q, \frac{\partial L}{\partial \dot{q}}(q,\dot{q})\right)$$

for v_q, $w_q \in TQ$. A Lagrangian is called *regular*, if its fiber derivative is locally an isomorphism. If it is a global isomorphism, L is called *hyperregular*. If the Hamiltonian is defined by $H(q,p) = \mathbb{F}L(q,\dot{q}) \cdot \dot{q} - L(q,\dot{q})$ (recall the calculation in the beginning) and L is hyperregular, then H is hyperregular as well and the Legendre transform is invertible (cf. [MW01]). In this case, the Lagrangian and Hamiltonian vector fields and flows are related by $\mathbb{F}L$. In other words, Hamilton's equations are equivalent to the Euler-Lagrange equations. Conversely, from a Hamiltonian on T^*Q that is hyperregular, it follows that there is a connection to a Lagrangian on TQ.

Hamiltonian and Lagrangian forces can be also transformed by the Legendre transform, i.e. $f_L = f_H \circ \mathbb{F}L$. Then, the above statement holds for the forced Hamiltonian and the forced Euler-Lagrange equations, since the pull-back under $\mathbb{F}L$ also relates the forced vector fields, i.e. $(\mathbb{F}L)^*(X_H^u) = X_L^u$.

Throughout this thesis, we will generally assume hyperregularity of the Lagrangian, such that we can always transform velocities into momenta and vice versa.

2.2 Discrete Mechanics

In this section, a discrete framework for Lagrangian mechanics is presented and related to a special class of numerical integrators, so-called *variational* or *symplectic integrators*. *Discrete forced Euler-Lagrange equations* later play a crucial role in the numerical treatment of optimal control problems, cf. Section 3.3, in particular.

2.2.1 Discrete Forced Euler-Lagrange Equations

For a discrete variational approach to Lagrangian mechanics, recalled from [MW01] and [OJM11], we define the discrete state space to be $Q \times Q$ with the same configuration manifold Q as before. So instead of a point $(q_0, \dot{q}_0)$, we now consider two configurations q_0 and q_1, which we can interpret as being two points on a curve q one time step h apart, such that they can approximate the local velocity information. Formally speaking, $Q \times Q$ is locally isomorphic to TQ.

Based on the time step h, we introduce a time grid $\Delta t = \{t_k = kh \,|\, k = 0, \dots, N\}$ with $Nh = T$. The *discrete path space*, denoted by $\mathcal{Q}_d$ is defined by

$$\mathcal{Q}_d = \mathcal{Q}_d(\{t_k\}_{k=0}^N, Q) = \{q_d : \{t_k\}_{k=0}^N \to Q\}$$

and for a discrete trajectory $q_d \in \mathcal{Q}_d$ we write $\{q_k\}_{k=0}^N$ with $q_k = q_d(t_k)$. A discrete Lagrangian is a function $L_d : Q \times Q \times \mathbb{R} \to \mathbb{R}$ which can be interpreted as the approximation of the action integral between two points q_k and q_{k+1},

$$L_d(q_k, q_{k+1}, h) \approx \int_{kh}^{(k+1)h} L(q(t), \dot{q}(t))dt.$$

For shortness, in the following, we neglect the h and simply write L_d as a function on $Q \times Q$, whenever the dependence on h is clear from the context. The discrete action map $\mathfrak{S}_d : \mathcal{Q}_d \to \mathbb{R}$ is defined by

$$\mathfrak{S}_d(q_d) = \sum_{k=0}^{N-1} L_d(q_k, q_{k+1}).$$

$\mathcal{Q}_d$ is isomorphic to $Q \times \cdots \times Q$ ($N+1$ copies) and can therefore be equipped with a smooth product manifold structure. The discrete action $\mathfrak{S}_d$ inherits the smoothness of the discrete Lagrangian. The tangent space $T_{q_d}\mathcal{Q}_d$ is defined to be the set of maps $v_{q_d} : \{t_k\}_{k=0}^N \to TQ$ such that $\pi_Q \circ v_{q_d} = q_d$, which are denoted by $v_{q_d} = \{(q_k, v_k)\}_{k=0}^N$.

To define a discrete formulation for Lagrangian control forces (cf. [OJM11]) we introduce a refined grid $\Delta\tilde{t} = \{t_{kl} = t_k + c_l h \,|\, k = 0, \dots, N-1; \, l = 1, \dots, s\}$ with control points $0 \leq c_1 < \cdots < c_s \leq 1$. The discrete control path space is

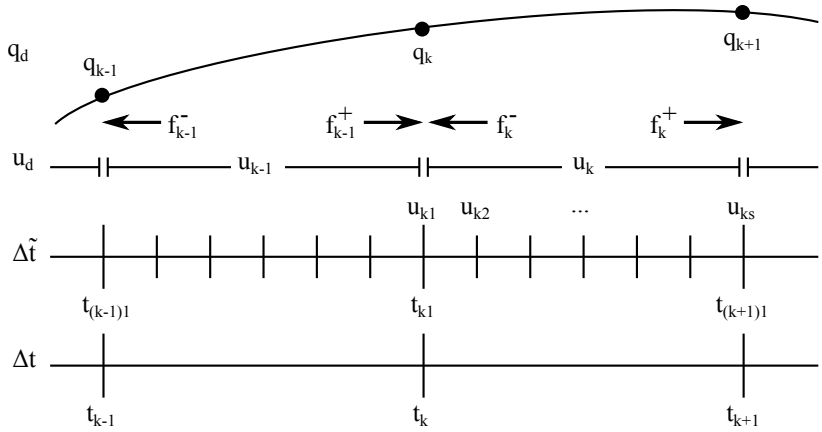

Figure 2.1: Definition of discrete configurations, controls and forces.

then defined to be $\mathcal{U}_d = \{u_d : \Delta\tilde{t} \to U\}$. Let the intermediate control samples $u_k = (u_{k1}, \ldots, u_{ks}) \in U^s$ on $[t_k, t_{k+1}]$ be the values of the control parameters guiding the system from q_k to q_{k+1} with $u_{kl} = u_d(t_{kl})$ for $l \in \{1, \ldots, s\}$. Then the left and the right discrete Lagrangian control forces $f_d^+, f_d^- : Q \times Q \times U^s \to T^*Q$ are given in coordinates as

$$f_d^+(q_k, q_{k+1}, u_k) = (q_{k+1}, f_d^+(q_k, q_{k+1}, u_k)), \text{ and}$$
$$f_d^-(q_k, q_{k+1}, u_k) = (q_k, f_d^-(q_k, q_{k+1}, u_k)).$$

They are interpreted as families of discrete fiber-preserving Lagrangian forces $f_d^{u_k,\pm} : Q \times Q \to T^*Q$ in the sense that $\pi_Q \circ f_d^{u_k,\pm} = \pi_Q^\pm$ with fixed $u_k \in U^s$, $\pi_Q^+(q_k, q_{k+1}) = q_{k+1}$ and $\pi_Q^-(q_k, q_{k+1}) = q_k$. The combination of the two discrete control forces finally leads to a single one-form $f_d^{u_k} : Q \times Q \to T^*(Q \times Q)$ defined by

$$f_d^{u_k}(q_k, q_{k+1}) \cdot (\delta q_k, \delta q_{k+1}) = f_d^{u_k,+}(q_k, q_{k+1}) \cdot \delta q_{k+1} + f_d^{u_k,-}(q_k, q_{k+1}) \cdot \delta q_k.$$

To simplify the notation, we set $f_k^\pm = f_d^\pm(q_k, q_{k+1}, u_k)$ and $f_k = f_d(q_k, q_{k+1}, u_k)$. We interpret the left discrete force f_{k-1}^+ (the right discrete force f_k^-, respectively) as the force resulting from the continuous control force acting during the time span $[t_{k-1}, t_k]$ ($[t_k, t_{k+1}]$, respectively) on the configuration node q_k. Figure 2.1 gives an illustration.

As in the continuous case, a discrete Hamiltonian principle can be applied which leads to discrete Euler-Lagrange equations in the unforced case. Since we additionally consider Lagrangian forces, we apply the discrete Lagrange-d'Alembert principle (cf. [OJM11]). Therefore, the virtual work can be approximated via the discrete left

and right forces,

$$\mathfrak{W}_d(q_d, u_d) = \sum_{k=0}^{N-1} f_k^- \cdot \delta q_k + f_k^+ \cdot \delta q_{k+1} \approx \int_0^T f_L(q(t), \dot{q}(t), u(t)) \cdot \delta q(t) dt.$$

Then, the *discrete Lagrange-d'Alembert principle* seeks discrete curves $\{q_k\}_{k=0}^N$ satisfying

$$\delta \mathfrak{S}_d + \mathfrak{W}_d(q_d, u_d) = \delta \sum_{k=0}^{N-1} L_d(q_k, q_{k+1}) + \sum_{k=0}^{N-1} \left[f_k^- \cdot \delta q_k + f_k^+ \cdot \delta q_{k+1} \right] = 0 \quad (2.10)$$

for all variations δq_k vanishing at the endpoints. This is equivalent to the *discrete forced Euler-Lagrange equations*

$$D_1 L_d(q_k, q_{k+1}) + D_2 L_d(q_{k-1}, q_k) + f_k^- + f_{k-1}^+ = 0, \quad \text{for } k = 1, \dots, N-1. \quad (2.11)$$

Here, we use the slot derivative notation, i.e. D_i denotes the derivative w.r.t. the i-th argument. These equations implicitly define the forced discrete Lagrangian map $F_{L_d}^{u_{k-1}, u_k} : Q \times Q \to Q \times Q$ which maps (q_{k-1}, q_k) to (q_k, q_{k+1}) for fixed controls $u_{k-1}, u_k \in U^s$.

The forced discrete Legendre transforms $\mathbb{F}^{\pm} L_d : Q \times Q \to T^*Q$ (cf. [MW01]) are defined as

$$\begin{aligned} &\mathbb{F}^{f+} L_d : (q_k, q_{k+1}, u_k) \mapsto (q_{k+1}, p_{k+1}^+) = (q_{k+1},\, D_2 L_d(q_k, q_{k+1}) + f_k^+), \text{and} \\ &\mathbb{F}^{f-} L_d : (q_k, q_{k+1}, u_k) \mapsto (q_k, p_k^-) = (q_k,\, -D_1 L_d(q_k, q_{k+1}) - f_k^-). \end{aligned}$$

By $\mathbb{F}^{f\pm} L_d^{u_k}$ we denote the forced discrete Legendre transform for fixed controls $u_k \in U^s$. Then, according to [OJM11], the corresponding forced discrete Hamiltonian map $\tilde{F}_{L_d}^{u_k} = \mathbb{F}^{f\pm} L_d^{u_{k+1}} \circ F_{L_d}^{u_k, u_{k+1}} \circ (\mathbb{F}^{f\pm} L_d^{u_k})^{-1}$ is given by the map $\tilde{F}_{L_d}^{u_k} : (q_k, p_k) \mapsto (q_{k+1}, p_{k+1}))$, with

$$\begin{aligned} p_k &= -D_1 L_d(q_k, q_{k+1}) - f_d^{u_k, -}(q_k, q_{k+1}), \text{ and} \\ p_{k+1} &= \quad D_2 L_d(q_k, q_{k+1}) + f_d^{u_k, +}(q_k, q_{k+1}). \end{aligned}$$

The discrete momenta p_k and p_{k+1} belong to the boundaries of the interval $[t_k, t_{k+1}]$. Comparing these formulas to Equations (2.11), we see that the discrete forced Euler-Lagrange equations can be written as

$$\begin{aligned} & D_2 L_d(q_{k-1}, q_k) + f_{k-1}^+ = -D_1 L_d(q_k, q_{k+1}) - f_k^- \\ \Leftrightarrow \quad & \mathbb{F}^{f+} L_d(q_{k-1}, q_k, u_{k-1}) = \mathbb{F}^{f-} L_d(q_k, q_{k+1}, u_k), \end{aligned}$$

i.e. they enforce the momentum at node k evaluated from the left interval $[t_{k-1}, t_k]$ to be the same as if evaluated from the right interval $[t_k, t_{k+1}]$. For further details on discrete mechanics from the Hamiltonian viewpoint, we refer to [MW01].

2.2.2 Variational Integrators

The use of discrete variational mechanics plays an important role for the numerical treatment of Lagrangian systems, meaning the discrete Lagrangian system is used to approximate a continuous Lagrangian system. Equations (2.11) provide a time stepping scheme for the simulation of the mechanical system, a so-called *variational integrator* (cf. [HLW06] or [MW01]).

Assuming a non-forced system with regular Lagrangian (such that the Legendre transform is well defined) the Euler-Lagrange equations simplify to

$$D_2 L_d(q_{k-1}, q_k, h) = -D_1 L_d(q_k, q_{k+1}, h).$$

Given the discrete trajectory up to q_k, the discrete Lagrangian map, denoted by $F_{L_d} : Q \times Q \times \mathbb{R} \to Q \times Q$, calculates q_{k+1} according to the equation above. Equivalently, the integrator can be implemented as a map

$$F : (q_k, p_k) \mapsto (q_{k+1}, p_{k+1})$$

using the implicit equation $p_k = -D_1 L_d(q_k, q_{k+1})$ to solve for q_{k+1} and then the explicit update $p_{k+1} = D_2 L_d(q_k, q_{k+1})$ to get p_{k+1}. Regularity of L_d ensures that both derivatives are local isomorphisms.

The discrete Lagrangian map and therefore the integrator as well are symplectic. One way to show this is by directly calculating the preservation of the discrete Lagrangian one-form (its push forward respectively, cf. [MW01]). Alternatively, one can apply the well known theorem that every symplectic map has a generating function (cf. [HLW06]). For mechanical systems, this is the discrete Lagrangian. More precisely, a generating function S of a symplectic mapping $F : (q, p) \to (Q, P)$ satisfies $\mathbf{d}S = P\,dQ - p\,dq$. Setting $S(q_n, q_{n+1}) = L_d(q_n, q_{n+1})$ we see that the discrete Lagrangian is a generating function of $F : (q_n, p_n) \mapsto (q_{n+1}, p_{n+1})$, since

$$\begin{aligned}\mathbf{d}S(q_n, q_{n+1}) = \mathbf{d}L_d(q_n, q_{n+1}) &= D_1 L_d(q_n, q_{n+1}) dq_n + D_2 L_d(q_n, q_{n+1}) dq_{n+1} \\ &= p_{n+1} dq_{n+1} - p_n dq_n.\end{aligned}$$

Thus, for mechanical systems, the classes of variational integrators and symplectic integrators are the same ([HLW06]).

At the end of the following section we will see that the discrete Lagrangian inherits the symmetry groups of the continuous system and therefore, the integrator additionally preserves the corresponding momentum maps (or changes them consis-

tently with the applied forces). This is why F_{L_d} is called *structure-preserving* or a *symplectic-momentum integrator* (cf. e.g. [MW01]).

In addition, variational integrators are known to have an excellent long-time energy behavior. This is due to the fact that although they do not preserve the true energy of the system given by the (continuous time) Hamiltonian, at least a so-called *modified Hamiltonian*, which is close to the original Hamiltonian (cf. [HLW06]), is preserved. The approximation order depends on the quadrature rule used to approximate the relevant integrals, e.g. second order using a midpoint rule approximation (cf. e.g. [OJM11]).

2.3 Symmetry

Many mechanical systems show symmetry properties, which we formally introduce in this section. We mainly follow the concept of [MW01]. For a detailed description of symmetries in unforced Lagrangian systems we also refer to [Mar94, MR99, Blo03, MS93, MRS00, Mar93]. An important motivation to study symmetries of mechanical systems is given by symmetry based reduction. The aim of reduction techniques is to give a simplified description of a mechanical system, sometimes even in lower dimensions, which is nonetheless exact, i.e. the original (full-dimensional) description can be reconstructed at any time. Here, we focus on reduction from the Lagrangian point of view. In the simple case of cyclic variables, reduced Euler-Lagrange equations can be derived by *Routh reduction* (cf. Section 2.3.2). This concept is generalized by the *Lagrangian reduction* procedure, described in [MS93, MRS00], for example. *Relative equilibria*, introduced in Section 2.3.3, later play a central role in the motion planning approach presented in Chapter 5.

2.3.1 Invariance of the Lagrangian and Momentum Maps

We consider a mechanical system given by a Lagrangian L on a configuration manifold Q as introduced in the previous section. Assume there exists a *Lie group* G (cf. Definition A.12) which acts on Q by a *left-action* $\Phi : G \times Q \to Q$. For each $g \in G$ we denote by $\Phi_g : Q \to Q$ the diffeomorphism defined by $\Phi_g = \Phi(g, \cdot)$. Let $\Phi^{TQ} : G \times TQ \to TQ$ for $(q, \dot{q}) \in TQ$ be the tangent lift of the action given by

$$\Phi_g^{TQ}(q, \dot{q}) = T(\Phi_g) \cdot (q, \dot{q}) = \left(\Phi^i(g, q), \frac{\partial \Phi^i}{\partial q^j}(g, q) \dot{q}^j \right).$$

The group action Φ is called a *symmetry* of the mechanical system, if the Lagrangian is *invariant* under the group action, i.e. $L \circ \Phi_g^{TQ} = L$ for all $g \in G$. Symmetries of Lagrangian systems lead to the existence of *momentum maps* that

are preserved by the Lagrangian flow or, in other words, are equivariant with respect to the symmetry action (cf. [MW01]).

The Lie algebra (cf. Definition A.15) corresponding to a Lie group G is denoted by $\mathfrak{g}$. For an element $\xi \in \mathfrak{g}$, we define the *infinitesimal generators* (cf. Definition A.18) $\xi_Q : Q \to TQ$ and $\xi_{TQ} : TQ \to T(TQ)$ by

$$\xi_Q(q) = \frac{d}{dg}\left(\Phi_g(q)\right) \cdot \xi, \text{ and } \xi_{TQ}(q,v) = \frac{d}{dg}\left(\Phi_g^{TQ}(q,v)\right) \cdot \xi,$$

respectively. For $t \in \mathbb{R}$, $\exp(t\xi)$ is a t-parametrized curve in G (cf. Definition A.18), and therefore, $\Phi_{\exp(t\xi)} : Q \to Q$ is a flow on Q with corresponding vector field given by ξ_Q, both generated by $\xi \in \mathfrak{g}$. Then, the *Lagrangian momentum map* $J : TQ \to \mathfrak{g}^*$ for a G-invariant Lagrangian L is defined by

$$J(q,v) \cdot \xi = \Theta_L \cdot \xi_{TQ}(q,v)$$

or, equivalently, by

$$\langle J(q,v), \xi \rangle = \langle\langle v, \xi_Q(q) \rangle\rangle = \left\langle \frac{\partial L}{\partial \dot{q}}(q,v), \xi_Q(q) \right\rangle. \tag{2.12}$$

Theorem 2.2 (Noether's Theorem, cf. e.g. [MW01])**:** Let $L : TQ \to \mathbb{R}$ be invariant under the lift of the action $\Phi : G \times Q \to Q$ as defined above, then the corresponding Lagrangian momentum map $J : TQ \to \mathfrak{g}^*$ is a conserved quantity for the flow, i.e. $J \circ F_L^t = J$ for all times t.

In general, arbitrary forcing in a mechanical system would destroy the symmetry of Lagrangian systems since it breaks the conservation of the momentum map. However, as the forced Noether's theorem states, forcing orthogonal to the group action preserves symmetry.

Theorem 2.3 (Forced Noether's Theorem, cf. e.g. [MW01])**:** Let the Lagrangian L and the symmetry action Φ be as in Theorem 2.2. Consider a force $f_L : TQ \times U \to T^*Q$ such that $\langle f_L(q,\dot{q},u), \xi_Q(q) \rangle = 0$ for all $(q,\dot{q}) \in TQ$, $u \in U$ and all $\xi \in \mathfrak{g}$. Then the Lagrangian momentum map $J : TQ \to \mathfrak{g}^*$ is preserved by the forced Lagrangian flow, i.e. $J \circ (F_L^u)^t = J$ for all t.

Since G leaves the set of solutions of the variational principle invariant, the group action commutes with the Lagrangian flow [MPS98]. In case of forced mechanical systems, we make use (in particular in Chapter 5) of the following definition of equivalent solutions of the corresponding forced Euler-Lagrange equations.

Definition 2.4 (Equivalence of Trajectories)**:** Let $\pi_1 : t \in [t_{i,1}, t_{f,1}] \mapsto (q_1(t), \dot{q}_1(t), u_1(t))$ and $\pi_2 : t \in [t_{i,2}, t_{f,2}] \mapsto (q_2(t), \dot{q}_2(t), u_2(t))$ be two solution trajectories of the forced Euler-Lagrange equations (2.9)[2]. Then, π_1 and π_2 are called equivalent, if it holds that

(i) $t_{f,1} - t_{i,1} = t_{f,2} - t_{i,2}$,

(ii) and there exist a group element $g \in G$ and a time shift parameter $\bar{t} \in \mathbb{R}$, such that

$$(q_1, \dot{q}_1)(t) = \Phi_g^{TQ}((q_2, \dot{q}_2)(t - \bar{t})), \text{ and } u_1(t) = u_2(t - \bar{t}) \quad \forall\, t \in [t_{i,1}, t_{f,1}].$$

Example 2.5 (Kepler Problem)**:** The Kepler problem is a two body system for which we describe the motion of a (small) point mass m relative to the gravitational field of a second (larger) point mass M. In polar coordinates, i.e. we choose $q = (r, \theta)$ as coordinates of the configuration manifold $Q = \mathbb{R} \times S^1$, for $r \neq 0$, the Lagrangian is given by

$$L(r, \theta, \dot{r}, \dot{\theta}) = \frac{1}{2} m(\dot{r}^2 + r^2\dot{\theta}^2) + \gamma \frac{Mm}{r}.$$

The system has a rotational symmetry, so $G = S^1$ with $\Phi_g(r, \theta) = (r, \theta + g)$. Thus, the tangent lift equals $\Phi_g^{TQ}(r, \theta, \dot{r}, \dot{\theta}) = (r, \theta + g, \dot{r}, \dot{\theta})$. Since the Lagrangian is independent of θ, which is the only coordinate that is affected by the symmetry action, the identity $L \circ \Phi^{TQ} = L$ obviously holds. The infinitesimal generator for $\xi \in \mathfrak{g}$ is $\xi_Q(r, \theta) = \frac{d}{dg}(\Phi_g(q)) \cdot \xi = (0, \xi)$ with $\xi \in \mathbb{R}$. Therefore, the momentum map is given by

$$J(r, \theta, \dot{r}, \dot{\theta}) = \frac{\partial L}{\partial \dot{\theta}}(r, \theta, \dot{r}, \dot{\theta}) = mr^2\dot{\theta}.$$

In Figure 2.2, examples of equivalent trajectories are shown. The momentum is constant for all solutions, in other words, it is invariant of the flow. Since not only the Lagrangian and therefore the energy is invariant of θ, but the momentum J as well, the equivariance of the momentum map w.r.t. the symmetry action simply reads $J = J \circ \Phi_g^{TQ}$.

As a second example we consider the spherical pendulum. This system is a popular example to study symmetries of a mechanical system (see, among others, [Mar93, AM87, BL04]). In this thesis, it will be revisited several times and

[2]For simplicity, we normally consider the path space and hence solutions of the Euler-Lagrange equations on the time interval $[0, T] \subset \mathbb{R}$, $T \in \mathbb{R}_0^+$. A more general notation with arbitrary starting point, e.g. $[t_i, t_f] \subset \mathbb{R}, 0 \leq t_i \leq t_f \in \mathbb{R}$, is straight forward though, since we restrict to autonomous Lagrangian.

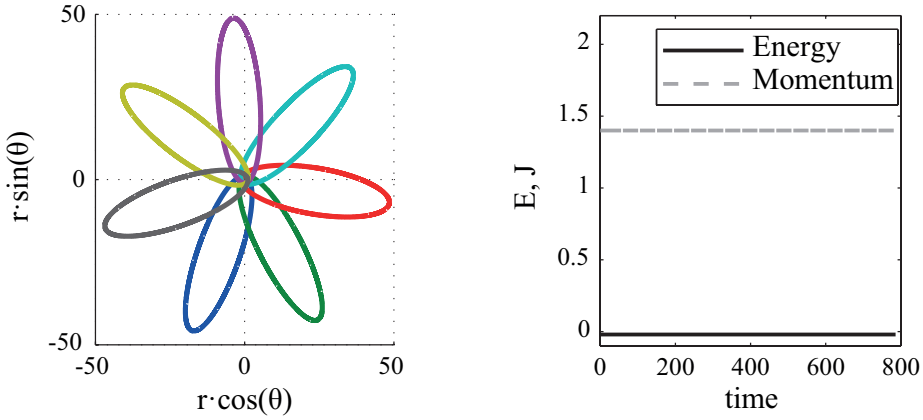

Figure 2.2: Examples of equivalent trajectories of the symmetric Kepler problem (all parameters set to 1.0). The blue elliptic curve (with initial value $(q_0, \dot{q}_0) = (1.0, 1.2, 0.0, 1.4)$) can be rotated by elements $g \in G$ to match the other trajectories. All solutions have a constant energy of $E = -0.02$ and a constant momentum of $J = 1.4$.

used to demonstrate the motion planning approach (cf. Chapter 5). From the application point of view, industrial robots can be idealized as spherical pendula: a double spherical pendulum is a simplified two-link manipulator, for instance. Therefore, the optimal control of spherical pendulua is of high interest.

Example 2.6 (Spherical Pendulum)**:** The single spherical pendulum consists of a point mass with mass m that is connected by a massless rod of length r to a spherical joint on the ground. Thus, the configuration space of this two degree of freedom system is a sphere, $Q = S^2$. In coordinates, it can be described by a vertical angle, denoted by φ and a horizontal angle, denoted by θ (cf. Figure 2.3). The Lagrangian is given by

$$\begin{aligned} L(\varphi, \dot{\theta}, \dot{\varphi}) &= K(\varphi, \dot{\theta}, \dot{\varphi}) - V(\varphi) \\ &= \frac{1}{2} mr^2(\dot{\varphi}^2 + \dot{\theta}^2 \sin^2(\varphi)) - mgr(\cos(\varphi) + 1), \end{aligned}$$

where we have some freedom in choosing the zero level of the potential. Here, again, we have a cyclic coordinate, since L is independent of the horizontal angle θ. Thus, it follows directly from $\frac{\partial L}{\partial \theta} = 0$ that the corresponding Euler-Lagrange equation simplifies to $\frac{\partial L}{\partial \dot{\theta}} = \text{const}$. In other words, the system is symmetric w.r.t. rotations about the vertical axis and the symmetry group is $G = S^1$, acting by addition only in the horizontal coordinate, $\Phi_g(\theta, \varphi) = (\theta + g, \varphi)$ and $\Phi^{TQ}(\theta, \varphi, \dot{\theta}, \dot{\varphi}) = (\theta +$

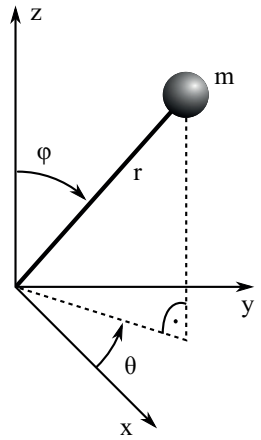

Figure 2.3: The spherical pendulum.

$g, \varphi, \dot{\theta}, \dot{\varphi}$). For the infinitesimal generator, we receive $\xi_Q(\theta, \varphi) = (\xi, 0)$. Therefore, the momentum map is

$$J(\theta, \varphi, \dot{\theta}, \dot{\varphi}) = p_\theta = mr^2 \sin^2(\varphi)\dot{\theta}.$$

For now, we finish the example with the Euler-Lagrange equations

$$\begin{aligned} \ddot{\theta} &= -2\frac{\cos(\varphi)}{\sin(\varphi)}\dot{\varphi}\,\dot{\theta} \\ \ddot{\varphi} &= \sin(\varphi)\cos(\varphi)\,\dot{\theta}^2 + \frac{g}{r}\sin(\varphi). \end{aligned}$$

This formulation is not valid for $\sin(\varphi) = 0$, though. A vertical angle of 0 or π (or multiplicities) corresponds to the pendulum's upper and lower fixed points, where the horizontal angle looses its meaning.

The special structure of the symmetries in the preceding examples can be used for reducing the system's equations of motion by the so-called Routh reduction.

2.3.2 Routh Reduction

The idea of Routh reduction is the classical reduction procedure for Abelian symmetry groups and is going back to the 19th century. We give a short description based on [MR99] and [Blo03], before we introduce the generalization of the method, the Lagrangian reduction as introduced by Marsden and Scheurle [MS93].

Here, we assume that the configuration space can be split into copies of the circle S^1 and the so-called shape space S, i.e. $Q = S \times (S^1 \times \ldots \times S^1)$. The S^1 copies belong to rotational symmetries, since Routh developed this method when studying rotating mechanical systems. However, they can be replaced by $\mathbb{R}$ with little change to account for translational symmetries, as well. To clearly distinguish the configuration space, in this section coordinates of S are denoted by $x^1, \ldots, x^m$, and for the number of copies of S^1 (say we have k factors) we introduce the coordinates $\theta^1, \ldots, \theta^k$. Assume now, that $G = S^1 \times \ldots \times S^1$ is a symmetry for the mechanical system on Q. Equivalently, it can be required that the Lagrangian is independent of $\theta^1, \ldots, \theta^k$. Then, these variables are called *cyclic*. It directly follows from the Euler-Lagrange equations for the cyclic variable that the corresponding momenta

$$p_i = \frac{\partial L}{\partial \dot{\theta}^i}$$

are conserved quantities. In other words (cf. Section 2.3.1), this defines k Lagrangian momentum maps.

Definition 2.7 (Classical Routhian, [MR99])**:** The classical Routhian is defined by setting $p_i = \mu_i = \text{const.}$ and performing a partial Legendre transformation in the variables θ^i:

$$R^\mu(x, \dot{x}) = \left[L(x, \dot{x}, \dot{\theta}) - \mu_i \dot{\theta}^i \right]_{p_i = \mu_i}, \tag{2.13}$$

where it is understood that the variable $\dot{\theta}^i$ is eliminated using the equation $p_i = \mu_i$ and μ_i is regarded as a constant.

Note that the momentum p_i depends on $\dot{\theta}^i$, in particular. The Routhian can be used to reduce the Euler-Lagrange equations from the former configuration manifold Q to the shape space S.

Proposition 2.8: The Euler-Lagrange equations for the shape space coordinates $\frac{d}{dt}\frac{\partial L}{\partial \dot{x}^i} - \frac{\partial L}{\partial x^i} = 0$, with $L(x, \dot{x}, \dot{\theta})$ together with the conservation laws $p_i = \mu_i$ are equivalent to the Euler-Lagrange equations for the Routhian $R^\mu(x, \dot{x})$ together with $p_i = \mu_i$.

Proof. The Euler-Lagrange equations with R^μ replacing the Lagrangian are

$$\frac{d}{dt}\frac{\partial R^\mu}{\partial \dot{x}^j} - \frac{\partial R^\mu}{\partial x^j} = \frac{d}{dt}\left(\frac{\partial L}{\partial \dot{x}^j} + \frac{\partial L}{\partial \dot{\theta}^i} \cdot \frac{\partial \dot{\theta}^i}{\partial \dot{x}^j} - \mu_i \cdot \frac{\partial \dot{\theta}^i}{\partial \dot{x}^j} \right) - \frac{\partial L}{\partial x^j} - \frac{\partial L}{\partial \dot{\theta}^i}\frac{\partial \dot{\theta}^i}{\partial x^j} + \mu_i \frac{\partial \dot{\theta}^i}{\partial x^j}$$

$$= \frac{d}{dt}\frac{\partial L}{\partial \dot{x}^j} - \frac{\partial L}{\partial x^j} + \frac{d}{dt}\left(\left(\frac{\partial L}{\partial \dot{\theta}^i} - \mu_i\right)\cdot\frac{\partial \dot{\theta}^i}{\partial \dot{x}^j}\right) - \left(\frac{\partial L}{\partial \dot{\theta}^i} - \mu_i\right)\cdot\frac{\partial \dot{\theta}^i}{\partial x^j}$$

and with $\mu_i = p_i = \frac{\partial L}{\partial \dot{\theta}^i}$ the third and fourth term vanish (cf. [Blo03]). □

The Euler-Lagrange equations for R^μ are therefore called the *reduced Euler-Lagrange equations*. They can be used to identify so-called *steady motions* of the system, i.e. uniform rotations about a fixed axis (cf. [MR99]), which correspond to equilibria of the reduced Euler-Lagrange equations. More generally, these symmetry induced motions are called *relative equilibria*, which we formally introduce in Section 2.3.3.

Example 2.9 (Kepler Problem)**:** Recall from Example 2.5 that the Kepler problem has rotational symmetry and the corresponding momentum map is $J = mr^2\dot{\theta}$. We have already seen that the Lagrangian is independent of θ, so this is a cyclic variable. Hence, the Routhian is given by

$$R^\mu(r, \dot{r}) = \frac{1}{2}m\dot{r}^2 - \frac{1}{2}\frac{\mu^2}{mr^2} + \gamma\frac{Mm}{r},$$

where we replace the cyclic coordinate's velocity by $\dot{\theta} = \frac{\mu}{mr^2}$. Then, the Euler-Lagrange equation for the Routhian is given by

$$m\ddot{r} = \frac{\mu^2}{m\cdot r^3} - \gamma\frac{Mm}{r^2} \qquad \text{with} \qquad \mu = mr^2\dot{\theta}$$

and can be shown to be equivalent to the original Euler-Lagrange equations

$$\ddot{r} = r\dot{\theta}^2 - \gamma\frac{M}{r^2}, \qquad \ddot{\theta} = -2\frac{\dot{r}\dot{\theta}}{r}.$$

There exist no equilibria of the original system. Fixed points of the reduced Euler-Lagrange equations have to fulfill $r = \frac{\mu^2}{\gamma M m^2}$, so by changing μ (assuming positive parameters), fixed points for every $r > 0$ can be found. Substituting $\dot{\theta}$ back into this fixed point condition, we get

$$\dot{\theta}^2 = \gamma\frac{M}{r^3}. \tag{2.14}$$

Any initial condition $q_0 = (r_0, \theta_0, 0, \dot{\theta}_0)$ that satisfies this equation leads to a trajectory which is a perfect circle with constant rotational velocity. These are the relative equilibria of the Kepler problem. In other words, any curve of the form $q(t) = (r_0, \theta_0 + \xi\cdot t, 0, \xi)$ where r_0 and ξ satisfy Equation (2.14) with $\xi = \dot{\theta}_0$ is a

solution of the Euler-Lagrange equations (θ_0 arbitrary). Note that $\xi \in \mathbb{R}$, the rotational velocity, is the Lie algebra element which generates the relative equilibrium's trajectory. $q(t)$ for $t \in [0, T]$ can be also interpreted as (part of) the group orbit $\mathrm{Orb}(q, \dot{q})$ since $\xi \cdot t$ is (part of) a one-parameter subgroup of $\mathbb{R}$.

Example 2.10 (Spherical Pendulum)**:** The Routhian for the spherical pendulum with $\mu = p_\theta$ (to eliminate $\dot{\theta}$) is

$$R^\mu(\varphi, \dot{\varphi}) = \frac{1}{2} m r^2 \dot{\varphi}^2 - \frac{1}{2} \frac{\mu^2}{m r^2 \sin^2(\varphi)} - mgr(\cos(\varphi) + 1).$$

Thus, the reduced Euler-Lagrange equation is

$$m r^2 \ddot{\varphi} = \frac{\mu^2 \cos(\varphi)}{m r^2 \sin^3(\varphi)} + mgr \sin(\varphi) \quad \text{with } \mu = m r^2 \sin^2(\varphi) \dot{\theta}.$$

The highest and the lowest pendulum positions induce that $\mu = 0$. They are still fixed points of the reduced system (although this cannot be directly seen in the formulation of the differential equation above). If $\mu = 0$ holds with φ not equal to $n\pi$, $n \in \mathbb{Z}$, we conclude that the horizontal rotational velocity $\dot{\theta}$ has to equal zero. In this case, the reduced equations of the spherical pendulum simplify to the equations of motion of a planar pendulum.

Fixed points of the reduced equation that belong to relative equilibria of the original system have to satisfy

$$\dot{\theta}^2 = -\frac{g}{r \cos(\varphi)}.$$

Solutions exist for vertical angles in the lower hemisphere. Since $\dot{\varphi} = 0$, the relative equilibria are purely horizontal rotations with constant rotational velocity $\dot{\theta}$ according to the height defined by the value of φ (cf. Figure 2.4).

2.3.3 Lagrangian Reduction and Relative Equilibria

The Lagrangian reduction method (cf. e.g. [MS93] or [Mar93]) is a generalization of the classical Routh reduction for cyclic variables to non-Abelian symmetry groups.

Consider again a Lagrangian system defined by L on a configuration manifold Q with symmetry group G. We assume that G acts freely on Q (Definition A.17) such that $Q \to Q/G$ is a principle G-bundle (Definition A.20). For each $q \in Q$ the *locked inertia tensor* $\mathbb{I}(q) : \mathfrak{g} \to \mathfrak{g}^*$ is defined by

$$\langle \mathbb{I}(q)\eta, \zeta \rangle = \langle\langle \eta_Q(q), \zeta_Q(q) \rangle\rangle$$

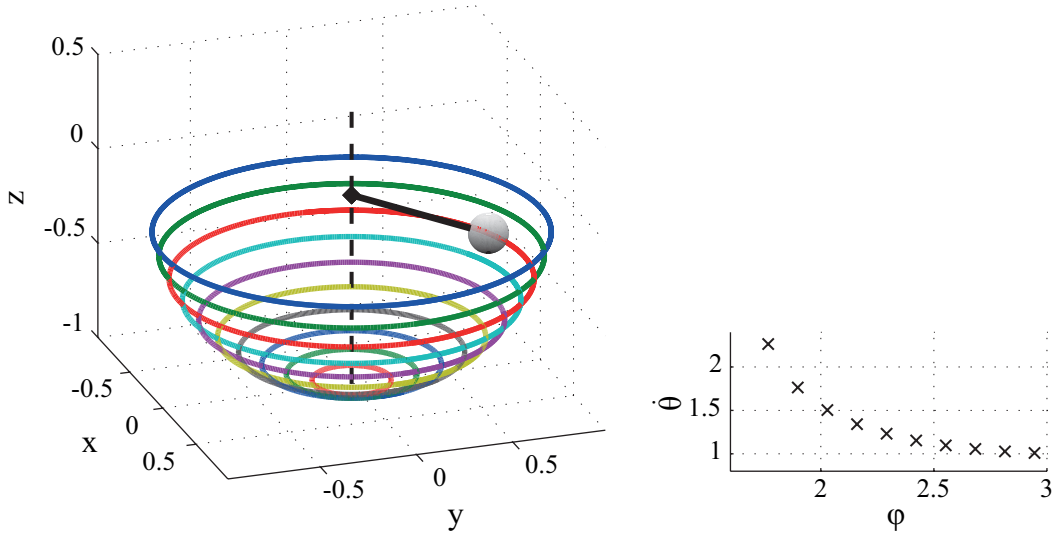

Figure 2.4: Relative equilibria of the spherical pendulum: horizontal rotations with constant rotational velocity $\dot{\theta}$ that depend on the height of the orbit defined by φ.

with η_Q, ζ_Q being the infinitesimal generators to $\eta, \zeta \in \mathfrak{g}$. It can be interpreted as the inertia tensor of a system which moves only in the direction of the infinitesimal generators of the symmetry action, such as e.g. a multibody system that has been locked to a rigid structure. The corresponding angular velocity, a map $\alpha : TQ \to \mathfrak{g}$, is then given by

$$\alpha(q, v) = \mathbb{I}(q)^{-1}(J(q, v)),$$

and is called the *mechanical connection* (cf. Definition A.21). Here, $J(q, v)$ is the momentum map induced by the symmetry group's action (cf. Equation (2.12)). For each $\mu \in \mathfrak{g}^*$, it leads to the definition of an one-form on Q, denoted by α_μ and defined by $\langle \alpha_\mu(q), v \rangle = \langle \mu, \alpha(q, v) \rangle$. The *amended potential*, which plays an important role in the reduction process, is defined by

$$V_\mu(q) = V(q) + \frac{1}{2}\langle \mu, \mathbb{I}(q)^{-1}\mu \rangle. \tag{2.15}$$

For a given value $\mu \in \mathfrak{g}^*$, the Routhian $R^\mu : TQ \to \mathbb{R}$ is defined as

$$R^\mu(q, v) = L(q, v) - \langle \alpha(q, v), \mu \rangle. \tag{2.16}$$

By fixing the level set of the momentum map to μ, i.e. $J(q, \dot{q}) = \mu$, it can be shown that the original Euler-Lagrange equations are equivalent to the Euler-Lagrange

equations of the Routhian R^μ with an additional gyroscopic forcing term reading

$$\frac{d}{dt}\frac{\partial R^\mu}{\partial \dot{q}} - \frac{\partial R^\mu}{\partial q} = \dot{q}^T \beta, \tag{2.17}$$

cf. [MS93] for the variational derivation via the Lagrange-d'Alembert principle. β is the *magnetic two form* on Q, $\beta(q) : T_qQ \times T_qQ \to \mathbb{R}$, defined by $\beta = \mathbf{d}\alpha_\mu$, i.e. in coordinates, $\beta_{ij} = \frac{\partial \alpha_j}{\partial q^i} - \frac{\partial \alpha_i}{\partial q^j}$. (The one form α_μ is given in coordinates by $\alpha_\mu = \alpha_i \, dq^i$ with dq^i being the basis vectors for T_q^*Q.)

Proposition 2.11: A curve $q(t)$ in Q is a solution of the Euler-Lagrange equations (2.7) for the Lagrangian L with $J(q, \dot{q}) = \mu$, if and only if it is a solution of the Euler-Lagrange equations for the Routhian R^μ with gyroscopic forcing given by β (see Equation (2.17)).

Proof. Confer [MS93] for a proof, which resembles the one of Proposition 2.8. Note however that in contrast to the classical Routhian, which only depends on the shape space coordinates (cf. Equation (2.13)), the new, generalized Routhian is still defined on the entire tangent bundle TQ. □

The mechanical connection α defines a splitting of tangent vectors of TQ in the following way: the corresponding horizontal space is given by

$$\mathrm{hor}_q = \{(q, v) | J(q, v) = 0\},$$

that is the space orthogonal to the G-orbits. The vertical space consists of vectors that are mapped to zero under the projection $Q \to Q/G$, i.e.

$$\mathrm{ver}_q = \{\xi_Q(q) | \xi \in \mathfrak{g}\}.$$

It can be verified (e.g. by using the coordinate expressions) that $\alpha(\xi_Q(q)) = \xi$ and thus, the corresponding one form α_μ takes values in $J^{-1}(\mu)$. Each vector $(q, v) \in T_qQ$ can be decomposed into its horizontal and its vertical part by

$$v = \mathrm{hor}_q v + \mathrm{ver}_q v,$$

where $\mathrm{ver}_q v = [\alpha(q, v)]_Q(q)$ and $\mathrm{hor}_q v = v - \mathrm{ver}_q v$.

Using this splitting of tangent vectors, the Routhian can be enlarged in a way that becomes suitable when we later constrain to level sets of J.

Proposition 2.12: For all $(q, v) \in TQ$ and $\mu \in \mathfrak{g}$, we can write

$$R^\mu = \frac{1}{2}\|\mathrm{hor}(q,v)\|^2 + \langle J(q,v) - \mu, \xi\rangle - (V + \frac{1}{2}\langle \mathbb{I}(q)\xi, \xi\rangle) \tag{2.18}$$

where $\xi = \alpha(q, v)$. If R^μ is restricted to the level sets of J, i.e. $J(q, v) = \mu$, the above expression simplifies to

$$R^\mu = \frac{1}{2}\|\mathrm{hor}(q,v)\|^2 - V_\mu.$$

Proof. The second formula for the restricted R^μ directly follows from the first expression with $J(q, v) = \mu$ and the definition of the amended potential, cf. Equation (2.15).

To relate Equation (2.18) to the definition of R^μ (cf. Equation (2.17)), one can compute

$$R^\mu = \frac{1}{2}\|v\|_q^2 - \langle\langle v, \xi_Q(q)\rangle\rangle + \frac{1}{2}\|\xi_Q(q)\|_q^2 + \langle J(q,v), \xi\rangle - \langle \mu, \xi\rangle - V - \frac{1}{2}\langle \mathbb{I}(q)\xi, \xi\rangle.$$

Here, the relation $\mathrm{hor}(q, v) = v - \xi_Q(q, v)$ can be used because the value of the connection is set to ξ. Then, by definition of the locked inertia tensor we can use $\|\xi_Q(q)\|_q^2 = \langle\langle \xi_Q(q), \xi_Q(q)\rangle\rangle = \langle \mathbb{I}(q)\xi, \xi\rangle$ and from the definition of the momentum map, we know $\langle J(q, v), \xi\rangle = \langle\langle v, \xi_Q(q)\rangle\rangle$. Thus, the second term cancels with the fourth and the third term with the last one. The remaining terms are equal to the definition of the Routhian, i.e. $R^\mu = L(q, v) - \langle \alpha(q, v), \mu\rangle = \frac{1}{2}\|v\|_q^2 - V(q) - \langle \alpha(q, v), \mu\rangle$.

□

The reduced Routhian (in contrast to the one previously defined in Proposition 2.11) is the analogue of the classical Routhian and in case of cyclic variables both are equivalent. In [MS93] and more detailed in [MRS00] the corresponding reduced variational principle is derived.

In the previous section a *relative equilibrium* has been introduced to be a dynamic state (q_e, v_e) that is also an one parameter group orbit of the symmetry group and therefore has been a fixed point of the Routh reduced Euler-Lagrange equations. More general, relative equilibria can be defined as follows.

Definition 2.13 (Relative Equilibrium)**:** A point $x_e = (q_e, v_e) \in TQ$ is called a relative equilibrium, if $X_L(x_e) \in T_{x_e}(G \cdot x_e)$, i.e. the Lagrangian vector field X_L at x_e points in the direction of the group orbit $G \cdot x_e = \{x = (q, v) | (q, v) = \Phi_g^{TQ}(q_e, v_e)$ for $g \in G\}$.

A helpful characterization of relative equilibria is given by the following propo-

sition (see [Mar93] for various alternative characterizations of relative equilibria, mostly based on the Hamiltonian).

Proposition 2.14 (cf. [MS93])**:** A point $x_e = (q_e, v_e) \in TQ$ is a relative equilibrium if and only if q_e is a critical point of the amended potential V_μ with $\mu = J(q_e, v_e)$.

Example 2.15 (Spherical Pendulum)**:** For the spherical pendulum, the Lagrangian reduction simplifies to the Routh reduction, i.e., in particular, it leads to the same conditions for relative equilibria as deduced in Example 2.10. The amended potential is given by $V_\mu(q) = V(q) + \frac{1}{2}\langle \mu, \mathbb{I}^{-1}\mu \rangle = mgr(\cos(\varphi)+1) + \frac{1}{2}\mu^2(mr^2\sin^2(\varphi))^{-1}$ with $\mathbb{I}(\theta,\varphi) = mr^2\sin^2(\varphi)$, so the connection equals $\alpha(\theta,\varphi,\dot\theta,\dot\varphi) = \dot\theta$. Therefore, the splitting of velocity vectors is simply the decomposition into the vertical part of the velocity, $\mathrm{hor}_q(\dot\theta,\dot\varphi) = (0,\dot\varphi)$, and the horizontal part $\mathrm{ver}_q(\dot\theta,\dot\varphi) = (\dot\theta, 0)$. The critical points of the amended potential, i.e. the relative equilibria of the original system require again $\dot\theta^2 = -\frac{g}{r\cos(\varphi)}$, leading to purely horizontal rotations with constant velocities.

Example 2.16 (Double Spherical Pendulum)**:** The configuration space of two 3D pendula – idealized as mass points m_1 and m_2 on massless rods – is $Q = S^2_{l_1} \times S^2_{l_2}$, where $S^2_{l_1}$, $S^2_{l_2}$ denote the two dimensional spheres of radius l_1, l_2. As a minimal set of coordinates, we choose horizontal and vertical angles ($q = (\theta_1, \theta_2, \varphi_1, \varphi_2)$), such that the mass points' positions are given by (cf. Figure 2.5)

$$q_1 = \begin{pmatrix} x_1 \\ y_1 \\ z_1 \end{pmatrix} = \begin{pmatrix} l_1\cos(\theta_1)\sin(\varphi_1) \\ l_1\sin(\theta_1)\sin(\varphi_1) \\ l_1\cos(\varphi_1) \end{pmatrix}, \quad q_2 = \begin{pmatrix} x_2 \\ y_2 \\ z_2 \end{pmatrix} = \begin{pmatrix} x_1 \\ y_1 \\ z_1 \end{pmatrix} + \begin{pmatrix} l_2\cos(\theta_2)\sin(\varphi_2) \\ l_2\sin(\theta_2)\sin(\varphi_2) \\ l_2\cos(\varphi_2) \end{pmatrix}.$$

The following computations could alternatively be performed only in terms of q_1, q_2 without substituting the coordinates until in the end as it has been done in [MS93]. However, note that we take a different set of coordinates than in [MS93], motivated by the previously considered simple spherical pendulum.

The Lagrangian as the difference of kinetic and potential energy can be written as: $L(q(t), \dot q(t)) = K(q(t), \dot q(t)) - V(q(t))$, where the potential is

$$V(q(t)) = (m_1 + m_2)gl_1(\cos(\varphi_1)+1) + m_2 g l_2(\cos(\varphi_2)+1),$$

and $K(q(t), \dot q(t)) = \frac{1}{2}\dot q^T(t) M(q(t)) \dot q(t)$ with the symmetric mass matrix

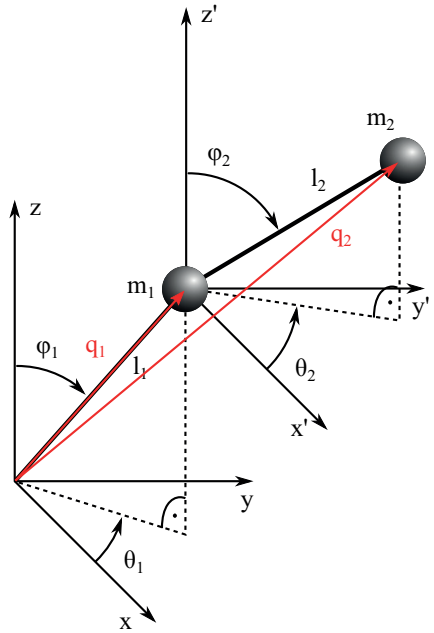

Figure 2.5: The double spherical pendulum.

$$M = M^T = \left(\begin{array}{c|c|c|c} (m_1+m_2)l_1^2 \cdot \sin^2(\varphi_1) & m_2 l_1 l_2 \cdot \cos(\theta_1-\theta_2) \cdot \sin(\varphi_1)\sin(\varphi_2) & 0 & -m_2 l_1 l_2 \sin(\theta_1-\theta_2) \cdot \sin(\varphi_1)\cos(\varphi_2) \\ \hline * & m_2 l_2^2 \sin^2(\varphi_2) & m_2 l_1 l_2 \cdot \sin(\theta_1-\theta_2) \cdot \cos(\varphi_1)\sin(\varphi_2) & 0 \\ \hline 0 & * & (m_1+m_2)l_1^2 & m_2 l_1 l_2((\cos(\theta_1-\theta_2) \cdot \cos(\varphi_1)\cos(\varphi_2)) + \sin(\varphi_1)\sin(\varphi_2)) \\ \hline * & 0 & * & m_2 l_2^2 \end{array}\right).$$

As for the simple spherical pendulum, the symmetry group is $G = S_1$, acting by rotation of both pendula about the z-axis:

$$\Phi : G \times Q \to Q,\ \Phi(g,(\theta_1,\theta_2,\varphi_1,\varphi_2)) = (g+\theta_1, g+\theta_2, \varphi_1, \varphi_2)$$

with tangent lift to TQ by $\Phi_g^{TQ}(q,\dot{q}) = (\Phi_g(q), \dot{\theta}_1, \dot{\theta}_2, \dot{\varphi}_1, \dot{\varphi}_2)$. We note that $V(q)$ is independent of θ_1, θ_2 so in particular invariant w.r.t. Φ_g. Then, the infinitesimal

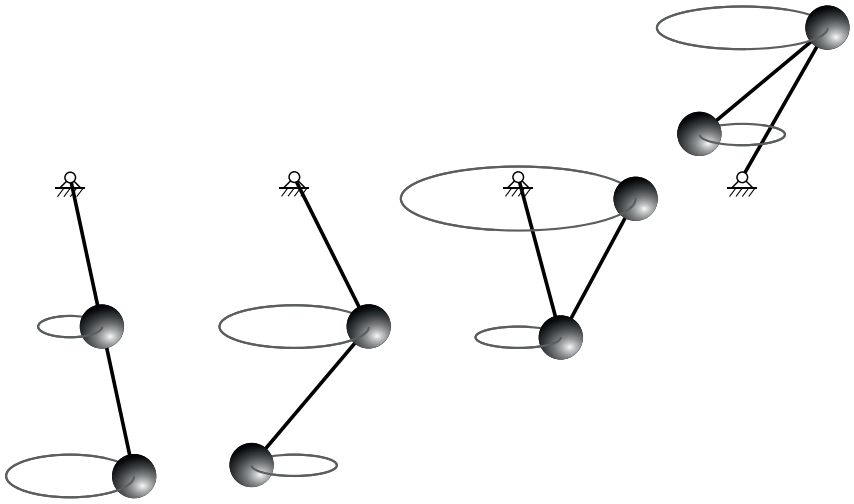

Figure 2.6: Shapes of the relative equilibria of the double spherical pendulum.

generator can be determined to be $\xi_Q(q) = (\xi, \xi, 0, 0)^T$ with $\xi \in \mathbb{R}$. Hence, the conserved quantity is the total angular momentum about the z-axis

$$\begin{aligned} J_{\theta_1\theta_2}(q,\dot{q}) =& \frac{\partial L}{\partial \dot{\theta}_1} + \frac{\partial L}{\partial \dot{\theta}_2} \\ =& \left((m_1+m_2)l_1^2 \cdot \sin^2(\varphi_1) + m_2 l_1 l_2 \cdot \cos(\theta_1-\theta_2)\cdot \sin(\varphi_1)\sin(\varphi_2)\right)\dot{\theta}_1 \\ &+ \left(m_2 l_1 l_2 \cdot \cos(\theta_1-\theta_2)\cdot \sin(\varphi_1)\sin(\varphi_2) + m_2 l_2^2 \sin^2(\varphi_2)\right)\dot{\theta}_2 \\ &+ \left(m_2 l_1 l_2 \cdot \sin(\theta_1-\theta_2)\cdot \cos(\varphi_1)\sin(\varphi_2)\right)\dot{\varphi}_1 \\ &- \left(m_2 l_1 l_2 \sin(\theta_1-\theta_2)\cdot \sin(\varphi_1)\cos(\varphi_2)\right)\dot{\varphi}_2, \end{aligned} \tag{2.19}$$

and the locked inertia tensor equals (compare this to the upper left 2×2 block of M)

$$\mathbb{I} = (m_1+m_2)l_1^2 \sin^2(\varphi_1) + m_2 l_2^2 \sin^2(\varphi_2) + 2m_2 l_1 l_2 \cos(\theta_1-\theta_2)\cdot \sin(\varphi_1)\sin(\varphi_2).$$

The mechanical connection $\alpha : TQ \to \mathfrak{g}$ can be computed by $\alpha(q,v) = \mathbb{I}^{-1}(q)\cdot J(q,v)$, assigning to each (q,v) the angular velocity of the locked system. Then, the amended potential with $\mu = J(q,\dot{q})$ is

$$V_\mu(q) = V(q) + \frac{\mu^2}{2\mathbb{I}(q)}.$$

Relative equilibria are classified in [MS93] in an elegant way by introducing two

shape defining parameters and then computing the critical points of the amended potential. Besides the four true equilibria (each pendulum either pointing straight upwards or downwards), all relative equilibria are given by a one parameter curve and they look similar to one of the four sketched types in Figure 2.6.

2.3.4 Relation to Other Symmetry Reduction Methods

The previous sections present only a very small part of the huge amount of research on symmetry and symmetry reduction in mechanical systems. For completeness, we shortly discuss alternative methods and relate them to the previously introduced approaches. This summary is mainly based on the thorough overview given in [MRS00].

Mechanical systems on Lie groups can be either described by a Lagrangian $L : TG \to \mathbb{R}$ or a Hamiltonian $H : T^*G \to \mathbb{R}$ (note that in this case, the entire state space is a Lie group). If the Lagrangian is invariant w.r.t. G, reduced equations of motion, *Euler-Poincaré equations*, can be derived for the reduced Lagrangian $l : \mathfrak{g} \to \mathbb{R}$. Analogously, an invariant Hamiltonian can be reduced to $h : \mathfrak{g}^* \to \mathbb{R}$ by *Lie-Poisson reduction*.

In a *reduction by stages* procedure, the idea of the Lie-Poisson reduction can be transferred to G-invariant Hamiltonian systems on $T^*G \times V^*$ with V being a vector space. The Lagrangian counterpart of this semidirect product theory generalizes the Euler-Poincaré reduction procedure to (left) G-invariant Lagrangian $L : TG \times V^* \to \mathbb{R}$. This leads to a special case of *Lagrange-Poincaré equations* (also called *reduced Euler-Lagrange equations*) for $l : (TQ)/G \to \mathbb{R}$.

In the general case of a symplectic manifold P, for a *symplectic reduction* the value μ of the equivariant momentum map $J : P \to \mathfrak{g}^*$ is fixed such that the reduced space is $J^{-1}(\mu)/G_\mu$, again a symplectic manifold. (Here, G_μ is the isotropy subgroup for the coadjoint action of G, $G_\mu = \{g \in G \mid Ad^*_g \mu = \mu\}$.)

The *Lagrangian reduction*, which we studied in detail in the previous section, is the Lagrangian counterpart of symplectic reduction. Historically, it extends the classical Routh reduction procedure to non-Abelian groups. Furthermore, in the classical Routh procedure it is typically assumed that the state space Q is globally a product $S \times G$ of shape space and Lie group. This means, the bundle $Q \to Q/R$ is a trivial bundle, which is not the case in general systems to which Lagrangian reduction can be applied. As already mentioned, Lagrangian reduction is based on reducing the variational principle. In contrast to the Lagrange-Poincaré procedure, the momentum map constraint $J = \mu$ is imposed as in symplectic reduction. In [MRS00] it is then shown that $J^{-1}(\mu)/G_\mu$ can be identified (via a global bundle isomorphism) with $T(Q/G) \times_{Q/G} Q/G_\mu$ and how the variational principle can be reduced to that space finally leading to reduced *Lagrange-Routh* equations.

2.3.5 Symmetry in Discrete Mechanics

Finally, a short introduction into symmetry of discrete mechanics is given. A discrete Lagrangian map inherits symplecticity from the continuous Lagrangian flow (see e.g. [MW01]) and there also exists a discrete analogue of Noether's theorem. As anticipated in Section 2.2.2, this is the reason why the mechanical integrators that we constructed above are symplectic-momentum conserving. In the following chapters, we will introduce and apply an optimal control method that is based on variational integrators and by that it implicitly makes use of the consistency of the symmetry induced momenta. However, the explicit exploitation of symmetry properties in mechanical systems (i.e. the identification of trim primitives, cf. Chapter 5) will be done in the previously introduced continuous time setting.

The left action $\Phi : G \times Q \to Q$ for a Lie group on Q is lifted to $Q \times Q$ (recall that this is the discretization of TQ) by

$$\Phi_g^{Q\times Q}(q_k, q_{k+1}) = (\Phi_g(q_k), \Phi_g(q_{k+1}))$$

leading to an infinitesimal generator $\xi_{Q\times Q} : Q \times Q \to T(Q \times Q)$ given by

$$\xi_{Q\times Q}(q_k, q_{k+1}) = (\xi_Q(q_k), \xi_Q(q_{k+1})).$$

The two discrete Lagrangian momentum maps can be written as

$$\begin{aligned} J^+_{L_d}(q_k, q_{k+1}) \cdot \xi &= \langle D_2 L_d(q_k, q_{k+1}), \xi_Q(q_{k+1})\rangle, \text{ and} \\ J^-_{L_d}(q_k, q_{k+1}) \cdot \xi &= \langle -D_1 L_d(q_k, q_{k+1}), \xi_Q(q_k)\rangle. \end{aligned}$$

If for a discrete Lagrangian $L_d : Q \times Q$, it holds $L_d \circ \Phi_g^{Q\times Q} = L_d$ for all $g \in G$, then L_d is invariant under the lifted action and Φ is called a symmetry of L_d. It follows that the two discrete momentum maps are equal and the unique single discrete Lagrangian momentum map is than denoted by $J_{L_d} : Q \times Q \to \mathfrak{g}^*$. Another consequence is that J_{L_d} is equivariant.

Theorem 2.17 (Discrete Noether's Theorem)**:** Consider a discrete Lagrangian system $L_d : Q\times Q \to \mathbb{R}$ which is invariant under the lift of the left action $\Phi : G\times Q \to Q$. The corresponding Lagrangian momentum map $J_{L_d} : Q \times Q \to \mathfrak{g}^*$ is a conserved quantity of the discrete Lagrangian map $F_{L_d} : Q \times Q \to Q \times Q$, i.e. $J_{L_d} \circ F_{L_d} = J_{L_d}$.

Proof. Again, cf. [MW01]. □

The theorem can also be directly extended to discrete Lagrangian systems with control forces, see e.g. [OJM11]. For initial works on a reduction theory for discrete

mechanical systems, we refer to [MPS98] or [MRS00] and the references discussed therein.

CHAPTER 3

Optimal Control

The presence of control inputs in dynamical systems offers the ability to influence the systems' natural dynamics, e.g. in order to guide a mechanical system from one location to another or to regulate a machine or a process into a desired operating point. In *optimal control*, control maneuvers are searched for that steer the system for a given control problem in an optimal way, i.e. minimizing a given cost functional.

Depending on the structure of the dynamical system, it may be even possible to derive a *feedback control law* that defines a control from any initial state to the desired final state. However, designing optimal feedback laws for complex dynamical systems with nonlinear dynamics is not a trivial task. Thus, a widely used approach is to split up the problem: Firstly, the optimal trajectory for an ideal situation, i.e. no unknown disturbances of any kind, is computed. Secondly, a feedback regulator is designed to ensure that the system can follow the optimal trajectory despite disturbances during operation (cf. Section 3.4 for an application of this *two degree of freedom controller* approach and [vNM98] for an early reference to this concept). The focus of this thesis lies in the development of numerical design strategies for optimal trajectories, sometimes also called *feedforward* or *open loop controls*. Therefore, dynamical systems with general nonlinear dynamics, but without any unknown, e.g. stochastic, disturbances are considered.

To begin with, we give an introduction to optimal control theory including the necessary optimality conditions given by the well-known Pontryagin maximum principle (cf. [PBGM86]) in Section 3.1.2. Then, in Section 3.2 an overview of existing numerical techniques for solving optimal control problems is given. Section 3.3 is dedicated to a presentation of DMOC (*Discrete Mechanics and Optimal Control*). This is a numerical optimal control method especially tailored to mechanical systems, which has been developed in [JMO05, Obe08, LOMO10, OW10, OJM11]. In Section 3.4, the concept of DMOC is extended to mechatronic systems and applied to the computation of optimal current profiles of a reluctance drive.

This chapter can be seen as a preliminary for the main part of the thesis. In Chapter 4, control strategies based on inherent dynamical properties of the system are developed and integrated into a broader motion planning approach in Chapter 5. In the following, we give the basic definitions for general (smooth) dynamical systems but again focus on mechanical systems when introducing DMOC. An extension of optimal control theory for *non-smooth dynamical systems* is postponed to Chapter 6, where it can be discussed in the framework of *hybrid systems*.

3.1 Basic Definitions and Concepts

Mechanical systems with Lagrangian control forces, as studied in the previous chapter, are examples of general *control systems*, i.e. dynamical systems defined by

$$\dot{x}(t) = \mathcal{F}(t, x(t), u(t)) \quad x(t_0) = x_0 \tag{3.1}$$

where $x \in \mathbb{R}^n$ is the state, $u \in U \subset \mathbb{R}^m$ is the control input and $t \in \mathbb{R}$ is the time with initial time t_0 and corresponding initial state x_0. Both, the state and the control are time-dependent. In the following, we will restrict to control systems that do not explicitly depend on time, i.e. the right hand side simplifies to $\mathcal{F}(x(t), u(t))$ and $t_0 = 0$ can be chosen without loss of generality. To guarantee existence and uniqueness of solutions, we always assume that $\mathcal{F}$ is locally Lipschitz in x. Further, the control u is assumed to be piecewise continuous (cf. e.g. [Lib12]).

Note that we consider dynamical systems on vector spaces now rather than on manifolds (e.g. mechanical systems on configuration manifolds) as in the previous chapter. Having in mind that in the end, numerical techniques are going to be applied, it is reasonable to assume that the system's dynamics are given in (local) coordinate expressions. In Section 3.3, numerical optimal control for mechanical systems is discussed in detail. For a study of mechanical control systems or optimality conditions in a geometric mechanical framework, we refer to [BL04] and [Blo03].

3.1.1 Formulation of Optimal Control Problems

As a basic form of a cost functional, which has to be minimized by an optimal control, we consider

$$J(x, u) = \int_0^T C(x(t), u(t))\, dt + \Psi(x_T) \tag{3.2}$$

with T denoting the final time and x_T the corresponding final state of a control system (3.1). The map $C : \mathbb{R}^n \times U \to \mathbb{R}$ is called the *running cost*[1] and $\Psi : \mathbb{R}^n \to \mathbb{R}$ the *terminal cost*, respectively. Later, the cost functions are required to be continuous and continuously differentiable w.r.t. the state x.

We formulate an optimal control problem as the problem of *minimizing* the costs $J(x, u)$ with respect to the dynamics of the control system and subject to some boundary constraints $r(x(0), x(T)) = 0$ depending on the initial and final state of the system. Additional constraints may be posed in terms of inequality constraints $h(x(t), u(t)) \geq 0$ for all time points $t \in [0, T]$ and are therefore sometimes called the *path constraints* in the literature.

Problem 3.1 (Optimal Control Problem)**:** An optimal control problem for a control system $\dot{x}(t) = \mathcal{F}(x(t), u(t))$, with a cost functional J, boundary and path constraints r and h as defined above, is given by

$$\min_{x,u} J(x, u) = \int_0^T C(x(t), u(t))\, dt + \Psi(x_T), \tag{3.3}$$

$$\text{w.r.t.} \quad \dot{x}(t) = \mathcal{F}(x(t), u(t)), \tag{3.4}$$

$$h(x(t), u(t)) \geq 0, \quad \text{for all } t \in [0, T], \text{ and} \tag{3.5}$$

$$r(x(0), x(T)) = 0. \tag{3.6}$$

Problem 3.1 generalizes a number of important special subclasses of problem formulations. Polak (cf. [Pol97]), for instance, lists no fewer than ten different types of optimal control problems. Regarding the type of cost functional, Problem 3.1 is said to be of *Bolza form*. Problems without terminal costs ($\Psi \equiv 0$), i.e.

$$J(x, u) = \int_0^T C(x(t), u(t))\, dt,$$

are called *Lagrange problems*. The terminal cost is also called a *Mayer term* and thus, cost functionals consisting only of this term,

$$J(x, u) = \Psi(x_T),$$

belong to *Mayer problems*. The cost functional of a time-minimal control problem is given by $J(x, u, T) = \int_0^T 1\, dt$, with T as an additional optimization parameter.

[1] Another common notation of C originates from variational calculus and is the cost functional's *Lagrangian*. However, we do not use this term to avoid confusion with the mechanical system's Lagrangian.

In general, we distinguish between *fixed final time* and *free final time* problems. It is possible to transform between Bolza, Lagrangian and Mayer problems (cf. e.g. [Lib12]). For instance, a new state variable defined by $\dot{z}(t) = C(x(t), u(t))$, $z_0(0) = 0$ has the final value $z_T = \int_0^T C(x(t), u(t))\, dt$ and thus can be used to replace the running costs by a Mayer term. Similarly, an auxiliary variable of the form $z(t) = t$ can be used to transform between fixed and free final time constraints.

For an analysis of optimality principles, it is convenient to split up the additional constraints $h(x(t), u(t)) \geq 0$ into pure state constraints and mixed state/control constraints (cf. e.g. [Ger12]). The boundary constraints can define either fixed initial and final state values, or initial/final regions from/to which the system has to be steered.

The aim of optimal control is to find the minimizing solution of the cost functional which is admissible to the constraints. Since for a given control trajectory, the corresponding state trajectory can be obtained from the differential equation, we primarily speak of *admissible controls* and *optimal controls*.

Definition 3.2 (Admissible Control, Optimal Control)**:** A control $u(\cdot)$ that satisfies the constraints (3.4) – (3.6) on the time interval $[0, T]$ is called an *admissible control*. Together with the corresponding trajectory $x(\cdot)$ it generates, $(x(\cdot), u(\cdot))$ is called an *admissible pair*.

An admissible pair $(x^*(\cdot), u^*(\cdot))$ for Problem 3.1 that satisfies

$$J(x^*, u^*) \leq J(x, u) \tag{3.7}$$

for all admissible $(x(\cdot), u(\cdot))$ is called a *global optimal solution* or an *optimal pair* with *global optimal control* $u^*(\cdot)$. If Equation (3.7) only holds in a neighborhood $\mathcal{B}_\delta(x^*(\cdot), u^*(\cdot))$, $\delta > 0$, the pair $(x^*(\cdot), u^*(\cdot))$ is called *locally optimal*.

3.1.2 Necessary Optimality Conditions

Following the recently published textbook [Lib12], we begin with a formulation of the famous Pontryagin maximum principle for an optimal control problem as Problem 3.1 without path constraints and with a fixed endpoint. Several related problem formulations and their versions of the maximum principle will be discussed subsequently. As in the original work of Pontryagin (cf. [PBGM86] for the translated version) we give a true maximum formulation, i.e. the Hamiltonian of the optimal control problem is maximized by the optimal control. Nowadays, it is also very common to formulate the theorem as a minimum principle (cf. e.g. [Loc01, Ger12]).

Theorem 3.3 (Pontryagin Maximum Principle)**:** Assume that f and C are continuous and continuously differentiable w.r.t. x. Further, assume the terminal cost is

absent, i.e.

$$J(x,u) = \int_0^T C(x(t),u(t))\,dt,$$

and consider a fixed endpoint problem $x(T) = x_T$ with free final time T. Let $u^* : [0,T] \to U$ be an optimal control (in the global sense) and let $x^* : [0,T] \to \mathbb{R}^n$ be the corresponding optimal state trajectory. Then there exist a function $\rho^* : [0,T] \to \mathbb{R}^n$ and a constant $\rho_0^* \leq 0$ satisfying $(\rho_0^*, \rho^*(t)) \neq (0,0)$ for all $t \in [0,T]$ and having the following properties:

(1) x^* and ρ^* satisfy the canonical equations

$$\begin{aligned} \dot{x}^* &= H_\rho(x^*, u^*, \rho^*, \rho_0^*) \\ \dot{\rho}^* &= -H_x(x^*, u^*, \rho^*, \rho_0^*) \end{aligned} \tag{3.8}$$

with the boundary conditions $x^*(0) = x_0$ and $x^*(T) = x_T$, where the *Hamiltonian* $H : \mathbb{R}^n \times U \times \mathbb{R}^n \times \mathbb{R} \to \mathbb{R}$ is defined as

$$H(x,u,\rho,\rho_0) = \langle \rho, \mathcal{F}(x,u) \rangle + \rho_0 C(x,u) \tag{3.9}$$

and H_ρ, H_x denote the partial derivatives w.r.t. ρ and x, respectively.

(2) For each fixed t, the function $u \mapsto H(x^*(t), u, \rho^*(t), \rho_0^*)$ has a global maximum at $u = u^*(t)$, i.e., the inequality

$$H(x^*(t), u^*, \rho^*(t), \rho_0^*) \geq H(x^*(t), u, \rho^*(t), \rho_0^*)$$

holds for all $t \in [0,T]$ and all $u \in U$.

(3) $H(x^*(t), u^*(t), \rho^*(t), \rho_0^*) = 0$ for all $t \in [0,T]$.

Proof. See e.g. [Lib12]. □

The n-dimensional vector $\rho(t)$ is the *costate* or *adjoint variable* of the Hamilton equations of optimal control, Equation (3.8). The scalar ρ_0 is called the *abnormal multiplier*. In the abnormal case, it holds $\rho_0 = 0$, and otherwise, the multiplier can be normalized to $\rho_0 = -1$.

Theorem 3.3 can be extended to a *variable endpoint* $x(T)$ by defining some target set $S = [0,\infty) \times S_T$, where S_T is a k-dimensional surface in $\mathbb{R}^n$ ($0 \leq k \leq n$). This surface can be defined via equality constraints, $S_T = \{x \in \mathbb{R}^n : h_1(x) = h_2(x) = \cdots = h_{n-k}(x) = 0\}$, with scalar, differentiable functions $h_1, \ldots, h_{n-k}$. It is assumed that every $x \in S_T$ is a regular point. Then, the boundary constraint of the final time in property (1) of Theorem 3.3 is replaced by $x^*(T) \in S_T$. Additionally, we

receive as a fourth property that the vector $\rho^*(T)$ is orthogonal to the tangent space to S_T at $x^*(T)$:

$$\langle \rho^*(T), d \rangle = 0 \quad \forall d \in T_{x^*(T)} S_T. \tag{3.10}$$

This is called the *transversality condition*. Together with the boundary constraints, it always gives a total number of $2n$ conditions to specify a solution of Equation (3.8). While the original formulation of Theorem 3.3 is the special case with $S_T = \{x_T\}$ and no restrictions on $\rho^*(T)$ (since the tangent space is zero), in the other extremal case, it holds $S_T = \mathbb{R}^n$ and Equation (3.10) simplifies to $\rho^*(T) = 0$. In all other cases with $0 < k < n$ we have n constraints from the initial point, k degrees of freedom for the final state and $n - k$ degrees of freedom for the final adjoint state.

Since we consider autonomous dynamical systems and time-independent cost functions only, the restriction to time intervals $[0, T]$ starting at $t = 0$ holds without loss of generality. Furthermore, the free final time formulation of Theorem 3.3 can be transformed into a *fixed terminal time* version by a change of variables. Namely, an additional state variable $x_{n+1} := t$ has to be introduced with corresponding differential equation $\dot{x}_{n+1} = 1$, $x_{n+1}(0) = 0$. Then, the target set is extended to $[0, \infty) \times S_T \times T$ such that Theorem 3.3 or the variable endpoint version can be applied. This gives us a new Hamiltonian that satisfies property (3), i.e. $\overline{H}(x^*(t), x^*_{n+1}(t), u^*, \rho^*(t), \rho^*_{n+1}(t), \rho^*_0) = 0$. However, one can show that it differs only by a constant from the original Hamiltonian and therefore, for fixed final time problems, property (3) is replaced by

$$H(x^*(t), u^*, \rho^*(t), \rho^*_0) = \text{ const.} \quad \text{for all } t \in [0, T].$$

Finally, one can consider types of Problem 3.1 including a *terminal cost* $\Psi(x_T)$. The necessary conditions can be derived from the previously discussed variable end point version by rewriting the terminal cost in integral formulation via $\Psi(x(T)) - \Psi(x(0)) = \int_0^T \Psi_x(x(t)) \cdot \mathcal{F}(x, u)\, dt$. In [Lib12], the adapted constraints are derived.

3.1.3 Multiobjective Optimal Control

In many applications, there arise several cost functionals that have to be minimized simultaneously. This leads to vector valued cost functionals, denoted by $\mathbf{J}(x, u)$ with $\mathbf{J} = (J_1, \ldots, J_k)$, $k \geq 1$ and J_i of Bolza form (3.2) for all $i \in \{1, \ldots, k\}$. The minimization of the vector valued functional $\mathbf{J}(x, u)$ is defined by the partial order $<_p$ on $\mathbb{R}^k$. Let $v, w \in \mathbb{R}^k$, then the vector v is *less than* w ($v <_p w$), if $v_i < w_i$ for all $i \in \{1, \ldots, k\}$. The relation $\leq_p$ is defined analogously. By this relation, we can introduce the concept of dominance and Pareto optimality (cf. [Mie99] or [Ehr05], for instance).

Definition 3.4 (Dominated and Pareto Optimal Solutions)**:** Let $(x(\cdot), u(\cdot))$ and $(x^*(\cdot), u^*(\cdot))$ be admissible solutions of Problem 3.1 with a vector valued cost functional $\mathbf{J}(x, u)$ as introduced above.

(a) The solution $(x(\cdot), u(\cdot))$ is *dominated* by a solution $(x^*(\cdot), u^*(\cdot))$ w.r.t. $\mathbf{J}(x, u)$, if $\mathbf{J}(x^*, u^*) \leq_p \mathbf{J}(x, u)$ and $\mathbf{J}(x, u) \neq \mathbf{J}(x^*, u^*)$, otherwise $(x(\cdot), u(\cdot))$ is non-dominated by $(x^*(\cdot), u^*(\cdot))$.

(b) A solution $(x^*(\cdot), u^*(\cdot))$ is called *Pareto optimal* if there exists no $(x(\cdot), u(\cdot))$ which dominates $(x^*(\cdot), u^*(\cdot))$.

(c) The set of all Pareto optimal solutions $(x^*(\cdot), u^*(\cdot))$ is called the *Pareto set* and its image under $\mathbf{J}$ the *Pareto front*.

We will be faced with multiobjective optimization problems that arise from optimal control problems with multiple objectives in several application examples throughout the following chapters. A numerical technique for solving multiobjective optimization problems, a so called *scalarization technique* based on *reference points*, is presented in Section B.2 in the appendix.

3.2 Numerical Treatment of Optimal Control Problems

Finding analytical solutions to optimal control problems with multiple states and nonlinear dynamics is often impossible. This gives rise to the development of numerical methods to approximate optimal control and state trajectories. The solution techniques can be categorized into *indirect* and *direct methods*. Their similarities and differences are sketched in the diagram of Figure 3.1 together with the method DMOC, which is introduced later in Section 3.3.

3.2.1 Indirect and Direct Solution Methods

Indirect Methods Indirect solution methods are based on the Pontryagin maximum principle. The Hamilton equations (3.8) of the states and the adjoints together with the boundary constraints form a *boundary value problem*. Thus, controls have to be synthesized which (point-wise) maximize the Hamiltonian and, at the same time, solve the boundary problem. Examples of indirect methods are given for instance in [Kir70] or [BBB+01]. Gradient methods, also called methods of steepest descent, iteratively maximize the Hamiltonian w.r.t. the controls. In every step of a corresponding algorithm, the state equation has to be integrated forward in time and the adjoint equation backward in time. This requires a discrete representation of the control trajectory as well as a discretization of the state and adjoint differential equations. Alternative indirect methods are collocation or multiple shooting, which

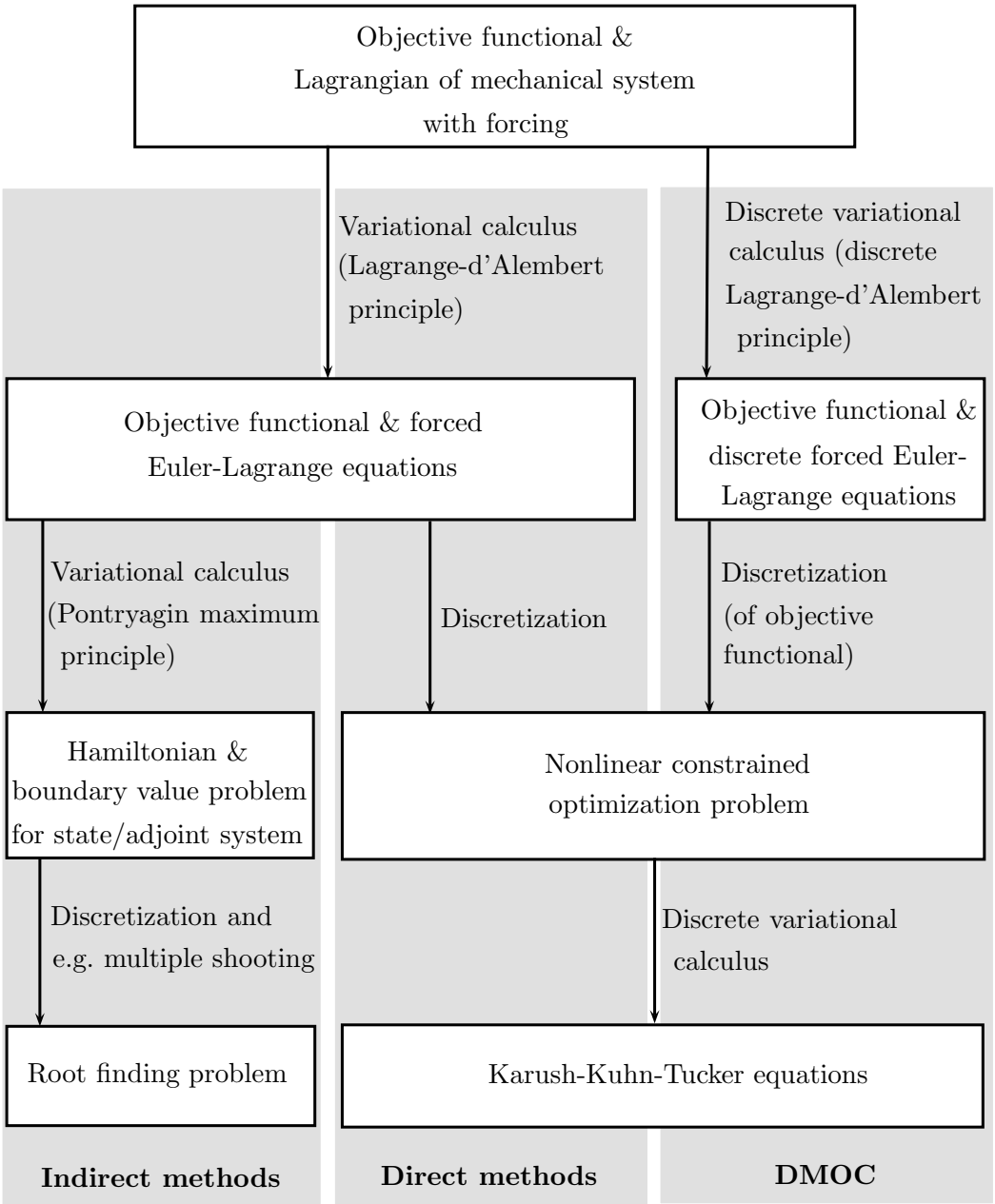

Figure 3.1: Comparison of indirect and direct methods for solving optimal control problems for mechanical systems (left and middle branch) and DMOC (right branch)

numerically solve the multi-point boundary value problem (cf. e.g. the overview given in [BBB+01] and the references therein). Drawbacks of indirect methods are that formulating the necessary optimality conditions can be quite cumbersome for high dimensional systems and, additionally, the methods require good initial guesses to start from. The latter problem is particularly severe if active constraints cause switches in the control subject to an a priori unknown switching structure (cf. [Ger12, BBB+01]).

Direct Methods On the contrary, direct methods start with a discretization of Problem 3.1. This means, a discrete time grid

$$\Delta t = \{t_0 < t_1 < \cdots < t_N\}$$

is introduced with $t_0 = 0$ and $t_N = T$, e.g. an equidistant partition with step size $h_j = t_{j+1} - t_j = \text{const.}$ for all $j = 0, \ldots, N-1$. A discretization of the controls $u_d = (u_0, \ldots, u_N)$ has to be chosen according to the time grid. The differential equation (3.4) can be discretized by any integration scheme, e.g. by Runge-Kutta methods. For illustration, we show the idea for an explicit Euler integration scheme, i.e.

$$x_{j+1} = x_j + h_j \mathcal{F}(x_j, u_j), \quad \text{for } j = 0, \ldots, N-1.$$

Finally, the cost functional and, if present, the constraints are discretized. Assuming a general Lagrange problem has been transformed into a Mayer problem (with fixed final time) beforehand, such that J has no integral term, the discretization just means an evaluation at the discrete time points. Thus one obtains the following *nonlinear restricted optimization problem* as a discretization of Problem 3.1

$$\begin{aligned} &\min \Psi(x_N) \\ \text{w.r.t. } &x_j + h_j \mathcal{F}(x_j, u_j) - x_{j+1} = 0, \quad j = 0, \ldots, N-1, && (3.11) \\ &r(x_0, x_N) = 0, && (3.12) \\ &h(x_j, u_j) \geq 0, \quad j = 0, \ldots, N. && (3.13) \end{aligned}$$

This is called the *full discretization approach* (see e.g. [Ger12]) with optimization variables $(x_0, x_1, \ldots, x_N, u_0, u_1, \ldots, u_N)$, equality constraints (3.11), (3.12), and inequality constraints (3.13).

Alternatively, a *reduced discretization approach* can be applied by exploiting the fact that x_{j+1} is completely defined by (x_j, u_j) and h_j. We define $X_0(x_0) = x_0$ and, recursively,

$$X_j(x_0, u_0, \ldots, u_{j-1}) = x_j \quad \text{for } j = 1, \ldots, N.$$

Then, eliminating the equality constraints (3.11) results in a nonlinear constrained

optimization problem with solely the optimization variables $(x_0, u_0, u_1, \ldots, u_N)$, i.e.

$$\begin{aligned} &\min\ \Psi(X_N(x_0, u_0, \ldots, u_{N-1})) \\ \text{w.r.t. } &r(X_0(x_0), X_N(x_0, u_0, \ldots, u_{N-1})) = 0, \\ &h(X_j(x_0, u_0, \ldots, u_{j-1}), u_j) \geq 0, \quad j = 0, 1, \ldots, N. \end{aligned} \tag{3.14}$$

Direct Single Shooting The reduced discretization approach is a formulation of the *direct single shooting method* (cf. e.g. [BBB+01]): the controls are parameterized by the finite dimensional vector $(u_0, \ldots, u_N)$ and in every iteration, the state equations are implicitly solved by some integration scheme. Because of the sequential simulation and optimization, the dynamics of the underlying system are fulfilled (up to the discretization error) in every iteration step.

On the contrary, in the full discretization approach, the differential equation has been transformed into nonlinear equality constraints of the optimization problem. Therefore, this approach is called a *simultaneous simulation and optimization strategy* (cf. [BBB+01]). Here, current iterates of an optimization algorithm need not be admissible solutions to the dynamics. However, when converged, the method provides an admissible and optimal solution to the discretized problem.

Direct Multiple Shooting The *direct multiple shooting method* is a combination of the sequential and the simultaneous approach. A finite parametrization of the controls is defined on a discrete time grid as before. Additionally, so called node values $s_0, s_1, \ldots, s_N$ are introduced. They serve as initial values of the decoupled problem which is generated by considering the original problem on each time interval $[t_j, t_{j+1}]$ separately, i.e. $x(t_j) = s_j$ for all $j = 0, \ldots, N$. The decoupling requires additional equality constraints of the form

$$s_{j+1} - \tilde{x}_j(t_{j+1}, s_j, u_j) = 0, \quad j = 0, \ldots, N-1,$$

where $\tilde{x}_j(t_{j+1}, s_j, u_j)$ is the piece of the solution trajectory on $[t_j, t_{j+1}]$ evaluated at the right boundary. It depends on the initial value s_j and the control u_j. Typically, in an implementation, a finer grid is used for the control discretization than for the node values. The inequality constraints of Problem 3.1 are again only evaluated at discrete grid points (e.g. on the grid for the nodes) and the initial and final values lead to the constraints $s_0 = x_0$ and $s_N = x_N$, respectively. Using a reduced discretization approach for the states on the intervals $[t_j, t_{j+1}]$, $j = 0, \ldots, N-1$ (cf. Equations (3.14)), we end up with a nonlinear constrained optimization problem with optimization parameters $(s_0, \ldots, s_N, u_0, \ldots, u_N)$. Compared to the alternative formulations, this is a high number of parameters. However, when computing the derivatives, the sparsity structure of the Jacobian can be exploited very well. This leads to quite efficient optimization algorithms (cf. e.g. [BBB+01, Ger12] and the

references therein). Furthermore, this approach is highly suitable for parallel computation.

Direct Collocation As another alternative method, we briefly sketch the idea of *direct collocation methods*, referencing to the short overview given in [BBB+01]. Here, the state and control functions are represented by polynomials, again separately on each subinterval of the time grid. The shape parameters, i.e. the coefficients of the polynomials, form the optimization parameters of the optimization problem. Matching conditions are imposed to guarantee that the polynomials are continuous (or even differentiable up to a higher order) at the boundaries of the subintervals. Additionally, on each subinterval, collocation points are defined and the differential equation in which the polynomials are substituted has to hold at these points only. Since both the state and control function are fully discretized, the collocation method leads to high dimensional optimization problems. However, it is again possible to exploit the special discretization structure in the computation of derivatives.

In comparison, the single shooting method leads to the smallest nonlinear optimization problem, while the collocation method requires the highest number of optimization variables. In general, the multiple shooting method lies in between (cf. [BBB+01]). However, since the single shooting method uses the reduced discretization approach, the derivatives do not show the sparsity structure which is obtained from a full discretization approach (cf. [Ger12]) and which is typically exploited for implementations of the multiple shooting and the collocation method.

3.2.2 Nonlinear Constrained Optimization Methods

All direct optimal control methods described above have in common that, in the end, a nonlinear problem of the following form has to be solved.

Problem 3.5: A finite nonlinear constrained optimization problem is given by

$$\begin{aligned} & \min J(z) \\ \text{w.r.t. } & z \in S, \\ & G(z) \leq 0, \\ & H(z) = 0, \end{aligned}$$

with $J : \mathbb{R}^{n_z} \to \mathbb{R}$, $G : \mathbb{R}^{n_z} \to \mathbb{R}^{n_G}$ and $H : \mathbb{R}^{n_z} \to \mathbb{R}^{n_H}$ being continuously differentiable and $S \subseteq \mathbb{R}^{n_z}$ being closed and convex. The admissible set is given by $\Sigma = \{z \in S \,|\, G(z) \leq 0, H(z) = 0\}$.

The following theorem, taken from [Ger12], gives the necessary conditions for an optimal solution of Problem 3.5.

Theorem 3.6 (First Order Necessary Optimality Conditions)**:** Let $\hat{z}$ be a local minimum of Problem 3.5 and $S \subseteq \mathbb{R}^{n_z}$ satisfies $\text{int}(S) \neq \emptyset$. Further, let the *linear independence constraint qualification* hold at $\hat{z}$, i.e. $\hat{z} \in \text{int}(S)$ and the derivatives $G_i'(\hat{z})$ for all $i \in \{1, \ldots, n_G\}$ with $G_i(\hat{z}) = 0$ and $H_i'(\hat{z})$, for all $i = 1, \ldots, n_H$, are linearly independent. Then there exist unique multipliers $\mu \in \mathbb{R}^{n_G}$ and $\lambda \in \mathbb{R}^{n_H}$ not all zero such that

$$\begin{aligned} \nabla_z L(\hat{z}, \mu, \lambda) &= 0, \\ \mu_i G_i(\hat{z}) &= 0, \text{ and} \\ \mu_i &\geq 0, \quad \text{for } i = 1, \ldots, n_G, \end{aligned}$$

where

$$L(z, \mu, \lambda) = J(z) + \mu^T G(z) + \lambda^T H(z)$$

is the *Lagrangian* of Problem 3.5.

Proof. Cf. [Ger12], Theorem 2.3.28 in combination with Corollary 2.3.39. □

The necessary optimality conditions of Theorem 3.6 are also known as the *Karush-Kuhn-Tucker (KKT) conditions* and, therefore, a point $\hat{z}$ satisfying the conditions is called a *KKT point*.

Sequential Quadratic Programming (SQP) In the last decades, SQP methods turned out to be very suitable for nonlinear optimization problems and became a state of the art technique available in many implementations (cf. e.g. [Pow78, BGR98, GJL+00, BBB+01, GMS05, Ger12] for an introduction to SQP and its implementation).

The basic idea of the SQP method is to iteratively solve the nonlinear optimization problem by a sequence of quadratic subproblems. For a brief overview of the method, we consider Problem 3.5 with $S = \mathbb{R}^{n_z}$ and J, G, and H being twice continuously differentiable. At some iterate $(z^{(k)}, \mu^{(k)}, \lambda^{(k)})$, a local approximation of the original

problem is given by the quadratic optimization problem

$$\begin{aligned} & \min \frac{1}{2} d^T L_{zz}(z^{(k)}, \mu^{(k)}, \lambda^{(k)}) d + \nabla J(z^{(k)})^T d \\ \text{w.r.t. } & d \in \mathbb{R}^{n_z}, \\ & G(z^{(k)}) + G'(z^{(k)}) d \leq 0, \\ & H(z^{(k)}) + H'(z^{(k)}) d = 0. \end{aligned}$$

This problem is obtained from a quadratic approximation of the original Lagrangian together with a linearization of the constraints. L_{zz} denotes the Hessian of the Lagrangian. In many implementations of SQP algorithms, it is replaced by a positive definite matrix as an approximation of the real Hessian.

An SQP algorithm starts with some triple $(z^{(0)}, \mu^{(0)}, \lambda^{(0)})$ and iteratively computes KKT points $(d^{(k)}, \mu^{(k+1)}, \lambda^{(k+1)})$ of the quadratic optimization problem (the *minor iterates*), until the update $z^{(k+1)} := z^{(k)} + d^{(k)}$ (a *major iteration step*) is a KKT point of the original problem. To ensure global convergence (to local minima), the step length into the search direction $d^{(k)}$ has to be adjusted by some step size. Here, for instance, Armijo line search can be applied, together with a merit function obtained by augmenting the Lagrangian by penalty terms (cf. [BBB+01], for instance).

SQP algorithms require derivative information of the constraints and the objective. For optimal control problems, derivative formulas can be derived directly in the discrete version for the finite optimization problem: either based on sensitivity equations or on discrete adjoint equations (cf. [Ger12]). Depending on the choice of discretization (e.g. full, reduced or by collocation polynomials), structural sparsity of the Jacobians can be exploited in specially tailored SQP algorithms. For an implementation, the derivatives can be approximated by finite differences, which is straightforward but computationally expensive and often inaccurate, or, advantageously, they can be computed by *algorithmic differentiation* (cf. e.g. [GW08]).

However, in general, the drawback of gradient-based optimization is that good initial guesses have to be chosen to make an algorithm converge to local minima that are at least close to global optimal solutions. This problem motivates the structure exploiting motion planning approach presented in the main part of this thesis (cf., in particular, Chapters 4 and 5).

3.3 The Method DMOC (Discrete Mechanics and Optimal Control)

DMOC is a direct solution method for optimal control problems of mechanical systems (see e.g. [OJM11]). The basic idea is to perform the discretization of the optimal control problem by *discrete mechanics*, a concept which has already been

introduced in Section 2.2. Recall that the state space X of a controlled Lagrangian system is the tangent bundle TQ and the differential equations (3.4) can be replaced by the forced Euler-Lagrange equations (2.9). This leads to the following specification of the optimal control problem 3.1 for mechanical systems.

Problem 3.7 (Optimal Control Problem for Mechanical Systems)**:** An optimal control problem for a mechanical system on state space TQ with forced Euler-Lagrange equations $\frac{\partial}{\partial q}L(q,\dot{q}) - \frac{d}{dt}\frac{\partial}{\partial \dot{q}}L(q,\dot{q}) + f_L(q,\dot{q},u) = 0$ depending on the system's state $(q(t),\dot{q}(t))$ and on the control path $u(t)$, is given by

$$\begin{aligned}\min_{q,u,(T)} J(q,u,(T)) &= \int_0^T C(q(t),\dot{q}(t),u(t))\,dt + \Psi(q(T),\dot{q}(T)),\\ \text{w.r.t.}\quad & \frac{\partial}{\partial q}L(q,\dot{q}) - \frac{d}{dt}\frac{\partial}{\partial \dot{q}}L(q,\dot{q}) + f_L(q,\dot{q},u) = 0,\\ & h(q(t),\dot{q}(t),u(t)) \geq 0, \qquad \text{for all } t \in [0,T],\\ & r(q(0),\dot{q}(0),q(T),\dot{q}(T)) = 0,\end{aligned}$$

where $C : TQ \times U \to \mathbb{R}$, $\Psi : TQ \to \mathbb{R}$ are running costs and terminal costs, respectively.

Equivalently, instead of the Euler-Lagrange equations, the variational equation of the Lagrange-d'Alembert principle (cf. Equation (2.8) in Section 2.1.2) depending on the Lagrangian and the forcing can be considered as part of the optimal control problem for mechanical systems.

Using concepts from discrete variational mechanics, the discretization in DMOC is based on the discrete Lagrange-d'Alembert principle. Thereby, the method captures the advantage of discrete variational mechanics for the discrete optimal control problem, namely that the discrete approximation inherits the same qualitative behavior (e.g. symplecticity or conserved momenta due to symmetries) as the original continuous system. In detail, the continuous optimal control problem is transformed into a finite dimensional constrained optimization problem using a discretization of the states and the controls. Again, let Δt denote a discrete time grid,

$$\Delta t = \{t_0 = 0 < t_1 < \cdots < t_N = T\}.$$

We replace the state space TQ by $Q \times Q$, and represent the configuration path $q : [0,T] \to Q$ by a discrete path $q_d = \{q_0, q_1, \ldots, q_N\}$ on the grid. The control path is represented on a possibly finer grid with $u_k = (u_{k1}, \ldots, u_{ks}) \in U^s$ on $[t_k, t_{k+1}]$ (cf. Section 2.2.1). The Lagrangian $L : TQ \to \mathbb{R}$ and the force function are approximated by the discrete Lagrangian and discrete forces, respectively, as described

in Section 2.2.1. Then, the discrete Lagrange-d'Alembert principle can be applied, leading to the discrete forced Euler-Lagrange equations (cf. Equation (2.11))

$$D_1 L_d(q_k, q_{k+1}) + D_2 L_d(q_{k-1}, q_k) + f_k^- + f_{k-1}^+ = 0 \tag{3.15}$$

for each $k = 1, \ldots, N-1$.

The next step is the discretization of the cost functional. To this end, a function C_d is introduced that approximates the integral of the running costs on every time slice $[t_k, t_{k+1}]$,

$$C_d(q_k, q_{k+1}, u_k) \approx \int_{t_k}^{t_{k+1}} C(q(t), \dot{q}(t), u(t))\, dt.$$

The discrete terminal cost $\Psi_d : Q \times Q \times U^s \to \mathbb{R}$ depends on the two last points of the discrete trajectory and the control force on $[t_{N-1}, t_N]$. Together, this yields the *discrete objective function*

$$J_d(q_d, u_d) = \sum_{k=0}^{N-1} C_d(q_k, q_{k+1}, u_k) + \Psi_d(q_{N-1}, q_N, u_{N-1}).$$

Discrete boundary constraints can be derived via the Legendre transforms (cf. Sections 2.1.4 and 2.2). While velocities in the discrete setting belong to the intervals, conjugate momenta can be computed for each node via the discrete Legendre transforms, e.g. for the final node, $p_N = D_2 L_d(q_{N-1}, q_N) + f_d^+(q_{N-1}, q_N, u_{N-1})$. Thus, for example, for the continuous problem with fixed initial and final states $(q^0, \dot{q}^0)$ and $(q^T, \dot{q}^T)$ as boundary constraints, the discretization reads

$$\begin{aligned} &r_d((q_0, q_1, u_0), (q_{N-1}, q_N, u_{N-1}))) \\ &= \begin{pmatrix} q_0 - q^0 \\ D_2 L(q^0, \dot{q}^0) + D_1 L_d(q_0, q_1) + f_d^-(q_0, q_1, u_0) \\ q_N - q^T \\ -D_2 L(q^T, \dot{q}^T) + D_2 L_d(q_{N-1}, q_N) + f_d^+(q_{N-1}, q_N, u_{N-1}) \end{pmatrix} = 0. \end{aligned} \tag{3.16}$$

Finally, the path constraints have to be discretized. Following [Obe08], we define the discrete path constraints on each interval $[t_k, t_{k+1}]$ by some function

$$h_d(q_k, q_{k+1}, u_k) \geq 0 \quad \text{for } k = 0, \ldots, N-1.$$

All together, this yields a discretization of the optimal control problem for mechanical systems.

Problem 3.8 (Discrete Optimal Control Problem for Mechanical Systems)**:** A discrete optimal control problem for a discrete mechanical system as defined above is

given by

$$\begin{aligned}
&\min_{q_d,u_d} J_d(q_d,u_d) = \sum_{k=0}^{N-1} C_d(q_k,q_{k+1},u_k) + \Psi_d(q_{N-1},q_N,u_{N-1}) \\
\text{w.r.t.}\quad & D_1L_d(q_k,q_{k+1}) + D_2L_d(q_{k-1},q_k) + f_k^- + f_{k-1}^+ = 0, \quad k = 1,\dots,N-1, \\
& h_d(q_k,q_{k+1},u_k) \geq 0, \quad k = 0,\dots,N-1, \\
& r_d((q_0,q_1,u_0),(q_{N-1},q_N,u_{N-1})) = 0.
\end{aligned}$$

It can be easily seen that Problem 3.8 is a finite nonlinear constrained optimization problem in the form of Problem 3.5: the optimization parameters are $(q_0,\dots,q_N,u_0,\dots,u_N)$, equality constraints are given by the discrete forced Euler-Lagrange equations and by the boundary constraints, and inequality constraints arise from the discrete path constraints. If the terminal time is free, the step sizes, in the simplest case one step size parameter h of an equidistant grid $\Delta t = \{t_k = kh \,|\, k = 0,\dots,N\}$, is an additional optimization parameter. Thus, a DMOC problem can be addressed by nonlinear optimization methods of any kind, e.g. by SQP methods (cf. Section 3.2.2).

A detailed analysis of DMOC can be found in [Obe08] and [OJM11], including higher order discretization by Runge-Kutta schemes. Also, a proof of convergence is given, showing that discrete solutions of the discrete optimal control problem converge to continuous solutions of the original problem for vanishing step sizes. The approximation order of the optimal control scheme depends on the quadrature rule, e.g. second order is obtained by using a midpoint rule approximation and assuming constant control parameters on each time interval with $l = 1$ and $c_1 = \frac{1}{2}$ (cf. Section 2.2.1). The optimization scheme generated by DMOC is symplectic-momentum consistent, i.e. the symplectic structure and the momentum maps which correspond to symmetry groups are consistent with the control forces for the discrete solution, independent of the step size h.

3.4 Technical Application

The optimal control method DMOC has been successfully used in various applications, e.g. in space mission design (cf. e.g. [DJK+06, DOP+09, MOM12]), in the optimal control of multibody systems (cf. [LOMO07, OT09, LOMO10]), or to compute swing-up trajectories for a double pendulum on a cart (see [TKOT11]). In the following, we present an extension of DMOC to electro-mechanical systems and use this method to compute optimal current profiles for a switched reluctance drive.

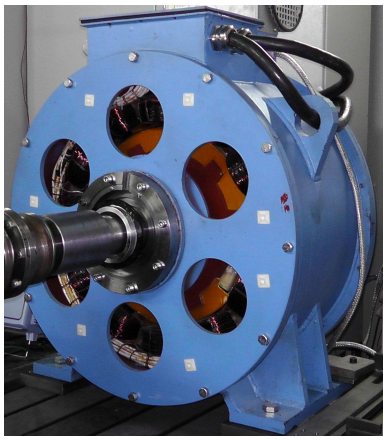

(a) Prototype of a switched reluctance drive

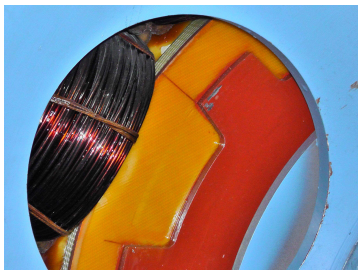

(b) Photograph of the coil and the rotor poles.

Figure 3.2: Prototype of the 12/10 SRM, a switched reluctance motor with twelve stator poles and ten rotor poles.

This application results from a cooperation with the *Chair of Power Electronics and Electrical Drives*[2]*, University of Paderborn* within the *CRC 614, Collaborative Research Center "Self-Optimizing Concepts and Structures in Mechanical Engineering"*[3] at the University of Paderborn and has been published in [FOR+11].

3.4.1 The Electro-Mechanical Model of a Reluctance Drive

Many dynamical systems arising in engineering science, e.g. electronic components of electro-mechanical systems, can be modeled by a Lagrangian in an analogous way as classical mechanical systems (cf. [DK05], [MW07] or [OTC+13], for instance). Thus, Euler-Lagrange equations can also be derived for entire electro-mechanical systems, as it is described for the example of a switched reluctance drive in the following. The modeling of electro-mechanical systems by a variational approach is advantageous since it allows a unified treatment of electrical and mechanical subsystems.

Switched Reluctance Drive Rising fuel costs and increasingly restrictive environmental guidelines require environmentally friendly transport concepts. Thus, the interest in electric vehicles has risen enormously in the last years, not only for road traffic but also for rail traffic. These developments motivate – amongst many other interesting problems in the field of optimization and control of mechatronic systems – the research in switched reluctance drives (cf. e.g. [IMDD02, KKP+08]).

[2] wwwlea.uni-paderborn.de
[3] www.sfb614.de

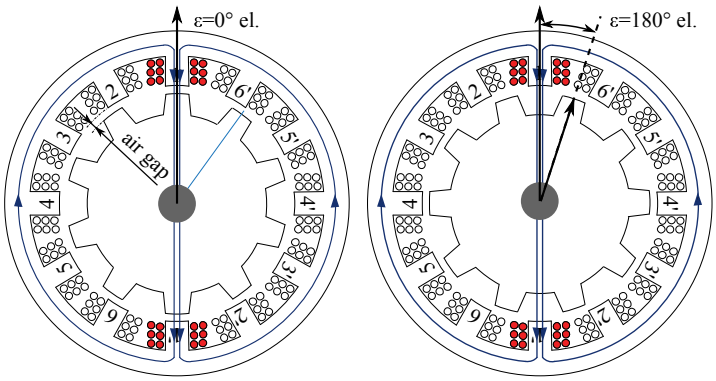

Figure 3.3: The action principle of a switched reluctance drive is based on magnetic reluctance. Sketch of the motor's aligned position (left) and unaligned position (right) w.r.t. the top pole.

In the course of research activities of the group "Neue Bahntechnik Paderborn" (*NBP – New Rail Technology Paderborn*[4]), two prototypes of switched reluctance drives have been built. One is designed in original linear form to test its static performance and the other one is built in rotary form as depicted in Figure 3.2 (cf. also [KKP+08]), to test its dynamic performance and efficiency for so-called *RailCabs*, rail-bound vehicles which drive autonomously and offer individual connections.

The switched reluctance drive of Figure 3.2 has a stator of twelve poles with coils. They form six pole pairs, so called *phases*, which can be energized independently. The principle of the drive is based on a minimization of the magnetic resistance, the *magnetic reluctance* (cf. [Kri01] for a detailed description of the action principle of reluctance drives). The rotor has ten poles only, such that, in any position, there are pairs of stator and rotor poles for which a non-minimal air gap occurs, i.e. *unaligned positions*, depicted in Figure 3.3 on the right for the top pole. A smaller air gap leads to lower magnetic resistance, in turn raising the reciprocal inductivity. In order to minimize the magnetic reluctance while a coil is supplied with current, the rotor tends to a position with a minimal air gap, the so called *aligned position* (cf. Figure 3.3, on the left). This in turn rotates the drive. However, it inevitably leads to a larger air gap at another stator pole and thus, suitable, oscillating phase currents can be used to obtain a steady rotation of the drive. With one full phase in the stator currents (360° electrical angle), the rotor is moved one pole forward, which results in a mechanical rotation of 36°. The inductivity of each phase for a constant current w.r.t. a varying electrical angle is depicted in Figure 3.4. As it can be seen, between the inductivity of two neighboring phases there is a shift of 60°.

[4] www.railcab.de

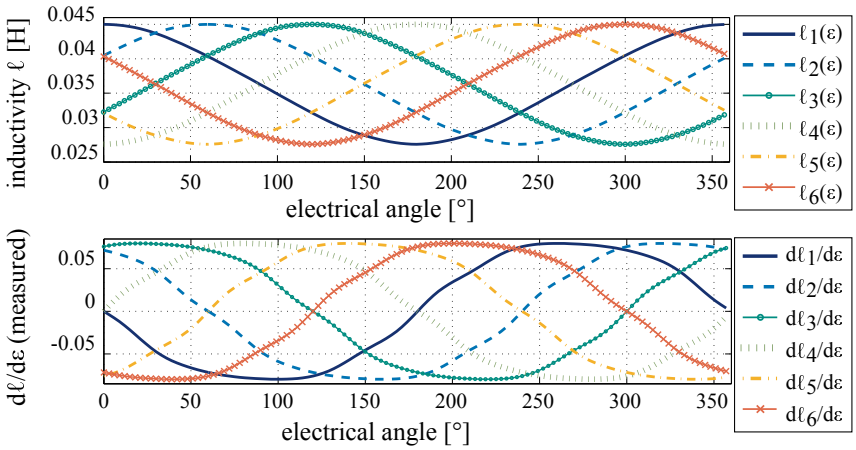

Figure 3.4: Measured inductivity of the coils depending on their position (electrical angle) and their (measured) derivatives, cf. [FOR+11].

We denote the electrical angle by ϵ and the inductivity of the phases by $\ell_k(\epsilon)$ for $k = 1, \dots, 6$.

Euler-Lagrange Equations The Lagrangian of the reluctance drive is given by the magnetic energy of the coils[5] and the kinetic energy of the drive. Let $q(t) = (q^1(t), \dots, q^6(t))$ denote the charges of the coils and $i(t) = (i^1(t), \dots, i^6(t))$ the currents as derivatives of the charges. Further, by a slight abuse of notation, we use $\epsilon(t)$ also to denote the mechanic angle, such that $\omega(t) = \dot{\epsilon}(t)$ is the rotational velocity. Then, the generalized configurations are given by $(q(t), \epsilon(t))$ with corresponding generalized velocities $(i(t), \omega(t))$. With Θ denoting the inertia of the drive, the Lagrangian reads

$$L(q, i, \epsilon, \omega) = \frac{1}{2} \left(\sum_{k=1}^{6} \ell_k(\epsilon(t)) \cdot (i^k(t))^2 + \Theta \cdot \omega(t)^2 \right),$$

where the dependence of all arguments of L on time is dropped for shortness at the left hand side. The forces acting on each coil are the dissipative forces from ohmic losses due to the ohmic resistors R (assumed to be identical for all coils) and the control forces generated by the supply voltage $u^k(t)$, $k = 1, \dots, 6$. Friction losses are

[5] In general, the *coenergy* has to be chosen for the Lagrangian. However, if the inductance is linear, e.g. due to a large air gap, it is acceptable to choose the stored field energy in a good approximation.

neglected, so only a load $M_L(t)$ is acting on the mechanical subsystem, i.e. we have

$$f^k(q^k, i^k, u^k) = -R \cdot i^k(t) + u^k(t), \quad \text{for } k = 1, \dots, 6, \text{ and}$$
$$f^7(\epsilon, \omega, M_L) = M_L(t).$$

Since no direct coupling between the coils is modeled (which is, of course, an idealization), we receive six Euler-Lagrange equations for the coils and an additional Euler-Lagrange equation for the magnetic subsystem

$$\ell_k(\epsilon(t))\frac{d}{dt}i^k(t) = -\frac{\partial \ell_k(\epsilon(t))}{\partial \epsilon}\dot{\epsilon}(t) \cdot i^k(t) - R \cdot i^k(t) + u^k(t), \quad \text{for } k = 1, \dots, 6,$$
$$\Theta \cdot \frac{d}{dt}\omega(t) = \frac{1}{2}\sum_{k=1}^{6} \frac{\partial \ell_k(\epsilon(t))}{\partial \epsilon} \cdot (i^k(t))^2 - M_L(t). \tag{3.17}$$

The *air gap torque* is given by $M_\delta = \frac{1}{2}\sum_{k=1}^{6} \frac{\partial \ell_k(\epsilon(t))}{\partial \epsilon} \cdot (i^k(t))^2$. Together with the bottom plot of Figure 3.4, it can be seen that the derivatives of the inductivities, $\frac{\partial \ell_k}{\partial \epsilon}$, $k = 1, \dots, 6$ influences the value and also the sign of the terms in M_δ. To generate a positive torque with minimal effort, coils for which the inductivity is momentarily increasing have to be energized. Depending on the position, this can be up to three coils at the same time.

3.4.2 Optimal Operating Point Control

For the switched reluctance drive, we are interested in optimal controls for a given operating point, i.e. a given constant torque M_L. This is a so called quasi stationary point, because a constant rotational velocity of the drive is required, i.e. $\dot{\epsilon}(t) = \omega(t) = \text{const}$. This simplifies the Euler-Lagrange equation (3.17) to $M_L(t) = \frac{1}{2}\sum_{k=1}^{6} \frac{\partial \ell_k(\epsilon(t))}{\partial \epsilon} \cdot (i^k(t))^2$, such that it can be regarded as a constraint in the optimal control problem.

Optimal Control Problem The cost functional is given by the losses in each coil of the six phases, i.e. $J(i) = \int_0^T \sum_{k=1}^{6} R \cdot (i^k)^2(t)\, dt$, and does not directly depend on the controls u^k. However, it is, of course, indirectly dependent on the controls through the currents, since a specific supply voltage is necessary to guarantee a given torque at any time. The final time T corresponds to a full electrical period and is defined by the desired rotational speed of the drive. Together with box constraints on the voltage, defined by u_{max} and thermic constraints on the currents given by

i_{max}, we are faced with the following optimal control problem

$$\begin{aligned}
&\min_{i^1,\dots,i^6,u^1,\dots,u^6} J(i) = \int_0^T \sum_{k=0}^{6} R \cdot (i^k(t))^2 \, dt \\
\text{w.r.t. } &\ell_k(\epsilon(t)) \frac{d}{dt} i^k(t) = -\frac{\partial \ell_k(\epsilon(t))}{\partial \epsilon} \dot{\epsilon}(t) \cdot i^k(t) - R \cdot i^k(t) + u^k(t), \quad \text{for } k = 1, \dots, 6, \\
&M_L(t) = \frac{1}{2} \sum_{k=1}^{6} \frac{\partial \ell_k(\epsilon(t))}{\partial \epsilon} \cdot (i^k(t))^2 \qquad \forall t \in [0, T], \\
&|u^k(t)| \leq u_{\max} \text{ and } 0 \leq i^k(t) \leq i_{\max} \qquad \forall\, t \in [0, T], \quad \text{for } k = 1, \dots, 6, \\
&i^k(0) = i^k(T) \qquad \text{for } k = 1, \dots, 6.
\end{aligned}$$

The boundary terms originate from a periodicity constraint, i.e. we are searching for a control signal that can be applied periodically. Therefore, initial and final value of the currents have to coincide.

Discretization We discretize the system's charges and the voltage control according to the DMOC principle (cf. Section 3.3) choosing a time grid $\Delta t = \{t_0, t_1, \dots, t_N\}$ with step size h and the midpoint rule for the approximation of the integrals, i.e.

$$\begin{aligned}
L_d(q_n, q_{n+1}, \epsilon_n, \epsilon_{n+1}) &= h \cdot L\left(\frac{q_{n+1} + q_n}{2}, \frac{q_{n+1} - q_n}{h}, \frac{\epsilon_{n+1} + \epsilon_n}{2}\right) \\
&\approx \int_{nh}^{(n+1)h} L(q, i, \epsilon) \, dt \quad \text{for } n = 0, \dots, N-1.
\end{aligned}$$

Together with a discretization of the forcing term, the discrete Euler-Lagrange equations read

$$\begin{aligned}
&\ell_k\left(\frac{\epsilon_n + \epsilon_{n-1}}{2}\right) \cdot \frac{q_n^k - q_{n-1}^k}{h} - \ell_k\left(\frac{\epsilon_{n+1} + \epsilon_n}{2}\right) \cdot \frac{q_{n+1}^k - q_n^k}{h} \\
&- \frac{1}{2} R \cdot (q_{n+1}^k - q_{n-1}^k) + h \cdot (u_{n-1}^k + u_n^k) = 0
\end{aligned}$$

for $n = 1, \dots, N-1$ and $k = 1, \dots, 6$. For the discrete cost functional, we have

$$J_d(q_d) = h \sum_{k=1}^{6} \sum_{n=0}^{N-1} R \left(\frac{q_{n+1}^k - q_n^k}{h}\right)^2.$$

Analogously, the constraints have to be discretized to transform the optimal control problem into a nonlinear constrained optimization problem.

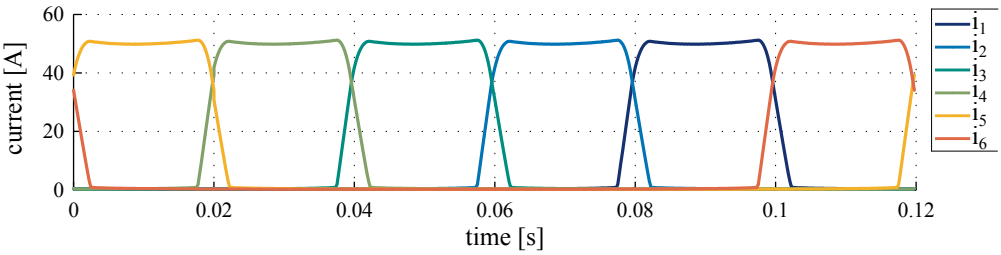

Figure 3.5: Optimized current profiles for an operation point of the switched reluctance drive with a motor torque of 100 Nm and a rotational speed of 50 min^{-1}.

Implementation and Numerical Results The previously described steps are implemented in *C*. Derivatives are computed by the algorithmic differentiation software ADOL-C[6] (*Automatic Differentiation by OverLoading in C++*) (cf. [GW08]) and passed to the state of the art nonlinear optimization solvers NAG[7] and Ipopt[8] (cf. [WB06]).

The numerical results (cf. Figure 3.5 for an example) show a symmetry of the currents in the coils, i.e. for $\overline{T} = \frac{T}{6}$, it holds $i^k(t+\overline{T}) = i^{k+1}(t)$ for $t \in \Delta t$, $k = 1, \ldots, 5$ and $i^6(t+\overline{T}) = i_1(t)$. This is in accordance with the construction of the drive, which is symmetric w.r.t. rotations of 60° electrical angle[9]. Therefore, the complexity can be reduced by solving the optimal control problem on the shorter time interval $[0, \overline{T}]$ and replacing the boundary condition by $i^{k+1}(0) = i^k(\overline{T})$, $k = 1, \ldots, 5$ and $i^1(0) = i^6(\overline{T})$.

Validation at Test Rig In Figure 3.6, the structure of the control strategy is sketched. The optimal current profiles serve as a feed forward trajectory. They are computed for several combinations of rotational speeds and load torques (see Figure 3.7a for an exemplary operation point with a motor torque of 100 Nm and a rotational speed of 50 min^{-1}) and are stored in a data table that is used for a validation at the test rig. An underlying feedback loop is added with six independent PI controllers for the current in the phases. Tests validate that the drive is indeed able to follow the precomputed current profiles very well (cf. Figure 3.7b and [FOR+11] for a detailed discussion of the control strategy's performance).

Finally, the optimal control solution for an exemplary operation point is applied to

[6] https://projects.coin-or.org/ADOL-C

[7] Numerical Algorithms Group (NAG): www.nag.co.uk/

[8] Ipopt is an open source software for nonlinear optimization and uses HSL, a collection of Fortran codes for large-scale scientific computation. See www.hsl.rl.ac.uk.

[9] This is a discrete symmetry, i.e. the corresponding symmetry group consists of a finite number of elements, and should not be mixed up with the continuous symmetries studied in Section 2.3.

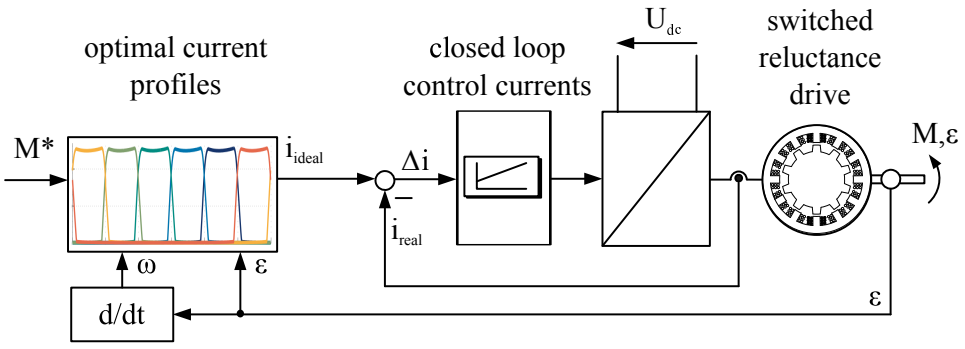

Figure 3.6: Sketch of the control strategy: the optimal current profiles are used as feedforward trajectories and are combined with an individual feedback controller for the current in each coil.

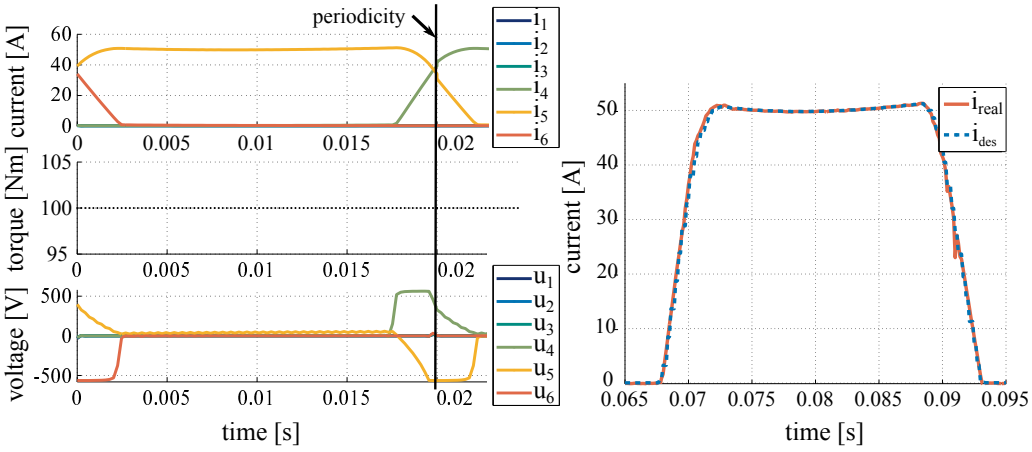

(a) Optimal current and voltage profiles.

(b) Desired trajectory and real trajectory of one phase current.

Figure 3.7: Optimal solution for an operation point with 50 min^{-1} and an air gap torque of 100 Nm and comparison between desired trajectory (dashed) and real trajectory (solid) of one phase current.

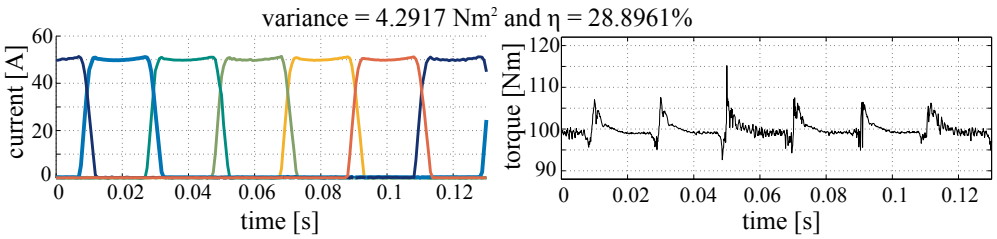

Figure 3.8: Measurements of the torque and the real currents of the reluctance drive using the optimal current profiles via the control strategy of Figure 3.6. The performance of the strategy is very good in variance of the torque as well as in efficiency η of the drive.

the test rig for several periods in order to validate its performance regarding variance and efficiency compared to state of the art control techniques (as e.g. proposed in [Kri01]). The efficiency of the drive η is calculated as the ratio of the mechanical motor power and the electrical input power, thus considering not only the losses in the copper coils, but also in the inverters. The variance of the torque is used as a quality criterion to determine to what extend the desired motor torque is kept constant in the real system. Here, the motor torque is measured via a torque shaft at the test rig. A comparison with solutions obtained by state of the art control concepts (cf. [FOR+11] for details) shows that the control strategy with optimal current profiles is a good compromise between efficiency and uniformity of the motor torque (see Figure 3.8). Recall that the motor torque is perfectly constant up to numerical accuracy in the optimal solution for the ideal case, since it was considered as a constraint in the optimal control problem (cf. Figure 3.7a). However, at the real test rig, the motor torque has a variance of 4.2917 Nm^2. The highest errors can be traced back to the limited dynamics of the feedback regulators that overshoot when the current is rapidly commutated. Since the currents influence the torque quadratically and two currents are non-zero at all times, even small deviations lead to significant ripple in the torque (cf. the small deviation of the measured current to the desired current profile in Figure 3.7b between 0.07 s and 0.0725 s and the corresponding periodicity of the errors in Figure 3.8). The amount of variance of the desired torque is still acceptable, though. The low efficiency of less than 30% is caused by the specific operating point with low rotational speed and load and also because the motor geometry is based on the RailCab system, which requires a large air gap of 12 mm due to wear and tear of the wheels and tracks. Even with purely efficiency oriented control concepts (i.e. block shaped desired current profiles which are non admissible to the drive's dynamics) one cannot provide more than 30% efficiency and this control strategy comes with the drawback of a much higher variance. The concept of [Kri01] (applied to the switched reluctance drive

in [FOR+11]) reduces the variance by using wider but lower current profiles, but has a poor efficiency of only 14.5%.

In conclusion, these results validate the benefit of the optimal control approach based on discrete variations in this application. Two possible directions of future research are at hand. Firstly, in the field of electrical drive systems, reluctance drives that are able to work with smaller air gaps than the RailCab's drives considered here are of particular interest. Such drives would have to be modeled with nonlinear inductances, which qualitatively change the Euler-Lagrange equations and thus, may also influence the performance of the optimal control method. Secondly, the applicability and the performance of the *DMOC–method for electro-mechanical systems* have to be evaluated further in other applications arising in the optimal control of mechatronic systems.

CHAPTER 4

Energy Optimal Control by Exploiting Inherent Dynamics

In this chapter, we begin to address one of the pivotal points of this thesis: how can *inherent dynamical properties* of dynamical systems be efficiently exploited for control purposes? Specifically, we focus on *energy optimal control* for mechanical systems. As mentioned in the introduction of this thesis, numerical tools for the analysis and control of spacecrafts have been successfully combined in space mission design in the past years. Based on these motivating examples, in this chapter we develop similar techniques for the optimal control of mechanical systems, using double pendula as illustrating examples. The methodology is based on numerical tools for the global analysis of dynamical systems (introduced in Section 4.1) and on the optimal control method DMOC (cf. Section 3.3).

In contrast to linear systems, nonlinear dynamical systems may exhibit complicated dynamical structures, e.g. local attractors or invariant manifolds (cf. [GH83], for instance) that "organize" the state space. These structures are typically not at all obvious up to a careful and systematic analysis. The effort for this analysis is justified though, since it may reveal motions of the unforced system that can be of great interest in control problems when searching for energy efficient solutions. In Section 4.3, it is shown how sequences of trajectories, partly moving along (un)stable manifolds, can be generated using optimal control techniques. In the second step of the approach, these sequences are used as *sophisticated initial guesses for a post optimization*. For the double pendula examples, we show that this procedure outperforms a "black-box optimization" with a simple, e.g. linearly interpolated, initial guess, that does not use any knowledge of the inherent system properties.

The sequencing of uncontrolled solutions on (un)stable manifolds with appropriate controlled maneuvers is an example of a *hybrid control strategy*. This concept

is later generalized in the motion planning approach based on motion primitives, which is introduced in Chapter 5.

4.1 Global Dynamics of Mechanical Systems

In this section, we give a short review of methods to analyze the system's *natural dynamics*, i.e. the unforced dynamics of e.g. a mechanical system. More precisely, we will formally introduce the concept of invariant (un)stable manifolds. (Un)stable manifolds are dealt with in a number of textbooks on dynamical systems (cf. [GH83, KH98], for instance, or [AM87] for a notation tailored to mechanics). The following definitions are basically taken from the latter with a slightly different notation at some points.

Consider a Lagrangian vector field X_L on the tangent bundle TQ with flow $F_L^t : TQ \to TQ$. A *critical element* is either an *equilibrium*, i.e. a point $\bar{x} \in TQ$ such that $X_L(\bar{x}) = 0$ and, hence, $F_L^t(\bar{x}) = \bar{x}$ for all $t \in \mathbb{R}$, or a *closed orbit*, i.e. the orbit of a periodic point (it holds $F_L^t(\bar{x}) = F_L^{t+\tau}(\bar{x})$ with $\tau > 0$ being the smallest value that satisfies this condition). In the following, a critical element is denoted by γ.

Given an equilibrium $\bar{x}$, we are interested in the eigenvalues of $X_L'(\bar{x})$, i.e. the *linearization* of X_L at $\bar{x}$, $X_L'(\bar{x}) : T_{\bar{x}}(TQ) \to T_{\bar{x}}(TQ)$ defined by $X_L'(\bar{x}) \cdot v = \frac{d}{dt}(TF_L^t(\bar{x}) \cdot v)\big|_{t=0}$. In coordinates, the matrix $X_L'(\bar{x})$ is given by $\left(\frac{\partial X_L^i}{\partial x^j}\right)\Big|_{x=\bar{x}}$. It is a well known stability criterion that a system is asymptotically (un)stable if all eigenvalues have strictly negative (positive, respectively) real parts. In the following, we will study the case where there are eigenvalues on both sides of the imaginary axis. An equilibrium is called *hyperbolic*, if none of the eigenvalues has zero real part.

To investigate the dynamic behavior near closed orbits, the Poincaré map of a transversal section S is studied. A *transversal section* of X_L at a point x on the orbit is a submanifold $S \subset TQ$ of codimension one with $x \in S$ and for all $s \in S$, $X_L(s)$ is not contained in T_sS. Then, roughly speaking, the *Poincaré map* of a closed orbit γ is a diffeomorphism Θ between neighborhoods of x in S that assigns to each neighboring point $s \in S$ the point, where the orbit $F_L^{\rho(s)}(s)$ intersects S again for the first time. Here, $\rho(s)$ is the corresponding return time. For a detailed introduction of Poincaré maps we refer to [AM87], for instance. Having identified a closed orbit γ of a vector field X_L, the *characteristic multipliers* of X_L at γ are the eigenvalues of $T_x\Theta$ for any Poincaré map Θ at any $x \in \gamma$. γ is called *hyperbolic*, if none of the characteristic multipliers has modulus one. Analogous to the stability criterion of Lyapunov for equilibria, a periodic orbit is asymptotically (un)stable, if the modulus of all characteristic multipliers is less (greater, respectively) than one.

4.1.1 (Un)Stable Invariant Manifolds

The following theorem is taken from [AM87]. For an earlier reference on the existence of stable and unstable invariant manifolds for *hyperbolic* invariant sets (e.g. hyperbolic equilibria), we refer to [HPS77] and the discussion of previous works therein (see [HPS77, Section 1]).

Theorem 4.1: If $\gamma \subset TQ$ is a critical element of X_L, there exist submanifolds of TQ, i.e. local stable (W^s_{loc}), center-stable (W^{cs}_{loc}), center (W^c_{loc}), center-unstable (W^{cu}_{loc}), and unstable (W^u_{loc}) manifolds, respectively, with the following properties:

(i) each submanifold is invariant under X_L and contains γ,

(ii) For $x \in \gamma$, $T_x(W^s_{\text{loc}})$ is the sum of the eigenspace in $T_x(TQ)$ of the characteristic multipliers of modulus < 1 and the subspace $T_x\gamma$;
$T_x(W^{cs}_{\text{loc}})$ (and $T_x(W^c_{\text{loc}})$, $T_x(W^{cu}_{\text{loc}})$, $T_x(W^u_{\text{loc}})$, respectively) is the sum of the eigenspace in $T_x(TQ)$ of the characteristic multipliers of modulus ≤ 1 (and $= 1, \geq 1, > 1$, respectively) and the subspace $T_x\gamma$.

(iii) If $x \in W^s_{\text{loc}}$, then the ω-limit[1], given by $\omega(x) = \bigcap_{T=0}^{\infty} \overline{(\bigcup_{t \geq T} F_L^t(x))}$, is equal to γ.
If $x \in W^u_{\text{loc}}$, then the α-limit is γ, with $\alpha(x) = \bigcap_{T=0}^{-\infty} \overline{(\bigcup_{t \leq T} F_L^t(x))}$.

(iv) W^s_{loc} and W^u_{loc} are locally unique.

Thus, all points of the local stable manifold W^s_{loc} tend to the critical element under the evolution. Conversely, the local unstable manifold W^u_{loc} consists of all points in TQ which show this behavior if time runs backwards. The dynamics on the center manifold is subject to a further analysis (see e.g. [AM87] and the references therein) but this is out of the scope for this work.

Remark 4.2: In case of a critical point, i.e. an equilibrium $\gamma = \bar{x}$, the tangent space is trivial, $T_{\bar{x}}\gamma = \{0\}$ and therefore, $T_{\bar{x}}(W^s_{\text{loc}})$ equals the eigenspace in $T_{\bar{x}}(TQ)$ of the characteristic multipliers of modulus < 1. Further, for $\gamma = \bar{x}$, the characteristic multipliers have to be interpreted as the eigenvalues of $T_{\bar{x}}F_L^t$, i.e. $\mathrm{e}^{t\lambda_1}, \ldots, \mathrm{e}^{t\lambda_n}$ where $\lambda_1, \ldots, \lambda_n$ are the eigenvalues of $X_L'(\bar{x})$ (also called characteristic exponents). In other words, the stable manifold W^s_{loc}, for example, is defined by the eigenvalues that lie in the strict left plane ($\mathfrak{Re}(\lambda_i) < 0$). Concretely, for some neighborhood $U_{\bar{x}}$

[1] For this definition of the ω- and α-limit set, we refer to [KH98].

of $\bar{x}$, we have

$$W^s_{\mathrm{loc}}(\bar{x}) = \{x \in U_{\bar{x}} \,|\, F^t_L(x) \to \bar{x} \text{ for } t \to \infty \text{ and } F^t_L(x) \in U_{\bar{x}}\, \forall t \geq 0\}\,, \text{ and}$$
$$W^u_{\mathrm{loc}}(\bar{x}) = \{x \in U_{\bar{x}} \,|\, F^t_L(x) \to \bar{x} \text{ for } t \to -\infty \text{ and } F^t_L(x) \in U_{\bar{x}}\, \forall t \leq 0\}.$$

Of special interest is the hyperbolic case, where there are no center eigenspaces. Then, the orbits in the neighborhood of γ behave qualitatively like the linear case, i.e. for a hyperbolic critical point, the flow nearby looks like that of the linearization at γ. The following corollary, which goes back to Smale (cf. e.g. [AM87]), shows how the local (un)stable manifolds can be expanded to global manifolds by applying the flow of the vector field.

Corollary 4.3: If γ is hyperbolic, then the stable manifold, $W^s(\gamma) = \{x \in TQ \,|\, \omega(x) \subset \gamma\}$ and the unstable manifold, $W^u(\gamma) = \{x \in TQ \,|\, \alpha(x) \subset \gamma\}$ are immersed submanifolds. Also, $\gamma \subset W^s(\gamma) \cap W^u(\gamma)$ and for $x \in \gamma$, $T_x W^s(\gamma)$ and $T_x W^u(\gamma)$ generate $T_x(TQ)$. If n_s is the number of characteristic multipliers of γ of modulus < 1, and n_u the number of modulus > 1, then the dimension of $W^s(\gamma)$ (of $W^u(\gamma)$, respectively) is n_s (n_u, respectively) if γ is a critical point, or $n_s + 1$ ($n_u + 1$, respectively) if γ is a closed orbit.

(Un)Stable Manifolds of Lagrangian Systems So far, we have not uncovered all of the structure of critical points of Lagrangian systems. Recall that a regular Lagrangian system can be transformed into a Hamiltonian system by the Legendre transformation (cf. Section 2.1.4). From the Euler-Lagrange equations interpreted as a system of first order differential equations in the variables (q, v), it directly follows that an equilibrium $\bar{x}$ satisfies $\bar{x} = (\bar{q}, 0)$. Considering a Lagrangian of the form $L(q, v) = \frac{1}{2} v^T M(q) v - V(q)$ with corresponding Hamiltonian $H(q, p) = \frac{1}{2} p^T M(q)^{-1} p + V(q)$, it follows that $\bar{p} = 0$ holds as well (since $M(\cdot)$ is assumed to be regular for all $q \in Q$) and $\bar{q}$ is determined by $\frac{\partial}{\partial q} V(\bar{q}) = 0$.

It is a well known result (see e.g. [AM87]), that the linearization of a Hamiltonian system is a linear Hamiltonian system. Therefore, if λ is an eigenvalue of $X'_H(\bar{x})$, then so are $\bar{\lambda}, -\lambda$ and $-\bar{\lambda}$, i.e. the eigenvalue spectrum is symmetric w.r.t. to both, the real and the imaginary axis. Consequently, stable and unstable manifolds of a critical point always have the same dimension and the center manifold, if it exists, is even dimensional. Additionally, for a Lagrangian that equals kinetic minus potential energy, solely the second-order partial derivatives of the potential, i.e. $\frac{\partial^2}{\partial q^2} V(\bar{q})$ determine the spectral characteristics. From the Lagrange-Dirichlet stability criterion (see e.g. [AM87, Mar93]), it follows that the system is stable, if the matrix $\frac{\partial^2}{\partial q^2} V(\bar{q})$ evaluated at the equilibrium is positive definite. Then, the eigenvalues lie on the imaginary axis. Otherwise, the system is unstable because there has to be at least

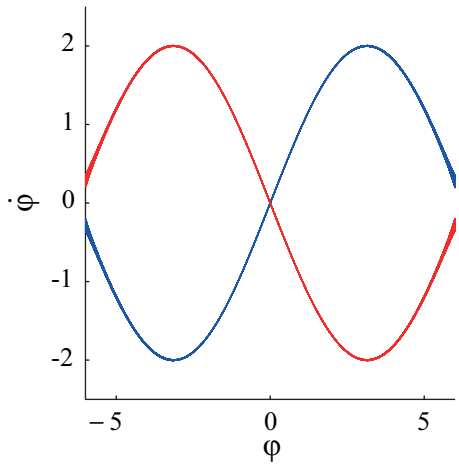

(a) Stable (red) and unstable (blue) manifold of the simple planar pendulum.

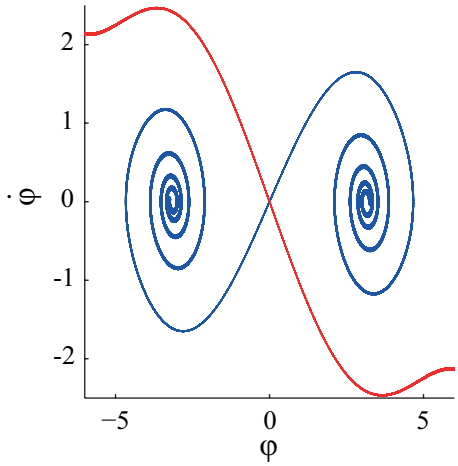

(b) Stable (red) and unstable (blue) manifold of the damped planar pendulum.

Figure 4.1: (Un)stable manifolds of the undamped and damped pendulum's upward equilibrium $(\bar{\varphi}, \dot{\bar{\varphi}}) = (0, 0)$, computed by GAIO.

one eigenvalue with positive real part giving rise to an unstable manifold.

Numerical Computation of (Un)Stable Manifolds In most cases, it is not possible to compute global invariant manifolds analytically. For that reason, a number of numerical techniques for approximating (un)stable manifolds have been developed within the last decades (see [KOD+05] for an overview of existing approaches and a comprehensive comparison of the methods for the example of the Lorenz system). The different methods all share the idea to successively grow the (un)stable manifold from a local neighborhood of the equilibrium. Among these techniques is the software package GAIO[2] (*Global Analysis of Invariant Objects*, cf. [DFJ01, DJ02]), which is based on set-oriented methods for approximating the invariant objects by box-coverings. A short description of the continuation algorithm for invariant manifolds, which we will use in the following examples, is given in Section B.1 in the appendix. GAIO has been used for the computation of invariant manifolds in [DJPT06] and [DOP+09], for instance. In these works, (un)stable manifolds have been used to compute low energy trajectories for space mission design problems.

Example 4.4 (Hamiltonian Planar Pendulum)**:** The simplest version of a mathematical pendulum is a single, planar pendulum without any damping. This results in a one-degree-of-freedom Hamiltonian system, i.e. an energy preserving sys-

[2] www.math.upb.de/~agdellnitz

tem[3]. Its Lagrangian is given by $L(\varphi, \dot{\varphi}) = \frac{1}{2}mr^2\dot{\varphi}^2 - mgr(\cos(\varphi) + 1)$, where φ denotes the angle, measured from the upright position, r is the length of the massless rod, m the mass, concentrated at the tip of the rod and g denotes the gravitational constant. Computing the Euler-Lagrange equation, we receive the well known pendulum equation $\ddot{\varphi}(t) = \frac{g}{r} \cdot \sin(\varphi)$ of second order. The two-dimensional system of first order has two fixed points, the upright equilibrium $\bar{x}^0 = (\varphi^0, \dot{\varphi}^0) = (0, 0)$ and the downward equilibrium $\bar{x}^1 = (\varphi^1, \dot{\varphi}^1) = (\pi, 0)$. Analyzing the eigenvalue spectra at the corresponding linearization reveals that the downward equilibrium is stable while the upright equilibrium possesses one-dimensional stable and unstable manifolds. These can be computed analytically (without knowing the Lagrangian flow explicitly) by use of the energy conservation, i.e. for all $x \in W^s(\bar{x}^0) \cup W^u(\bar{x}^0)$ it holds $E(x) = E(\bar{x}^0) = 2mgr$ and from that it follows $\dot{\varphi} = \pm\sqrt{2\frac{g}{r}(1 - \cos(\varphi))}$. Locally around $\bar{x}^0$, the stable manifold is given by $W^s_{\text{loc}}(\bar{x}^0) = \left\{x = (\varphi, \dot{\varphi}) \,|\, \dot{\varphi} = -\text{sign}(\varphi)\sqrt{2\frac{g}{r}(1 - \cos(\varphi))}\right\}$. However, globally, the stable and unstable manifolds form homoclinic orbits, i.e. connecting orbits from $\bar{x}^0 = (\varphi^0, \dot{\varphi}^0) = (0, 0)$ to $\bar{x}^2 = (\varphi^0, \dot{\varphi}^0) = (2\pi, 0)$, for instance, due to the 2π-periodicity of the pendulum. In Figure 4.1a, a numerical approximation of the manifolds is shown, which has been computed by GAIO for normalized parameters $l = m = g = 1.0$. By a closer look, one observes that the manifolds grew thicker while tending away from $(0, 0)$. This is caused by numerical inaccuracies due to the homoclinic connection in this Hamiltonian system (cf. [Jun00] for a detailed study of this property) – an interesting effect which is, however, not in the scope of this thesis.

Example 4.5 (Damped Planar Pendulum)**:** Damping effects, e.g. due to air drag or friction in the joint can be modeled by a Lagrangian forcing $f_L(\varphi, \dot{\varphi}) = -d\dot{\varphi}$ with $d > 0$. This leads to the modified second order differential equation $\ddot{\varphi}(t) = \frac{g}{r} \cdot \sin(\varphi) - \frac{d}{mr^2}\dot{\varphi}$. The system is not energy preserving anymore and thus shows a qualitatively different dynamical behavior. The downward equilibrium is asymptotically stable and the eigenvalue spectrum of the upright equilibrium is not symmetric anymore, but still has one stable and one unstable eigenvalue. In Figure 4.1b, the numerical approximation of the stable and unstable manifolds, computed by GAIO is depicted for $d = 0.2$ and all other parameters as before. Compared to the undamped case, the symmetry of stable and unstable manifold is broken: points on the stable manifold need higher velocities now to reach the equilibrium due to the energy dissipation caused by the damping. The unstable manifold spirals around the stable downward equilibrium and never reaches the upwards position again.

[3]It is identical to the spherical pendulum, which as been introduced before in Example 2.6, when this system is restricted to $(\theta, \dot{\theta}) = (0, 0)$.

4.1.2 Strong (Un)Stable Manifolds

On an (un)stable manifold of dimension higher than one, the dynamics can sometimes be investigated further. Here, strong (un)stable manifolds (cf. e.g. [OLT04]) can be identified as the regions of the state space with the highest contraction to or expansion from the fixed point. In this section, for shortness of notation, let us consider a dynamical system of general form[4] $\dot{x} = \mathcal{F}(x)$. Then, let λ^{uu} be the eigenvalue with largest real part of the linearization at an equilibrium[5] $\bar{x} = 0$ and we assume λ^{uu} to be unique. Thus, the corresponding eigenvector v^{uu} spans the one-dimensional, so called *strong unstable eigenspace*, i.e. it shows the direction with fastest expansion from the fixed point in forward time of the linear system. The *strong unstable manifold* of the nonlinear system is tangent to v^{uu} at $\bar{x}$ and a one-dimensional submanifold of the unstable manifold. Analogously, *strong stable manifolds* correspond to (unique) eigenvalues λ^{ss} with smallest real part.

Numerical Computation of Strong (Un)Stable Manifolds For the computation of strong (un)stable manifolds, GAIO can be used in combination with a system transformation. We shortly sketch the idea for the computation of strong stable manifolds. Let us assume we have n eigenvalues and a unique smallest eigenvalue λ^{ss}, i.e. $\mathfrak{Re}(\lambda^{ss}) < \mathfrak{Re}(\lambda_2) \leq \ldots \leq \mathfrak{Re}(\lambda_n)$ and $\mathfrak{Re}(\lambda^{ss}) < \mathfrak{Re}(\lambda_2) < 0$, i.e. there exists a stable manifold of dimension two at least. As a prerequisite to the application of GAIO, the original dynamical system has to be transformed appropriately. The aim is to shift its eigenvalue spectrum at the fixed point $\bar{x} = 0$ to the right until λ^{ss} is the last remaining eigenvalue on the left side of the complex plane. Therefore, a parameter $\mu \in \mathbb{R}$ is chosen that satisfies $|\mathfrak{Re}(\lambda^{ss})| < \mu < |\mathfrak{Re}(\lambda_2)|$. Then, the system is transformed by setting $\tilde{x}(t) := \exp(\mu t)x(t)$ leading to the differential equation

$$\dot{\tilde{x}}(t) = \mu\tilde{x}(t) + \exp(\mu t)\mathcal{F}(\exp(-\mu t)\tilde{x}(t)) =: \tilde{\mathcal{F}}(t, \tilde{x}).$$

Corollary 4.6: The transformed system $\dot{\tilde{x}}(t) = \tilde{\mathcal{F}}(t, \tilde{x})$ still has 0 as a fixed point, but the eigenvalue spectrum of the linearization at 0 is shifted by μ to the right.

Proof. Evaluating $\tilde{\mathcal{F}}(t, \tilde{x})$ at $\bar{\tilde{x}} = 0$ yields $\tilde{\mathcal{F}}(t, \bar{\tilde{x}}) = 0$ and thus, zero is an equilibrium

[4] For any mechanical system with regular Lagrangian $L(q, v) = \frac{1}{2}v^T M(q)v - V(q)$ the vector field $\mathcal{F} : x = (q, v) \mapsto \mathcal{F}(x)$ is obtained by $\mathcal{F}(q, v) = \begin{pmatrix} v \\ M(q)^{-1} \cdot \left(\frac{\partial L}{\partial q} - \frac{\partial}{\partial q}(M(q)v\right) \end{pmatrix}$.

[5] We can assume $\bar{x} = 0$ without loss of generality, since any system with a fixed point $\bar{x} \neq 0$ can be shifted such that $\bar{x} = 0$ is the equilibrium.

for any $t \in \mathbb{R}$. The linearization of $\tilde{\mathcal{F}}$ at $\bar{\tilde{x}} = 0$ is

$$\frac{\partial}{\partial \tilde{x}} \tilde{\mathcal{F}}\Big|_{\bar{\tilde{x}}=0} = \mu \cdot \mathbb{1} + \exp(\mu t) \cdot \frac{\partial}{\partial x} \mathcal{F}\Big|_{\bar{x}=0} \cdot \exp(-\mu t) \cdot \mathbb{1}.$$

So, $\tilde{\lambda}$ is an eigenvalue of $\frac{\partial}{\partial \tilde{x}} \tilde{\mathcal{F}}\Big|_{\bar{\tilde{x}}=0}$ if and only if

$$\det\left(\tilde{\lambda} \cdot \mathbb{1} - \frac{\partial}{\partial \tilde{x}} \tilde{\mathcal{F}}\Big|_{\bar{\tilde{x}}=0}\right) = 0 \quad \Leftrightarrow \quad \det\left((\tilde{\lambda} - \mu) \cdot \mathbb{1} - \frac{\partial}{\partial x} \mathcal{F}\Big|_{\bar{x}=0}\right) = 0,$$

that is $\tilde{\lambda} - \mu$ is an eigenvalue of the linearization of $\mathcal{F}$ at $\bar{x} = 0$. Since μ is chosen to satisfy $|\mathfrak{Re}(\lambda^{ss})| < \mu < |\mathfrak{Re}(\lambda_2)|$, we have $\tilde{\lambda}^{ss} = \lambda^{ss} + \mu$ and thus $\mathfrak{Re}(\tilde{\lambda}^{ss}) < 0$, but $\mathfrak{Re}(\tilde{\lambda}_2), \ldots, \mathfrak{Re}(\tilde{\lambda}_n) > 0$. □

Then, GAIO can be applied to the transformed system, which is non-autonomous (for a study of invariant manifolds in non-autonomous systems, cf. [ARS05, ARS06]). For the implementation, the time is considered as an additional variable $\theta(t)$ with differential equation $\frac{d}{dt}\theta(t) = 1$. Finally, the resulting stable manifold of the non-autonomous system can be transformed back, yielding an approximation of the strong stable manifold of the original system (cf. [Sch99] for a detailed discussion on the computation of strong stable manifolds and implementation details for GAIO).

In order to use the manifolds for the design of optimal control maneuvers, trajectories on the (un)stable or strong (un)stable manifolds have to be generated. This is explained in detail in Section 5.4 in the context of motion primitives on (un)stable manifolds. At the moment, we just assume to have an appropriate method at hand.

Example 4.7 (Stable and Strong Stable Manifold of a Double Pendulum)**:** Here, we use a double pendulum system that models the dynamics of the double pendulum subsystem of a real test rig (cf. [TKOT11]). Details on its geometry and system parameters can be found in Section C.1 in the appendix. The double pendulum has four equilibria, in which each of the pendulum's arms point straight up- or downwards. The *up-up equilibrium* is the position where both of the pendulum's arms points upwards – in coordinates, this is $\bar{x} = (\varphi_1^0, \varphi_2^0, \dot{\varphi}_1^0, \dot{\varphi}_2^0) = (0, 0, 0, 0)$. The linearization of the dynamics at this point has two stable and two unstable eigenvalues, so the fixed point is a hyperbolic equilibrium. Thus, it follows from Theorem 4.1 and the succeeding corollary that the system has two-dimensional stable and unstable manifolds. In Figure 4.2a, an approximation of the stable manifold is shown, which has been computed by GAIO. The three axes show the projection on the φ_1, φ_2 and $\dot{\varphi}_1$ coordinates, while the fourth coordinate, $\dot{\varphi}_2$, defines the color coding. One observes that the box collection is indeed – approximately – a two dimensional object. The red and blue lappets, which correspond to areas with high velocity in

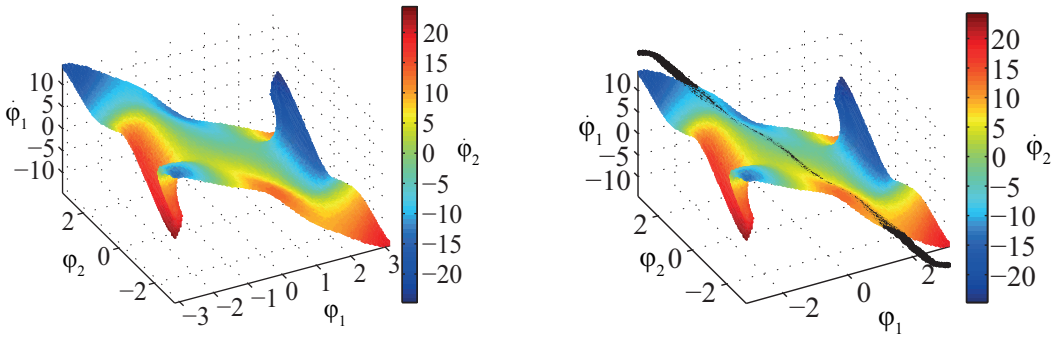

(a) Stable manifold of the up-up equilibrium.

(b) Strong stable manifold of the up-up equilibrium (black)

Figure 4.2: Approximations of the stable and strong stable manifolds (excerpts on $(\varphi_1, \varphi_2) \in [-\pi, \pi] \times [-\pi, \pi]$) of the double pendulum's up-up equilibrium $\bar{x} = (\varphi_1^0, \varphi_2^0, \dot{\varphi}_1^0, \dot{\varphi}_2^0) = (0, 0, 0, 0)$, computed by GAIO.

both angles, tend in the direction of the position of the down-down equilibrium, but with increasing velocities. In the next step, we compute the strong stable manifold using GAIO for the transformed system, as explained above. Its approximation is depicted in Figure 4.2b in black. As one can see, it forms a submanifold of the stable manifold. A trajectory along the strong stable manifold will be used to design an energy efficient swing-up of the double pendulum in the following section.

4.2 Control Strategies on (Un)Stable Manifolds

In this section, we describe the general idea of the control methodology, which aims at computing energy efficient controlled trajectories partly using the strong stable manifold orbit. Since the solutions strongly depend on the maneuver's duration, we compare the results regarding time duration as a second objective in a multiobjective fashion. Afterwards, the approach is validated for two different double pendulum examples. This work has been done in cooperation with the *Chair of Control Engineering and Mechatronics*[6]*, Heinz Nixdorf Institute, University of Paderborn* and has been published in [FTO+12] and [FTOT13].

Our control approach basically consists of the following steps:

1. At first, relevant equilibria of the system under consideration have to be identified.

[6] www.hni.uni-paderborn.de/rtm/

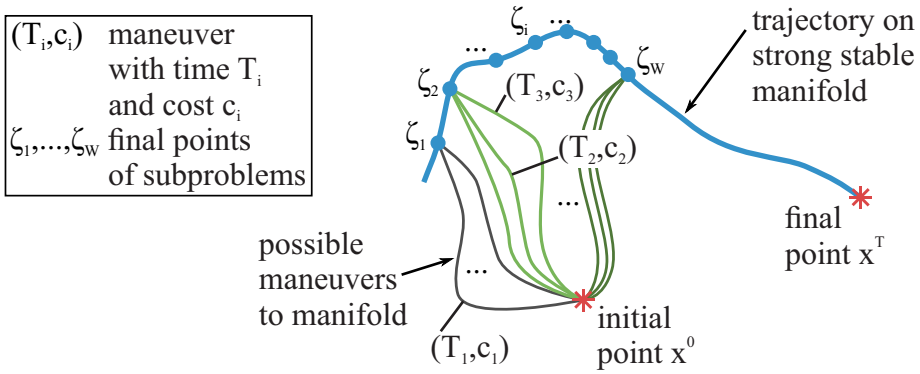

Figure 4.3: Sketch of different sequences comprised of controlled maneuvers and trajectories on the strong stable manifold, e.g. a maneuver with time T_1 and costs c_1 to the point ζ_1 on the manifold orbit concatenated with the uncontrolled trajectory from ζ_1 to x^T forms an admissible sequence. Alternative sequences can be generated e.g. with either the maneuver (T_2, c_2) or (T_3, c_3) to the intermediate point ζ_2 together with a trajectory on the manifold orbit $\Delta\tau$ shorter in time.

2. For those points, (un)stable manifolds are computed and appropriate trajectories on these manifolds are chosen and stored.

3. Optimal control subproblems for maneuvers that start or end on the manifold trajectories are formulated and then solved numerically. The resulting maneuvers can be sequenced with appropriate pieces of the manifold trajectories.

4. In the final step, the sequences can be used as initial guesses for a post optimization of the original problem.

We start with a discussion of the approach's first and second step. In engineering applications, operating points of dynamical systems often coincide with the system's equilibria or periodic solutions. Thus, a typical control task is to steer the system from one operating point to another. Methods for the computation of (un)stable manifolds for these equilibria and the generation of trajectories have been presented in the previous section. In the following, we denote the exemplary manifold orbit by $x_{\mathrm{mnf}} : [0, T_{\mathrm{mnf}}] \ni t \mapsto x_{\mathrm{mnf}}(t)$ with T_{mnf} being a fixed final time.

The trajectories on the manifolds are advantageous for the design of energy efficient maneuvers, because the system moves without control effort on them. However, such trajectories alone do not provide admissible solutions to the control problem, in general. Therefore, in the next step, control subproblems have to be formulated that connect the initial and final point of the control problem with the manifold

orbits. In Figure 4.3, this is sketched for the computation of maneuvers from an initial equilibrium point x^0 to a strong stable manifold orbit, which belongs to another equilibrium, namely the desired final point x^T. We illustrate the following steps for this scenario.

Different solution sequences can be obtained by varying the *switching point*, the *time on the manifold orbit*, and *the final time of the controlled maneuver* to the manifold. The switching point denotes the state on the manifold orbit at which the controlled maneuver ends, such that a solution sequence can (continuously) switch to the uncontrolled manifold trajectory. Since we consider the manifold orbit x_{mnf}, the first and second design parameter are correlated, i.e. by choosing a switching point on the orbit, it is automatically defined how long the motion on the manifold takes until reaching the final point. Thus, we define a discretization of the time interval $[0, T_{\text{mnf}}]$ with step size $\Delta\tau$ by $\Gamma := \{T^0_{\text{mnf}} + \eta \cdot \Delta\tau \,|\, \eta = 1, \dots, W\}$. Here, T^0_{mnf}, $\Delta\tau$, and W have to be chosen appropriately for the specific application in order to generate a representative family of switching points. These switching points are denoted by $\zeta_1, \dots, \zeta_W$ (cf. the blue dots in Figure 4.3) and it holds $\zeta_i = x_{\text{mnf}}(T^0_{\text{mnf}} + i \cdot \Delta\tau)$ for $i = 1, \dots, W$. Additionally, for the final time of the controlled maneuver, a time grid $\mathcal{T} = \{T_1, \dots, T_Y\}$ is defined for $Y \in \mathbb{N}$ and $T_j \in \mathbb{R}^+$ for $j = 1, \dots, Y$. Then, for each final point ζ_i, $i \in \{1, \dots, W\}$, an optimal control problem can be stated for every final time $T_j \in \mathcal{T}$ ($j \in \{1, \dots, W\}$). This leads to different optimal solutions, sketched by the green to gray lines in Figure 4.3. All together, $W \cdot Y$ sequences can be generated from this family of connecting maneuvers. Making use of the fact that the uncontrolled system is autonomous, i.e. not explicitly dependent on time, the part of the manifold orbit can be shifted in time to generate a solution to the entire control problem, e.g. the (i, j)-solution sequence is given by

$$
\begin{aligned}
&(x_{i,j}, u_{i,j}) \,:\, [0, T_j + T_{\text{mnf}} - (T^0_{\text{mnf}} + i \cdot \Delta\tau)] \ni t \\
&\quad \mapsto \begin{cases} (x^*(t), u^*(t)) & \text{for } t \in [0, T_j], \\ (x_{\text{mnf}}(t + T^0_{\text{mnf}} + i \cdot \Delta\tau - T_j), 0) & \text{for } t \in [T_j, T_j + T_{\text{mnf}} - (T^0_{\text{mnf}} + i \cdot \Delta\tau)], \end{cases}
\end{aligned}
$$

where $(x^*(\cdot), u^*(\cdot))$ is the optimal solution of the energy optimal control problem from the initial point x^0 to the final point ζ_i in time T_j. Since at a transition point, the configurations and velocities of the maneuver and the manifold trajectory coincide, all resulting sequences are continuous.

Remark 4.8: Optionally, in a fourth step, the resulting sequences can be used as an initial guess for a post optimization of the entire optimal control problem. Only with this additional optimization we can ensure the optimality of a resulting sequences because it cannot be assumed that two optimal parts (in our case, the solution of the optimal subproblem and the piece of the manifold orbit) result in an optimal

solution for the entire optimal control problem. This is due to the fact that we fix the transition point on the strong stable manifold as one point of the solution sequence. Thus, this procedure does not give any information on the existence of better solutions not containing this point.

In the post optimization process, we propose to choose the control effort as the objective functional and to take the (i,j)-sequence's final time $T_j + T_{\mathrm{mnf}} - (T^0_{\mathrm{mnf}} + i \cdot \Delta\tau)$ to be fixed. However, the optimal solution is allowed to deviate from the sequence's transition point. Alternatively, the final time of the controlled maneuver could be left free in the optimization in order to compute only one controlled maneuver to every discretization point on the manifold orbit. This approach is not followed here since we aim at analyzing in particular the trade-off between energy efficient and time-optimal solutions. This can be done with the concept of Pareto optimality (cf. Section 3.1.3): Sequences or post optimized solutions are dominated if there exists another solution that is cheaper and at the same time faster. Non-dominated solutions are candidates for local optima that are – fixing the duration of the maneuver – close to the globally most energy efficient solution. In the following, this will be numerically evaluated for swing-up scenarios of double pendula.

4.3 Application to Swing-Ups of Double Pendula

To start with, we consider again the double pendulum that is mounted to the ground, as introduced in Example 4.7, now with a torque control applied to the inner arm as depicted in Figure 4.4a. This can be seen as an intermediate step towards the modeling for a test rig of a double pendulum on a cart (cf. Figure 4.4c and Figure 4.4b for a model of the test rig), to which we apply the control strategy afterwards.

4.3.1 Double Pendulum with Torque Control

A swing-up of the double pendulum is an admissible solution to the following optimal control problem

$$\begin{aligned} \min_{q,u,T} J_1(q,u) &= \int_0^T u(t)^2 \, dt \\ \text{w.r.t. } & \frac{d}{dt}\frac{\partial}{\partial \dot{q}} L(q,\dot{q}) - \frac{\partial}{\partial q} L(q,\dot{q}) = F(q,\dot{q},u), \\ & (q^0, \dot{q}^0) = (-\pi, \pi, 0, 0), \\ & (q^T, \dot{q}^T) = (0, 0, 0, 0). \end{aligned}$$

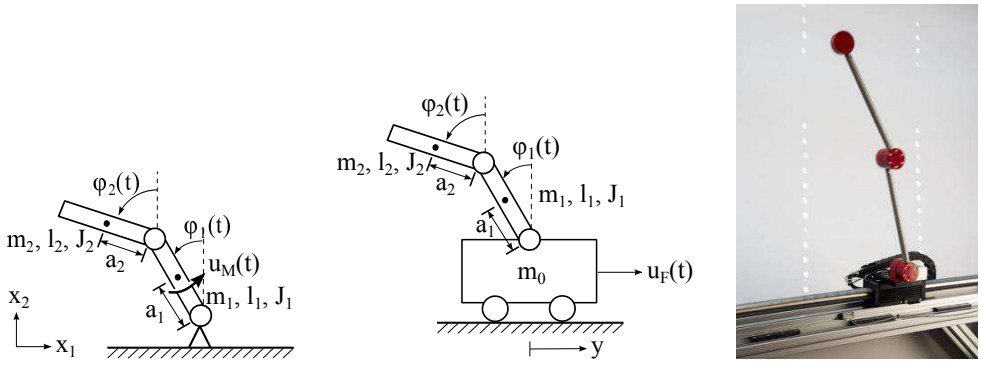

(a) Double pendulum with torque control.

(b) Double pendulum on a controlled cart

(c) Test rig

Figure 4.4: Models of double pendula and the test rig.

The forced Euler-Lagrange equations for the configuration coordinates $q = (\varphi_1, \varphi_2, \dot{\varphi}_1, \dot{\varphi}_2)^T$ are given in the appendix, cf. Section C.1. $F(\cdot, \cdot, \cdot)$ is comprised of the friction forces and the control force, which acts as a torque on the inner joint. We are primarily interested in energy efficient swing-ups, i.e. solutions that minimize J_1. However, since the costs and dynamic behavior of the solutions strongly depend on their duration, we compare them regarding a secondary cost function $J_2 = \int_0^T 1\, dt = T$. For all numerical solutions of the optimal control problem or subproblems, we use a variational integrator with step size $h = 0.005\,\mathrm{s}$ and the control method DMOC with a nonlinear optimization function from NAG.

As discussed in Example 4.7, the up-up equilibrium $\bar{x} = (0, 0, 0, 0)$ has two-dimensional stable and unstable manifolds, while the down-down equilibrium is stable. Therefore, we generate a trajectory on the strong stable manifold: referring to Figure 4.2b, a trajectory from the upper left corner of the depicted manifold excerpt to the equilibrium point. This corresponds to a shearing movement of the pendulum arms.

Then, a set of connecting control maneuvers from the down-down equilibrium to this orbit is computed as explained in Section 4.2. We compare the results from the post optimization of these sequences with solutions from a black-box optimization, i.e. with a linearly interpolated initial guess that does not require any knowledge about the inherent system dynamics. The objective values "maneuver time" and "control effort" of the computational results are presented in Figure 4.5a. The clouds of grey dots belong to the designed sequences: the time is the sum of the maneuver duration and the time spent on the manifold orbit and the costs are those of the controlled maneuver pieces only since the motion along the manifold orbit is for free. The cyan asterisks represent solutions obtained from a post optimization of

the sequence and the results of the black-box optimization are given by green circles.

It is clearly visible that the costs of the sequences could be considerably improved by the post optimization. This is due to the fact that the post optimization smoothes out the transition from the controlled maneuver onto the manifold (also cf. Figure 4.6), which leads to a reduction of the costs in almost all computations. Secondly, it becomes evident that there are "branches" of local optimal solutions and even for one fixed time, there exist several local optima with different costs. Such solutions belong to initial guesses from different sequences with the same overall duration but different times spent on the manifold (cf. Figure 4.3). Obviously, the optimization algorithm often converged to different local minima. Besides the branches, one observes scattered asterisks in the upper right corner. These solutions correspond to post optimized trajectories which have left the manifold. Since those solutions additionally show an unrealistic behavior from an engineering point of view, we have not considered them further. However, by construction of the post optimization, we cannot assure that the post optimized sequences stay as close to the manifold as it is the case in Figure 4.6 and we observed other solutions deviating from the manifold orbit in the post optimization as well. Regarding the trade-off between energy-efficient and fast solutions, the non-dominated points, i.e. the points in Figure 4.5b have to be considered. Here, one observes that there are quite large areas where the sequencing approach provides the best solutions and thus outperforms the black-box optimizations. In some smaller sections the black-box optimization is just as good (in this case the solution trajectories from both computations are the same), but never better than the sequence approach.

A more detailed analysis of representative solutions with same duration but different costs shows that the resulting motions from the two approaches have crucial structural differences. In Figure 4.6, a three-dimensional projection of these solutions onto the φ_1, φ_2, and $\dot{\varphi}_1$ components is shown. The sequence consisting of the optimal control maneuver to the manifold represented by the green line and the subsequent section of the strong stable manifold orbit (cyan) has a duration of 1.4 s. Its post optimization (yellow), which is not directly located on the strong stable manifold but is winding around it, yields a control effort of 12.142 N^2s. In contrast to that the black-box optimization for the same time results in a – also qualitatively different – solution with 45.217 N^2s control effort, i.e. it is 3.7 times more expensive.

Finally, we compare the numerical effort of the optimizations performed by the NAG-solver (cf. Figure 4.7). Since we use the constant step size of $h = 0.005\,\mathrm{s}$ in the discretization, a longer maneuver duration uniquely corresponds to a higher number of nodes. For the sequencing approach, the sum of the computation times to generate the control maneuvers and the computation for the post optimizations is taken. Then, for each number of nodes, we average the values obtained from the different initial guesses (blue asterisks). Taking into account the computation times of the black-box optimizations (green circles) for reference, the novel approach has a

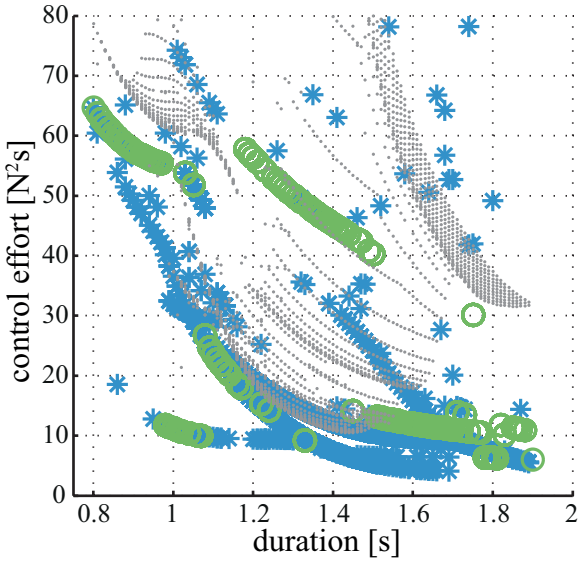

(a) Duration and control effort of the solutions.

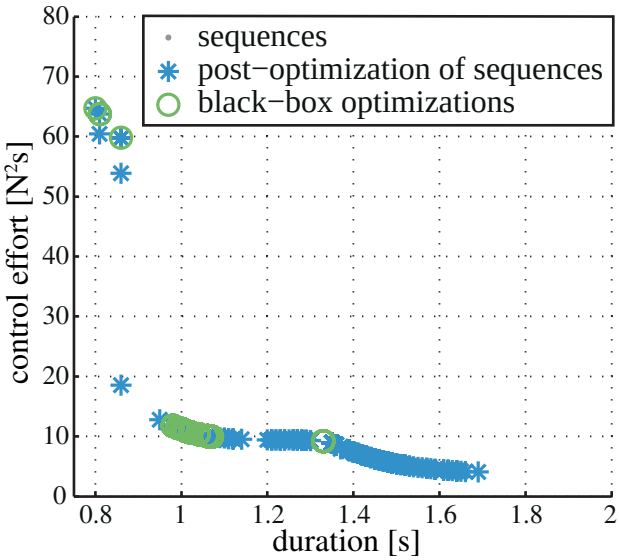

(b) Non-dominated points of Figure 4.5a

Figure 4.5: Objective values and non-dominated solutions for the swing-up of the double pendulum with torque control: black-box optimizations are performed for final times $T \in [0.8, 1.9]$ s (green circles). For each final time, the novel approach leads to different sequences (grey dots) which are used as initial guesses for a post optimization (cyan asterisks).

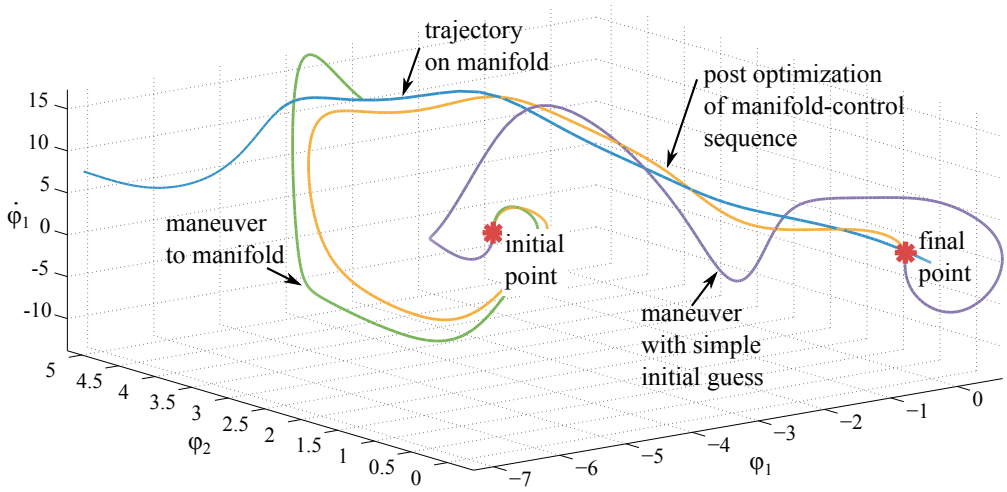

Figure 4.6: Comparison of swing-up solutions: maneuver with simple initial guess from "black-box optimization" (purple) versus the sequence consisting of the controlled maneuver (green) together with the appropriate part of the manifold trajectory (cyan) and versus the post optimization of this sequence (yellow).

comparable computational effort, although it includes two optimizations. While for shorter durations, i.e. a smaller number of nodes, the novel approach requires less computation time than the black-box optimization, for a higher number of nodes, it is the other way around.

In conclusion, this example shows that using the sequencing approach which exploits the natural dynamics of the system is a helpful method in finding energy efficient solutions. Additionally, we have to validate if solution trajectories from the control strategy can be realized on the real test rig. Therefore, we consider the double pendulum on a cart system in the following section.

4.3.2 Double Pendulum on a Cart

The swing-up problem for the double pendulum can be stated as before, but now the cart's position $y(t)$ is appended to the configuration vector. For the initial and final point, we take $(y^0, \dot{y}^0) = (y^T, \dot{y}^T) = (0, 0)$. Later, we extend the problem by the task to stabilize the double pendulum in the up-up equilibrium. Therefore, a two-degree of freedom controller is designed. While the sequencing approach provides the feedforward control, an additional feedback controller takes care of perturbations during the swing-up and realizes the stabilization at the end of the feedforward

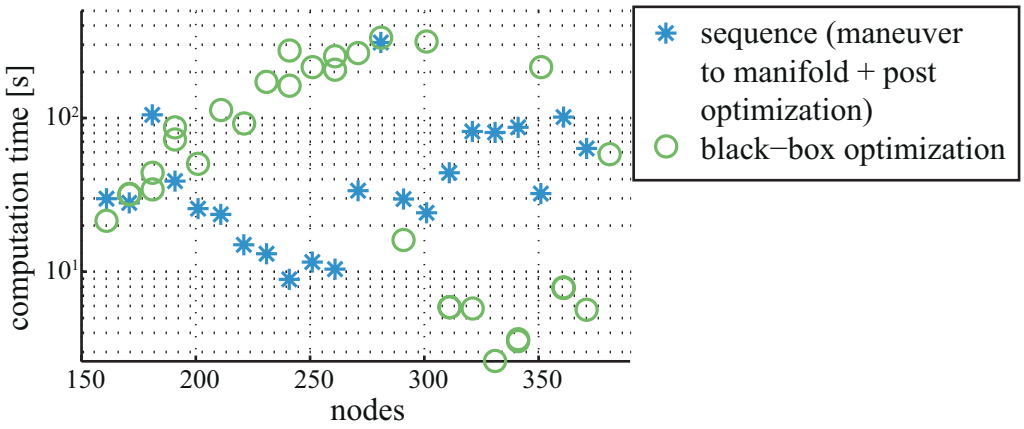

Figure 4.7: Comparison of the computation time of the averaged sum from the maneuver to the manifold and the post optimization with the black-box optimization regarding the number of nodes used for the discretization

trajectory[7].

Because of the structural similarity to the previous double pendulum examples we reuse the strong stable manifold orbit. This is justified by the fact that the corresponding model of the uncontrolled double pendulum coincides with the new one if the cart stands still. Thanks to various sources of friction in the real test rig, this situation could indeed be realized at the technical system with nearly no control. While using the ideal model of a double pendulum on a cart, the exact control forces for the cart, which turn the manifold orbit into an admissible trajectory for the system, can be computed (cf. Section C.1 for details).

However, new controlled maneuvers from the down-down equilibrium to the stable manifold orbit have to be computed for the more complex model for the double pendulum on a cart. For validation at the test rig, a sequence with a maneuver to the manifold orbit with time 1.55 s and overall duration $T = 2.4\,\mathrm{s}$ is chosen. As described before, a post optimization is performed with DMOC. The resulting maneuver is then taken as the nominal trajectory for the two-degree-of-freedom controller.

In Figure 4.8, the feedforward trajectory (dashed blue lines) together with the measurements for the pendulum's angles $\varphi_1(t)$ and $\varphi_2(t)$ and for the cart's position $y(t)$ in test runs with (solid green lines) and without the feedback controller (dotted red lines) are depicted. It can be seen that the cart and the pendulum arms follow the nominal trajectories quite well. Near the up-up equilibrium the cart has to

[7]For details on the feedback controller and also on further tests for this system, it is referred to [FTOT13].

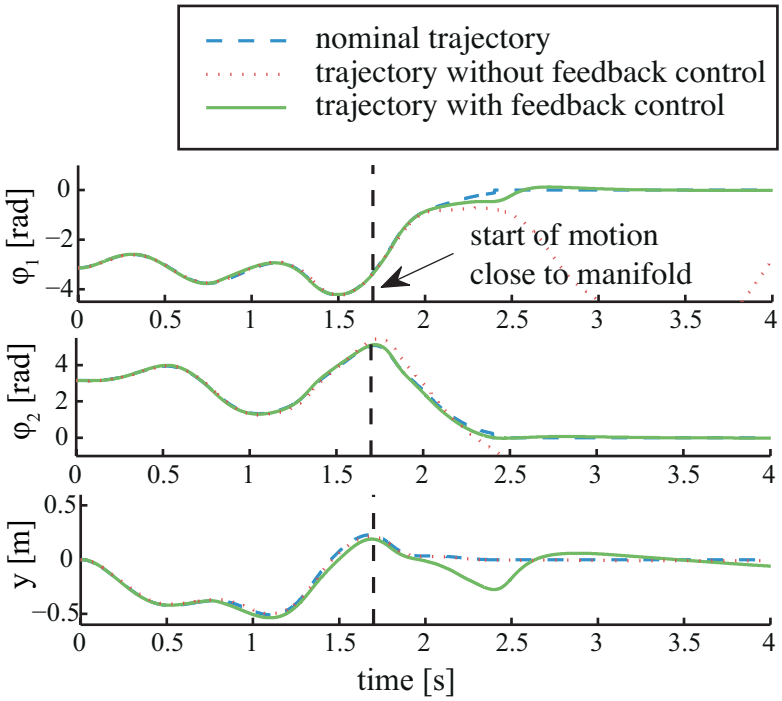

(a) Angles and cart postion.

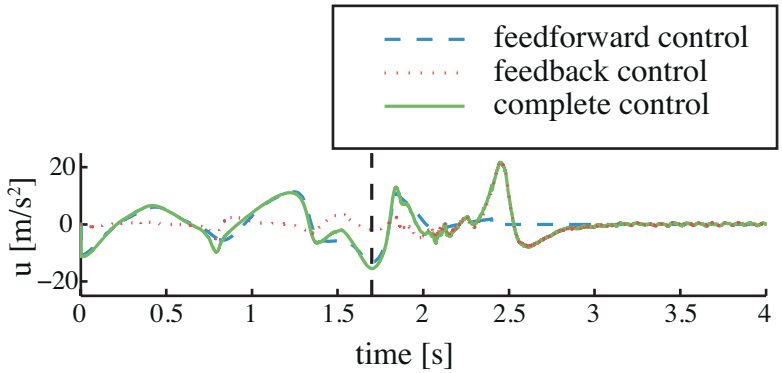

(b) Control trajectory.

Figure 4.8: Angles, cart position, and control trajectory of the swing-up of the double pendulum on a cart at the real test rig. The vertical dashed line indicates where the motion close to the strong stable manifold trajectory starts.

perform additional motions to stabilize the arms due to deviations from the nominal trajectory. In the measured trajectories, especially when there is no feedback control, one still recognizes the characteristics of the maneuver-manifold-sequence. In the first part, the linear motor moves in an appropriate way to steer the pendulum towards the strong stable manifold. In the second part, beginning at the vertical dashed lines in Figure 4.8, almost no additional motion of the cart is necessary because the pendulum arms move uncontrolled on the manifold towards the up-up equilibrium. In a feedback controlled run at the test rig, the additive feedback control trajectory is comparably small during the swing-up but higher at the end of the nominal trajectory, when the pendulum has to be stabilized in the up-up position.

In conclusion, the experiments showed that the proposed sequence approach provides the opportunity to find qualitatively new solutions for the swing-up of the double pendulum on a cart. In particular, the resulting trajectories are more complex compared to the previously tested optimal swing-up control design in [TKOT11].

CHAPTER 5

Motion Planning with Motion Primitives

As it has already been discussed in the previous two chapters, solving optimal control problems for mechanical systems, which typically exhibit highly nonlinear behavior, is a challenging task. In Chapter 4, we have focused on the computation of energy efficient control strategies and the general problem of providing good initial guesses for local optimizers has been discussed. The list of challenges can be easily extended by problems including collision avoidance with other obstacles, cooperative control problems, recalculation of optimal solutions during operation time, or problems with multiple objectives. While research e.g. in robotics in the last decades often addressed path planning problems (i.e. a computation of optimal configuration trajectories not taking into account the dynamics, in particular the way of forcing), optimal control or *motion planning*[1] aims at solving the actual optimal control problem, i.e. optimal solutions that are admissible to the dynamics are required (see [CLH+05], for instance).

A novel approach to meet these challenges is *motion planning with motion primitives*, introduced by Frazzoli, [Fra01], and co-workers in [FDF99, FDF00, FB02, Fra03, FDF05]. Basically, the approach consists of two phases:

1. Generating a motion planning library: Simple and short pieces of trajectories, so called *motion primitives* (cf. Section 5.1), are computed and stored in a motion planning library that can be represented by a graph, the *maneuver automaton* (cf. Section 5.2).

[1] To avoid confusion about the term "planning", we always speak of "path planning" in case of purely kinematical problems, in which only admissible or optimal configuration trajectories are searched for. Contrarily, "*motion* planning" addresses the same kind of (time continuous) problems as classical optimal control does. In the literature, "planning" often refers to discrete (or finite or combinatorial) optimization problems and, in fact, the approach of Frazzoli et al., [FDF05], has some aspects in common with combinatorial optimization.

2. Solving the optimal control problem: The optimal sequence of motion primitives in the maneuver automaton is determined.

Besides providing a practicable solution method to the nominal optimal control problem, the idea of splitting up the problem suggests to divide the steps into the design and the operational phase of the system. While the computationally costly generation of the motion planning library can be performed offline during the design phase, the actual optimal control problem can be solved online during operation, when current environmental restrictions can be taken into account. In particular, the maneuver automaton is not limited to solving one specific optimal control problem, e.g. with one fixed set of initial and final points.

The key assumption for the applicability of this method is that the dynamical system under consideration provides some symmetry. However, as we have seen in Chapter 2, mechanical systems typically exhibit symmetries by invariances. The exploitation of these inherent structures in the planning approach (leading to the existence of so called *trim primitives*) is explained in more detail in Section 5.1.

The motion planning with motion primitives method is based on human-inspired control strategies. More detailed, in [FDF05], the authors observed that very skilled and experienced pilots of acrobatic helicopters solve their steering tasks by sequencing (a) simple flight phases, that is e.g. with constant height and velocity and (b) short, intermediate, highly controlled maneuvers in between. We later give a formal definition of these different types of motion primitives.

After introducing Frazzoli's approach in more detail in Section 5.1 and Section 5.2, we turn our attention to the substantial extensions of the method which have been developed in the course of this thesis. Namely, we address the following aspects.

Lagrangian Systems with Symmetries Frazzoli and co-workers introduced the motion planning approach for general dynamical systems and studied its application to autonomous vehicles, in particular. However, focusing on symmetric mechanical systems, or, more precisely, on Lagrangian systems with symmetries, provides a deeper insight into the existence and computation of trim primitives (cf. Section 5.3). In this thesis, we relate trim primitives to the concept of relative equilibria in the Lagrangian setting and extend the necessary condition for the existence of relative equilibria to forced Lagrangian systems.

Motion Primitives on (Un)Stable Manifolds The concept of the motion planning library can be extended to accept further types of motion primitives. Therefore, we use this framework to structurally include motions on (un)stable manifolds of the uncontrolled dynamics in the maneuver automaton (cf. Section 5.4). This generalizes the idea presented in Chapter 4 on how to provide solution sequences as good initial guesses leading to globally energy efficient solutions. As it is shown for the spherical

pendulum examples in Section 5.6, trajectories on (un)stable manifolds can be used beneficially by the motion planning method if energy optimal solutions are required. From another point of view, besides symmetries, this is a second kind of inherent dynamical property that we are going to make use of in the extended planning method presented in Section 5.5.

Pareto Optimal Maneuvers The method's possible split-up into design and operation phase makes it well suited for the development of self-optimizing systems[2]. The precomputed motion planning library can be seen as a knowledge base to which online planning methods refer during operation of a technical system. The framework of the maneuver automaton even allows to store several alternative controlled maneuvers, e.g. several Pareto optimal solutions (cf. Section 5.5 and Section 5.6.3 for an application). Thus, an actual prioritization of objectives, given by a decision maker or current environmental influences, can be taken into account when finding the optimal sequence during operation time.

Regarding the computational aspects, our extended motion planning approach uses a simple search tree method (cf. Section 5.5) that we developed in cooperation with Marin Kobilarov in [FOK10] and [FOK12]. Real world applications would require faster optimization methods, e.g. sampling based roadmap algorithms using random tree search techniques, which have been successfully applied by Kobilarov in the context of motion planning with primitives for the optimal control of an autonomous helicopter [Kob08].

In Section 5.6, the extended motion planning method is applied to three examples focusing on the different aspects of the extended approach. The spherical and double spherical pendulum examples from Chapter 2 are revived to illustrate the computation of trim primitives by means of the *controlled amended potential* introduced in Section 5.3 and the benefit of (un)stable manifold primitives in a planning library. A simple mobile robot is used to demonstrate the motion planning with Pareto optimal maneuvers.

5.1 Types of Motion Primitives

In the following, we refer to the findings of [FDF05] if not stated otherwise. In this work, a general controlled dynamical system $\dot{x} = \mathcal{F}(x, u)$ on an n-dimensional manifold $\mathcal{X}$ with controls $u \in U \subset \mathbb{R}^m$ is considered. It is assumed that a unique solution of the differential equation for any piecewise continuous control function u

[2]See [GRS09] for an introduction to self-optimizing systems, a concept which has been developed in the CRC 614, Collaborative Research Center "Self-Optimizing Concepts and Structures in Mechanical Engineering" at the University of Paderborn.

exists, e.g. by requiring $\mathcal{F}$ to be Lipschitz continuous. The symmetry is given by a Lie group G with symmetry action $\Psi : G \times \mathcal{X} \to \mathcal{X}$. It leads to a definition of equivalent trajectories that is consistent with our definition for forced Euler-Lagrange equations (cf. Definition 2.4). Concretely, trajectories $\pi_1 = (x_1(t), u_1(t))$ and $\pi_2 = (x_2(t), u_2(t))$ are equivalent, if they are defined on (fixed) time intervals of the same length and if there exists a $g \in G$ and a $\bar{t} \in \mathbb{R}$, such that $(x_1(t), u_1(t)) = (\Psi(g, x_2(t-\bar{t})), u_2(t-\bar{t}))$ holds for all time points.

Definition 5.1 (Motion Primitive)**:** Let $\pi : [0, t_f] \to \mathcal{X} \times U$ be a solution of $\dot{x} = \mathcal{F}(x, u)$. Then, the class of trajectories equivalent to π is called a *motion primitive* and denoted by π as well.

For mechanical systems with dynamics given by forced Euler-Lagrange equations, the motion primitive is a triple $\pi = (q(t), \dot{q}(t), u(t))$ and equivalent trajectories are generated with the lifted symmetry action Φ^{TQ} (cf. Section 2.3). It can be verified that, indeed, a motion primitive defines an equivalence class. Reflexivity trivially holds by construction. Assuming π_1 is equivalent to π_2 with a time shift T and a group element g, i.e. $(x_1(t), u_1(t)) = (\Psi(g, x_2(t-\bar{t})), u_2(t-\bar{t}))$, then, alternatively, π_1 can be shifted by g^{-1} and $-\bar{t}$ leading to $(x_2(t), u_2(t)) = (\Psi(g^{-1}, x_1(t+\bar{t})), u_1(t+\bar{t}))$. Here we make use of basic Lie group properties (cf. A.12) and the requirement that both trajectories have the same time duration. In the same manner, transitivity of the equivalence relation can be verified.

Definition 5.2 (Concatenation)**:** A *concatenation* of two motion primitives $\pi_1 : t \in [0, t_{f,1}] \mapsto (x_1(t), u_1(t))$ and $\pi_2 : t \in [0, t_{f,2}] \mapsto (x_2(t), u_2(t))$ on the time interval $[0, t_{f,1} + t_{f,2}]$ is defined by

$$\pi_1\pi_2(t) := \begin{cases} (x_1(t), u_1(t)) & \text{for } 0 \leq t \leq t_{f,1}, \\ (\Psi(g_{12}, x_2(t - t_{f,1})), u_2(t - t_{f,1})) & \text{for } t_{f,1} \leq t \leq t_{f,1} + t_{f,2} \end{cases} \tag{5.1}$$

if there exists a group element g_{12} such that the second motion can be shifted compatibly, i.e. it holds $x_1(t_{f,1}) = \Psi(g_{12}, x_2(0))$.

The motion planning approach is based on concatenating motion primitives such that the sequence forms a solution to the given control problem. A special type of motion primitives, namely the *trim primitives*, are of particular importance since they can be continuously parametrized and therefore, they allow for a great variety of sequence trajectories.

Definition 5.3 (Trim Primitive)**:** A trim primitive $\alpha : t \in [0, t_f] \mapsto (x_\alpha(t), u_\alpha(t))$

is defined as a motion primitive that satisfies

$$x_\alpha(t) = \Psi(\exp(\xi_\alpha t), x_\alpha(0)), \quad u_\alpha(t) = u_\alpha = \text{const.} \quad \forall t \in [0, t_f], \tag{5.2}$$

with ξ_α being an element of the corresponding Lie algebra.

A trim primitive can be parametrized by its time duration, called the *coasting time* τ, leading to a family of trims, $\alpha(\tau) : t \in [0, \tau] \mapsto (\Psi(\exp(t\xi_\alpha, x_\alpha(0))), u_\alpha)$. Therefore, trim primitives allow for an infinite number of sequences even in a finite set of motion primitives, which is an important property of this motion planning approach. The simplest example of trim primitives are natural or controlled fixed points. For mechanics, some resemblance to trajectories on relative equilibria is obvious and we postpone a detailed discussion to Section 5.3. The term "trim primitives" originates from aeronautics, where trajectories that can be flown with constant ("trimmed") controls are called "trim trajectories" as explained in [FDF05].

A second class of motion primitives are *maneuvers*, which can be any kind of controlled maneuver that connects trims.

Definition 5.4 (Maneuver)**:** A maneuver π is a motion primitive that is compatible with some trim α from the left and with a trim β from the right, such that $\alpha\pi\beta$ is a valid concatenation.

Thus, there exist group elements $g_{\alpha\pi}$ and $g_{\pi\beta}$, such that $x_\pi(0) = \Psi(g_{\alpha\pi}, x_\alpha(0))$ and $x_\pi(t_f) = \Psi(g_{\pi\beta}, x_\beta(0))$. The *group displacement*, an invariant characteristic of a maneuver, is defined as $g_\pi = g_{\alpha\pi}^{-1} g_{\pi\beta}$. Together with *trim displacements*, which depend on the time spend on a trim, they become important in the generation of feasible motion plans.

5.2 Maneuver Automaton

A finite number of motion primitives, i.e. trim primitives and maneuvers, form a *motion planning library*. To solve optimal control problems, it has to be searched for admissible sequences in this library. Therefore, a *maneuver automaton* is introduced to organize the primitives. It can be depicted as a graph with trim primitives defining the vertices and edges representing the maneuvers. For a detailed description of the formal language belonging to this finite state machine, we refer to [FDF05]. A sketch of a maneuver automaton's graph is given in Figure 5.1.

The motion planning approach transforms an infinite-dimensional optimal control problem (cf. Chapter 3) into a search problem on the maneuver automaton, i.e. a finite dimensional algebraic problem. It is therefore characterized as a quantization

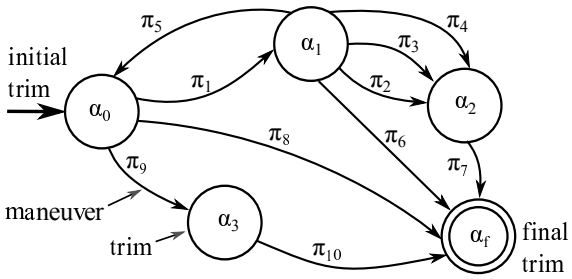

Figure 5.1: Sketch of a maneuver automaton with vertices corresponding to trim primitives and edges to connecting maneuvers (cf. [FDF05]).

method. Every path connecting the initial state x_0 with a final state x_f belongs to a sequence of motion primitives which forms an admissible curve, i.e. a trajectory to the system dynamics. Here, the class of control problems has to be restricted to those with initial and final states on trim primitives. However, this limitation is not severe, since operating points of technical systems are typically either fixed points or some kind of steady-state motion. In general, the maneuver automaton has – depending on the connectivity of the graph, of course – very good controllability properties, cf. [FDF05] for an analysis.

Let α_0 and α_f denote the given boundary trims with initial states $x_{\alpha_0}(0)$ and $x_{\alpha_f}(0)$. Then there exist some group elements $g_0, g_f \in G$ such that $x_0 = \Psi(g_0, x_{\alpha_0}(0))$ and $x_f = \Psi(g_f, x_{\alpha_f}(0))$. Finding a motion from x_0 to x_f amounts to finding a proper sequence of trim primitives $\alpha_0, \alpha_1, ..., \alpha_N, \alpha_f$, coasting times $\tau_0, \tau_1, ..., \tau_N, \tau_f$, and connecting maneuvers $\pi_0, \pi_1, ..., \pi_N$. The sequence forms the trajectory ρ (cf. Figure 5.2) defined by

$$\rho = \alpha_0(\tau_0)\pi_0\alpha_1(\tau_1)\pi_1...\alpha_N(\tau_N)\pi_N\alpha_f(\tau_f).$$

The states along ρ are expressed, for $k \geq 0$, by

$$\rho(t) = \begin{cases} (\Psi(g_k \exp((t-t_k)\xi_{\alpha_k}), x_{\alpha_k}(0)), u_{\alpha_k}), & t \in [t_k, t_k + \tau_k], \\ (\Psi(g_k \exp(\tau_k \xi_{\alpha_k}), x_{\pi_k}(t')), u_{\pi_k}(t')), & t \in [t_k + \tau_k, t_{k+1}], \end{cases}$$

where $g_k = g_0 \prod_{i=0}^{k-1} \exp(\tau_i \xi_{\alpha_i}) g_{\pi_i}$, $t_k = \sum_{i=0}^{k-1} (\tau_i + |\pi_i|)$, with duration $|\pi_i|$ of maneuver π_i, and $t' = t - t_k - \tau_k$. The group elements $\exp(\tau_i \xi_{\alpha_i})$ are trim displacements, whereas g_{π_i} are the displacements of the maneuvers π_i. Without loss of generality, we assume that all maneuvers in the automaton have been shifted in advance such that if a maneuver π is compatible with a preceding trim α to a concatenation $\alpha\pi$, then for the group element $g_{\alpha\pi}$ which assures $x_\pi(0) = \Psi(g_{\alpha\pi}, x_\alpha(0))$, it holds

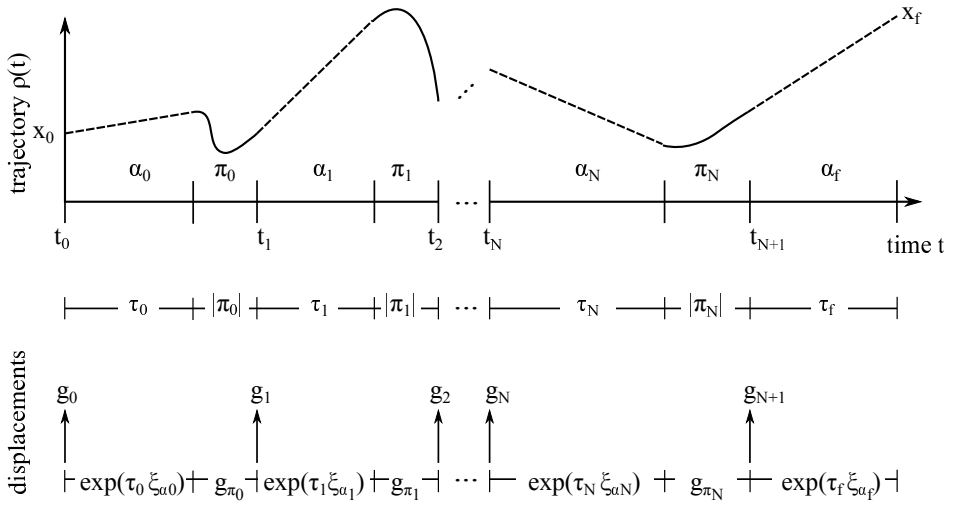

Figure 5.2: Sketch of a trajectory generated by motion primitives with their corresponding group displacements.

$g_{\alpha\pi} = e$, the identity element of the group. The total group displacement along ρ is

$$g_\rho = \left[\prod_{i=0}^{N} \exp(\tau_i \xi_{\alpha_i}) g_{\pi_i}\right] \exp(\tau_f \xi_{\alpha_f}).$$

Thus, computing a motion from x_0 to x_f amounts to finding a motion plan ρ such that $g_\rho = g_0^{-1} g_f$.

It is reasonable to assume that the cost functional of the optimal control problem (cf. Section 3.1), $J(x,u) = \int_0^T C(x(t),u(t))\,dt$, is invariant w.r.t. G as well, such that trajectories belonging to the same motion primitive have the same costs. For trim primitives, we can further define a *unit cost* for a trim α by the costs per time unit, $c_\alpha = \int_0^1 C(x_\alpha(t),u_\alpha(t))\,dt$. Then, the *cost functional for a motion plan* $\rho(t)$ with trims $\alpha_0,\ldots,\alpha_N,\alpha_f$, coasting times $\tau_0,\ldots,\tau_N,\tau_f$, and maneuvers $\pi_0,\ldots,\pi_N$ simplifies to

$$J(\rho) = \int_0^T C(\rho(t))\,dt = \sum_{i=1}^{N} (J_{\pi_i} + c_{\alpha_i}\tau_i) + c_{\alpha_f}\tau_f, \tag{5.3}$$

with the costs of the maneuvers given by

$$J_{\pi_i} = \int_0^{|\pi_i|} C(x_{\pi_i}(t),u_{\pi_i}(t))\,dt \tag{5.4}$$

for $0 \leq i \leq N$. Finally, we can state the motion planning problem as follows.

Problem 5.5 (Motion Planning Problem)**:** Let MA be a maneuver automaton as described above with initial state x_0 and final state x_f. The *motion planning problem* is then given by

$$\min_{\rho} J(\rho) = \sum_{i=1}^{N} (J_{\pi_i} + c_{\alpha_i}\tau_i) + c_{\alpha_f}\tau_f,$$

$$\begin{aligned}
\text{w.r.t. } & \left[\prod_{i=0}^{N} \exp(\tau_i \xi_{\alpha_i}) g_{\pi_i}\right] \exp(\tau_f \xi_{\alpha_f}) = g_0^{-1} g_f, \\
& (\alpha_0, \pi_0, \alpha_1, \pi_1, \ldots, \alpha_N, \pi_N, \alpha_f) \text{ is a path in MA}, \\
& \tau_i \geq 0, \forall i = 0, \ldots, N, \ \tau_f \geq 0, \\
& \Psi(g_0, x_{\alpha_0}(0)) = x_0, \Psi(g_f, x_{\alpha_f}(0)) = x_f, \text{ and} \\
& x_f = \rho\left(\left(\sum_{i=0}^{N} \tau_i + |\pi_i|\right) + \tau_f\right). \qquad (5.5)
\end{aligned}$$

The *optimal solution* ρ^* is the sequence $(\alpha_0^*, \pi_0^*, \alpha_1^*, \pi_1^*, \ldots, \alpha_{N^*}^*, \pi_{N^*}^*, \alpha_f^*)$ of optimal length N^* and optimal coasting times $\tau_0^*, \ldots, \tau_N^*$.

Except for g_0 and g_f, which can be seen as internal auxiliary variables, the parameters of the optimization problem are the coasting times as well as the length and the elements of the sequence. Thus, the motion planning problem is a *finite dimensional*, but *mixed-integer optimization problem*. While problems of this kind are normally quite difficult to solve, knowing the structure of the symmetry group and of the trims in the maneuver automaton often helps to essentially narrow down the number of different types of sequences. Further, for typical symmetry groups, the optimization of the coasting times simplifies to polynomial or even linear problems, see [FDF05] for a discussion.

So far, additional constraints of the original motion planning problem have not been discussed, since they are not within the scope of this thesis. In principle, restrictions on the states or control can be considered in both phases of the motion planning approach: as constraints on trims and maneuvers while the maneuver automaton is generated (cf. [FDF05]), and also during sequencing (cf. e.g. [Kob08]). The latter is important when dealing with obstacles, in particular during an online application of this planning method.

5.3 Trim Primitives for Mechanical Systems

Based on the framework of motion primitives introduced in the previous two sections, in the remainder of this chapter, we describe our extended concept, which has been developed in course of this thesis, in more detail. To study the origin of trim primitives and a convenient way of computing them, we make use of concepts from mechanics and symmetry, which have already been discussed in Chapter 2. Relative equilibria have been introduced in Section 2.3.3 as states $x_e = (q_e, v_e) \in TQ$ at which the Lagrangian vector field X_L points in the direction of the group orbit $G \cdot x_e = \{(q,v) \,|\, (q,v) = \Phi_g^{TQ}(q_e, v_e) \text{ for } g \in G\}$ (cf. Definition 2.13). One characterization of relative equilibria is based on the amended potential, which has been defined by $V_\mu(q) = V(q) + \frac{1}{2}\langle \mu, \mathbb{I}(q)^{-1}\mu \rangle$. Now, we aim for a method to compute relative equilibria for forced, in particular, controlled mechanical systems. We maintain the terminology introduced in Section 5.1 and Section 5.2 and define trim primitives for mechanical systems as follows.

Definition 5.6 (Trim Primitives for Mechanical Systems)**:** A point $x_e = (q_e, v_e) \in TQ$ together with some control value $u_e \in U$ is called a *trim primitive* (or, briefly, a *trim*), if it holds that $X_L^{u_e}(x_e) \in T_{x_e}(G \cdot x_e)$ with the forced Lagrangian vector field $X_L^{u_e}$.

This is in line with Definition 5.3, since trim primitives for mechanical systems generate solutions $(q(t), \dot{q}(t))$ on $[0, t_f]$ of the forced Euler-Lagrange equations with control $u(t)$ for a G-invariant Lagrangian L and forcing f_L, that can be written as

$$(q, \dot{q})(t) = \Phi^{TQ}(\exp(t\xi), (q_e, v_e)), \quad u(t) = u_e = \text{const.} \quad \forall t \in [0, t_f], \tag{5.6}$$

with $\xi \in \mathfrak{g}$ and $\exp : \mathfrak{g} \to G, \xi \mapsto \exp(t\xi) \in G$. Thus, trims are uniquely defined by their initial value $(q_0, \dot{q}_0, u_0)$ and the Lie algebra element ξ. Additionally, they can be parametrized by time; altogether, this makes them easy to store and handle in a library of motion primitives.

Besides fixed points, the simplest class of trim primitives are uncontrolled motions along the group orbits, i.e. relative equilibria. They are of special importance for sequences of motion primitives with minimal control effort (cf. e.g. the pendulum applications in Section 5.6). However, in general, maneuver automata solely with uncontrolled trim primitives would be too restrictive. In the following we will therefore introduce the concept of controlled potentials that provides a method to construct controlled trim primitives based on the computation of relative equilibria.

We augment the original potential $V(q)$ by a parameter-dependent term ν which represents a *potential force*, a special kind of forcing that can be defined in terms of a potential (cf. [BL04]). That means, we replace $V : Q \to \mathbb{R}$ by $V^u : Q \to \mathbb{R}$,

$V^u(q) = V(q) - \nu(q)$ with $\nu : Q \to \mathbb{R}$ having the property that $\frac{\partial}{\partial q}\nu(q) = u$ for some control value $u \in U$, where we assume that $U \subseteq \mathbb{R}^n$.

This type of potential force is intrinsically restricted to depend on configurations, so it cannot be used to model dissipative, i.e. velocity dependent forces. However, many examples of control forces on mechanical systems fit into this structure. The following theorem describes how a trim primitive for a controlled Lagrangian system can be computed by means of the concept of controlled potentials.

Theorem 5.7: Let $L = T - V$ be a G-invariant Lagrangian and $V^u(q) = V(q) - \nu(q)$ the augmented, G-invariant controlled potential. The critical points of the amended controlled potential V^u_μ are trim primitives according to Definition 5.6.

Proof. Amending the controlled potential V^u leads to the amended controlled potential $V^u_\mu = V^u + \frac{1}{2}\langle \mu, \mathbb{I}(q)^{-1}\mu\rangle = V(q) - \nu(q) + \frac{1}{2}\langle \mu, \mathbb{I}(q)^{-1}\mu\rangle = V_\mu - \nu(q)$. Since we assume V^u to be G-invariant, Proposition 2.14 can be applied to the modified system given by the Lagrangian $L^u = T - V^u$. Thus, relative equilibria are given by the critical points of V^u_μ:

$$\frac{\partial}{\partial q} V^u_\mu = 0 \quad \Leftrightarrow \quad \frac{\partial}{\partial q}\left(V_\mu - \nu(q)\right) = 0 \quad \Leftrightarrow \quad \frac{\partial}{\partial q} V_\mu = u\,.$$

In other words, if a pair $(x_e, u_e) = ((q_e, v_e), u_e)$ satisfies $\frac{\partial}{\partial q}V_\mu(q_e) = u_e$ with $\mu = J(q_e, v_e)$, the definition of a relative equilibrium, $X_{L^u}(x_e) \in T_{x_e}(G \cdot x_e)$, is fulfilled. The Euler-Lagrange equations of L^u read as follows: $\frac{\partial}{\partial q}(T(q,\dot q) - V^u(q)) - \frac{d}{dt}\frac{\partial}{\partial \dot q}T(q,\dot q) = \frac{\partial}{\partial q}(T(q,\dot q) - V(q)) - \frac{d}{dt}\frac{\partial}{\partial \dot q}T(q,\dot q) + u = 0$ and hence are equal to the forced Euler-Lagrange equations for L with forcing $f(q,\dot q, u) = \frac{\partial}{\partial q}\nu(q) = u$. Thus, the vector fields $X_{L^u} = X^u_L$ coincide and therefore, $X^{u_e}_L(x_e) \in T_{x_e}(G\cdot x_e)$ and (x_e, u_e) is a trim primitive as defined in Definition 5.6. □

Note that in Theorem 5.7 the condition that the controlled potential is G-invariant implicitly gives restrictions on ν and thus on the control u. The forced Noether's theorem 2.3 suggests candidates for trim primitives, namely all trajectories with such controls that act orthogonally to the group action. Indeed the following corollary states that this orthogonality condition is in fact necessary for the construction of trim primitives.

Corollary 5.8: If $x_e = (q_e, v_e)$ with control u_e is a trim primitive of a Lagrangian system with symmetry group G and G-invariant controlled potential $V^{u_e} = V(q) - \nu(q)$ with $\frac{\partial}{\partial q}\nu(q) = u_e$, it necessarily holds that $u_e \cdot \xi_Q(q_e) = 0$, with $\cdot$ denoting the standard scalar product. Here, ξ_Q is the infinitesimal generator of $\xi \in \mathfrak{g}$ such that $(q,\dot q)(t) = \Phi^{TQ}(\exp(t\xi), (q_e, v_e))$, $u(t) \equiv u_e$ is a solution of the forced Euler-Lagrange

equations.

Proof. It follows from the G-invariance of L that the original V is G-invariant, because we assume G to act by isometries and the kinetic energy is given in terms of a metric thus it is invariant w.r.t. G by itself. Then, from the G-invariance of V^{u_e} ($V^{u_e}(\Phi(g,q)) = V^{u_e}(q)$) it can be deduced:

$$V(\Phi(g,q)) - \nu(\Phi(g,q)) = V(q) - \nu(q) \quad \Leftrightarrow \quad \nu(\Phi(g,q)) - \nu(q) = 0. \tag{5.7}$$

As g is a point in the one-parameter subgroup $\mathbb{R} \ni s \mapsto \exp(s\xi) \in G$ generated by $\xi \in \mathfrak{g}$, we can replace g by $\exp(s\xi)$, set q to the trim primitive value x_e and then differentiate with respect to s and evaluate at $s = 0$:

$$\begin{aligned} 0 &= \frac{d}{ds}(\nu(\Phi(\exp(s\xi), q_e)) - \nu(q_e)))\Big|_{s=0} \\ &= \frac{\partial}{\partial q}\nu(\Phi(\exp(s\xi), q_e)) \cdot \frac{d}{ds}\Phi(\exp(s\xi), q_e)\Big|_{s=0} = u_e \cdot \xi_Q(q_e). \end{aligned}$$

□

5.4 Motion Primitives on (Un)Stable Manifolds

We extend the motion planning concept by a third type of motion primitives, namely orbits on (un)stable manifolds. Pieces of trajectories on (un)stable manifolds have already been used in Chapter 4 to compute energy efficient solutions for optimal control problems. Using the motion planning concept we are now able to generalize the proposed approach.

The first step is a global analysis of the uncontrolled system, by searching for fixed points, possibly higher dimensional invariant critical objects and corresponding (un)-stable manifolds (cf. Section 4.1).

Proposition 5.9 (Trim Primitives of the Natural Dynamics)**:** Equilibria of the natural dynamics (either hyperbolic or non-hyperbolic) form trim primitives with zero control.

Proof. Let $\bar{x} = (\bar{q}, 0)$ denote an equilibrium of a mechanical system with symmetry group G and corresponding Lie algebra $\mathfrak{g}$. We let $\mathfrak{e} = 0$ being the identity element

of $\mathfrak{g}$. For a trim α with $u_\alpha = 0$, it follows

$$\begin{aligned}\alpha(t) &= (q(t), \dot{q}(t), u_\alpha) = (\Phi^{TQ}(\exp(t\mathfrak{e}), (\bar{q}, 0)), 0) = (\Phi^{TQ}(e, (\bar{q}, 0)), 0) \\ &= ((\bar{q}, 0), 0) \quad \forall t \in [0, t_f].\end{aligned}$$

□

Remark 5.10 (Trim Primitives of the Natural Dynamics)**:** An extension of Proposition 5.9 to one-dimensional critical objects, i.e. periodic orbits in the natural dynamics does not hold in general. There exist examples with rotational symmetry in which uncontrolled trim primitives, the relative equilibria, belong to periodic orbits (e.g. the trims of a single or a double spherical pendulum, cf. Section 5.6). However, the periodic motions of an undamped planar single or double pendulum, for instance, do not form trim primitives, since there does not exist any symmetry group from which the motions could be generated via the corresponding Lie algebra's vector fields.

Of greater interest are motion primitives on the (un)stable manifolds of the critical objects. In the following, we restrict to the (un)stable manifolds of hyperbolic equilibria. To fit manifold trajectories into the motion planning library, first, a finite set of orbits on (un)stable manifolds, denoted by $\mathcal{O}$, has to be chosen.

Assuming one has attained a global overview of the (un)stable manifolds, e.g. from numerical approximations of the invariant objects performed by GAIO (cf. Section B.1), single trajectories have to be chosen. In case of one-dimensional (un)stable manifolds, this means defining an initial point x_O on the manifold and a final time t_f, such that the orbit $\mathcal{O} \ni O : t \in [0, t_f] \mapsto F_L(x_O, t)$, defined by the Lagrangian flow F_L can be approximated by numerical integration. Since relevant (un)stable manifold structures exist in nonlinear dynamical systems only, it is quite unlikely that the flow of the system is known analytically such that exact solutions could be generated. Therefore, numerical integration schemes, e.g. variational integrators (cf. Section 2.2.2) are required.

In case of two- or higher dimensional manifolds, different trajectories along the manifold are possible. To narrow down the number of motion primitive candidates, we propose to take – if present – orbits on strong (un)stable manifolds[3] (cf. Section 4.1.2). These orbits perform a fast dynamical transition, contracting to or expanding from the fixed point, respectively.

The initial point x_O for a manifold orbit cannot be placed onto the fixed point directly, since this is an invariant object itself. Furthermore, points too close to the

[3] One-dimensional strong (un)stable manifolds exist, if the eigenvalue with the largest or smallest real part is unique.

equilibrium are not desirable, either. Recall that points on the unstable manifold approach the fixed point (backwards in time) only asymptotically and therefore, the dynamics close to the fixed point are extremely slow (cf. e.g. [OLT04] for a discussion of this effect). For control purposes, it is preferable to choose x_O on the approximated manifold, but a small distance away from the equilibrium. However, for the sequencing of motion primitives, it then follows immediately that even if the corresponding fixed point is a trim in the library, the manifold orbit cannot be directly concatenated behind (or before, in case of stable manifold orbits) the trim. Instead, short connecting maneuvers have to be computed, as we discuss in detail in the following section.

For the computation of stable manifold orbits, time has to be reversed to provide stable numerical integration on the manifold, which is then attractive (cf. Section B.1). Then, we denote by O the reversed orbit with initial point $x_O = x(0)$ and final point $x(t_f)$ close to the fixed point. Figure 5.3 roughly sketches the idea of computing motion primitives on stable manifold orbits in the direction of the strong stable manifold. As the starting point for a strong stable manifold orbit, we take $x(t_f) = \bar{x} + \delta \cdot v^{ss}$ with some small $\delta \in \mathbb{R}$, which can be found by shifting the equilibrium point a reasonable amount in the direction of the largest eigenvector v^{ss}, which is real valued since the strong stable eigenvalue is assumed to be unique. The value of δ has to be chosen manually, such that the resulting trajectory shows a sufficient expansion from the fixed point in final time but still starts close enough to $\bar{x}$. Except for reversing the integration time, orbits on unstable manifolds can be computed analogously.

Note that by varying t_f, a whole family of motion primitives on one single manifold orbit can be generated. This fact will be considered in our extended maneuver automaton (in Section 5.5) such that it is sufficient to store only the manifold orbit with the maximal time. To be even more flexible in the planning, we allow a *manifold primitive* to also start at any point on the orbit, i.e. to be any piece of the manifold orbit. Recall that the dynamical system is assumed to be autonomous, so time shifts do not affect the validity of the trajectories on the manifold.

Definition 5.11 (Manifold Primitive)**:** Let $O : [0, t_f] \ni t \mapsto x_O(t)$ be a manifold orbit. Then, a manifold primitive is an (uncontrolled) motion primitive $\kappa : [0, t_\kappa] \ni t \mapsto (x_\kappa(t), 0)$ on O, i.e. there exists a $\tilde{t} \in [0, t_f]$ with $t_\kappa \leq t_f - \tilde{t}$, such that

$$x_\kappa(0) = x_O(\tilde{t})$$

and, therefore $x_\kappa(t) = x_O(t + \tilde{t})$ for all $t \in [0, t_\kappa]$.

In conclusion, motion primitives on manifold orbits play an ambiguous role in the motion planning approach. On the one hand, they originate from the natural

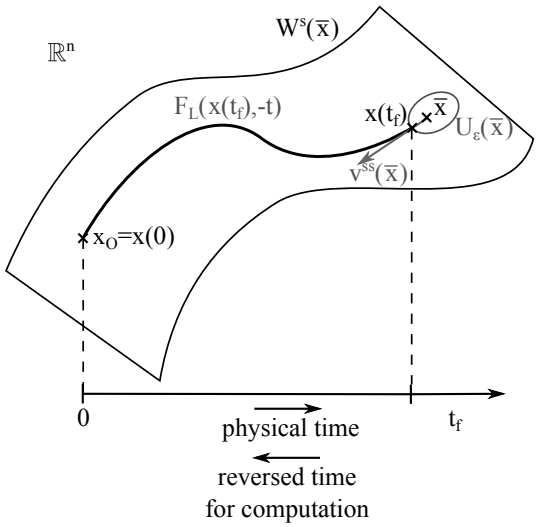

Figure 5.3: Sketch of the computation of stable manifold orbits. A starting point is defined in the neighborhood of the fixed point $\bar{x}$ and a trajectory is generated by numerical integration in backward time. Then, the trajectory is flipped by reversing the time again, such that x_O is the initial point for the manifold orbit that is stored in the motion planning library.

dynamics and aim to exploit the inherent system structures, as trims are supposed to do as well. On the other hand, orbits on manifolds exhibit a fixed final time and have to be computed and stored as discretized trajectories prior to the actual planning in the maneuver automaton. In this respect, they resemble maneuvers without control. However, since manifold orbits, in general, cannot be concatenated with trim primitives, the motion planning library has to provide connecting maneuvers such that trims and manifold orbits can be sequenced. These facts lead to our definition of an extended maneuver automaton.

5.5 Extended Motion Planning

Based on the motion planning concept of [FDF05], we develop an extended approach with the following main novelties: extended maneuvers are introduced to integrate manifold orbits into the maneuver concept, optimal control problems are stated and different sets of boundary conditions are discussed, and multiobjective optimal control maneuvers are introduced. Finally we present our search tree method for the computation of admissible and optimal sequences, which is applied to several examples in Section 5.6.

5.5.1 Extended Maneuvers

A concatenation of two motion primitives is possible, if there exists a group element which shifts the second prim, such that its initial point matches the final point of the first prim (cf. Definition 5.2). If both primitives start at $t = 0$, the second prim has to be time-shifted by the duration of the first one. Now, we introduce the definition of an *extended maneuver* for the concatenation of trim primitives, manifold primitives and maneuvers.

Definition 5.12 (Extended Maneuver)**:** Let x_α and x_β ($\alpha \neq \beta$) be trim trajectories and let $O \in \mathcal{O}$ be an (un)stable manifold orbit with manifold primitive $\kappa : [0, t_\kappa] \ni t \mapsto (x_\kappa(t), 0)$. Further, let $\pi_1 = (x_1, u_1)$ be a maneuver of duration t_1 that is compatible with α and that ends at $x_\kappa(0)$ and, finally, let $\pi_2 = (x_2, u_2)$ be a maneuver with $x_2(0) = x_\kappa(t_\kappa)$ and which is compatible with x_β. Then, an *extended maneuver* π is defined as $\pi = \pi_1 \kappa \, \pi_2$.

Requiring compatibility between maneuvers, trim and manifold primitives in the definition above, it is implicitly understood that there always exist group elements such that the individual motion primitives can be shifted by the symmetry action to form concatenations of primitives.

Proposition 5.13 (Extended Maneuver)**:** The extended maneuver $\pi = \pi_1 \kappa \pi_2$ is a maneuver in the sense of Definition 5.4.

Proof. Since $\pi(0) = \pi_1(0)$ and π_1 is a maneuver starting on a trim x_α, π is compatible with x_α. Let t_2 denote the duration of the maneuver π_2 such that the final point of the maneuver (started at $t = 0$) is $\pi_2(t_2)$. Then, we have $\pi(t_1 + t_\kappa + t_2) = \pi_2(t_2)$, i.e. π ends on the trim x_β. Thus, $\alpha\pi\beta$ is a valid concatenation and π is a connecting maneuver for α and β according to Definition 5.4. □

It directly follows that any extended maneuver can also be shifted by Lie group elements to start or end, respectively, at any point of the compatible trims.

Proposition 5.14 (Existence of Extended Maneuvers)**:** Let α and β be trims and O a manifold orbit as in Definition 5.12. Let $\pi_1 = (x_1, u_1)$ be a maneuver on $[0, t_1]$ that is compatible to α from the left and $\pi_2 = (x_2, u_2)$ a maneuver on $[0, t_2]$ that can be concatenated with β from the right. If there exists a manifold primitive $\kappa : [0, t_\kappa] \ni t \mapsto (x_\kappa(t), 0)$ on O and group elements $g_{1\kappa}$ and $g_{\kappa 2}$ with $x_1(t_1) = \Phi^{TQ}(g_{1\kappa}, x_\kappa(0))$ and $x_\kappa(t_\kappa) = \Phi^{TQ}(g_{\kappa 2}, x_2(0))$, then, an extended maneuver compatible with α and β and using O in between exists.

Proof. The following trajectory π on $[0, t_1 + t_\kappa + t_2]$ starts on α, ends on β and satisfies the requirements of an extended maneuver using π_1, π_2 and κ.

$$\pi(t) := \begin{cases} (x_1(t), u_1(t)), & t \in [0, t_1], \\ (\Phi^{TQ}(g_{1\kappa}, x_\kappa(t - t_1)), 0), & t \in [t_1, t_1 + t_\kappa], \\ (\Phi^{TQ}(g_{\kappa 2}^{-1} g_{1\kappa}, x_2(t - t_1 - t_\kappa)), u_2(t - t_1 - t_\kappa)), & t \in [t_1 + t_\kappa, t_1 + t_\kappa + t_2]. \end{cases}$$

That is, for $t_1 \leq t \leq t_1 + t_\kappa$ and with some $\tilde{t} \in [0, t_f]$, denoting the arrival time of the maneuver on the manifold, we have

$$\pi(t) = (\Phi^{TQ}(g_{1\kappa}, x_\kappa(t - t_1)), 0) = (\Phi^{TQ}(g_{1\kappa}, x_O(\tilde{t} + t - t_1)), 0)$$

with x_O denoting the manifold orbit of duration t_f starting at $t = 0$. Thus, for the existence of an extended maneuver, it is crucial that $t_\kappa \leq t_f - \tilde{t}$, i.e. that the incoming maneuver enters the manifold orbit before the outgoing maneuver leaves it. From this point of view, the compatible manifold primitive is defined by the points where the maneuvers enter and leave the manifold orbit, whenever this leads to an admissible trajectory x_κ, that is when $t_\kappa \geq 0$. □

Since the extended maneuvers can be seen as classical maneuvers, controllability of the maneuver automaton as proved in [FDF05] still holds in the same sense for the extended maneuver automaton.

For the construction of a motion planning library, a finite set of trim primitives and orbits on manifolds has to be chosen. The computation of trim primitives via the controlled amended potentials offers different ways on how to quantize the set of trim primitives. One approach is to start by gridding the values of the momentum map which is strongly related to fixing the Lie algebra elements. Then, configurations and controls have to be chosen to match the condition of critical points of the amended potential. The other way round, one can also start by fixing configuration variables and control inputs and search for the admissible momentum map's value which then leads to the corresponding Lie algebra element. For an example, recall the simple relation between height and rotational velocity of relative equilibria of the spherical pendulum shown in Example 2.10 and confer to Section 5.6.1 for a further discussion.

It is sufficient to select and store only a trim's initial value $\alpha(0) = (x_\alpha(0), u_\alpha(0))$ and its generating Lie algebra element ξ_α, because an orbit of arbitrary length can be constructed via Equation (5.6). Since generating the flow on a manifold orbit would require the original Lagrangian flow, which is typically not known explicitly, the entire discretized manifold orbit as it can be computed by numerical integration, is stored in one data file. One manifold orbit can generate a family of manifold primitives, as it has been explained above. For different manifold orbits, e.g. trajectories

that leave the critical object in different directions, orbits of stable and unstable manifolds, or even orbits belonging to different critical objects, several data files have to be provided.

In the next step, the motion planning library has to be enriched by maneuvers, such that extended maneuvers including manifold primitives can be generated during the sequencing process at planning. Thus, maneuvers have to be designed to connect pairs of trim primitives and pairs of orbits on manifolds as well as pairs of a trim primitive and a manifold orbit. It is not necessary to construct a fully connected graph, but a good connectivity is important for a large number of reachable states (cf. [FDF05]). For the generation of maneuvers, optimal control problems can be stated and solved, such that the connecting maneuvers are optimal w.r.t. some predefined objectives. In this thesis, we follow the idea of [Kob08] and use DMOC (cf. Section 3.3) for computing the connecting maneuvers.

5.5.2 Optimal Maneuvers

An *optimal maneuver* π for a mechanical system is approximated by the solution of the following discrete optimal control problem for $\Delta t = \{t_0 = 0, t_1, \ldots, t_N = |\pi|\}$

$$\begin{aligned} \min_{q_d, u_d} & J_{\pi,d}(q_d, u_d) = \sum_{k=0}^{N-1} C_d(q_k, q_{k+1}, u_k) \\ \text{w.r.t. } & D_1 L_d(q_k, q_{k+1}) + D_2 L_d(q_{k-1}, q_k) + f_k^- + f_{k-1}^+ = 0, \quad k = 1, \ldots, N-1, \\ & r_\pi((q_0, p_0), (q_N, p_N)) = 0, \end{aligned}$$

where the costs of the maneuver are approximated by $J_{\pi,d}(q_d, u_d)$. The crucial part is the explicit definition of the boundary condition, denoted by r_π. Here, several variants can be chosen due to the symmetry invariance and the definition of trim and manifold primitives. For simplicity, we consider the boundary conditions as functions of the initial and final discrete configurations and discrete momenta since then, the discrete forced Legendre transforms can be used to reformulate the conditions into constraints of (q_0, q_1) and (q_{N-1}, q_N), respectively (cf. Equation (3.16)). The other way round, if trim or manifold primitives are given in configuration and velocity coordinates, the continuous Legendre transform can be used to obtain the corresponding boundary points in (q, p) coordinates. Further, we distinguish between the following types of connecting maneuvers:

(i) starting at trim α and ending at trim β,

(ii) starting at trim α and ending at manifold orbit O_2,

(iii) starting at manifold orbit O_1 and ending at trim β, or

(iv) starting at manifold orbit O_1 and ending at manifold orbit O_2.

Fixed Boundaries In the simplest case, points on both, the preceding and the succeeding primitive, either a trim or a manifold primitive, are fixed. The boundary condition then reads

$$r_\pi((q_0,p_0),(q_N,p_N)) = \begin{pmatrix} q_0 - q^0 \\ p_0 - p^0 \\ q_N - q^{|\pi|} \\ p_N - p^{|\pi|} \end{pmatrix}, \text{ with } \begin{array}{lll} \text{(i)} & (q^0,p^0) \in \alpha, & (q^{|\pi|},p^{|\pi|}) \in \beta, \\ \text{(ii)} & (q^0,p^0) \in \alpha, & (q^{|\pi|},p^{|\pi|}) \in O_2, \\ \text{(iii)} & (q^0,p^0) \in O_1, & (q^{|\pi|},p^{|\pi|}) \in \beta, \\ \text{(iv)} & (q^0,p^0) \in O_1, & (q^{|\pi|},p^{|\pi|}) \in O_2, \end{array}$$

fixed. Here, we implicitly fix the displacement of the maneuvers as well. On the one hand, this can be seen as ignoring the symmetry properties of the system. On the other hand, parametrizing over e.g. the final points allows to design a family of maneuvers with varying displacements. An entire family of maneuvers can become quite beneficial in the planning when staying on the trims is not for free such that sequences with suitable maneuver displacements are cheaper than solutions with long coasting times on the trims to meet the predefined total displacement.

Free Group Displacement To reduce the number of maneuvers which have to be computed for a motion planning library and also the number of constraints in the optimization problem, the group displacement can be left undefined and thereby implicitly becomes an additional optimization variable. Let us therefore assume that there exists a mapping $\varpi : T^*Q \to T^*Q\backslash G$ which subtracts out the invariant coordinate. In the simple case of cyclic variables, this means that the corresponding boundary constraints can be omitted and only the shape variables of q^0, p^0, $q^{|\pi|}$ and $p^{|\pi|}$ have to be defined. Since the maneuvers, i.e. in particular their boundary points, are invariant w.r.t. group actions, the mapping ϖ can be applied equivalently either simultaneously to the initial and final points or to one boundary only. Thus, as boundary conditions, one can choose for instance

$$r_\pi((q_0,p_0),(q_N,p_N)) = \begin{pmatrix} \varpi(q_0,p_0) - \varpi(q^0,p^0) \\ \varpi(q_N,p_N) - \varpi(q^{|\pi|},p^{|\pi|}) \end{pmatrix},$$

$$\text{with either } \begin{array}{lll} \text{(i)} & \varpi(q^0,p^0)) \in \varpi(\alpha), & \varpi(q^{|\pi|},p^{|\pi|}) \in \varpi(\beta), \\ \text{(ii)} & \varpi(q^0,p^0)) \in \varpi(\alpha), & \varpi(q^{|\pi|},p^{|\pi|}) \in \varpi(O_2), \\ \text{(iii)} & \varpi(q^0,p^0)) \in \varpi(O_1), & \varpi(q^{|\pi|},p^{|\pi|}) \in \varpi(\beta), \\ \text{(iv)} & \varpi(q^0,p^0)) \in \varpi(O_1), & \varpi(q^{|\pi|},p^{|\pi|}) \in \varpi(O_2) \end{array} \text{ fixed.}$$

In Section 5.6.1, this set of boundary conditions is discussed and illustrated for the spherical pendulum example.

Free Boundary Values On Manifold Orbits As a third alternative, instead of fixing points on the manifold orbits, the image of the orbit is used as the initial and/or final target set (cf. Section 3.1.2 for a discussion of target sets in optimal control problems). This could be combined with a free group displacement, but for clarity we restrict to free boundary values on manifold orbits here.

$$
\begin{aligned}
&r_\pi((q_0,p_0),(q_N,p_N)) \\
&= \begin{cases}
\left(\begin{pmatrix} q_0 \\ p_0 \end{pmatrix} - \begin{pmatrix} q^0 \\ p^0 \end{pmatrix}, \begin{pmatrix} q_N \\ p_N \end{pmatrix} - \begin{pmatrix} q^{|\pi|} \\ p^{|\pi|} \end{pmatrix} \right)^T & \text{in (i) with } (q^0,p^0),\ (q^{|\pi|},p^{|\pi|}) \text{ fixed,} \\
\left(\begin{pmatrix} q_0 \\ p_0 \end{pmatrix} - \begin{pmatrix} q^0 \\ p^0 \end{pmatrix}, \zeta_{O_2}(q_N,p_N) \right)^T & \text{in (ii) with } (q^0,p^0) \text{ fixed,} \\
\left(\zeta_{O_1}(q_0,p_0), \begin{pmatrix} q_N \\ p_N \end{pmatrix} - \begin{pmatrix} q^{|\pi|} \\ p^{|\pi|} \end{pmatrix} \right)^T & \text{in (iii) with } (q^{|\pi|},p^{|\pi|}) \text{ fixed,} \\
\left(\zeta_{O_1}(q_0,p_0), \zeta_{O_2}(q_N,p_N) \right)^T & \text{in (iv).}
\end{cases}
\end{aligned}
$$

An implementation of these boundary conditions requires a representation of the manifold orbits, i.e. a function $\zeta_O : T^*Q \to \mathbb{R}$, such that $\zeta(q,p) = 0$ if and only if $(q,p) \in O$. Ideally, one should choose the analytic expression of the manifold orbit here. Since analytic solutions for manifolds are rarely at hand, the boundary target sets could be alternatively approximated by splines, for instance. The advantage of this choice of boundary conditions is that a solution to the corresponding problem is the – unique, up to local optima – *optimal transition* between the motion primitive orbits and therefore, the size of the motion planning library is reduced. However, this local optimality does not automatically lead to global optimal sequences, if, for example, the maneuver's displacement is suboptimal for the specific planning problem. This can be improved by providing different alternative maneuvers for the specific transition. Further, recall from Proposition 5.14 and the discussion thereafter that it has to be checked if the resulting maneuvers lead to valid extended maneuvers. Although this is automatically ensured if the maneuvers are used in the sequencing procedure later on, the automaton's designer may want to consider this fact early on for general reachability questions.

To sum up, the choice of boundary conditions is a design problem which has to be solved as a trade off between limiting the computational effort, while generating a flexible maneuver automaton. An even more detailed specification of boundary conditions can be made for complex examples with a higher dimensional Lie group, for instance, but this is omitted at this point. Instead, we finally discuss another type of a maneuver family connecting one pair of trim or manifold primitives, namely Pareto optimal maneuvers.

5.5.3 Pareto Optimal Maneuvers

Recall that the costs of a motion plan ρ were defined as $J(\rho) = \int_0^T C(\rho(t))\,dt = \sum_{i=1}^{N}(J_{\pi_i} + c_{\alpha_i}\tau_i) + c_{\alpha_f}\tau_f$ (cf. Equation 5.3) and, in particular, the connecting maneuvers are designed to be optimal with respect to a cost functional $J_\pi(q,u) = \int_0^{|\pi|} C(q(t),\dot{q}(t),u(t))\,dt$ (cf. Section 5.5.2), i.e. $J_\pi(\cdot,\cdot)$ is a real-valued scalar functional. Thus, either the minimization of only a single objective is of interest, or a weighted sum of objectives has been formed already. For the latter case, assuming K objectives $C_k : TQ \times U \to \mathbb{R}$, $k = 1,\dots,K$ are of interest, a weighting vector $\lambda \in \mathbb{R}^K$, typically with $\lambda_k \in \mathbb{R}_0^+$ for all $k = 1,\dots,K$ and $\sum_{k=1}^{K}\lambda_k = 1$, is introduced. Then, a scalar-valued cost functional can be generated by

$$\begin{aligned} J_\pi(q,u) &= \int_0^{|\pi|} \sum_{k=1}^{K} \lambda_k \cdot C_k(q(t),\dot{q}(t),u(t))\,dt \\ &= \int_0^{|\pi|} \lambda^T \cdot \mathbf{C}_\pi(q(t),\dot{q}(t),u(t))\,dt, \end{aligned}$$

with $\mathbf{C}_\pi = (C_1,\dots,C_K) : TQ \times U \to \mathbb{R}^K$.

The weighting of the objectives corresponds to a prioritization; objectives of major importance are weighted with multipliers λ_k close to one, such that minor important objectives are multiplied with factors which are almost zero. However, oftentimes, such a prioritization is not known a priori in motion planning problems. Therefore, one considers the optimal control problem in a multiobjective sense; we refer to Section 3.1.3 for a definition of multiobjective optimal control problems.

A *Pareto optimal maneuver* (for a mechanical system) is a motion primitive which solves the following multiobjective optimal control problem with the vector of cost functionals $\mathbf{J}_\pi = (J_1,\dots,J_K)$

$$\begin{aligned} \min_{q,u} \mathbf{J}_\pi(q,u) &= \begin{pmatrix} \int_0^{|\pi|} C_1\,dt \\ \vdots \\ \int_0^{|\pi|} C_K\,dt \end{pmatrix}, \\ \text{w.r.t. } \frac{\partial}{\partial q}L(q,\dot{q}) - \frac{d}{dt}\frac{\partial}{\partial \dot{q}}L(q,\dot{q}) + f_L(q,\dot{q},u) &= 0, \\ r_\pi((q(0),\dot{q}(0)),(q(|\pi|),\dot{q}(|\pi|))) &= 0. \end{aligned}$$

A Pareto optimal maneuver can be approximated by the corresponding *discrete* multiobjective optimal control problem. Then, r_π can be chosen as one of the boundary conditions discussed in Section 5.5.2. Typically, there exists a whole set of Pareto optimal maneuvers solving the multiobjective optimal control problem,

denoted by the *Pareto set of optimal maneuvers*.

Applying multiobjective optimization techniques allows us to approximately compute the entire set of optimal compromises. An approximation of the entire Pareto set of an optimal control problem provides crucial information for deciding on a particular control maneuver. In the motion planning with primitives approach, alternative Pareto optimal maneuvers can be incorporated in the maneuver automaton (cf. e.g. the maneuvers π_2, π_3 and π_4, which connect the trims α_1 and α_2 in Figure 5.1). Thereby, the decision making, e.g. a prioritization of one objective over another, can be postponed until the sequencing phase. In principle, it would be even possible to change the prioritization during the sequencing, e.g. if the sequencing is performed online during a system's operation.

Typical examples of contradictory objectives from many applications are energy efficiency of a steering maneuver and time optimality (cf. e.g. the examples in Section 5.6). For illustration, a motion planning problem of an autonomous robot with these objectives is given in Section 5.6.3. One possible method for the computation of Pareto optimal maneuvers is a scalarization approach based on a reference point technique to approximate the Pareto set (cf. e.g. [LHDV10, ORZ12]). A short description of this method, which combines the optimization of the scalarized auxiliary problems with DMOC is given in Section B.2 in the appendix.

5.5.4 Motion Primitives Search Tree

Having an extended library of motion primitives at hand, the final step is to apply a sequencing method that solves the planning problem stated in Section 5.2. We emphasize that a motion planning library, formally organized by a maneuver automaton, provides solution sequences for any combinations of initial and final trim primitives that can be connected by a path through the graph (cf. [FDF05]). Regarding an online applicability, a concrete planning problem has to be specified just before the sequencing can start and the planning library can be reused for later planning problems. Thus, let us assume now that a planning problem is given in the form of Problem 5.5.

Our sequencing method is based on a search tree (see Figure 5.4) which expands all possible sequences of trims and manifold orbits and connecting maneuvers. The tree is grown in depth-first manner so that each trajectory contains at most $\dim(G) + 2$ trim primitives. Here, $\dim(G)$ denotes the dimension of the symmetry group. The length of admissible sequences and thereby the number of required primitives is usually known in advance, but depends on the concrete system and the structure of the maneuver automaton. For example, in case that equilibrium trims exist, these trims cannot be used to reduce the group displacement between initial and final point of the control problem.

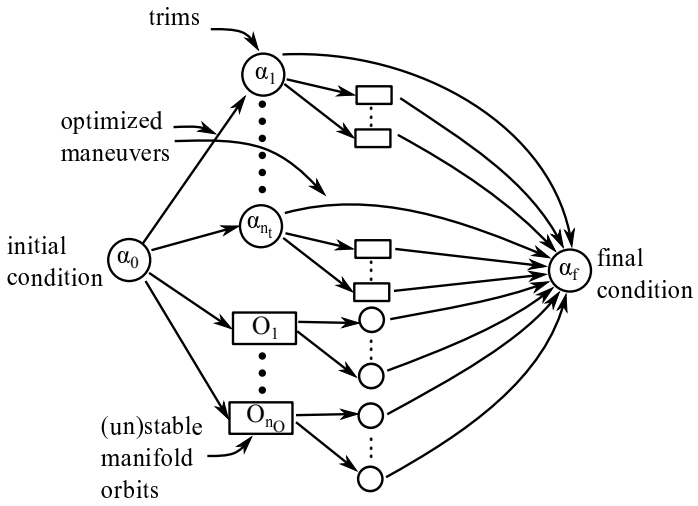

Figure 5.4: An example of a search tree expanding paths of various sequences of primitives. This particular tree provides sequences with three trim primitives each.

Example 5.15: In the following, we list a few examples of motion primitive sequences for illustration.

(a) Consider a one-dimensional Lie group, i.e. $\dim(G) = 1$. If either the initial trim, α_0, or the final trim, α_f, (or both) are non-equilibrium, the shortest admissible sequence is of the form $\alpha_0\pi_0\alpha_f$ using one maneuver π_0. The shortest sequence including a manifold orbit is $\alpha_0\pi_0 O_1\pi_1\alpha_f$ with two connecting maneuvers, i.e. $\pi_0\kappa_1\pi_1$ forms an extended maneuver with κ_1 being the appropriate part of the manifold orbit O_1.

(b) Consider a system with $\dim(G) = 2$ and non-equilibrium trims α_0 and α_f. Then, the shortest solution sequence is still $\alpha_0\pi_0\alpha_f$ or, including a part of a manifold orbit, $\alpha_0\pi_0 O_1\pi_1\alpha_f$. However, an initial or final equilibrium trim may require an additional intermediate trim to overcome the group displacement between α_0 and α_f and thus an additional connecting maneuver as well.

(c) For a system with $\dim(G) = 3$, a number of different types of sequences may exist, in particular depending on the chosen trim primitives. Even for non-equilibrium trims, but if we assume that each trim primitive corresponds to a motion that changes the group displacement in exactly one dimension of G, each sequence generally contains three primitives, leading to the combinations

- $\alpha_0\pi_0\alpha_1\pi_1\alpha_f$, with two maneuvers,
- $\alpha_0\pi_0 O_1\pi_1\alpha_1\pi_2\alpha_f$, with three maneuvers,

- $\alpha_0\pi_0\alpha_1\pi_2 O_1\pi_3\alpha_f$, including also three maneuvers, or
- $\alpha_0\pi_0 O_1\pi_1\alpha_1\pi_2 O_2\pi_3\alpha_f$, with even four connecting maneuvers.

Thus, for general non-equilibrium α_0 and α_f, the number of motion primitives along trajectories in the tree varies from $2 \cdot \dim(G) - 1$ (when no manifolds are visited) to $4 \cdot \dim(G) - 3$ (when alternating between visiting trims and manifolds).

By the construction of the maneuver automaton, the sequence, or motion plan, ρ is an admissible solution for the optimal control problem from the initial state x_0 to the final state x_f. Our sequencing method simply compares the cost of each admissible sequence to the best solution found so far and thereby determines the optimal sequence to the given planning problem. The best sequence can be used as a sophisticated initial guess for a post optimization, e.g. performed by DMOC again. If the maneuver automaton is small, i.e. the gridding of trim and manifold state space is rough and the number of different connecting maneuvers is small, a post optimization is useful to smooth out the changes between controlled and uncontrolled pieces of the sequence trajectory (cf. the post optimization technique in Section 4.3 that was used for similar reasons).

In multiobjective planning problems, there are two possibilities how to perform the sequencing:

- choosing one objective or a fixed prioritization first, and then searching for the sequence(s) which minimize the corresponding cost function (this reduces the problem to the ordinary single objective case), or

- searching for all admissible sequences which are Pareto optimal to provide a knowledge base of alternative Pareto optimal choices.

In Section 5.6.3, the sequencing method is applied to an automaton with Pareto optimal maneuvers and the resulting admissible sequences are illustrated. In general, for large real-world applications, the search tree method should be replaced by an appropriate mixed-integer multiobjective optimization method (cf. Problem 5.5). In [Kob08], for instance, (single objective) motion planning problems have been addressed by random tree search methods.

5.6 Applications

The following three examples illustrate the motion planning with motion primitives focussing on the different aspects of the approach. The simple spherical pendulum and, in particular, the double spherical pendulum example show the benefit of

manifold orbits in the motion planning library for the computation of energy efficient solutions. The example with the car-like robot is used to illustrate the motion planning with Pareto optimal maneuvers.

5.6.1 Motion Planning for a Spherical Pendulum

The first example is the spherical pendulum, which has been already introduced in Example 2.6 in Chapter 2. Recall that the two angles for describing the pendulum's position on the sphere $Q = S^2$ (with radius r) are denoted by φ for the vertical and θ for the horizontal component. Now, we add control forces to the system. Concretely, two controls u_θ and u_φ are introduced via the Lagrangian forcing

$$f(u_\theta, u_\varphi) = \begin{pmatrix} u_\theta \\ u_\varphi \end{pmatrix}.$$

For consistency, all parameter values are still fixed to 1 for the numerical computations. Before a planning problem is considered, we study the different kind of motion primitives for the controlled spherical pendulum.

Trim Primitives In Example 2.10, relative equilibria of the spherical pendulum have been identified as horizontal rotations in the lower hemisphere with constant velocity. As it has been shown in Section 5.3, these motions form uncontrolled trim primitives for the mechanical system. Now, using a constant control u_φ and setting u_θ to zero, the class of trim primitives can be extended. For a chosen rotational velocity $\dot{\theta}$ and an arbitrary vertical angle φ, even in the upper hemisphere,

$$u_\varphi = -mgr\sin(\varphi) - mr^2\sin(\varphi)\cos(\varphi)\dot{\theta}^2$$

satisfies the definition of a trim and still leads to purely horizontal rotations with constant rotational velocity $\dot{\theta}$. Trim defining triples $(\varphi, \dot{\theta}, u_\varphi)$ are shown in Figure 5.5a.

(Un)stable Manifolds The *planar pendulum* exhibits a hyperbolic equilibrium in the upper fixed point. This gives rise to one-dimensional stable and unstable manifolds; together they form the separatrix in the well known phase portrait of a simple pendulum (cf. Example 4.4). For purely vertical initial conditions ($\dot{\theta} = 0$), the spherical pendulum behaves like a planar pendulum. This, together with the horizontal symmetry, explains why the stable and unstable manifold of the upper equilibrium $\bar{x} = (\bar{q}, 0)$ of the spherical pendulum are given by

$$\begin{aligned} W^{u,s}(\bar{x}) &= \{(q,\dot{q}) \in TQ \,|\, J(q,\dot{q}) = 0,\, E(q,\dot{q}) = V(\bar{q}) = 2mgr\} \\ &= \{(\theta,\varphi,\dot{\theta},\dot{\varphi}) | \theta = \text{const.}, \dot{\theta} = 0, \dot{\varphi}^2 = 2\frac{g}{r}(1-\cos(\varphi))\}, \end{aligned}$$

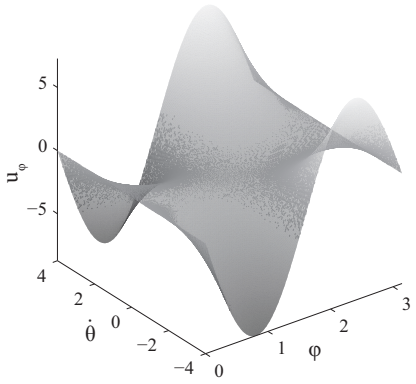

(a) Trim primitive generating control values u_φ for horizontal angles $0 \leq \varphi \leq \pi$ and horizontal velocities $-4 \leq \dot{\theta} \leq 4$.

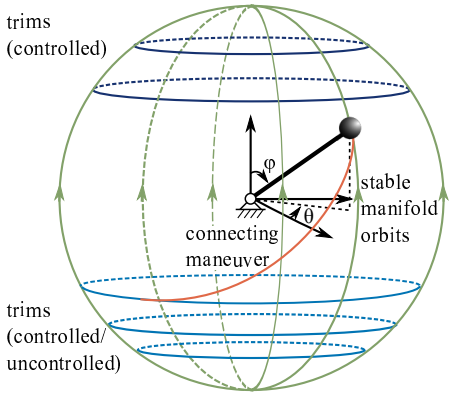

(b) Motion primitives sketched in configuration space: trims are purely horizontal motions ($\dot{\varphi} = 0$), whereas the stable manifold orbits are vertical motions ($\dot{\theta} = 0$).

Figure 5.5: Motion primitives for the spherical pendulum.

i.e. the manifolds of the planar pendulum with an arbitrary, but fixed horizontal angle (cf. also [LSE99] for a definition of the stable manifold of the spherical pendulum's upper equilibrium by means of the energy and the momentum function). $E(q, \dot{q}) = K(q, \dot{q}) + V(q)$ denotes the system's energy; for all points on the manifolds, it is identical to the potential energy in the equilibrium configuration $\bar{q}$. The orbits on the (un)stable manifolds are purely vertical motions. Since the trim primitives are horizontal rotations, we definitely need controlled maneuvers as a third type of motion primitives to be able to generate sequences of primitives. All three types of motion primitives for the spherical pendulum are depicted on the configuration manifold of the spherical pendulum in Figure 5.5b.

Connecting Maneuvers and Motion Planning For the motion planning library, we store a set of uncontrolled and controlled trim primitives as well as an orbit on the stable and on the unstable manifold for the upper equilibrium. Connecting maneuvers are computed by DMOC. Here we allow forcing in both coordinate directions and search for solutions that minimize

$$J(x, u) = \int_0^1 \left(u_\theta(t)^2 + u_\varphi(t)^2 \right) \, dt.$$

We fix the boundary points on the manifold but for the initial or final points on trims, we allow an arbitrary value of the horizontal coordinate, such that the group

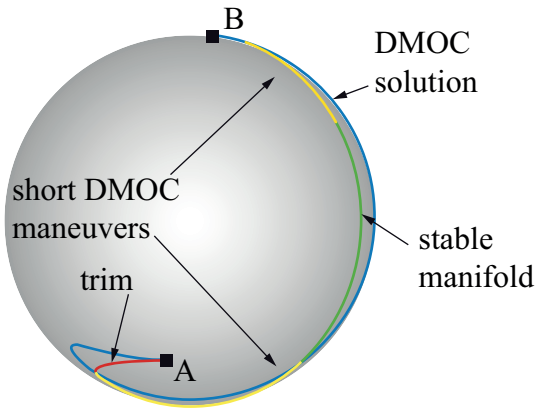

(a) Optimal sequence of motion primitives and DMOC maneuver.

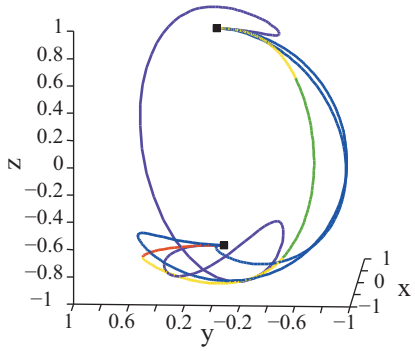

(b) Sequence of motion primitives and direct solutions with different durations (purple).

Figure 5.6: Optimal sequence for a scenario from trim A to trim B consisting of the trims, two controlled maneuvers and a trajectory on the stable manifold in between. The blue curve is the solution of a DMOC optimization with the sequence as initial guess. The additional purple curves in the right figure are DMOC maneuvers with durations $t_f = 2$ and $t_f = 12$.

displacement of the maneuvers is determined by the optimization as well.

As an exemplary scenario we choose a starting point A and a final point B on trims ($\varphi_A = \frac{13}{16}\pi$ on an uncontrolled trim, $\varphi_B = \frac{1}{8}\pi$ for a controlled trim with $\dot{\theta} = -\pi$) and search for sequences with minimal control effort that connect these trims via a stable or unstable manifold orbit.

The resulting trajectory (cf. Figure 5.6a) has the costs $J = 3.2211$ and the final time $t_f = 4.3335$, which is the sum of the time spent on the trims, the fixed durations of the maneuvers and the time that the sequence stays on the manifold orbit. The sequence is then used as an initial guess for a post optimization by DMOC, that reduces the costs of the sequence to $J = 1.3821$. This is compared to optimal solutions of naive, direct optimizations[4] with simple linearly interpolated initial guesses, i.e. we interpolate each coordinate between its initial and final point. Such an initial guess can be constructed without any knowledge of the dynamical system, however, the resulting curve is by no means an admissible solution. It turns out

[4]In the numerical tests for direct or post-optimized DMOC solutions, we observed problems with the pendulum's singularity in the lower equilibrium point, i.e. we obtained solutions with kinks at this point. To avoid this behavior, we used an alternative implementation of the spherical pendulum as a differential algebraic system. Afterwards, the solutions, in particular the resulting control trajectories, have been transformed back in order to compare the control effort to the motion planning solutions.

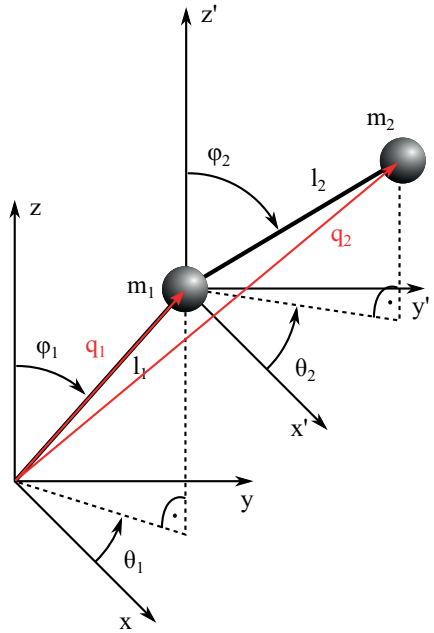

Figure 5.7: The double spherical pendulum.

that the information about the duration of the optimal trajectory that we obtain from the sequencing approach is important for finding energy efficient maneuvers: direct solutions for $t_f = 2$ or $t_f = 12$ (cf. Figure 5.6b) have much higher costs of $J = 6.3427$ and $J = 2.6084$. For the time t_f defined by the sequence, the resulting direct solution is similar to the sequence in its costs and its qualitative behavior. However, in more complicated systems, such as a double spherical pendulum, it is much harder to find any reasonable, admissible solution without starting from a sophisticated initial guess.

5.6.2 Motion Primitives for Energy Efficient Control of a Double Spherical Pendulum

In case of a double spherical pendulum, motion primitives are computed by numerical techniques, as described in the following. Afterwards, we show results for specific optimal control scenarios, where the motion primitives sequence is compared to results from simple black-box optimizations. Recall from Example 2.16 in Chapter 2 that the double spherical pendulum has four degrees of freedom, for which we choose the vertical and the horizontal angles of both pendula as configuration coordinates (for convenience, we repeat its sketch in Figure 5.7).

Trim Primitives Trims of the uncontrolled system, i.e. relative equilibria, are presented in Example 2.16 (cf., in particular, Figure 2.6) based on the presentation in [MS93]. According to Corollary 5.8, additional trims with nonzero constant control values can be generated by controls that do not influence the conservation of the angular momentum, i.e. the total momentum w.r.t. the z-axis, denoted by $J_{\theta_1\theta_2}$ (cf. Equation (2.19)). Hence, we add a potential force to the original potential $V(q)$ and obtain

$$V^u(q,u) = V(q) - \varphi_1 \cdot u_{\varphi_1} - \varphi_2 \cdot u_{\varphi_2}$$

with $u = (u_{\theta_1}, u_{\theta_2}, u_{\varphi_1}, u_{\varphi_2})$ as the general control force for the double spherical pendulum. Theorem 5.7 is applied to the controlled potential and thus $\frac{\partial}{\partial q} V_\mu = u$ for constant $u = (0, 0, u_{\varphi_1}, u_{\varphi_2})^T$ has to be solved for additional, controlled trims. As before, this constrains the two pendula to purely horizontal motions with identical horizontal starting angles and a joint fixed horizontal velocity. Additionally to the uncontrolled trims, constant control values $(u_{\varphi_1}, u_{\varphi_2})$ admit trims with both pendula pointing upwards as well as arbitrary rotating velocities in all shapes.

(Un)stable Manifolds The motion planning problem which we discuss in the following will be a variant of the swing-up problem to the pendulum's up-up equilibrium. Therefore, the stable manifold of this equilibrium ($\bar{x} = (\bar{q}, \dot{\bar{q}}) = 0$) may be of interest for energy efficient motion primitive sequences. In this point, the system's energy equals $E_{\bar{x}} = V(\bar{q})$ while the angular momentum is zero. Hence the (un)stable manifolds are part of the set $\{x \in TQ \,|\, E(x) = E_{\bar{x}},\, J_{\theta_1\theta_2}(x) = 0\}$. This includes in particular the motion on (un)stable manifolds of a planar double pendulum and, thus, we restrict the computation of the manifolds to the planar case ($\dot{\theta}_1 = \dot{\theta}_2 = 0$). The stable and unstable manifold of the up-up equilibrium of a planar double pendulum are both two-dimensional (cf. the pendulum examples discussed in Chapter 4). Thus, we have to choose manifold orbits that are stored in the motion planning library. Here, we follow the concept proposed in Section 5.4, that is we choose a manifold orbit along the strong stable manifold. In Figure 5.8 a box covering is given for the stable manifold together with an approximation of the strong stable manifold in black, both computed with GAIO (cf. Section B.1).

Motion Planning Scenario For the numerical computations, we choose the following parameter values: $m_1 = m_2 = 1\,kg$, $l_1 = l_2 = 1\,m$, and $g = 9.81\frac{m}{s^2}$. The strong stable manifold orbit and a couple of trims are generated and stored in the motion planning library. Then, connecting maneuvers have to be computed and stored in the library, as well. To this aim, we consider the fully actuated system

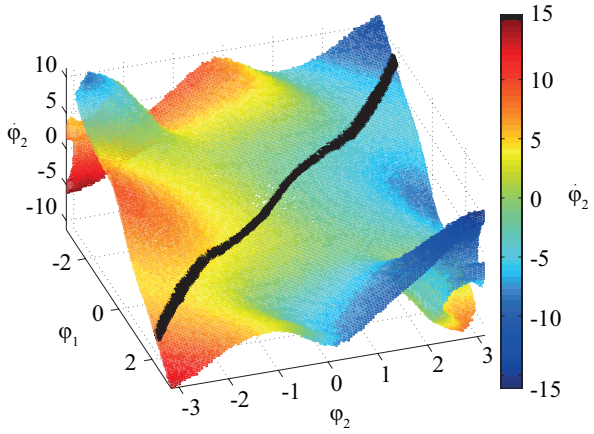

Figure 5.8: Stable manifold of the double pendulum's up-up equilibrium in φ_1-φ_2-$\dot{\varphi}_1$-space with color coding according to the $\dot{\varphi}_2$-coordinate and covering of the strong stable manifold in black, both computed by GAIO.

$(u = (u_{\theta_1}, u_{\theta_2}, u_{\varphi_1}, u_{\varphi_2})^T)$ and choose the control effort as the cost functional, i.e.

$$J(x,u) = \int_0^{t_f} u(t)^2 \, dt \, .$$

For the connecting maneuvers, we allow arbitrary boundary points on the specific trims, i.e. the point is fixed except for the horizontal coordinates, which only have to fulfill $\theta_1 = \theta_2$ since on a trim, the double pendulum horizontally rotates as a rigid structure with both arms in one vertical plane, i.e. with $\theta_1 = \theta_2$ (cf. Section 5.5.2 on boundary conditions with free group displacement). The optimal control problems are solved by the DMOC method, using a sparse SQP algorithm from NAG and derivatives generated from ADOL-C. Since the double spherical pendulum is modeled in minimal coordinates that are not globally valid, we are faced with singularities in our numerical computations. If one of the pendulum's vertical angle equals 0 or π (or multiplicities of that), the horizontal angle becomes meaningless. The NAG algorithm is nonetheless able to perform the optimization for our scenarios. However, to overcome this problem in principle, a global system description by e.g. differential algebraic models could be used alternatively, but is not in the scope of this thesis.

The motion planning is performed for the following scenario: the starting point is chosen to lie on an uncontrolled trim ($\varphi_1 = 2.4087$, $\varphi_2 = 2.2532$), where the double pendulum is in the outstretched shape. The final point is the up-up equilibrium, i.e. where both pendula pointing straight upwards. According to the defined scenario, a sequence is searched for that consists of a maneuver from the trim to the stable

manifold orbit and then a second, very short maneuver to bridge the gap from the orbit's endpoint to the equilibrium itself.

Figure 5.9a shows a resulting sequence with duration $t_f = 3.28$ and costs $J = 548.76$. The durations of the maneuvers have been fixed in advance, such that the entire duration depends on how long the sequence stays on the manifold orbit. The dashed lines refer to the results of a post optimization performed by DMOC, which reduces the costs to $J = 296.51$. One can see that the post optimization smoothes out the (suboptimal) switch from the controlled maneuver to the uncontrolled trajectory on the manifold. In comparison, when DMOC is directly applied to the problem with a simple, linearly interpolated initial guess, the obtained (local) optimal solution (cf. Figure 5.9b) has much higher costs of $J = 5.85 \cdot 10^3$.

In this scenario, we considered sequences involving only one manifold and therefore restricted to the stable manifold of the upper equilibrium. However, it might be possible that a sequence of higher depth including other manifolds as well would even lead to further improvement. This has to remain for future work, though.

5.6.3 Multiobjective Optimal Control of a Simple Mobile Robot

As a third example, we consider the very simplified model of an autonomous robot in order to illustrate the computation and usage of Pareto optimal maneuvers (cf. Section 5.5.3).

Dynamics Simplified dynamics of a mobile robot moving in the plane (cf. Figure 5.10) are given by the Lagrangian

$$L(x, y, \theta, \dot{x}, \dot{y}, \dot{\theta}) = \frac{1}{2} m(\dot{x}^2 + \dot{y}^2) + \frac{1}{2} \Theta \cdot \dot{\theta},$$

with mass m and inertia Θ. Both parameters, as well as the length r are normalized to 1.0. We consider a forcing as depicted in Figure 5.10, such that the robot's equations of motion yield

$$\begin{aligned} m \cdot \ddot{x}(t) &= \cos(\theta) \cdot u_1(t) - \sin(\theta) \cdot u_2(t), \\ m \cdot \ddot{y}(t) &= \sin(\theta) \cdot u_1(t) + \cos(\theta) \cdot u_2(t), \\ \Theta \cdot \ddot{\theta}(t) &= -r \cdot u_2(t). \end{aligned}$$

In the optimal control problem, two objectives are considered: "minimal duration time" and "minimal control effort", i.e. the two cost functionals are

$$J_1(T) = \int_0^T 1 \, dt, \qquad J_2(u_1, u_2, T) = \int_0^T \left(u_1(t)^2 + u_2(t)^2 \right) \, dt.$$

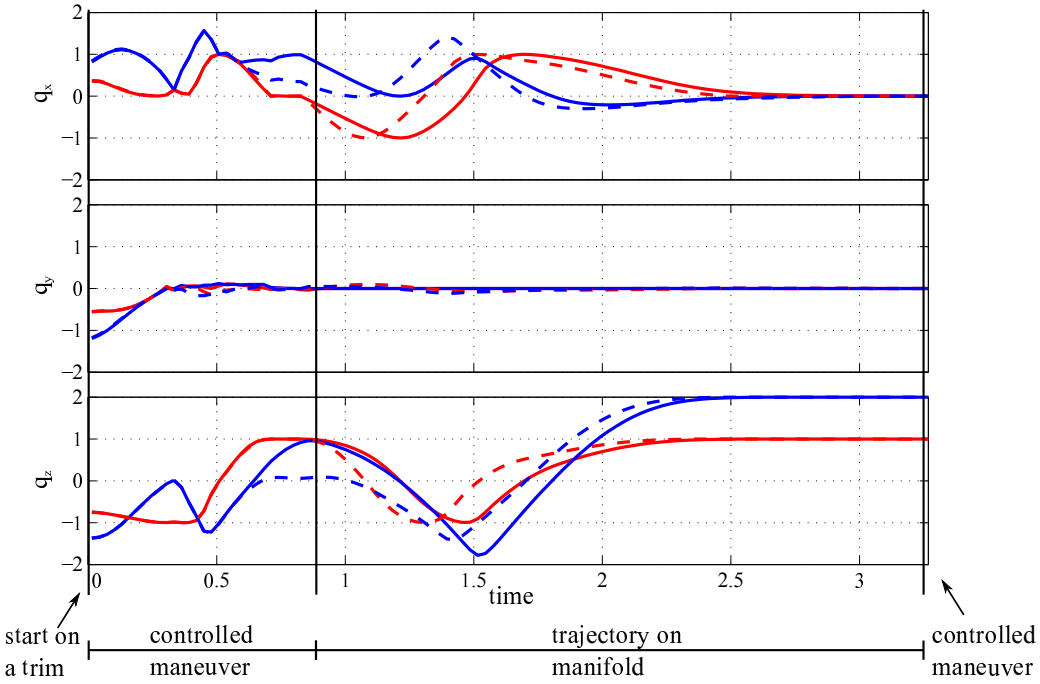

(a) Optimal motion primitives sequence (solid lines) and post optimization (dashed lines).

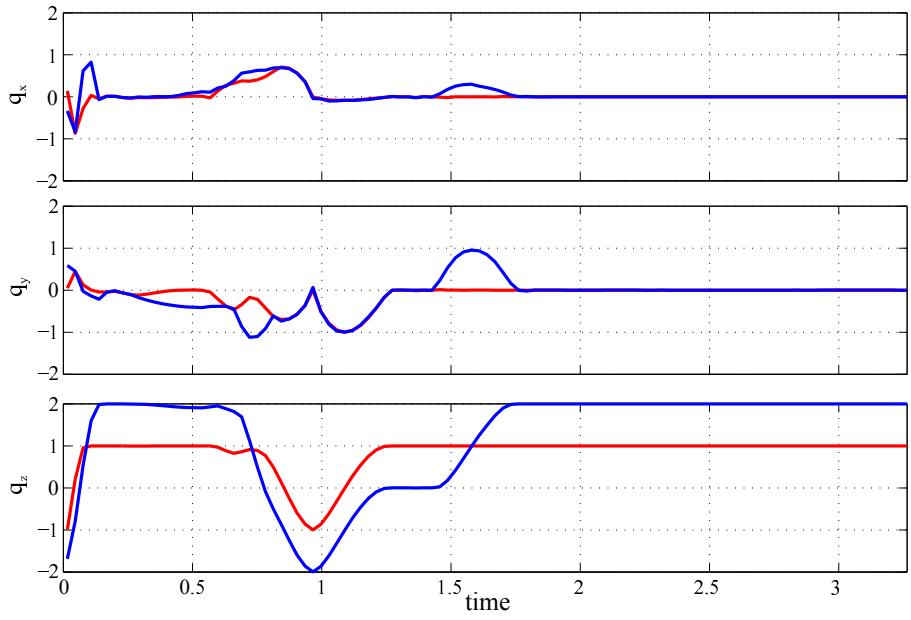

(b) Optimal solution from optimization with simple initial guess.

Figure 5.9: Solutions of the motion planning problem for the double spherical pendulum. The motions of the inner and outer pendulum are drawn in red and blue, respectively, and are given in cartesian coordinates for an easier interpretation.

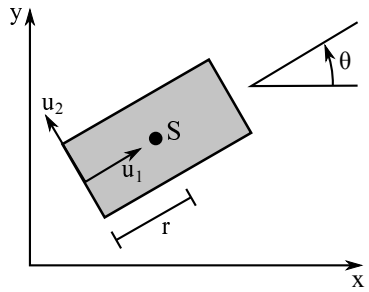

Figure 5.10: Simple model of an autonomous robot in the plane.

Pareto Optimal Maneuvers Pareto optimal control maneuvers can be computed with the reference point technique applied to the DMOC discretization (cf. Section B.2) taking into account the two objectives. In Figure 5.11, one Pareto front and the corresponding Pareto optimal solutions are shown exemplarily for maneuvers from from the point $(x^0, y^0, \theta^0, \dot{x}^0, \dot{y}^0, \dot{\theta}^0) = (60, 0, 0, 0, 0, 0)$ to the final point $(x^T, y^T, \theta^T, \dot{x}^T, \dot{y}^T, \dot{\theta}^T) = (80, 30, 1.5, 0, 0, 0)$.

Motion Planning Scenario The robot is a *mechanical system on a Lie group*, i.e. the entire configuration manifold $Q = \mathbb{R}^2 \times S^1$ is the symmetry group, since the uncontrolled system is invariant w.r.t. translations as well as w.r.t. rotations. Thus, trim primitives are all motions with constant translational and/or rotational velocity and $u_1 = u_2 = 0$.

Since this is an academic example, only a small maneuver automaton is built, designed for the specific planning scenario we want to solve afterwards (cf. Figure 5.12a). More precisely, the robot should start at $A = (0, 0, 0)$ with zero velocity and come to rest at $B = (100, 80, 3\pi/4)$. Thus, the initial and final trim are equilibrium trims. Three further trim primitives, $\alpha_1, \alpha_2, \alpha_3$ are chosen, which corresponds to motions in exactly one direction each (cf. Figure 5.12b). Pareto optimal control maneuver are computed as described above for every edge depicted in the automaton's graph in Figure 5.12a. For simplicity, we restrict to a few representative Pareto optimal maneuvers only. Then, the tree-expansion algorithm, which was presented in Section 5.5.4, is applied to the planning problem. Since sequences with different length may lead to admissible solutions, we rerun the algorithm with depth 5, 7 and 9. Resulting admissible sequences are depicted in the x-y-plane in Figure 5.13.

Among the admissible sequences of length 9, the minimal control effort is $J_2 = 1.608 \cdot 10^3$ and the corresponding sequence has a duration of $J_1 = T = 1.003 \cdot 10^2$. For depth 7, the algorithm returns a sequence with $J_2 = 1.307 \cdot 10^2$ as the one with minimal control effort and this needs a duration of $J_1 = 6.509 \cdot 10^1$. The minimal control effort among all sequences of length 5 is $J_2 = 5.69 \cdot 10^3$ and the

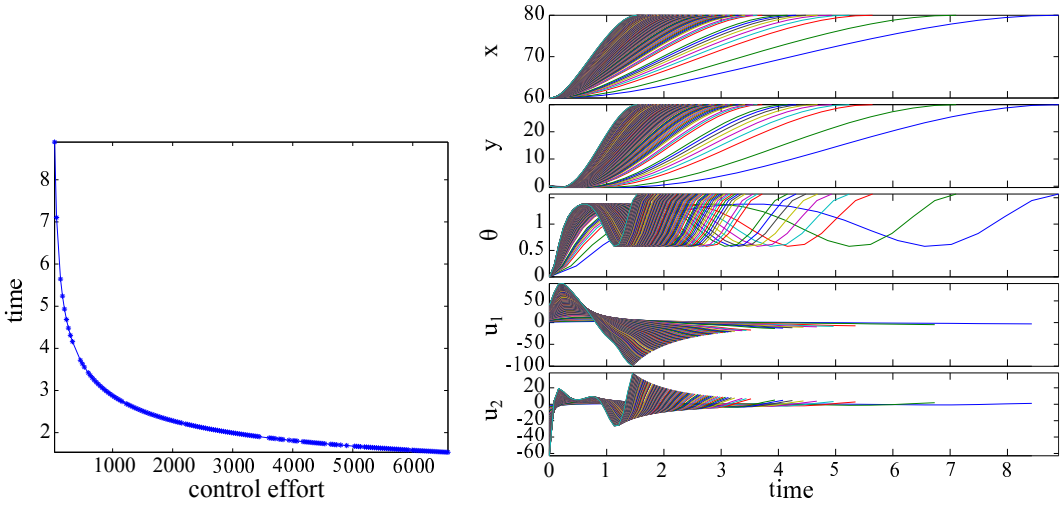

(a) Pareto front.

(b) Pareto optimal configurations and controls.

Figure 5.11: Pareto set and Pareto optimal solutions for an example maneuver from $(x^0, y^0, \theta^0, \dot{x}^0, \dot{y}^0, \dot{\theta}^0) = (60, 0, 0, 0, 0, 0)$ to $(x^T, y^T, \theta^T, \dot{x}^T, \dot{y}^T, \dot{\theta}^T) = (80, 30, 1.5, 0, 0, 0)$.

duration of the corresponding sequence is $J_1 = 2.416 \cdot 10^1$. Thus, if control effort is of prior importance, the sequence of length 7 with $J_2 = 1.307 \cdot 10^2$ would be chosen. If the duration gets a higher priority, other sequences, also of a different length, become interesting as well. Since the different sequences share some of the trim primitives, it would be even possible to switch from one maneuver sequence to another in case the priority changes during operation. For a more detailed discussion on motion planning with Pareto optimal maneuvers for self-optimizing systems, we refer to [FO13].

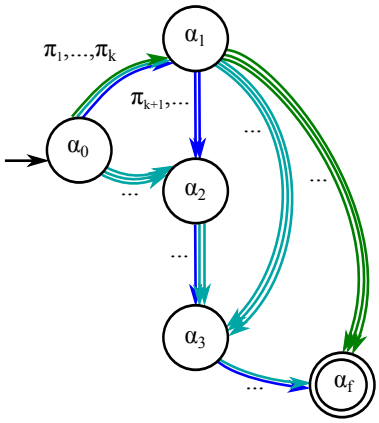

(a) Maneuver automaton with Pareto optimal maneuvers.

Trims:	$\xi = (\dot{x}, \dot{y}, \dot{\theta})$
α_0	$\xi_0 = (0, 0, 0)$
α_1	$\xi_1 = (1.5, 0, 0)$
α_2	$\xi_2 = (0, 1.5, 0)$
α_3	$\xi_3 = (0, 0, 1.5)$
α_f	$\xi_f = (0, 0, 0)$

(b) Trim primitives.

Figure 5.12: Maneuver automaton for robot motion planning. Here, each edge represents a set of Pareto optimal maneuvers. The color of the edges depicts solution sequences of different length (cf. the scenario results in Figure 5.13).

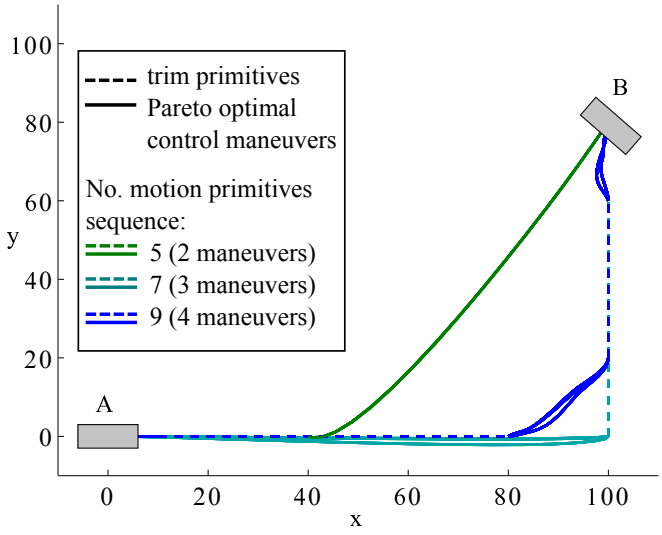

Figure 5.13: Motion primitive sequences for a robot's motion planning scenario: the robot starts at $A = (0, 0, 0)$ and has to be steered to $B = (100, 80, 3\pi/4)$. Admissible solution sequences of length $5, 7$ or 9 include different numbers of controlled maneuvers.

CHAPTER 6

Hybrid Mechanical Systems and Optimal Control

The dynamic behavior of a *hybrid system* is characterized by the interaction of continuous and discrete dynamics. A widely used modeling framework for hybrid systems is the hybrid automaton (cf. Section 6.1), for a thorough introduction we refer to the textbook [SS00].

Classifying mechanical systems as hybrid systems allows us to treat various discrete effects on the continuous dynamics of mechanical systems in a unified way. For instance, impacts of mechanical systems – a bouncing ball in the simplest case, a walking robot touching the ground as a more complex example – are typically modeled as instantaneous events that cause a discontinuity in the velocities. Other examples are changing topologies in multibody systems because of (de)coupling, simplified models of internal or environmental parameters, e.g. nonsmooth friction laws or control units that switch instantaneously between different control policies. In Section 6.2, we extend the variational principle for Lagrangian systems to *hybrid Lagrangian systems*, in order to generate equations of motion for hybrid mechanical systems.

In the third part of this chapter, optimal control problems for hybrid mechanical systems are studied. The optimal control of hybrid systems is a challenging task since it consists of optimizing not only the continuous dynamics, but also the occurrence of discrete events, i.e. the *switching times* and – even though not considered in this thesis – the switching sequence as a discrete variable. Thus, it is favorable to split up the numerical optimization in several layers as proposed in Section 6.3.

A crucial subproblem is the *switching time optimization*, which we study in detail in Section 6.4. It is shown that the time-discretized problem, which has to be used for numerical optimization, does not inherit the smoothness properties of the original

(time-continuous) problem and thus, nonsmooth optimization techniques have to be applied.

The link between this chapter and Chapter 5 is then studied in Chapter 7 by formulating the maneuver automaton generated by the motion primitives as a hybrid system and by extending the definition of trim primitives to hybrid mechanical systems.

6.1 Basic Definitions for Hybrid Systems

There exist a number of different modeling approaches for hybrid systems, e.g. hybrid automata, switched systems, mixed logical dynamical systems, complementarity systems or hybrid inclusions (cf. e.g. [LL09] for an overview of the models and equivalences between them).

In this thesis, we use *hybrid automata* as a basis for the description of hybrid dynamics. Hybrid automata provide a quite general modeling framework, meaning that other models of hybrid systems, e.g. switched systems, can in principle be considered as special subclasses of hybrid automata. The definition of a hybrid automaton follows [SJSL05].

Definition 6.1 (Hybrid automaton)**:** A hybrid automaton is a 6-tuple $\mathcal{H} = (\Gamma, \mathcal{E}, \mathcal{D}, \mathcal{X}, \mathcal{G}, \mathcal{R})$, where

- $\Gamma = \{1, \ldots, k\}$ is a finite set of discrete states ($k \in \mathbb{N}$),
- $\mathcal{E} \subset \Gamma \times \Gamma$ is a collection of edges,
- $\mathcal{D} = \{D_i : i \in \Gamma\}$ is a collection of domains, where $D_i \subset \{i\} \times \mathbb{R}^n$ for all $i \in \Gamma$,[1]
- $\mathcal{X} = \{X_i : i \in \Gamma\}$ is a collection of vector fields X_i on D_i such that X_i is Lipschitz for all $i \in \Gamma$,
- $\mathcal{G} = \{G_e : e \in \mathcal{E}\}$ is a collection of guards, where for each $e = (i, j) \in \mathcal{E}, G_e \subset D_i$, and
- $\mathcal{R} = \{R_e : e \in \mathcal{E}\}$ is a collection of resets, where for each $e = (i, j) \in \mathcal{E}$, R_e is a map $G_e \to D_j$.

The definition of the continuous dynamics can be also generalized to vector fields on smooth manifolds, cf. [LJS+03].

[1] Thus, the domains are distinct copies in $\{i\} \times \mathbb{R}^n$ because of the factor $\{i\}$. Whenever the discrete state is clear from context, we drop the i and write e.g. $D_i \subset \mathbb{R}^n$ for simplicity, cf. also [SJSL05].

Roughly speaking, the behavior of a hybrid system in terms of a hybrid automaton is as follows: the system starts at $x^0 \in D_i$ in a chosen domain D_i and continuously flows inside according to the vector field X_i until it reaches a guard, say $G_{(i,j)}$. Then, a discrete transition $R_{(i,j)}$ into another domain D_j takes place, possibly with a nonsmooth reset of the continuous variables before the system continues flowing according to the new vector field X_j.

Therefore, an appropriate concept of time for hybrid systems requires information on the durations the system spends inside each domain as well as an identification of the time instants of the discrete transitions between different domains. We define the hybrid interval as follows.

Definition 6.2 (Hybrid time interval)**:** Let $\Lambda = \{0, 1, \dots, N\} \subset \mathbb{N}$ be an indexing set. A *hybrid time interval* $\mathcal{I} = \{I_\lambda\}_{\lambda \in \Lambda}$ is a sequence of intervals such that $I_\lambda = [\tau_\lambda, \tau_{\lambda+1}]$ for all $\lambda = 0, \dots, N-1$, and $I_N = [\tau_N, \tau_{N+1}]$ or $I_N = [\tau_N, \tau_{N+1})$. Here, $\tau_\lambda \in \mathbb{R}$, $\lambda = 0, \dots, N+1$ and $\tau_\lambda \leq \tau_{\lambda+1}$.

The boundary values of the sequenced intervals, $\tau_1, \dots, \tau_N$ are called *switching times*. In order to keep track of the actual discrete state and thus the according domain of the mechanical system, a switching sequence is introduced as follows.

Definition 6.3 (Switching sequence)**:** For an indexing set Λ, a *switching sequence* is determined by a map $\gamma : \Lambda \to \Gamma$ governing the visited discrete states.

Definition 6.4 (Execution)**:** An *execution* (also called *solution* or *trajectory*) of a hybrid system $\mathcal{H}$ is a triple $(\mathcal{I}, \gamma, x)$, where $\mathcal{I}$ is a hybrid time interval, $\gamma : \Lambda \to \Gamma$ the switching sequence, and $x = \{x_\lambda : \lambda \in \Lambda\}$ is a collection of C^1 maps such that x_λ is a map $I_\lambda \to D_{\gamma(\lambda)}$ satisfying $\dot{x}_\lambda(t) = X_{\gamma(\lambda)}(x_\lambda(t))$ for all $t \in I_\lambda$. Furthermore, for all $\lambda \in \Lambda \setminus \{N\}$, it holds $(\gamma(\lambda), \gamma(\lambda+1)) \in \mathcal{E}$, $x_\lambda(\tau_{\lambda+1}) \in G_{(\gamma(\lambda),\gamma(\lambda+1))}$, and $R_{(\gamma(\lambda),\gamma(\lambda+1))}(x_\lambda(\tau_{\lambda+1})) = x_{\lambda+1}(\tau_{\lambda+1})$.

Whenever it is clear from context, we will drop the subscript λ for the trajectories of the subparts of the interval. To distinguish between states before and after the reset, we write τ_λ^- to indicate the moment before the switch and τ_λ^+ for the instant right after the switch, i.e. $\tau_\lambda^- \in I_{\lambda-1}$ and $\tau_\lambda^+ \in I_\lambda$.

A hybrid automaton is called *deterministic*, if for each initial state there exists at most one (maximal time) execution. This property is also denoted by *well-posedness* in [SS00]. Regarding the existence of solutions, it is important that a hybrid automaton is *nonblocking*, i.e. for every initial state, there exists at least one solution. We assume that the vector fields are Lipschitz such that the existence of solutions in the interior of domains is ensured. Still, to guarantee the determinism and nonblocking

properties of the system, further assumptions on the underlying graph structure of the automaton have to be made, a study of which is not in the scope of this thesis. In the following, we simply assume that our model of a hybrid system is nonblocking for any starting point in any domain (cf. [LJS$^+$03, SJSL05]).

For our long-term goal, namely to deal with finite time optimal control problems (with a finite maximum number of switches), it is adequate to consider hybrid time intervals with only finite sequences of intervals, i.e. $N < \infty$. However, in general, it is not untypical that hybrid systems undergo infinitely many switches in finite time. This is called *zeno behavior*. We refer to [AZGS06] for a formal definition, examples of mechanical systems that show zeno behavior and a physically meaningful definition of executions beyond a zeno point, or to [SJSL05] for a study of zeno behavior from a geometric perspective. A fundamental reference for the analysis of hybrid systems' dynamics, including reachability conditions, stability results for equilibria and invariant sets, and theorems on existence and uniqueness of solutions is the work of Lygeros, Johansson, Simić et al., [LJS$^+$03].

Discrete events that are triggered when the state trajectory reaches a guard are called *state-controlled* events. Switchings can also be controlled from outside, e.g. triggered by time and thus called *time-controlled*. However, for a given hybrid automaton, time-controlled switchings can be remodeled as state-controlled events. To this aim, an additional continuous state is introduced, for which the vector field is equal to one, such that the state resembles a "clock". Let $x \in \mathbb{R}^n$ denote the normal states, which underlie the dynamics of the vector fields X_i, $i \in \Gamma$. Then, for the clock state $x_{n+1} \in \mathbb{T} \subseteq \mathbb{R}$, we consider the augmented vector fields $(X_i, 1)$. This state then triggers the guard, i.e. $G_{(i,j)} = \{(x, x_{n+1}) \in D_i \times \mathbb{T} \,|\, x_{n+1} - \tau = 0\}$ when τ is the desired switching time for a switch from discrete state i to discrete state j. Purely time-controlled systems are called *switched systems* in this thesis[2]. A switched system is a special kind of a hybrid automaton. More precisely, it is a hybrid automaton with a common (continuous time) domain for all discrete states, i.e. with the projection $\pi_{\mathcal{D}} : \Gamma \times \mathbb{R}^n \times \mathbb{T} \to \mathbb{R}^n$ that maps to the continuous state space of the domain, we have $\pi_{\mathcal{D}}(D_i) = \pi_{\mathcal{D}}(D_j)$ for all $i, j \in \Gamma$. Further, the resets are trivial (i.e. identity maps) for the states x and the guards do not depend on the continuous states except for the additional clock state x_{n+1}. Then, resembling an ordinary differential equation, the following system can be used to model a switched system.

Definition 6.5 (Switched System)**:** Let Γ be a finite set of discrete states (also called *modes*) and $\mathcal{X} = \{X_i : i \in \Gamma\}$ a collection of vector fields on a common state

[2]In the literature, there is no consensus on a definition of switched systems, i.e. in some works, switched systems can be arbitrarily state-controlled as well (see e.g. [LL09, Chapter 4]). However, throughout this thesis, we use the term switched systems for purely time-controlled systems only.

space $\mathcal{D}$. Further, let $\tau_1, \dots, \tau_N$ be a sequence of switching times with $\tau_i \leq \tau_{i+1}$, $i = 1, \dots, N-1$ and τ_0, τ_{N+1} being the initial and final time of the corresponding hybrid time interval. Let $\gamma : \Lambda \to \Gamma$ with indexing set $\Lambda = \{0, \dots, N\}$ be a switching sequence, also called the *mode sequence*. Then, a *switched system* is defined by

$$\dot{x}(t) = \begin{cases} X_{\gamma(0)}(x(t)) & \tau_0 \leq t < \tau_1, \\ X_{\gamma(1)}(x(t)) & \tau_1 \leq t < \tau_2, \\ \quad \vdots & \\ X_{\gamma(N)}(x(t)) & \tau_N \leq t \leq \tau_{N+1}. \end{cases} \tag{6.1}$$

It is then straight forward to generate the unique trajectory of the switched system for a given initial value $x(\tau_0) = x_0$, assuming again that the vector fields are all Lipschitz. Note that this definition includes a prescribed switching sequence, also called a *switching signal*. In the framework of a hybrid automaton, the switching signal can be modeled via clock states, as pointed out above. By this, one of all possible paths through the underlying graph $(\Gamma, \mathcal{E})$ of the hybrid system is chosen or, in other words, the switching signal induces a "small" hybrid subsystem on a subgraph of the larger hybrid automaton. From an alternative point of view, the model of the switched system with its switching signal designs a hybrid system (cf. [Hag12] for a detailed discussion on the relation between hybrid automata and switched systems).

In the *control of hybrid systems*, the optimization of switching times is an important control method. *Hybrid control systems*, in general, are hybrid systems with continuous and discrete controls inputs. In this thesis, we focus on continuous controls for hybrid systems, namely *optimal control for hybrid systems* (cf. e.g. [BGH$^+$02, Sus99b, SC07, PAM07] or [LL09, Chapter 3]) in Section 6.3 and *switching time optimization* in Section 6.4 (see also [XA02a, XA04, EWD03, AA04, EWA06, SDEL09, JM11, CM11, KT12]).

Continuous controls can be integrated into the concept of hybrid automata by introducing a control set $U \subset \mathbb{R}^m$ and replacing the uncontrolled vector fields in $\mathcal{X} = \{X_i : i \in \Gamma\}$ by *controlled vector fields* X_i on $D_i \times U$. We do not consider additional discrete inputs or guards which directly depend on the inputs.

6.2 Hybrid Mechanics

The automaton for a hybrid Lagrangian control system is sketched in Figure 6.1.

Definition 6.6 (Hybrid Lagrangian Control System)**:** A *hybrid Lagrangian control system* is an 8-tuple $\mathcal{H} = (Q, \Gamma, \mathcal{E}, \mathcal{L}, \mathcal{G}, \mathcal{R}, U, \mathcal{F})$, where

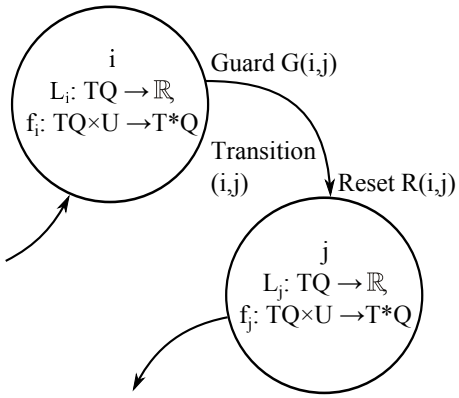

Figure 6.1: Sketch of a hybrid automaton for Lagrangian systems.

- Q is an n-dimensional smooth configuration manifold with associated state space (tangent bundle) given by TQ and cotangent bundle T^*Q,
- Γ is a (countable) set of discrete states,
- $\mathcal{E} \subset \Gamma \times \Gamma$ is a collection of discrete transitions,
- $\mathcal{L} = \{L_i : TQ \to \mathbb{R}\}_{i \in \Gamma}$ is a collection of hyperregular Lagrangian,
- $\mathcal{G} = \{G_e\}_{e \in \mathcal{E}}$ is a collection of guards with $G_e \subset TQ$ for $e = (i, j) \in \mathcal{E}$,
- $\mathcal{R} = \{R_e\}_{e \in \mathcal{E}}$ is a collection of reset maps $R_{(i,j)} : G_{(i,j)} \subset TQ \to TQ$,
- $U \subseteq \mathbb{R}^m$ is the set of admissible controls, and
- $\mathcal{F} = \{f_i : TQ \times U \to T^*Q\}_{i \in \Gamma}$ is a collection of Lagrangian forces.

Assumption 6.7: (i) In the following, we restrict ourselves to guards that depend on configurations only and not on the velocities, thus $G_{(i,j)} \subset Q$. Whenever it is clear from context, we abuse the notation $G_{(i,j)}$ to also denote the subset of TQ, given by configurations in the guard and arbitrary velocities. Further, we assume G to be the smooth boundary of some submanifold of codimension one in Q.

(ii) The reset maps $R_{(i,j)} : G_{(i,j)} \subset TQ \times TQ$ are assumed to act trivially on the configurations, that is, only the velocities are allowed to jump at the discrete events.

(iii) When considering solutions of the hybrid Lagrangian control system and variations of these solutions, we always assume the switching sequence to be fixed in advance.

Hybrid Lagrangian Control System with Two Discrete States For the development of a variational principle for hybrid Lagrangian control systems, we consider a system with two discrete states only and a single discrete event. That is, our hybrid interval equals $\mathcal{I} = \{[0, t_i], [t_i, T]\}$, where the switching time t_i is not fixed yet. As we will see below, the theory easily extends to systems with multiple discrete states and multiple switches but considering the smallest subclass simplifies the notation to some extent. By Assumption 6.7(iii), a switching sequence is given, i.e. $\gamma : \Lambda \to \Gamma$, $\Gamma = \{1, 2\}$, $\Lambda = \{0, 1\}$. Without loss of generality, we can assume $\gamma(0) = 1$, $\gamma(1) = 2$, i.e. the system switches from subsystem 1 to subsystem 2. For abbreviation, we write $G := G_{(1,2)}$ and $R := R_{(1,2)}$.

To be able to consider variations of the configuration curves and also of the switching time, we extend the Lagrangian dynamics by considering the time as an additional freely varying curve of some (artificial time) parameter τ. This is based on the approach of Fetecau et al. for nonsmooth mechanical systems (see [FMOW03]).

Definition 6.8 (Extended Path Space)**:** Define the *extended path space* to be

$$\mathcal{M} = \mathcal{T} \times \mathcal{Q}([0, 1], \tau_i, G, Q),$$

with

$$\mathcal{T} = \{c_t \in C^k([0, 1], \mathbb{R}) \,|\, c_t' > 0 \text{ in } [0, 1]\},$$

and

$$\mathcal{Q}([0, 1], \tau_i, G, Q) = \{c_q : [0, 1] \to Q \,|\, c_q \text{ is a piecewise } C^2 \text{ curve with at most one singularity at } \tau_i \in (0, 1) \text{ where } c_q(\tau_i) \in G\}.$$

A path $c \in \mathcal{M}$ consists of curves c_t and c_q, $c = (c_t, c_q)$, and the associated curve $q(t)$ is given by $q : [c_t(0), c_t(1)] \to Q$, $q(t) = c_q(c_t^{-1}(t))$ with $c_t(0) = 0$ and $c_t(1) = T$. In the following, let k with $2 \leq k < \infty$ denote the order of differentiability[3].

Lemma 6.9: $\mathcal{T}$ is a C^k manifold.

[3]In contrast to [FMOW03], in which C^∞ functions are considered, we use C^k functions with $k < \infty$ in order to model the various path spaces as infinite dimensional manifolds on Banach spaces. This cannot be done for C^∞ (cf. [KM97]).

Proof. $C^k([0,1],\mathbb{R})$ is a Banach space (together with the norm of bounded convergence for the functions and its derivatives up to order k) and thus a C^k manifold. $\mathcal{T}$ is an open subset of $C^k([0,1],\mathbb{R})$ and thus a submanifold and a C^k manifold by itself, see e.g. [AMR88]. □

Lemma 6.10: $\mathcal{Q}([0,1],\tau_i,G,Q)$ is a C^k manifold.

Proof. We only give a sketch of the proof here, since the formal proof requires results from the differential geometry for infinite dimensional manifolds, which go beyond the scope of this thesis[4].

The starting point is a chart (Y,κ) in Q, s.t. $Y \cap G \neq \emptyset$ and $(Y \cap G, \kappa|_{Y\cap G})$ is a submanifold of Q. Then, consider the set

$$\mathcal{Q}_Y = \mathcal{Q}_1([0,\tau_i],Y) \times \mathcal{Q}_2([\tau_i,1],Y) \times (Y \cap G)$$

with

$$\mathcal{Q}_1([0,\tau_i],Y) = \{c_1 : [0,\tau_i] \to Q \,|\, c_1 \text{ is a } C^k \text{ curve, } c_1(\tau_i) \in Y\},$$
$$\mathcal{Q}_2([\tau_i,1],Y) = \{c_2 : [\tau_i,1] \to Q \,|\, c_2 \text{ is a } C^k \text{ curve, } c_2(\tau_i) \in Y\}.$$

We define $g_Y : \mathcal{Q}_Y \to \mathbb{R}^{2n}$, $g_Y(c_1,c_2,q_i) = \begin{pmatrix}\kappa(c_1(\tau_i)) - \kappa(q_i)\\ \kappa(c_2(\tau_i)) - \kappa(q_i)\end{pmatrix}$. Note that $c_1(\tau_i)$ and $c_2(\tau_i)$ are the images of c_1 and c_2, respectively, under the map which evaluates curves at time τ_i. Then, we have $g_Y(c_1,c_2,q_i) = 0 \in \mathbb{R}^{2n}$ if and only if $c_1(\tau_i) = c_2(\tau_i) = q_i \in Y \cap G$ and $c_q : [0,1] \ni \tau \mapsto \begin{cases} c_1(\tau), & \tau \in [0,\tau_i],\\ c_2(\tau), & \tau \in [\tau_i,1]\end{cases}$ is a curve in $\mathcal{Q}([0,1],\tau_i,G,Q)$. This means, the preimages of $g_Y = 0$ define curves in $\mathcal{Q}([0,1],\tau_i,G,Q)$. The manifold structure that we will choose for $\mathcal{Q}_1([0,\tau_i],Y)$ and $\mathcal{Q}_2([\tau_i,1],Y)$ turns the evaluation map at τ_i and thus, g_Y into smooth mappings.

The set $C^k([0,\tau_i],Q)$ is an infinite dimensional manifold modeled on the Banach space $C^k([0,\tau_i] \leftarrow c_1^*TQ)$, where $C^k([0,\tau_i] \leftarrow c_1^*TQ)$ are the *sections* (see Definition A.23), i.e. $\sigma \in C^k([0,\tau_i],TQ)$ with $\pi_Q \circ \sigma = c_1$ and, analogously, for $C^k([\tau_i,1],Q)$ (cf. [KM97, Section 42] for details[5]). Thus, there exist for each curve $c_1 \in C^k([0,\tau_i],Q)$, for instance, a chart which maps curves close to c_1 to curves in

[4] Here, I gratefully acknowledge the helpful comments of A. Schmeding, who took care of the technical details of the proof and pointed out relevant references on smooth and C^k mappings between manifolds to me.

[5] In the proof of [KM97, Theorem 42.1], for our setting, C^∞ can be replaced by C^k and one can exploit the fact that we have mappings on compact intervals instead of arbitrary manifolds. Further, we use the Fréchet differential calculus as before, whereas [KM97] apply the so called *convenient calculus*. Earlier references for manifolds of C^k mappings are [Eel66] or [Mar74, Chap. 1].

$C^k([0,\tau_i] \leftarrow c^*TQ)$. Then, $\mathcal{Q}_1([0,\tau_i],Y)$ and $\mathcal{Q}_2([\tau_i,1],Y)$ are infinite dimensional manifolds, because they are open subsets of $C^k([0,\tau_i],Q)$ and $C^k([\tau_i,1],Q)$, respectively.

The next step is to show that zero is a regular value of g_Y, i.e. $T_z g_Y : T_z\mathcal{Q}_Y \to T_{g_Y(z)}\mathbb{R}^{2n} = \{g_Y(z)\} \times \mathbb{R}^{2n}$ is surjective for every z with $g_Y(z) = 0$. For simplicity, we drop the third factor of $\mathcal{Q}_Y$ for a moment and consider $q_i \in (Y \cap G)$ as being fixed. The derivatives of g_Y at z can be computed with the help of the charts into the Banach space, Riemannian geometry, and the chart κ from Q to $\mathbb{R}^n$ (cf. [KM97] for the explicit construction of charts). This shows that there can be always found maps (c_1, c_2) (with $c_1(\tau_i) = c_2(\tau_i) = q_i$) with tangent vectors $v_1 \in T_{c_1(\tau_i)}\mathcal{Q}_1$, $v_2 \in T_{c_2(\tau_i)}\mathcal{Q}_2$ such that $dg_Y((c_1,c_2),(v_1,v_2)) = w$ for any $w \in \mathbb{R}^{2n}$, which is the tangent space on $g(z) = 0 \in \mathbb{R}^{2n}$. This also holds if $q_i \in (Y \cap G)$ is reconsidered as the third parameter of g_Y. Therefore, $T_z g_Y$ is surjective. Then, the set $g_Y^{-1}(0)$ is a submanifold of $\mathcal{Q}_Y$ (by applying the *Submersion Theorem*, see e.g. [AMR88, Theorem 3.5.4]) and thus has its own manifold structure. Now, $\{g_Y^{-1}(0)\}_Y$ represents a covering of $\mathcal{Q}([0,1],\tau_i,G,Q)$ where each element of the covering is a manifold. Thus, $\mathcal{Q}([0,1],\tau_i,G,Q)$ is a manifold. □

6.2.1 Hybrid Lagrange-d'Alembert Variational Principle

A hybrid version of the Lagrange-d'Alembert variational principle can now be formulated on the extended state space. Because of the instantaneous changes of the system's Lagrangian, jumps in the energy as well as in the system's momenta may occur. These are considered in the impulsive energy effect and the impulsive momentum effect (Definition 6.14), both formally defined below.

Theorem 6.11 (Hybrid Lagrange-d'Alembert Principle)**:** Let $\mathcal{H}$ be a hybrid Lagrangian control system with two discrete modes. Let γ be a fixed switching sequence with one switch and $\mathcal{I} = \{[0,t_i],[t_i,T]\}$ a corresponding hybrid interval with unknown switching time t_i. A curve $q \in Q$ joining $q(0) = q_0$ and $q(T) = q_f$ with $q(t_i) \in G$ satisfies the forced Euler-Lagrange equations on each interval I_λ and the reset condition, $\dot{q}(t_i^+) = R(\dot{q}(t_i^-))$ if and only if for all variations $\delta c \in T_c\mathcal{M}$ it holds

$$\delta\mathfrak{S}(c) + W(c,u) + \mathfrak{M} = \mathfrak{E}, \tag{6.2}$$

where $\mathcal{M}$ is the extended path space, such that $q(t) = c_q(c_t^{-1}(t))$ for $c = (c_t, c_q) \in \mathcal{M}$, $\mathfrak{S}$ denotes the *hybrid action map* (cf. Definition 6.12), $W(c,u)$ is the *hybrid virtual work*, and $\mathfrak{M}$ and $\mathfrak{E}$ are the *impulsive momentum* and *impulsive energy effect* (cf. Definition 6.14), respectively.

Variations of the Hybrid Action Map In order to prove this theorem, we need a couple of preliminary results, the central one being on variations of the hybrid action map in the following paragraph.

Definition 6.12 (Hybrid Action Map)**:** For the hybrid interval $\mathcal{I}$, we define the *hybrid action map* $\mathfrak{S} : \mathcal{M} \to \mathbb{R}$ to be

$$\mathfrak{S}(c_t, c_q) = \int_0^{\tau_i} L_1\left(c_q(\tau), \frac{c_q'(\tau)}{c_t'(\tau)}\right) c_t'(\tau)\, d\tau + \int_{\tau_i}^1 L_2\left(c_q(\tau), \frac{c_q'(\tau)}{c_t'(\tau)}\right) c_t'(\tau)\, d\tau, \quad (6.3)$$

where c' denotes the derivative w.r.t. τ.

When substituting $c_t : [0,1] \to \mathbb{R}$ by $s = c_t(\tau)$, the hybrid action map $\mathfrak{S}$ can be written as

$$\begin{aligned}\mathfrak{S}(q) &= \int_{c_t(0)}^{c_t(\tau_i)} L_1(q(s), \dot{q}(s))\, ds + \int_{c_t(\tau_i)}^{c_t(1)} L_2(q(s), \dot{q}(s))\, ds \\ &= \int_{c_t(0)}^{t_i} L_1(q(s), \dot{q}(s))\, ds + \int_{t_i}^{c_t(1)} L_2(q(s), \dot{q}(s))\, ds,\end{aligned}$$

where $\dot{q}$, the derivative w.r.t. s, equals $\dot{q}(s) = \frac{c_q'(\tau)}{c_t'(\tau)}$.

We define the *extended configuration manifold* to be $Q_e = \mathbb{R} \times Q$ and the *second order submanifold* of $T(TQ_e)$ to be

$$\ddot{Q}_e = \{\omega \in T(TQ_e) \,|\, T\pi_{Q_e}(\omega) = \pi_{TQ_e}(\omega)\} \subset T(TQ_e),$$

with $\pi_{Q_e} : TQ_e \to Q_e$ and $\pi_{TQ_e} : T(TQ_e) \to TQ_e$ being the canonical projections. That is, $\ddot{Q}_e$ is the set of second derivatives $\frac{d^2c}{d\tau^2}(0)$ of C^2 curves $c : [0,1] \to Q_e$ (cf. [FMOW03]).

Lemma 6.13 (Variations of the Hybrid Action Map)**:** Given C^k Lagrangian L_1 and L_2, $k \geq 2$, there exist unique C^{k-2} mappings $D_{EL}L_i : \ddot{Q}_e \to T^*Q_e$ and unique C^{k-1} one-forms Θ_{L_i} on TQ_e $(i = 1, 2)$ such that for all variations $\delta c \in T_c\mathcal{M}$ of c we have

$$\mathbf{d}\mathfrak{S}(c)\cdot\delta c = \int_0^{\tau_i} D_{EL}L_1(c'')\cdot\delta c\, d\tau + \int_{\tau_i}^1 D_{EL}L_2(c'')\cdot\delta c\, d\tau + \Theta_{L_1}(c')\cdot\widehat{\delta c}|_0^{\tau_i} + \Theta_{L_2}(c')\cdot\widehat{\delta c}|_{\tau_i}^1 \quad (6.4)$$

where

$$\widehat{\delta c}(\tau) = \left(\left(c(\tau), \frac{\partial c}{\partial \tau}(\tau)\right), \left(\delta c(\tau), \frac{\partial \delta c}{\partial \tau}(\tau)\right)\right).$$

The *Euler-Lagrange map* $D_{EL}L_i$, $i = 1, 2$, has the coordinate expression

$$D_{EL}L_i(c'') = \left[\frac{\partial L_i}{\partial q}c_t' - \frac{d}{d\tau}\left(\frac{\partial L_i}{\partial \dot{q}}\right)\right] dc_q + \left[\frac{d}{d\tau}\left(\frac{\partial L_i}{\partial \dot{q}}\frac{c_q'}{c_t'} - L_i\right)\right] dc_t,$$

and the *Lagrangian one-form* is given in coordinates by $\Theta_{L_i}(c') = \left[\frac{\partial L_i}{\partial \dot{q}}\right] dc_q - \left[\frac{\partial L_i}{\partial \dot{q}}\frac{c_q'}{c_t'} - L_i\right] dc_t$.

Proof. Variations of the curve c are given by $\delta c = \frac{d}{d\epsilon}c(\tau, \epsilon)\big|_{\epsilon=0}$, where $c(\cdot, \epsilon)$ is a curve in $\mathcal{M}$ with $c(\cdot, 0) = c$ and we can split it into components $c(\cdot, \epsilon) = (c_t(\cdot, \epsilon), c_q(\cdot, \epsilon))$ such that we have $\delta c = (\delta c_t, \delta c_q)$ for the variations. When taking variations of $\mathfrak{S}$ (cf. Equation (6.3)), we apply the slot derivative notation do indicate derivatives of the Lagrangian w.r.t. the first, i.e. $D_1L_1(\cdot, \cdot)$, and the second factor, i.e. $D_2L_1(\cdot, \cdot)$ and we use $L_1(\tau)$ as short for $L_1\left(c_q(\tau), \frac{c_q'(\tau)}{c_t'(\tau)}\right)$. For the first half of the hybrid action map, we then obtain

$$\begin{aligned}
&\delta \int_0^{\tau_i} L_1\left(c_q(\tau), \frac{c_q'(\tau)}{c_t'(\tau)}\right) c_t'(\tau)\, d\tau \\
&\quad= \int_0^{\tau_i} \left[D_1L_1(\tau) \cdot \delta c_q \cdot c_t'(\tau) + D_2L_1(\tau) \cdot \left(\frac{\delta c_q'(\tau)}{c_t'(\tau)} - \frac{c_q'(\tau) \cdot \delta c_t'(\tau)}{(c_t'(\tau))^2}\right) \cdot c_t'(\tau)\right] d\tau \\
&\qquad+ \int_0^{\tau_i} L_1(\tau) \cdot \delta c_t'\, d\tau \\
&\quad= \int_0^{\tau_i} D_1L_1(\tau) \cdot c_t'(\tau)\delta c_q\, d\tau + [D_2L_1(\tau)\delta c_q]_0^{\tau_i} - \int_0^{\tau_i} \frac{d}{d\tau}D_2L_1(\tau) \cdot \delta c_q(\tau)\, d\tau \\
&\qquad- \left[D_2L_1(\tau)\frac{c_q'(\tau)}{c_t'(\tau)} \cdot \delta c_t\right]_0^{\tau_i} + \int_0^{\tau_i} \frac{d}{d\tau}\left(D_2L_1(\tau)\frac{c_q'(\tau)}{c_t'(\tau)}\right) \cdot \delta c_t\, d\tau + [L_1(\tau)\delta c_t]_0^{\tau_i} \\
&\qquad- \int_0^{\tau_i} \frac{d}{d\tau}L_1(\tau) \cdot \delta c_t\, d\tau \\
&\quad= \int_0^{\tau_i} \left[\left(D_1L_1(\tau)c_t'(\tau) - \frac{d}{d\tau}D_2L_1(\tau)\right) dc_q \right. \\
&\qquad\qquad\left. + \left(\frac{d}{d\tau}\left(D_2L_1(\tau)\frac{c_q'(\tau)}{c_t'(\tau)} - L_1(\tau)\right)\right) dc_t\right] \delta c\, d\tau \\
&\qquad+ \left[\, [D_2L_1(\tau)]_0^{\tau_i}\, dc_q - \left[\, D_2L_1(\tau)\frac{c_q'(\tau)}{c_t'(\tau)} - L_1(\tau)\right]_0^{\tau_i} dc_t\right] \hat{\delta}c(\tau_i),
\end{aligned}$$

where we use partial integration for the three terms involving either $\delta c_q'$ or $\delta c_t'$ in the second line. Analogous transformations can be made for variations of the second

integral $\int_{\tau_i}^{1} L_2\left(c_q(\tau), \frac{c_q'(\tau)}{c_t'(\tau)}\right) c_t'(\tau)\, d\tau$. Then, using the defined Euler-Lagrange map and the Lagrangian one-form we have

$$\delta\mathfrak{S}(c)\cdot\delta c = \int_0^{\tau_i} D_{EL}L_1(c'')\cdot\delta c\, d\tau + \int_{\tau_i}^{1} D_{EL}L_2(c'')\cdot\delta c\, d\tau + \Theta_{L_1}(c')\cdot\widehat{\delta c}|_0^{\tau_i} + \Theta_{L_2}(c')\cdot\widehat{\delta c}|_{\tau_i}^{1}.$$

□

Impulsive Momentum and Energy Effect Now, the effects of the discrete events have to be taken into account.

Definition 6.14 (Impulsive Momentum and Energy Effect)**:** The *impulsive momentum effect* $\mathfrak{M}$ and the *impulsive energy effect* $\mathfrak{E}$ are defined as

$$\begin{aligned}\mathfrak{M} &:= \left[D_2L_2\left(c_q(\tau_i), R\left(\frac{c_q'(\tau_i)}{c_t'(\tau_i)}\right)\right) - D_2L_1\left(c_q(\tau_i), \frac{c_q'(\tau_i)}{c_t'(\tau)}\right)\right]\delta c_q(\tau_i)\\ &= \left[p_2\left(c_q(\tau_i), R\left(\frac{c_q'(\tau_i)}{c_t'(\tau_i)}\right)\right) - p_1\left(c_q(\tau_i), \frac{c_q'(\tau_i)}{c_t'(\tau_i)}\right)\right]\delta c_q(\tau_i),\end{aligned}$$

and

$$\begin{aligned}\mathfrak{E} &:= \left[\left(D_2L_2(\tau)\cdot R\left(\frac{c_q'(\tau_i)}{c_t'(\tau_i)}\right) - L_2(\tau)\right) - \left(D_2L_1(\tau)\cdot\frac{c_q'(\tau_i)}{c_t'(\tau_i)} - L_1(\tau)\right)\right]\cdot\delta c_t(\tau_i)\\ &= \left[E_2\left(c_q(\tau_i), R\left(\frac{c_q'(\tau_i)}{c_t'(\tau_i)}\right)\right) - E_1\left(c_q(\tau_i), \frac{c_q'(\tau_i)}{c_t'(\tau_i)}\right)\right]\cdot\delta c_t(\tau_i)\end{aligned}$$

where $p_{1,2}$ are the conjugate momenta given by $p_i = \frac{\partial L_i}{\partial\dot{q}}$ and E_i denote the energies given by $E_i = p_i\cdot\dot{q} - L_i$ $(i = 1, 2)$. As before, $L_i(\tau)$ is used as short notation for $L_i\left(c_q(\tau), \frac{c_q'(\tau)}{c_t'(\tau)}\right)$.

Using the transformation $s = c_t(\tau)$, we have

$$\begin{aligned}\mathfrak{M} &= [p_2(q(t_i), R(\dot{q}(t_i))) - p_1(q(t_i), \dot{q}(t_i))]\cdot(\dot{q}(t_i)\delta t_i + \delta q(t_i)) \quad \text{and}\\ \mathfrak{E} &= [E_2(q(t_i), R(\dot{q}(t_i))) - E_1(q(t_i), \dot{q}(t_i))]\cdot\delta t_i,\end{aligned}$$

since $t_i = c_t(\tau_i)$ and the states transform as above, $q(s) = c_q(c_t^{-1}(s))$, $\dot{q}(s) = \frac{c_q'(c_t^{-1}(s))}{c_t'(c_t^{-1}(s))}$. A variation of $q(t)$ can be derived from the variations δc_q and δc_t, cf. Figure 6.2 for an illustration. To show this, we use the equality $c_q(\tau) = q(c_t(s))$ and

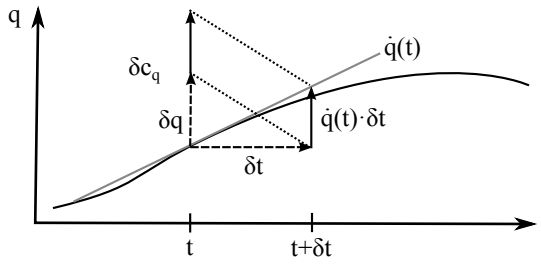

Figure 6.2: Variations of the time and of the induced curve $q(t) = c_q(c_t^{-1}(t))$.

compute

$$\begin{aligned}\delta c_q = \frac{d}{d\epsilon} c_q(\tau,\epsilon)\Big|_{\epsilon=0} &= \frac{d}{d\epsilon} q(c_t(\tau,\epsilon),\epsilon)\Big|_{\epsilon=0} = D_1 q(c_t(\tau,\epsilon),\epsilon)\cdot \frac{\partial}{\partial\epsilon} c_t(\tau,\epsilon)\Big|_{\epsilon=0} \\ &+ \frac{\partial}{\partial\epsilon} q(c_t(\tau,\epsilon),\epsilon)\Big|_{\epsilon=0} = \dot q(c_t(\tau))\cdot \delta c_t + \delta q(c_t(\tau)) = \dot q\cdot\delta c_t + \delta q.\end{aligned} \tag{6.5}$$

In the transformed expression, it is obvious why $\mathfrak{M}$ is called the impulsive momentum effect: it gives the jump in the momentum at switching time t_i. This quantity depends on variations of the switching time, δt_i, as well as on variations of the curve at this time point, $\delta q(t_i)$. Similarly, the impulsive energy effect describes the possible jump in the energy due to the singularity of the curve at t_i.

As an intermediate step we can now formulate Hamilton's principle for the hybrid setting.

Proposition 6.15 (Hybrid Hamilton's Principle)**:** Let $c = (c_t, c_q) \in \mathcal{M}$ be a curve for which $c_q(c_t^{-1}(0)) = q(0) = q_0$ and $c_q(c_t^{-1}(T)) = q(T) = q_f$. Considering variations δc that vanish at the boundary points, the curve is a solution of

$$\mathbf{d}\mathfrak{S}(c)\cdot\delta c + \mathfrak{M} = \mathfrak{E}, \tag{6.6}$$

if and only if it satisfies

(i) the Euler-Lagrange equations for L_1, $\frac{d}{dt}\frac{\partial L_1}{\partial \dot q} - \frac{\partial L_1}{\partial q} = 0$, on $[0, t_i]$,

(ii) and for L_2, $\frac{d}{dt}\frac{\partial L_2}{\partial \dot q} - \frac{\partial L_2}{\partial q} = 0$, on $[t_i, T]$, both with $q(t) = c_q(c_t^{-1}(\tau))$, and

(iii) the reset condition, that is $q(t_i^-) = q(t_i^+) \in G$ and $\dot q(t_i^+) = R(\dot q(t_i^-))$.

Proof. Variations of the hybrid action map have been computed in Equation (6.4) (cf. Lemma 6.13). To satisfy $d\mathfrak{S}(c)\cdot\delta c + \mathfrak{M} = \mathfrak{E}$, the different terms from variations

on the continuous parts w.r.t. c_q and c_t and of the switching, i.e. $c_q(\tau_i)$ and $c_t(\tau_i)$ have to hold independently

$$D_1 L_i \cdot c_t' - \frac{d}{d\tau} D_2 L_i = 0 \quad \text{for } i = 1 \text{ on } [0, \tau_i],\ i = 2 \text{ on } [\tau_i, 1], \tag{6.7}$$

$$\frac{d}{d\tau}\left(D_2 L_i \cdot \frac{c_q'}{c_t'} - L_i \right) = 0 \quad \text{for } i = 1 \text{ on } [0, \tau_i],\ i = 2 \text{ on } [\tau_i, 1], \tag{6.8}$$

$$\left(D_2 L_1|_{\tau=\tau_i^-} - D_2 L_2|_{\tau=\tau_i^+} \right) \delta c_q(\tau_i) + \mathfrak{M} = 0, \tag{6.9}$$

$$\left(\left(D_2 L_2 \cdot \frac{c_q'}{c_t'} - L_2 \right)\Big|_{\tau=\tau_i^+} - \left(D_2 L_1 \cdot \frac{c_q'}{c_t'} - L_1 \right)\Big|_{\tau=\tau_i^-} \right) \delta c_t(\tau_i) = \mathfrak{E}. \tag{6.10}$$

Using the transformation $s = c_t(\tau)$ (with $ds = c_t'(\tau) \cdot d\tau$, replacing s in the end by the conventional time parameter t and recalling that $c_t' > 0$ by definition), Equation (6.7) yields the ordinary Euler-Lagrange equations for the continuous parts, which hold by conditions (i) and (ii),

$$\frac{d}{dt}\frac{\partial L_i}{\partial \dot{q}} - \frac{\partial L_i}{\partial q} = 0 \quad \text{ on } [0, t_i] \text{ with } i = 1 \quad \text{and on } \ [t_i, T] \text{ with } i = 2.$$

Equation (6.8) with the same substitution reads $\frac{d}{dt}\left(\frac{\partial L_i}{\partial \dot{q}} \dot{q} - L_i \right) = 0$ on the appropriate time intervals. This equality, namely the energy conservation along the continuous part, holds automatically as soon as (i) does, because one can compute (cf. [MW01, FMOW03])

$$\frac{d}{dt}\left(\frac{\partial L_i}{\partial \dot{q}} \dot{q} - L_i \right) = \frac{d}{dt}\frac{\partial L_i}{\partial \dot{q}} \dot{q} + \frac{\partial L_i}{\partial \dot{q}} \ddot{q} - \frac{dL}{dt} = \frac{\partial L_i}{\partial q} \dot{q} + \frac{\partial L_i}{\partial \dot{q}} \ddot{q} - \frac{\partial L_i}{\partial q} \dot{q} - \frac{\partial L_i}{\partial \dot{q}} \ddot{q} = 0.$$

The boundary conditions at $\tau = 0$ and $\tau = 1$ of the Lagrangian maps vanish since $\delta c_t(0) = \delta c_t(1) = 0$. Equation (6.9), in which the variations $\delta c_q(\tau_i)$ are considered, is transformed into

$$\begin{aligned} &\frac{\partial}{\partial \dot{q}} L_1(q(\tau_i), \dot{q}(\tau_i)) - \frac{\partial}{\partial \dot{q}} L_2(q(\tau_i), R(\dot{q}(\tau_i))) \\ &- \frac{\partial}{\partial \dot{q}} L_1(q(\tau_i), \dot{q}(\tau_i)) + \frac{\partial}{\partial \dot{q}} L_2(q(\tau_i), R(\dot{q}(\tau_i))) = 0, \end{aligned}$$

which is trivially fulfilled by the definition of the impulsive momentum effect and

with the reset map from condition (iii). Similarly, from Equation (6.10), we receive

$$\frac{\partial}{\partial \dot{q}} L_2(q(t_i), R(\dot{q}(t_i))) \cdot R(\dot{q}(t_i)) - L_2(q(t_i), R(\dot{q}(t_i))) - \frac{\partial}{\partial \dot{q}} L_1(q(t_i), \dot{q}(t_i)) \cdot \dot{q}(t_i)$$
$$+ L_1(q(t_i), \dot{q}(t_i)) = E_2((q(t_i), R(\dot{q}(t_i))) - E_1(q(t_i), \dot{q}(t_i)),$$

where we use again condition (iii) on the reset map. To sum up, the impulsive effects defining the discontinuity of the momenta at the switching time, cancel with the inner boundary values of the Lagrangian one-forms. Altogether, we proved that conditions (i) to (iii) guarantee that the hybrid variational equation (6.6) holds. On the other hand, assuming $\mathbf{d}\mathfrak{S}(c) \cdot \delta c + \mathfrak{M} = \mathfrak{E}$ holds for arbitrary variations requires that conditions (i) - (iii) are satisfied. In particular, by the definition of curves c with $c_q(\tau_i) \in G$, the condition $q(t_i^-) = q(t_i^+) \in G$ in (iii) is satisfied. This completes the proof. □

Remark 6.16: Note the difference of our approach compared to [FMOW03]: We consider the reset map for the velocity at the switch as being previously defined, which allows for more general discrete effects in mechanical systems than impacts only. Therefore, we do not variationally derive the update formulae at the impulses, but take into account the impulsive changes in the system's momenta and energy due to the instantaneous reset in the hybrid Hamilton's principle.

Remark 6.17: A solution of the hybrid mechanical system for a chosen initial condition $(q(0), \dot{q}(0)) = (q_0, \dot{q}_0)$ is obtained by starting with the *flow corresponding to the first Lagrangian*, $F_1 : TQ \times \mathbb{R} \to TQ$. The flow can be defined on TQ instead of TQ_e since – up to the specific parametrization in τ – solutions $q(t)$ uniquely correspond to solutions $c(\tau)$, cf. [FMOW03]. At t_i, $q(t_i) \in G$ holds and since the reset map was assumed to be the identity in Q, we have $q(t_i^-) = q(t_i^+)$. The velocity is *updated according to the reset map*, that is $R(\dot{q}(t_i^-)) = \dot{q}(t_i^+)$. In applications, this may also be an implicit definition of the velocity behind the switch, $\dot{q}(t_i^+)$. From then on, the trajectory is determined by the *second Lagrangian flow*, $F_2 : TQ \times \mathbb{R} \to TQ$ until the final time T is reached.

Since our interest lies in the control of hybrid Lagrangian systems, we now introduce the hybrid virtual work and formulate a hybrid Lagrange-d'Alembert principle.

Hybrid Virtual Work Starting in the extended setting, we consider Lagrangian control forces $f_i : TQ_e \times U \to T^*Q_e$, given by a family $f_i^u : TQ_e \mapsto T^*Q_e$ of

fiber-preserving maps over the identity ($i \in \{1,2\}$) for fixed curves

$$u \in \mathcal{C}([0,1],\tau_i,U) = \{u : [0,1] \to U \,|\, u \text{ piecewise continuous with at most one singularity at } \tau_i \in (0,1)\}.$$

We can split the forces into the two components $f_i^u = (f_{i,t}^u, f_{i,q}^u)$, $(i = 1,2)$ as proposed in [FMOW03] as well. The *hybrid virtual work* is then given by

$$W(c,u) = \int_0^{\tau_i} f_1(c(\tau), c'(\tau), u(\tau)) \cdot \delta c(\tau) d\tau + \int_{\tau_i}^1 f_2(c(\tau), c'(\tau), u(\tau)) \cdot \delta c(\tau) d\tau.$$

Now, the theorem on the hybrid Lagrange-d'Alembert principle stated in the beginning of this section can be proved.

Proof of Theorem 6.11. We follow the steps of the proof of Proposition 6.15, now with the variational equation $\delta\mathfrak{S}(c)+W(c,u)+\mathfrak{M} = \mathfrak{E}$. The virtual work contributes to variations in c_q and in c_t, thus Equations (6.7) and (6.8) are replaced by

$$D_1 L_i \cdot c_t' - \frac{d}{d\tau} D_2 L_i + f_{i,q}^u = 0 \quad \text{for } i = 1 \text{ on } [0,\tau_i],\ i = 2 \text{ on } [\tau_i, 1], \tag{6.11}$$

$$\frac{d}{d\tau}\left(D_2 L_i \cdot \frac{c_q'}{c_t'} - L_i \right) + f_{i,t}^u = 0 \quad \text{for } i = 1 \text{ on } [0,\tau_i],\ i = 2 \text{ on } [\tau_i, 1]. \tag{6.12}$$

Since we do not consider forces that solely apply at the switching instant, the equations for the switching remain unchanged. Substituting $s = c_t(\tau)$ in Equation (6.11) yields

$$\frac{d}{dt}\frac{\partial L_i}{\partial \dot{q}} - \frac{\partial L_i}{\partial q} = \frac{1}{c_t'} \cdot f_{i,q}^u. \tag{6.13}$$

Equation (6.12) can be transformed into

$$\frac{d}{dt}\left(D_2 L_i \cdot \dot{q} - L_i \right) = -\frac{1}{c_t'} f_{i,t}^u. \tag{6.14}$$

For the left hand side of Equation (6.14), which is the time derivative of the energy E_i, we can derive

$$\begin{aligned} &\frac{d}{dt}\left(D_2 L_i \cdot \dot{q} - L_i \right) = \frac{d}{dt}\frac{\partial L_i}{\partial \dot{q}}\dot{q} + \frac{\partial L_i}{\partial \dot{q}}\ddot{q} - \frac{d}{dt} L_i = \frac{d}{dt}\frac{\partial L_i}{\partial \dot{q}}\dot{q} + \frac{\partial L_i}{\partial \dot{q}}\ddot{q} - \frac{\partial L_i}{\partial q}\dot{q} - \frac{\partial L_i}{\partial \dot{q}}\ddot{q} \\ &= \left(\frac{d}{dt}\frac{\partial L_i}{\partial \dot{q}} - \frac{\partial L_i}{\partial q} \right) \cdot \dot{q} \overset{Eq.\ (6.13)}{=} \frac{1}{c_t'(\tau)} \cdot f_{i,q}^u \cdot \dot{q}, \end{aligned}$$

such that we obtain the relation between $f^u_{i,t}$ and $f^u_{i,q}$:

$$f^u_{i,t} = -f^u_{i,q} \cdot \dot{q} = -f^u_{i,q} \cdot \frac{c'_q}{c'_t}.$$

With

$$\tilde{f}^u_i(q(t), \dot{q}(t)) := \frac{1}{c'_t(c_t^{-1})} f^u_{i,q}(c(c_t^{-1}), c'(c_t^{-1})), \tag{6.15}$$

we have the ordinary forced Euler-Lagrange equations (6.13) on the continuous parts of the hybrid time interval. Using Equation (6.15), the virtual work can be rewritten as a function of the associated curve $q(t)$, i.e.

$$\begin{aligned}
&W(c,u)\\
&= \int_0^{\tau_i} \left[f^u_{1,q}\delta c_q + f^u_{1,t}\delta c_t\right] d\tau + \int_{\tau_i}^1 \left[f^u_{2,q}\delta c_q + f^u_{2,t}\delta c_t\right] d\tau\\
&= \int_0^{\tau_i} \left[\tilde{f}^u_1 \cdot c'_t(\tau)\delta c_q - \tilde{f}^u_1 \cdot c'_q(\tau)\delta c_t\right] d\tau + \int_{\tau_i}^1 \left[\tilde{f}^u_2 \cdot c'_t(\tau)\delta c_q - \tilde{f}^u_2 \cdot c'_q(\tau)\delta c_t\right] d\tau\\
&= \int_0^{\tau_i} \tilde{f}^u_1 \cdot \left[\delta c_q - \frac{c'_q}{c'_t} \cdot \delta c_t\right] \cdot c'_t \, d\tau + \int_{\tau_i}^1 \tilde{f}^u_2 \cdot \left[\delta c_q - \frac{c'_q}{c'_t} \cdot \delta c_t\right] \cdot c'_t \, d\tau\\
&= \int_0^{t_i} \tilde{f}^u_1 \, \delta q \, dt + \int_{t_i}^T \tilde{f}^u_1 \, \delta q \, dt = W(q,u),
\end{aligned}$$

where the transformation of the variations as given in Equation (6.5) is used.

Thus, we see that the virtual work in the variational equation $\delta\mathfrak{S}(c) + W(c,u) + \mathfrak{M} = \mathfrak{E}$ leads to (ordinary) forced Euler-Lagrange equations on the continuous parts of the hybrid interval and vice versa, for a curve $q(t)$ that satisfies the forced Euler-Lagrange equations, Equations (6.11) and (6.12) are both fulfilled. Together with the reset condition at $t_i = c_t(\tau_i)$ and the impulsive effects, as shown in Proposition 6.15, we obtain the variational equation of the hybrid Lagrange-d'Alembert principle. □

Remark 6.18: The preliminary results are extendable to a fixed switching sequence with multiple switches possibly between multiple Lagrangian. However, the notation becomes confusingly complex then; cf. [FO11] for some ideas (without formal proofs) on how to deal with multiple switches.

Remark 6.19: The hybrid Lagrangian control system with two discrete states (cf. Definition 6.6 and the following specifications) can be modeled as a general hybrid automaton according to Definition 6.1. To this end, define the domains by $D_i = \{i\} \times TQ$ for $i \in \Gamma = \{1,2\}$, which are locally isomorphic to $D_i = \{i\} \times \mathbb{R}^{2n}$ when

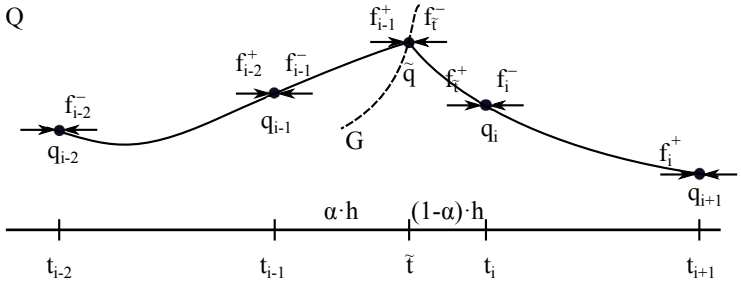

Figure 6.3: Sketch of the discrete curve q_d, the discrete time grid and the discrete forces.

choosing local coordinates. The vector fields are given by the Lagrangian vector fields X^{L_i} together with the forcing functions f_1 and f_2, as for controlled hybrid automata. Since we assumed the guard of the mechanical system, $G^{\text{mech}}_{(i,j)}$, to be a submanifold of Q, for $G_{(i,j)} \subset D_i$ we have $G_{(i,j)} = \bigcup_{q \in G^{\text{mech}}_{(i,j)}} \{(q,v) \in T_qQ\}$. As it has been already discussed in Assumption 6.7, the reset map can be extended by the identity on Q, i.e. $R_{(i,j)}(q,v) = (q, R^{\text{mech}}_{(i,j)}(v))$.

6.2.2 Discrete Hybrid Mechanical Systems

In the discrete setting, as for classical mechanical systems (cf. Section 2.2), we consider discrete Lagrangian $L_{d,1}$ and $L_{d,2}$ which approximate the continuous time action map.

Let $\Delta t = \{t_0 = 0, t_1, \ldots, t_N = T\}$ be a discrete time grid for the hybrid interval[6] $\mathcal{I} = \{[0,\tilde{t}], [\tilde{t},T]\}$, where i denotes the index of the subinterval for which $\tilde{t} \in [t_{i-1}, t_i]$.

We consider variations of the switching time in this (arbitrary) interval only, therefore it is sufficient to extend the discrete path space by a time component for this interval only. In analogy with the continuous case, let $\tilde{\tau}$ denote the fixed impact time and define $\tilde{\alpha} \in [0,1]$ by $\tilde{\tau} = t_{i-1} + \tilde{\alpha}h$. Then, let $t_d \in C^k([0,1],[0,1])$ (with $2 \leq k < \infty$) be a function that gives the real impact time $\tilde{t}$ via $\alpha = t_d(\tilde{\alpha})$ such that

$$\tilde{t} = t_{i-1} + t_d(\tilde{\alpha})(t_i - t_{i-1}) = t_{i-1} + \alpha(t_i - t_{i-1}) = (1-\alpha)t_{i-1} + \alpha\, t_i.$$

Thus, variations of $\tilde{t}$ can be generated by variations of α. To simplify notation, we assume a fixed step size $h = t_k - t_{k-1}$, $k = 1, \ldots, N$ (although the following derivations are in principle not restricted to equidistant time grids) and write $\tilde{t} = t_{i-1} + \alpha\, h$. See Figure 6.3 for an illustration.

[6] To avoid confusion with the discrete time points, the switching time is denoted by $\tilde{t}$ in this section.

The *discrete path space* is defined by

$$\mathcal{M}_d = \mathcal{T}_d \times \mathcal{Q}_d(\tilde{\alpha}, G, Q),$$

with $\mathcal{T}_d = \{t_d \in C^k([0,1],[0,1]), t_d \text{ onto}, t_d' > 0\}$ and

$$\mathcal{Q}_d(\tilde{\alpha}, G, Q) = \{q_d : \{t_0, \ldots, t_{i-1}, \tilde{\tau}, t_i, \ldots, t_N\} \to Q \,|\, \tilde{q} \in G\}.$$

Here, $\tilde{q} = q_d(\tilde{\tau})$ and we also write $q_d(t_k) = q_k$ for $k \in \{0, \ldots, N\}$. The discrete trajectory (t_d, q_d) can be identified with its image (α, q_d) in $[0,1] \times Q \times \ldots \times G \times Q \times \ldots \times Q$. Since this space is isomorphic to $\mathcal{M}_d$, the discrete path space can be given a smooth product manifold structure (cf. e.g. [MW01]).

Definition 6.20 (Discrete Hybrid Action Map)**:** The *discrete hybrid action map* $\mathfrak{S}_d : \mathcal{M}_d \to \mathbb{R}$ is defined by

$$\begin{aligned}\mathfrak{S}_d(\alpha, q_d) = &\sum_{k=0}^{i-2} L_{1,d}(q_k, q_{k+1}) + L_{1,d}(q_{i-1}, \tilde{q}, \alpha h) \\ &+ L_{2,d}(\tilde{q}, q_i, (1-\alpha)h) + \sum_{k=i}^{N} L_{2,d}(q_k, q_{k+1}, h).\end{aligned}$$

The tangent space to the discrete path space is $T\mathcal{M}_d = T\mathcal{T}_d \times T\mathcal{Q}_d$, where the tangent space $T_{q_d}\mathcal{Q}_d(\tilde{\alpha}, G, Q)$ at an element q_d is given by the set of all maps $v_{q_d} : \{t_0, \ldots, t_{i-1}, \tilde{\tau}, t_i, \ldots, t_N\} \to TQ$ such that $\pi_Q \circ v_{q_d} = q_d$ and $v_{q_d}(\tilde{\tau}) \in T_{\tilde{q}}G$. The following Lemma characterizes the variations of the discrete hybrid action map.

Lemma 6.21 (Variations of the Discrete Hybrid Action Map)**:** Given two C^k Lagrangian $L_{i,d} : Q \times Q \times \mathbb{R} \to \mathbb{R}$ ($k \geq 1$, $i = 1, 2$), there exist unique C^{k-1} mappings $D_{DEL}L_{d,i} : \ddot{Q}_d \to T^*Q$ on the discrete second order manifold $\ddot{Q}_d = Q \times Q \times Q$ and unique C^{k-1} one-forms $\Theta^-_{L_{1,d}}$ and $\Theta^+_{L_{2,d}}$ on the discrete phase space $Q \times Q$ such that,

for all variations $(\delta\alpha, \delta q_d) \in T_{(\alpha,q_d)}\mathcal{M}_d$ of (α, q_d), it holds

$$\begin{aligned} d\mathfrak{S}_d(\alpha, q_d)\cdot(\delta\alpha,\delta q_d) = &\sum_{k=1}^{i-2} D_{DEL}L_{1,d}(q_{k-1},q_k,q_{k+1})\cdot\delta q_k \\ &+ \sum_{k=i+1}^{N-1} D_{DEL}L_{2,d}(q_{k-1},q_k,q_{k+1})\cdot\delta q_k \\ &+ \Theta^+_{L_{2,d}}(q_{N-1},q_N)\cdot(\delta q_{N-1},\delta q_N) - \Theta^-_{L_{1,d}}(q_0,q_1)\cdot(\delta q_0,\delta q_1) \\ &+ [D_2L_{1,d}(q_{i-2},q_{i-1},h) + D_1L_{1,d}(q_{i-1},\tilde{q},\alpha h)]\cdot\delta q_{i-1} \\ &+ h\cdot[D_3L_{1,d}(q_{i-1},\tilde{q},\alpha h) - D_3L_{2,d}(\tilde{q},q_i,(1-\alpha)h)]\cdot\delta\alpha \\ &+ (D_2L_{1,d}(q_{i-1},\tilde{q},\alpha h) + D_1L_{2,d}(\tilde{q},q_i,(1-\alpha)h))\cdot\delta\tilde{q} \\ &+ [D_2L_{2,d}(\tilde{q},q_i,(1-\alpha),h) + D_1L_{2,d}(q_i,q_{i+1},h)]\ \cdot\delta q_i. \end{aligned} \tag{6.16}$$

The maps $D_{DEL}L_{d,j}$ $(j = 1, 2)$ are the *discrete Euler-Lagrange maps*,

$$D_{DEL}L_{d,j}(q_{k-1},q_k,q_{k+1}) = [D_2L_{d,j}(q_{k-1},q_k,h) + D_1L_{d,j}(q_k,q_{k+1},h)]\ dq_k$$

and the one-forms $\Theta^+_{L_{d,j}}$ and $\Theta^-_{L_{d,j}}$ $(j = 1, 2)$ are the *discrete Lagrangian one-forms*,

$$\begin{aligned} \Theta^+_{L_{d,j}}(q_k,q_{k+1}) &= D_2L_{d,j}(q_k,q_{k+1},h)dq_{k+1}, \\ \Theta^-_{L_{d,j}}(q_k,q_{k+1}) &= -D_1L_{d,j}(q_k,q_{k+1},h)dq_k. \end{aligned}$$

Proof. Equation (6.16) is obtained by taking variations $(\delta\alpha, \delta q_d) = (\delta\alpha, \delta q_0, \ldots, \delta q_{i-1}, \delta\tilde{q}, \delta q_i, \ldots, \delta q_N)$ and rearranging the sums (cf. [MW01] or [FMOW03]). □

Discretization of the Reset Map Recall that the reset map $R : TQ \to TQ$, $v_q \mapsto R(v_q)$ was assumed to be the identity on Q. Since the continuous state space TQ is replaced by discrete state space $Q \times Q$, the discrete reset map has to be defined as a function of the discrete states now. This can be done by using the discrete Legendre transformations $\mathbb{F}^{f+}L_{d,1}$ and $\mathbb{F}^{f-}L_{d,2}$. That is, $R_d : Q \times Q \to Q \times Q$, $(q_{i-1}, \tilde{q}) \mapsto (\tilde{q}, q_i)$ is defined via

$$R_d(q_{i-1},\tilde{q}) = (\mathbb{F}^{f-}L_{d,2})^{-1} \circ \mathbb{F}L_2 \circ R \circ (\mathbb{F}L_1)^{-1} \circ \mathbb{F}^{f+}L_{d,1}(q_{i-1},\tilde{q}). \tag{6.17}$$

Discrete Hybrid Virtual Work We consider discrete control paths (for simplicity, on the same discrete time grid as the configurations), $u_d : \{ t_0, \ldots, t_{i-1}, \tilde{\tau}, t_i, \ldots, t_{N-1}\} \to U$ with $u_d = \{u_0, \ldots, u_{i-1}, \tilde{u}, u_i, \ldots, u_{N-1}\}$ such that u_k approximates the control on the time interval $[t_k, t_{k+1}]$ for $k \neq i-1$ and u_i approximates

the control on $[t_{i-1}, \tilde{\tau}]$ while $\tilde{u}$ is assigned to the interval $[\tilde{\tau}, t_i]$. The discrete control path space is denoted by $\mathcal{U}_d$. Then, the discrete forces are (cf. Figure 6.3)

$$\begin{aligned}
f^{\pm}_{1,k} &= f_{d,1}(q_k, q_{k+1}, u_k) \text{ for } k = 0, \dots, i-2, \\
f^{\pm}_{2,k} &= f_{d,2}(q_k, q_{k+1}, u_k) \text{ for } k = i, \dots, N-1, \\
f^{\pm}_{1,i-1} &= f_{d,1}(q_{i-1}, \tilde{q}, u_{i-1}), \text{ and} \\
f^{\pm}_{2,\tilde{t}} &= f_{d,2}(\tilde{q}, q_i, \tilde{u}).
\end{aligned}$$

The discrete hybrid virtual work $W_d : \mathcal{Q}_d \times \mathcal{U}_d \to \mathbb{R}$ is defined as

$$\begin{aligned}
W_d(\alpha, q_d, u_d) = &\sum_{k=0}^{i-2} f^-_{1,k} \cdot \delta q_k + f^+_{1,k} \cdot \delta q_{k+1} + \sum_{k=i}^{N-1} f^-_{2,k} \cdot \delta q_k + f^+_{2,k} \cdot \delta q_{k+1} \\
&+ f^-_{1,i-1} \cdot \delta q_{i-1} + \left(f^+_{1,i-1} + f^-_{2,\tilde{t}} \right) \cdot \delta \tilde{q} + f^+_{2,\tilde{t}} \cdot \delta q_i.
\end{aligned} \tag{6.18}$$

Discrete Impulsive Effects For the discrete impulsive momentum effect, we apply the discrete forced Legendre transformations $\mathbb{F}^{f+}L^{u_k}_{1,d}(q_k, q_{k+1}) = (q_{k+1}, D_2 L_{1,d}(q_k, q_{k+1}) + f^+_{1,k})$ and $\mathbb{F}^{f-}L^{u_k}_{2,d}(q_k, q_{k+1}) = (q_k, -D_1 L_{2,d}(q_k, q_{k+1}) - f^-_k)$ to define the discrete momenta $p^+_{1,d}(q_k, q_{k+1})$ and $p^-_{2,d}(q_k, q_{k+1})$, respectively. Concretely, we define

$$\mathfrak{M}_d = \left[p^-_{2,d}(\tilde{q}, q_i, (1-\alpha)h) - p^+_{1,d}(q_{i-1}, \tilde{q}, \alpha h) \right] \cdot \delta \tilde{q}.$$

The discrete impulsive energy effect is defined by

$$\mathfrak{E}_d = [E_{d,2}(\tilde{q}, q_i, (1-\alpha)h) - E_{d,1}(q_{i-1}, \tilde{q}, \alpha h)] \cdot h \delta \alpha,$$

where $E_{d,i}(q_k, q_{k+1}) = -D_3 L_{d,i}(q_k, q_{k+1}, h)$ is the discrete energy of a discrete Lagrangian system (cf. e.g. [FMOW03]).

Now, we can state the discrete analogon of the hybrid Lagrange-d'Alembert principle.

Theorem 6.22 (Discrete Hybrid Lagrange-d'Alembert Principle)**:** Let $L_{i,d} : Q \times Q \times \mathbb{R} \to \mathbb{R}$, $(i = 1, 2)$ be C^k discrete Lagrangian, $\gamma(\Lambda) = (1, 2)$ a fixed switching sequence, $\mathcal{I}_d = \{ t_0, \dots, t_{i-1}, \tilde{t}, t_i, \dots, t_N \}$ a discrete hybrid interval with $\tilde{t}$ unknown, $G \subset Q$ a guard set and R_d a discretized reset map. Then, a discrete curve q_d joining q_0 and q_N is a solution to the discrete variational equation

$$\delta \mathfrak{S}_d(\alpha, q_d) + W_d(\alpha, q_d, u_d) + \mathfrak{M}_d = \mathfrak{E}_d$$

for all variations $(\delta\alpha, \delta q_d)$, if and only if the discrete forced Euler-Lagrange equations

are fulfilled before and after the switch, and the discrete reset condition $R_d(q_{i-1}, \tilde{q}) = (\tilde{q}, q_i)$ holds.

Proof. Since the boundary points q_0 and q_N are fixed, their variations have to be zero, $\delta q_0 = \delta q_N = 0$, and therefore, the discrete Lagrangian one-forms $\Theta^-_{L_{1,d}}(q_0, q_1)$ and $\Theta^+_{L_{2,d}}(q_{N-1}, q_N)$, as well as the corresponding terms of the discrete hybrid virtual work vanish. From the variations $\delta q_1, \ldots, \delta q_{i-1}$ and $\delta q_i, \ldots, \delta q_{N-1}$ we receive

$$
\begin{aligned}
&D_2L_{1,d}(q_{k-1}, q_k, h) + D_1L_{1,d}(q_k, q_{k+1}, h) + f^+_{1,k-1} + f^-_{1,k} = 0, \text{ for } k = 1, \ldots, i-2,\\
&D_2L_{1,d}(q_{i-2}, q_{i-1}, h) + D_1L_{1,d}(q_{i-1}, \tilde{q}, \alpha h) + f^+_{1,i-2} + f^-_{1,i-1} = 0,\\
&D_2L_{2,d}(\tilde{q}, q_i, (1-\alpha)h) + D_1L_{2,d}(q_i, q_{i+1}, h) + f^+_{2,\tilde{t}} + f^-_{2,i} = 0,\\
&D_2L_{2,d}(q_{k-1}, q_k, h) + D_1L_{2,d}(q_k, q_{k+1}, h) + f^+_{2,k-1} + f^-_{2,k} = 0, \text{ for } k = i{+}1, \ldots, N{-}1,
\end{aligned}
$$

and $\tilde{q} \in G$. These are the discrete forced Euler-Lagrange equations for $L_{d,1}$ before the switch, i.e. up to $(q_{i-2}, q_{i-1}, \tilde{q})$ and for $L_{d,2}$ after the switch, starting from $(\tilde{q}, q_i, q_{i+1})$. The variations w.r.t. $\tilde{q}$ lead to

$$
\Big(D_2L_{1,d}(q_{i-1}, \tilde{q}, \alpha h) + D_1L_{2,d}(\tilde{q}, q_i, (1-\alpha)h) + f^+_{1,i-1} + f^-_{2,\tilde{t}}\Big)\,\delta\tilde{q} + \mathfrak{M}_d = 0.
$$

By the definition of the discrete impulsive momentum effect,

$$
\begin{aligned}
\mathfrak{M}_d &= \Big[p^+_{2,d}(\tilde{q}, q_i, (1-\alpha)h) - p^-_{1,d}(q_{i-1}, \tilde{q}, \alpha h)\Big] \cdot \delta\tilde{q}\\
&= \Big(-D_1L_{2,d}(\tilde{q}, q_i, (1-\alpha)h) - f^-_{2,\tilde{t}} - D_2L_{1,d}(q_{i-1}, \tilde{q}, \alpha h) - f^+_{1,i-1}\Big) \cdot \delta\tilde{q},
\end{aligned}
$$

this term is indeed equal to zero. Finally, the variations $\delta\alpha$ of the discrete hybrid action map cancel with the discrete impulsive energy effect,

$$
\begin{aligned}
&[D_3L_{1,d}(q_{i-1}, \tilde{q}, \alpha h) - D_3L_{2,d}(\tilde{q}, q_i, (1-\alpha)h)] \cdot h \cdot \delta\alpha\\
&\qquad = [E_{d,2}(\tilde{q}, q_i, (1-\alpha)h) - E_{d,1}(q_{i-1}, \tilde{q}, \alpha h)] \cdot h \cdot \delta\alpha = \mathfrak{E}_d.
\end{aligned}
$$

Note that there is no discrete Euler-Lagrange equation defining the first configuration after the switch, i.e. at time node t_i. Instead, q_i is determined by the discrete hybrid reset map, $R_d(q_{i-1}, \tilde{q}) = (\tilde{q}, q_i)$ as defined above. Conversely, any pair (α, q_d) that satisfies the discrete Euler-Lagrange equations and the hybrid reset condition solves the variational equation. □

Hybrid Integrator The discrete forced Euler-Lagrange equations together with the guard and the reset map define an integrator for the discrete hybrid mechanical system. More detailed, given an initial condition $(q_0, \dot{q}_0)$ and a discretized control

function u_d, the initial velocity is transformed into an initial momentum p_0 via the continuous Legendre transform $\mathbb{F}L_1$. The next configuration q_1 is implicitly defined by the discrete forced Legendre transform, $p_0+D_1L_{1,d}(q_0,q_1,h)+f^-_{1,0}=0$. From then on, the discrete Euler-Lagrange equations $D_2L_{1,d}(q_{k-1},q_k,h)+D_1L_{1,d}(q_k,q_{k+1},h)+f^+_{1,k-1}+f^-_{1,k}=0$ can be solved for q_{k+1} until the interval, in which the guard is met, is reached. Denoting this interval by $[t_{i-1},t_i]$, the last configuration to be determined is q_{i-1}. Then, the Euler-Lagrange equations with the partial time step αh and the condition $\tilde{q}\in G$ can be used to compute $\tilde{q}$ and α. This is exactly the same procedure as described in [FMOW03]. After the switch, in our approach, we determine the next node q_i by means of the discrete reset map. This is different to [FMOW03] in which the equation obtained from the variation of the switching state $\tilde{q}$ – physically speaking, the reflection condition for the impact – together with the energy conservation condition is used. Thus, the discrete reset map can be the discretization of more general kinds of reset maps, modeling mechanical or other types of discrete events, as pointed out in the beginning of this section. After the discrete event, in both approaches, discrete Euler-Lagrange equations with $L_{d,2}$ are used; first with the partial time step $(1-\alpha)h$ between $\tilde{q}$ and q_i and with constant step size h afterwards.

6.2.3 Examples

The following examples show the modeling of different types of discrete effects in mechanical systems.

Example 6.23 (Special Cases of Theorem 6.11)**:** Given a hybrid Lagrangian system with two discrete modes, we consider a switch between subsystem 1 and subsystem 2. The reset map is chosen to be the identity on TQ. Assume that the Lagrangian differ only by a term depending on the configurations, i.e. $L_1(q,\dot{q})-L_2(q,\dot{q})=n(q)$ for some function $n:Q\to\mathbb{R}$ and for all $(q,\dot{q})\in TQ$, e.g. caused by different potentials. The momenta $p_1(t_i^-)=\frac{\partial L_1}{\partial\dot{q}}$ and $p_2(t_i^+)=\frac{\partial L_2}{\partial\dot{q}}$ coincide then. Thus, $\mathfrak{M}=0$ and the boundary terms of the variations of the hybrid action sum cancel out automatically. In other words, this is when a discrete event does not change the momentum in the switching point of the system. If additionally the Lagrangian L_1 and L_2 match exactly for the switching point, then it also holds that $E_2(t_i)=E_1(t_i)$. Hence, the impulsive energy effect $\mathfrak{E}$ is zero and the variations w.r.t. the switching time add up to zero. Here, the discrete effect does not lead to instantaneous changes neither in the velocity, nor in the momentum or energy. However, this does not automatically lead to the case of a single ordinary dynamical system, since, for instance, the potential energies may still vary for other states than the switching point.

Example 6.24 (Mechanical Systems with Impacts)**:** To model a mechanical system

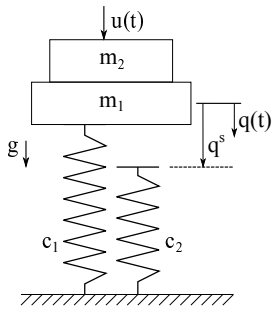

Figure 6.4: Sketch of the single-mass oscillator.

that undergoes an impact, the Lagrangian are identical, $L_2 = L_1 =: L$ and the guard G is chosen to be the contact manifold. More concretely, let us consider a mass point $q = (x, y)$ with mass m in $Q = \mathbb{R}^2$ and $L(q, \dot{q}) = \frac{1}{2}m(\dot{x}^2 + \dot{y}^2) - V(y)$ and the guard $G = \{(x, y) \,|\, y = 0\}$. We choose $R(x^-, y^-, \dot{x}^-, \dot{y}^-) = (x^+, y^+, \dot{x}^+, -\dot{y}^+)$ to model an elastic impact. The boundary terms of the variation of the hybrid action map leads to a momentum term that is canceled out by the impulsive momentum effect $\mathfrak{M}$ in the variational equation. Since, $E(q^-, \dot{q}^-) = E(q^+, \dot{q}^+)$, the corresponding parts of the Lagrangian one-form cancel out automatically and, at the same time, the impulsive energy effect is equal to zero. Thus, the Euler-Lagrange equations together with the reset map at discrete events, that is when $y = 0$, define the dynamics of the hybrid system. This is equivalent to what one obtains from the approach in [FMOW03], in which the reset map is derived from the Lagrangian one-form at the switch. The normal cone of G at some point x is $N_C = \lambda \cdot \big(0, 1\big)^T$ with $\lambda \in \mathbb{R}$. Therefore, we can write $\dot{q}^+ - \dot{q}^- \in N_C$ as $\dot{q}^+ = \dot{q}^- + \lambda \cdot \big(0, 1\big)^T$. Substituting this, i.e. $\dot{x}^+ = \dot{x}^-$, $\dot{y}^+ = \dot{y}^- + \lambda$, into the energy conservation constraint leads to the solution[7] $\dot{y}^+ = -\dot{y}^-$, which forms the modeling equations together with the ordinary Euler-Lagrange equations before and after the switch.

Example 6.25 (Hybrid Single Mass Oscillator)**:** The hybrid single-mass oscillator consists of two masses which are firmly connected[8] and a suspension system, cf. Figure 6.4. The suspension system is comprised of one linear and one nonlinear spring which are mounted parallel but differ in their lengths in the unloaded case.

The system is modeled as a hybrid Lagrangian control system by $\mathcal{H} = (Q, \Gamma, \mathcal{E}, \mathcal{L}, \mathcal{G}, \mathcal{R}, U, \mathcal{F})$ with

[7]The second solution from $\lambda = 0$ corresponds to $\dot{y}^+ = \dot{y}^-$. This is physically not meaningful, since the mass would interpenetrate with the contact manifold then (cf. [FMOW03]).

[8]This justifies the term single-mass oscillator. The mass parameters and actual spring lengths will become important when optimal control problems for the hybrid single mass oscillator are considered in Section 6.3.3.

- configuration manifold $Q = \mathbb{R}$ and state space $TQ = \mathbb{R}^2$,
- discrete states $\Gamma = \{1, 2\}$, given by the two cases "only one spring loaded" and "both springs loaded" and discrete transitions $\mathcal{E} = \{(1, 2), (2, 1)\}$,
- $\mathcal{L} = \{L_0, L_1\}$ with $m := m_1 + m_2$ given by

$$L_1(q, \dot{q}) = \frac{1}{2}m\dot{q}^2 - \frac{1}{2}c_1q^2 + mgq,$$
$$L_2(q, \dot{q}) = \frac{1}{2}m\dot{q}^2 - \frac{1}{2}c_1q^2 - \frac{1}{2}c_2(q - q^s)^4 + mgq,$$

- guards $\mathcal{G} = \{G_{(1,2)}, G_{(2,1)}\}$ with $G = G_{(1,2)} = G_{(2,1)} = \{(q, \dot{q}) \in TQ \,|\, q = q^s, \}$[9],
- trivial resets, $\mathcal{R} = \{R_{(1,2)}, R_{(2,1)}\}$ with $R_{(1,2)} = R_{(2,1)} = id$,
- the control set $U = \{u \in \mathbb{R} \,|\, -m_2g \leq u \leq 0\}$ (such that the force cannot "pick up" the second mass), and
- forces $\mathcal{F} = \{f_1, f_2\}$ with $f_1(q, \dot{q}, u) = f_2(q, \dot{q}, u) = u$.

In this example, the momenta at a switching point and also the energies corresponding to L_1 and L_2 are the same, since the potential of the second spring is zero at $q = q^s$. The forced Euler-Lagrange equations for the two Lagrangian and forces together with the reset map and the guard condition define the equations of motion for the hybrid system. Whenever passing $q(t) = q^s$, there is a switch in the controlled Lagrangian vector field and thus a nonsmooth point of the velocity, but $\dot{q}$ is at least continuous, since $R = id$, and one can check that the unforced Euler-Lagrange equations coincide for $q = q^s$ as well.

Note the two opposing points of view regarding the interaction of the switching time and the control trajectory: given a (nondegenerated) initial condition and a control trajectory, the evolution of the system, in general, will hit the guard once in a while and then switch into the other discrete state where it evolves according to the new Lagrangian. On the other hand, one can fix a sequence of switching times $\{\tau_1, \ldots, \tau_N\}$, and check if there is a control function that steers the system from an initial point to a desired target state and that hits the switching manifold at every switching time $\tau \in \{\tau_1, \ldots, \tau_N\}$. This is the viewpoint we take up in the following section when optimal control problems for hybrid systems are formulated and, in particular, when using the two layer approach.

[9]Strictly speaking, to guarantee that the system leaves the discrete state 1, $\dot{q}^s > 0$ has to be ensured while $\dot{q}^s < 0$ has to hold for a switch from discrete state 2 to discrete state 1.

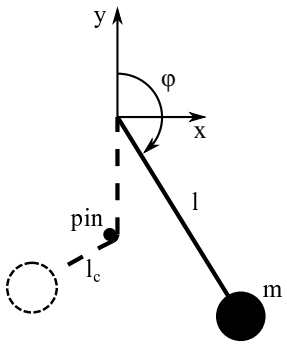

Figure 6.5: The planar pendulum, constrained by a pin.

Example 6.26 (Constrained Pendulum)**:** An example with a non-trivial reset map is the constrained pendulum, which is similar to the constrained pendulum example considered in [SS00]. As shown in Figure 6.5, the position of the pendulum with mass m on a rod with length l is described by the angle coordinate φ. For $\varphi = \pi$, there is a pin (distance $l - l_c$ below the center of the pendulum), which constrains the motion of the pendulum for $\varphi > \pi$. Thus, we have two discrete states and a guard given by $G = \{\varphi \in [0, 2\pi) \,|\, \varphi = \pi\}$. The Lagrangian for the unconstrained case is $L_1(\varphi, \dot{\varphi}) = \frac{1}{2} m l^2 \dot{\varphi}^2 - mgl\cos(\varphi)$, and for the constrained case we have $L_2(\varphi, \dot{\varphi}) = \frac{1}{2} m l_c^2 \dot{\varphi}^2 - mg(l_c \cdot (1 + \cos(\varphi)) - l)$. Since we want to model the discrete event, when the rod hits the pin, such that the lateral velocity of the pendulum is continuous, a nontrivial reset map for the angular velocity $\dot{\varphi}$ is required,

$$\dot{\varphi}^+ = R(\dot{\varphi}^-) = \frac{l}{l_c} \dot{\varphi}^-.$$

With this reset map, one can check that $E_1(\pi, \dot{\varphi}^-) = E_2(\pi, R(\dot{\varphi}^-))$ and $p_1(\pi, \dot{\varphi}^-) = p_2(\pi, R(\dot{\varphi}^-))$. The Euler-Lagrange equations follow from the hybrid variational principle.

6.3 Optimal Control of Hybrid Lagrangian Control Systems

In this section, we state the optimal control problem for hybrid Lagrangian control systems which is an extension of the optimal control problem for ordinary dynamical systems, cf. Problem 3.1. Let $\mathcal{H} = (Q, \Gamma, \mathcal{E}, \mathcal{L}, \mathcal{G}, \mathcal{R}, U, \mathcal{F})$ be a hybrid Lagrangian control system (cf. Definition 6.6), then we have seen in the previous section that the continuous dynamics are defined by the Euler-Lagrange equations for configuration and velocity variables $(q, \dot{q}) = x$. Now, a cost functional $J_i(x, u) = \int C_i(x(t), u(t))\, dt$

with $C_i : TQ \times U \to \mathbb{R}$ being continuously differentiable is assigned to each continuous subsystem $i \in \Gamma$.

For a given hybrid time interval $\mathcal{I} = \{I_\lambda\}_{\lambda\in\Lambda}$, a fixed switching sequence γ, a control trajectory $u : \mathcal{I} \to U$ and a corresponding hybrid execution $x : \mathcal{I} \to TQ$, the *hybrid cost functional* is given by

$$J(x,u) = \sum_{\lambda\in\Lambda} J_{\gamma(\lambda)}(x\big|_{I_\lambda}, u\big|_{I_\lambda}) = \sum_{\lambda\in\Lambda} \int_{I_\lambda} C_{\gamma(\lambda)}(x(t),u(t))\,dt. \tag{6.19}$$

If desired, costs for the discrete events can be added, namely by adding a Mayer term (cf. Section 3.1.1) as proposed in [BGH$^+$02], for instance.

Assumption 6.27: In the following, we assume that the number of switches in the hybrid interval, N, and the discrete sequence of modes, γ, are fixed.

Note that the switching times and, in particular, the final time $T := \tau_{N+1}$ are allowed to vary and are considered as additional optimization variables. We denote the switching times by $\mathcal{T} = \{\tau_0, \ldots, \tau_{N+1}\}$.

Problem 6.28: An *optimal control problem* for a hybrid Lagrangian control system $\mathcal{H}$ with switching sequence γ is stated as follows

$$\min_{\mathcal{T},(x,u)} J(x,u,\mathcal{T}) = \sum_{\lambda\in\Lambda} J_{\gamma(\lambda)}(x,u) \tag{6.20}$$

subject to

$$\begin{aligned}
&\tau_0 = 0,\ \ \tau_{N+1} = T,\ \ \tau_\lambda \le \tau_{\lambda+1} \ \text{ for } 0 \le \lambda \le N-1,\\
&x(\tau_0) = x^0 = (q^0, \dot{q}^0),\ \ x(\tau_{N+1}) = x^T = (q^T, \dot{q}^T),\\
&\frac{d}{dt}\frac{\partial L_{\gamma(\lambda)}}{\partial \dot{q}} - \frac{\partial L_{\gamma(\lambda)}}{\partial q} = f_{\gamma(\lambda)}(x,u) \quad \forall t \in I_\lambda \text{ and } \forall\, \lambda \in \Lambda,\\
&x(\tau_{\lambda+1}^-) \in G_{(\gamma(\lambda),\gamma(\lambda+1))} \quad \text{ for } 0 \le \lambda \le N-1, \text{ and}\\
&R_{(\gamma(\lambda),\gamma(\lambda+1))}(x(\tau_{\lambda+1}^-)) = x(\tau_{\lambda+1}^+).
\end{aligned}$$

Remark 6.29: When there are more than one hybrid cost functional which have to be minimized simultaneously, Problem 6.28 can be extended to a *multiobjective optimal control problem for a hybrid Lagrangian control system*. The vector of hybrid cost functionals is denoted by $\mathbf{J}$ with $\mathbf{J} = (J^1, \ldots, J^k)$, $k \ge 1$, and $J^1, \ldots, J^k$ being of Bolza form as defined in Equation (6.19). On the interval parts I_λ, we write $\mathbf{J}_{\gamma(\lambda)}(x,u) = \int_{I_\lambda} \mathbf{C}_{\gamma(\lambda)}(x(t),u(t))\,dt$, where $\mathbf{C}_{\gamma(\lambda)}(x(t),u(t))$ denotes the vector of

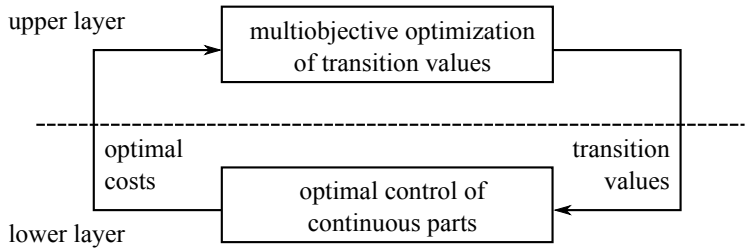

Figure 6.6: The single or multiobjective optimal control problem for hybrid systems can be split up into two layers.

running costs of subsystem $\gamma(\lambda)$, for which the integration is performed component wise.

For ordinary multiobjective optimal control problems, Pareto optimality has been defined in Section 3.1.3. This definition extends directly to hybrid solutions $(\mathcal{T}, x, u)$: a triple $(\mathcal{T}^*, x^*, u^*)$, which is admissible to the constraints of Problem 6.28, is Pareto optimal if there is no other admissible triple $(\mathcal{T}, x, u)$ for which $J^i(\mathcal{T}, x, u) \leq J^i(\mathcal{T}^*, x^*, u^*)$ for all $1 \leq i \leq k$ and $J^j(\mathcal{T}, x, u) < J^j(\mathcal{T}^*, x^*, u^*)$ for at least one $j \in \{1, \ldots, k\}$ (cf. Definition 3.4).

6.3.1 Two Layer Formulation

For the numerical computation of optimal solutions for the hybrid optimal control problem, we split up the problem into two layers. The basic idea is to decouple the continuous parts of a trajectory of the hybrid system at the discrete events, such that there remain a set of uncoupled ordinary optimal control problems. The coupling constraints, i.e. the switching times and states have to be optimized in an upper layer then. This procedure is depicted in Figure 6.6.

This approach resembles a method presented in [XA02b], which splits up hybrid control problems in multiple stages, as well. The authors additionally propose to perform the discrete optimization w.r.t. the switching sequence and the number of switches in a third optimization stage, but do not elaborate this idea further. However, our approach differ from the [XA02b] approach in the choice of numerical methods for the implementation (cf. Section 6.3.2). Furthermore, in [XA02b], they restrict to single cost functions and do not consider multiobjective hybrid optimal control problems.

In more detail, for our two layer formulation, we introduce the *transition states* as auxiliary optimization variables, $\mathcal{A} = \{a_\lambda\}_{\lambda \in \Lambda}$ and $\mathcal{B} = \{b_\lambda\}_{\lambda \in \Lambda}$ with a_λ and b_λ being the initial and final states of the interval I_λ. Then, the optimal control problems of the lower layer can be stated as follows.

Problem 6.30: The $N+1$ optimal control problems of the lower layer are of the form:

$$\min_{(x,u)} \mathbf{J}_{\gamma(\lambda)}(x,u) = \int_{I_\lambda} \mathbf{C}_{\gamma(\lambda)}(x(t),u(t))\,dt,$$

subject to $x(\tau_\lambda^+) = a_\lambda$, $x(\tau_{\lambda+1}^-) = b_\lambda$, and

$$\frac{d}{dt}\frac{\partial L_{\gamma(\lambda)}}{\partial \dot{q}} - \frac{\partial L_{\gamma(\lambda)}}{\partial q} = f_{\gamma(\lambda)}(x,u) \;\; \forall\, t \in I_\lambda$$

for all $\lambda \in \Lambda$ and with $a_0 = x^0$ and $b_N = x^T$.

Thus, in the lower layer, we have $N+1$ decoupled ordinary optimal control problems with fixed final time. Because of the fixed boundary conditions, the subproblems could be easily solved in parallel. In the upper layer, the switching times $\mathcal{T}$ and the transition states $\mathcal{A}, \mathcal{B}$ are optimized with respect to the hybrid cost functional (Equation (6.19)) which is evaluated at the optimal solutions $(x^*\big|_{I_\lambda}, u^*\big|_{I_\lambda})$ for the interval parts I_λ, $\lambda \in \Lambda$. Thus, the upper layer problem is a finite-dimensional, restricted optimization problem.

Problem 6.31: The optimization problem of the upper layer is of the form:

$$\min_{\mathcal{T},\mathcal{A},\mathcal{B}} \hat{\mathbf{J}}(\mathcal{T},\mathcal{A},\mathcal{B})$$

subject to

$$\begin{aligned}
&\tau_0 = 0, \;\; \tau_{N+1} = T, \;\; \tau_\lambda \le \tau_{\lambda+1} \;\text{ for } 0 \le \lambda \le N-1,\\
&a_0 = x^0 = (q^0, \dot{q}^0), \;\; b_{N+1} = x^T = (q^T, \dot{q}^T),\\
&b_\lambda \in G_{(\gamma(\lambda),\gamma(\lambda+1))} \quad \text{for } 0 \le \lambda \le N-1, \text{ and}\\
&a_{\lambda+1} = R_{(\gamma(\lambda),\gamma(\lambda+1))}(b_\lambda)),
\end{aligned}$$

where $\hat{\mathbf{J}} := \mathbf{J}(x^*, u^*)$ with $(x^*\big|_{I_\lambda}, u^*\big|_{I_\lambda})$ being the optimal solutions of Problem 6.30 with boundary values $\mathcal{A}$ and $\mathcal{B}$ and time intervals given by $I_\lambda \in \mathcal{I}$ with switching times $\mathcal{T}$.

Using similar concepts as in [JMO06], one can show that the two layer formulation is an equivalent reformulation.

Proposition 6.32: The two layer problem formulation is equivalent to the original hybrid optimal control problem.

Proof. Consider the original formulation of Problem 6.28 with given switching sequence γ, fixed final time T, and fixed initial and final states x^0, x^T. Assume that the guard sets can be modeled by functions $g_{(\lambda,\lambda+1)}$, such that $x \in G_{(\lambda,\lambda+1)}$ if and only if $g_{(\lambda,\lambda+1)}(x) = 0$. We start by adding the auxiliary variables for the boundary states, $\mathcal{A}$, $\mathcal{B}$. Together with the corresponding additional constraints, this does not change the problem. To simplify the notation, we introduce h_1 and h_2 for the equality constraints, i.e.

$$h_1(x, u, \mathcal{T}, \mathcal{A}, \mathcal{B}) = \begin{pmatrix} x(\tau_\lambda^+) - a_\lambda \\ x(\tau_{\lambda+1}^-) - b_\lambda \\ D_{EL}L_{\gamma(\lambda)} + f_{\gamma(\lambda)}(x, u), \end{pmatrix} \qquad (\text{for } \lambda = 0, \dots, N)$$

$$h_2(\mathcal{T}, \mathcal{A}, \mathcal{B}) = \begin{pmatrix} \tau_0 \\ \tau_{N+1} - T \\ a_0 - x^0 \\ b_N - x^T \\ a_{\lambda+1} - R_{(\gamma(\lambda),\gamma(\lambda+1))}(b_\lambda) \\ g_{(\gamma(\lambda),\gamma(\lambda+1))}(b_\lambda) \end{pmatrix} \qquad (\text{for } \lambda = 0, \dots, N-1)$$

and h_3 for the inequality constraints, i.e.

$$h_3(\mathcal{T}) = \begin{pmatrix} \tau_0 - \tau_1 \\ \tau_1 - \tau_2 \\ \vdots \\ \tau_N - \tau_{N+1} \end{pmatrix}.$$

Then, with $z = (x, u)$ and $y = (\mathcal{T}, \mathcal{A}, \mathcal{B})$ the one-layer problem formulation can be abstractly written as

$$\min_{y,z} J(y, z) \quad \text{w.r.t. } h_1(y, z) = 0,\ h_2(y) = 0,\ h_3(y) \leq 0.$$

Let Y denote the set of all y admissible to h_2 and h_3, $Y = \{y \,|\, h_2(y) = 0,\ h_3(y) \leq 0\}$, and $Z(y) = \{z \,|\, h_1(y, z) = 0\}$, which is the family of sets of admissible z, parametrized by y. The following steps lead to the hierarchical two layer formu-

lation

$$
\begin{aligned}
&\min_{y,z} \{J(y,z) \,|\, h_1(y,z) = 0,\, h_2(y) = 0,\, h_3(y) \leq 0\} \\
=&\min_{y,z} \left\{ J(y,z) \,\middle|\, (y,z) \in \bigcup_{y \in Y} \{y\} \times Z(y) \right\} \\
=&\min_{y,z} \bigcup_{y \in Y} \left\{ J(y,z) \,\middle|\, (y,z) \in \{y\} \times Z(y) \right\} \\
=&\min_{y} \left\{ \min_{z} \{J(y,z) \,|\, z \in Z(y)\} \;\middle|\; y \in Y \right\} \\
=&\min_{y} \left\{ \min_{z} \{J(y,z) \,|\, h_1(y,z) = 0\} \;\middle|\; h_2(y) = 0,\, h_3(y) \leq 0 \right\}.
\end{aligned}
$$

□

6.3.2 Implementation

The two layer formulation, as proposed in the previous section, allows to choose suitable state of the art computational techniques for both layers independently. For our implementation, we use DMOC (cf. Section 3.3) for solving the optimal control problems in the lower layer and therefore introduce the discretized hybrid optimal control problem.

Discretized Hybrid Optimal Control Problem Following the philosophy of DMOC as a direct optimal control method, the forced Euler-Lagrange equations are replaced by the discrete Euler-Lagrange equations and serve as equality constraints for the optimization problem. We introduce a *discrete hybrid time grid* Δt on the hybrid interval $\mathcal{I}$ by

$$\Delta t = \{\Delta t_\lambda\}_{\lambda \in \Lambda} = \{t_0^\lambda = \tau_\lambda, t_1^\lambda, \ldots, t_{M_\lambda - 1}^\lambda, t_{M_\lambda}^\lambda = \tau_{\lambda+1}\}_{\lambda \in \Lambda}.$$

Thereby, $\{t_0^\lambda = \tau_\lambda, t_1^\lambda, \ldots, t_{M_\lambda - 1}^\lambda, t_{M_\lambda}^\lambda = \tau_{\lambda+1}\}$ is a discrete time grid for $I_\lambda = [\tau_\lambda, \tau_{\lambda+1}]$. As discussed in Section 6.2.2, if the discrete hybrid time grid is based on an equidistant time grid for $[0, T]$, then the discretization on the subintervals is equidistant except for the first and the last time step. Let q_d denote the corresponding discrete curve with $q_d(t_k^\lambda) = q_k^\lambda$ for $\lambda \in \Lambda$ and $k = 0, \ldots, M_\lambda$, and u_d a discrete control, discretized on the same time grid to simplify the notation (cf. Section 3.3).

We define the discrete cost function by

$$J_d(q_d, u_d, \Delta t) = \sum_{\lambda \in \Lambda} J_{d,\gamma(\lambda)}(q_d, u_d, \Delta t_\lambda) \tag{6.21}$$
$$= \sum_{\lambda \in \Lambda} \sum_{k=0}^{M_\lambda - 1} C_{d,\gamma(\lambda)}(q_k^\lambda, q_{k+1}^\lambda, u_k, t_k^\lambda, t_{k+1}^\lambda).$$

As for the continuous case, if several discrete cost functions have to be minimized simultaneously, they can be collected in a vector $\mathbf{J}_d(q_d, u_d, \Delta t)$. We consider the discrete forced Euler-Lagrange equations and the discrete reset maps as introduced in Section 6.2.2. Then, the discrete counterpart of Problem 6.28 is stated as follows.

Problem 6.33: The *discrete optimal control problem* for a discrete hybrid system with switching sequence γ is given by

$$\min_{\mathcal{T}, (q_d, u_d)} \mathbf{J}_d(q_d, u_d, \mathcal{T})$$

subject to

$$\begin{aligned}
&\tau_0 = 0, \;\; \tau_{N+1} = T, \;\; \tau_\lambda \leq \tau_{\lambda+1} \text{ for } 0 \leq \lambda \leq N-1, \\
&\mathbb{F}^- L_{d,\gamma(0)}(q_0^0, q_1^0, u_0^0) = \mathbb{F} L_{\gamma(0)}(x^0), \\
&\mathbb{F}^+ L_{d,\gamma(N)}(q_{M_\lambda - 1}^N, q_{M_\lambda}^N, u_{M_\lambda - 1}^N) = \mathbb{F} L_{\gamma(N)}(x^T), \\
&D_1 L_{d,\gamma(\lambda)}(q_k^\lambda, q_{k+1}^\lambda) + D_2 L_{d,\gamma(\lambda)}(q_{k-1}^\lambda, q_k^\lambda) + f^-_{\gamma(\lambda),k} + f^+_{\gamma(\lambda),k-1} = 0 \\
&\qquad\qquad \forall \lambda \in \Lambda \text{ and } k = 1, \ldots, M_\lambda - 1, \\
&q_{M_\lambda}^\lambda \in G_{(\gamma(\lambda),\gamma(\lambda+1))}, \text{ and} \\
&(q_0^{\lambda+1}, q_1^{\lambda+1}) = R_{d,(\gamma(\lambda),\gamma(\lambda+1))}(q_{M_\lambda - 1}^\lambda, q_{M_\lambda}^\lambda), \text{ for } \lambda = 0, \ldots, N-1.
\end{aligned}$$

Recall that the continuous reset function is assumed to be the identity on Q and consequently, the discrete reset function $R_d : Q \times Q \to Q \times Q$, $(q_{i-1}, \tilde{q}) \mapsto (\tilde{q}, q_i)$ keeps its second argument (cf. Equation (6.17)). Thus, in the discrete setting we have $q_{M_\lambda}^\lambda = q_0^{\lambda+1}$ for all $\lambda = 0, \ldots, N-1$ as a constraint from the reset map, which is reasonable since we introduced two variables for the unique discrete state at $t_{M_\lambda}^\lambda = t_0^{\lambda+1} = \tau_{\lambda+1}$.

A discrete formulation of the lower layer problem 6.30 can be derived analogously, by using the discrete Legendre transforms $\mathbb{F}^\pm L_{d,i}$ to transform the auxiliary variables $\mathcal{A}$, $\mathcal{B}$ into discrete boundary conditions.

The discrete lower layer subproblems in case of single objectives are then in the ordinary DMOC formulation (cf. Section 3.3) and can be implemented as explained

before. For our implementation of the DMOC method, we use again a sparse SQP optimization algorithm provided by the NAG library as reported in Section 3.4 and Section 4.3. For multiobjective optimal control subproblems in the lower layer, DMOC can be combined with the reference point technique (cf. Section B.2) as it has been presented in Section 5.6.3.

The DMOC method has been used in similar two stage optimization schemes in [JMO06] for the optimal control of formation flying satellites, not in a hybrid system setting, but for a multi agent system and in [PAM07] to compute periodic orbits of a compass gait biped modeled as a mechanical system with impacts.

The numerical tool for the optimization of the upper layer is chosen depending on the type of problem. If only one objective has to be minimized, we use a state of the art nonlinear optimization algorithm of Matlab for which no derivative information is required. In case of multiobjective optimal control problems, we are interested in the computation of the entire Pareto set. Therefore, we use the set-oriented methods for multiobjective optimization implemented in the software package GAIO (cf. Section B.1.2). Here, we also propose a gradient-free technique. As we study in detail in Section 6.4, a switching time optimization problem on discretized dynamics, in general, is not differentiable everywhere. Thus, when choosing gradient-based methods, one has to adapt the classical techniques to the nonsmooth case.

6.3.3 Application: Optimal Control of a Hybrid Oscillator

The two layer approach is applied to an optimal control scenario for the hybrid single-mass oscillator, which has already been introduced in Example 6.25. These numerical results have also been published in [FO11].

The parameters of the hybrid single-mass oscillator are chosen such that in the equilibrium state of the first mass, only one spring is tensioned whereas both masses load the second spring as well, cf. Table 6.1 for details.

The initial point at which the control of the system starts is right after the second mass is put on top of the (up to now stationary) first mass. Since no damping effects are taken into account, the uncontrolled system would start to oscillate forever. However, by applying a control force as depicted in Figure 6.4, it is possible to steer the system into the equilibrium state of both masses.

Optimal Hybrid Trajectories for Fixed Final Time At first, we are interested in the optimal solution for a hybrid trajectory consisting of two parts and with fixed final time T, hence we take $\Lambda = \{0, 1\}$, $\mathcal{I} = \{[0, \tau_1], [\tau_1, T]\}$ and $\gamma(0) = 1, \gamma(1) = 2$. The cost functional for the optimal control problem is the control effort given by

$$J(x, u) = \int_{I_1} u_1^2(t)\, dt + \int_{I_2} u_2^2(t)\, dt. \tag{6.22}$$

Parameter	Value
1st mass (m_1)	1,500
2nd mass (m_2)	500
1st spring (c_1)	10,000
2nd sping (c_2)	20,000
gravity (g)	10
initial point (q_0)	1.5
final point (q_f)	1.96
switching point (q^s)	1.7

Table 6.1: Parameters of the hybrid single mass oscillator for the numerical computations (also cf. Figure 6.4).

Using the two layer formulation as presented in Section 6.3.1, we optimize the hybrid state trajectory with initial state $x^0 = x(0) = (q_0, 0)$ and final state $x^T = x(T) = (q_f, 0)$ with corresponding control trajectory in the lower layer and the switching time τ_1 together with the switching velocity $\dot{q}^s$ in the lower layer.

The resulting optimal trajectories (position and control) for the fixed final time $T = 5.98$ are shown in Figure 6.7.

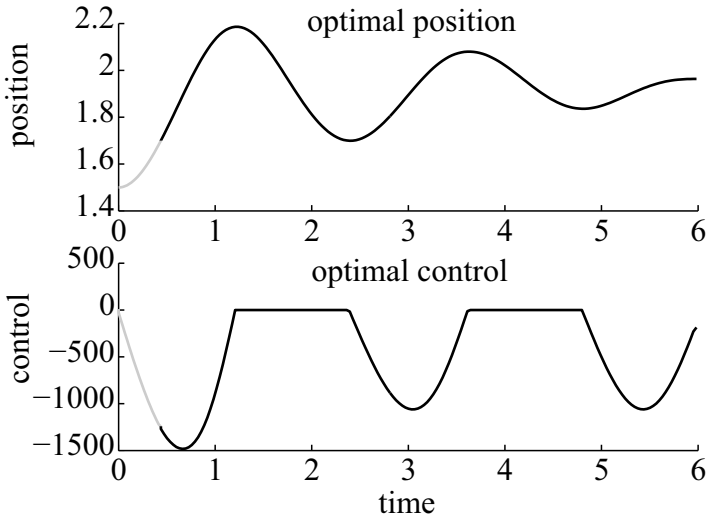

Figure 6.7: Hybrid optimal solution of the two layer implementation for one switching and fixed final time $T = 5.98$. The optimal switching time is $\tau_1 = 0.44$, the optimal switching velocity $\dot{q}^s = 0.79$ and the optimal costs are $J = 2.75 \cdot 10^6$.

Pareto Optimal Hybrid Trajectories with One Switch In the next step, we take a second objective into account, that is the duration T of the steering maneuver. This is intuitively contradictory to minimizing the control effort (6.22). Hence, we are faced with a multiobjective optimal control problem. However, the overall duration of the maneuver only depends on the switching times and not explicitly on the states and controls. Thus, the optimal control subproblems of the lower layer remain unchanged, while on the upper layer, a multiobjective optimization problem has to be solved. For the approximation of the Pareto front, we use an algorithm provided by the software package GAIO (cf. Section B.1.2). Figure 6.8 shows the resulting approximation of the Pareto front. Its shape shows the typical trade-off between control effort and duration, i.e. if one objective improves, the other one gets worse. The holes in the Pareto front occur, because the corresponding solutions

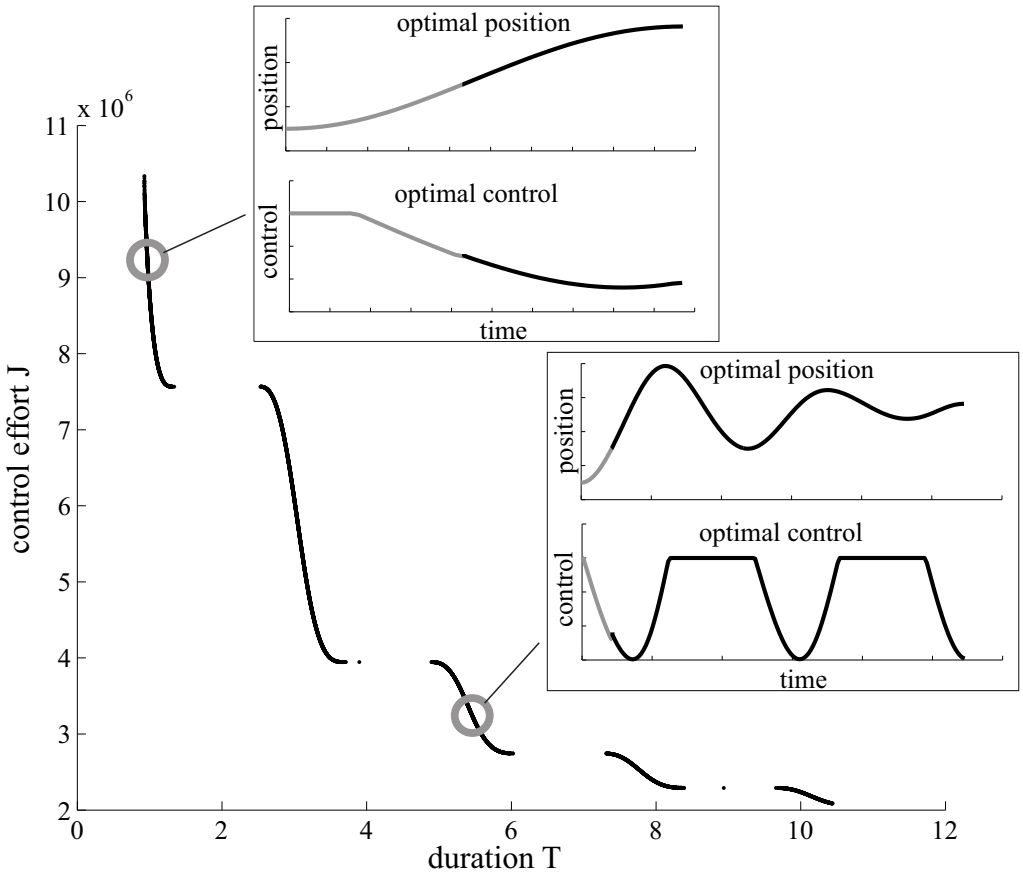

Figure 6.8: An approximation of the Pareto front with exemplary Pareto optimal solutions for the hybrid single-mass oscillator.

are dominated by Pareto optimal solutions which have the same control effort but reach the final state faster. Solutions with the same control effort but differing durations exist, since we steer the system into its equilibrium position, in which it stays without further control.

Pareto Optimal Hybrid Trajectories with Multiple Switches Finally, we investigate the optimal solutions with regard to the number of switches. By the choice of the initial and final points for the control problem, only an odd number of switches is reasonable, so we consider the control problem for $N = 1$, $N = 3$ and $N = 5$ switches. The resulting Pareto fronts are depicted in Figure 6.9. While for $N = 1$ only three parameters $(\tau_1, T, \dot{q}^s)$ have to be optimized in the upper layer, the problems with $N = 3$ and $N = 5$ lead to seven and eleven parameters, respectively.

Additionally, constraints on the velocity have been implemented to make sure that the system indeed switches between the two subsystems at the discrete events. As a consequence, it is not possible that switching points exactly coincide, thus solutions of the $N = 1$ problem are not contained in the set of admissible solutions of the $N = 3$ and $N = 5$ problems.

It is observed in Figure 6.9 that for longer duration times ($T > 8$), solutions with several switches become better, i.e. cheaper w.r.t. the control effort than solutions with only one switch. This is reasonable, because with less control, i.e. damping, but a long time horizon, higher oscillations occurs which need several switches between the discrete modes.

The numerical tests showed that the computational costs rapidly grew with an increasing number of switches, partly due to the switching velocities as additional parameters. To reduce the number of optimization parameters of the upper layer, the splitting approach could be reformulated without the additional parameters. Instead, the optimal control problem of the first subinterval could be solved with free final state and the resulting optimal final state is transferred as the initial state for the second control problem, which has to be solved subsequently then, and so forth. A numerical validation of this variant is left for future work. It would be also interesting to extend the two layer approach by another layer in which the switching sequence is optimized by appropriate discrete optimization techniques, as proposed in [BGH$^+$02], for instance.

6.4 Switching Time Optimization

In Section 6.3, it has been shown that the optimization of the switching times plays a crucial role in the optimal control of hybrid dynamical systems. For this reason, we focus on switching time optimization (STO) in this section. That means, we consider autonomous switched systems (cf. Definition 6.5), which are uncontrolled

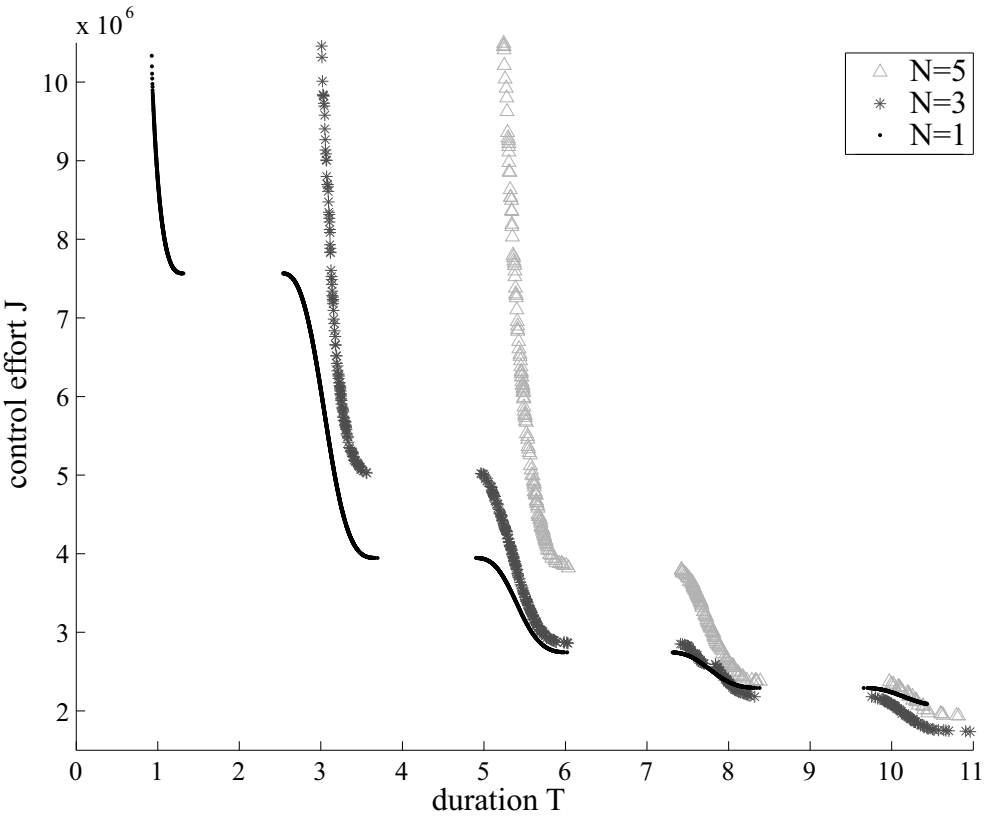

Figure 6.9: Approximation of the Pareto fronts for hybrid solutions with $N = 1$, $N = 3$ and $N = 5$ switches for the hybrid single-mass oscillator.

except for the switching times and the switching sequence. Such problems have been studied in various settings and from different perspectives in the last years (cf. among others [EWD03], [AA04], [EWA06], [SDEL09], [XA02a], [XA04], [CM11], and [JM11]).

In contrast to these works, in this thesis, we formulate and analyze the *discretized switching time optimization problem* that is obtained from a time-discretization by numerical integration schemes. For our analytical results presented below (cf. also [FMO13b] and, for preliminary results, [FMO12, FMO13a]), it is sufficient to consider switched systems with two vector fields and one single switching point. Also, the second part of Assumption 6.27 is still in effect, i.e. the switching sequence is fixed and we focus on the optimization of the switching times.

6.4.1 Switching Time Optimization for Continuous-Time Systems

We shortly recall results for the well studied case of continuous-time STO problems.

Problem 6.34: Let $\mathcal{X} \subset \mathbb{R}^n$ be a state space with $x_0 \in \mathcal{X}$. Let $T, \tau \in \mathbb{R}$ with $0 \leq \tau \leq T$, f_1, $f_2 \in C^2$ and $\ell \in C^2$. Then we consider the following problem

$$\min_{\tau} J(\tau) = \int_0^T \ell(x(t), t)\, dt \tag{6.23}$$

$$\text{w.r.t.} \quad \dot{x}(t) = \begin{cases} f_1(x(t)) & t < \tau \\ f_2(x(t)) & t \geq \tau, \end{cases} \quad \text{and} \quad x(0) = x^0. \tag{6.24}$$

Here, the hybrid trajectory $x(t) : t \in [0, T] \mapsto x(t) \in \mathcal{X}$ is in fact also a function of the switching time τ. Its derivative w.r.t. τ for $t \in (\tau, T)$ is given by (cf. [EWD03])

$$\frac{dx(t)}{d\tau} = \Phi(t, \tau)(f_1(x(\tau)) - f_2(x(\tau))), \tag{6.25}$$

with $\Phi(t, \tau)$ being the state transition matrix of the autonomous linear system $\dot{z} = \frac{\partial f_2(x(t))}{\partial x} z$.

Candidates for optimal switching times are given by the critical points of the cost function, i.e. τ^* with $\frac{d}{d\tau} J(\tau^*) = 0$. Thus, derivatives of the cost function w.r.t. the switching time have to be determined. They can be computed by means of costate, also called adjoint, differential equations, as it has been proven in several works (cf. e.g. [EWD03], [EWA06], [CM11]). We recall from [EWA06]:

Lemma 6.35: Let f_1, f_2 and ℓ be as in Problem 6.34 with $J(\tau) = \int_0^T \ell(x(t), t)\, dt$ and additionally assume that there exists a constant $K > 0$ such that, for every $x \in \mathbb{R}^n$, $\|f_i(x)\| \leq K(\|x\| + 1)$ for $i = 1, 2$ (cf. [EWA06, Asmp. 2.1]). For $t \in [\tau, T]$, define the costate by

$$\begin{aligned} \dot{\rho}(t) &= -\left(\frac{\partial f_2}{\partial x}(x(t))\right)^T \rho(t) - \left(\frac{\partial \ell}{\partial x}(x(t))\right)^T \\ \rho(T) &= 0. \end{aligned} \tag{6.26}$$

Then, $J'(\tau)$ has the following form,

$$J'(\tau) = \rho(\tau)^T [f_1(x(\tau)) - f_2(x(\tau))]. \tag{6.27}$$

A proof, also for several switching times, is given in [EWA06]. In particular, it is shown that the cost function is differentiable for any set of disjoint switching times, but not in case of coinciding switching times.

In [CM11], for instance, an additional final cost $m(x(T))$ (cf. Equation (6.23)) is considered. The boundary value of the adjoint at final point T is then $\rho(T) = \frac{\partial m}{\partial x}(x(T))$. Formulas for the second order derivative have been derived in [CM11] and [JM11]. Lemma 6.35 can be used to develop gradient-based optimization techniques for the computation of an optimal switching time $\tau_{opt} = \operatorname{argmin}_\tau J(\tau)$. Such numerical techniques are based on solving the state equation (6.24) and then the adjoint equation (6.26) to generate a descent direction for the next iteration of the optimization scheme. A feasible step size can be generated e.g. by the Armijo rule (cf. [EWA06] or [CM11]). In case of multiple switches, the algorithm presented in [EWA06] also deals with coinciding switching points.

6.4.2 Switching Time Optimization in Discretized Systems

Now, we consider the discretization of Problem 6.34 and study the differentiability of the discretized cost function.

Problem 6.36: Let $\{t_k\}_{k=0}^N = \{t_0, t_1, \dots, t_N\}$ be a discrete time grid with $t_0 = 0$, $t_N = T$ and $\tau \in (0, T)$. Let $\mathcal{X} \subset \mathbb{R}^n$ be the state space with $x_0 \in \mathcal{X}$, vector fields of the switched system $f_1,\ f_2 \in C^2$ and costs $\ell \in C^2$. Then we consider the following problem,

$$\min_\tau\ J_d(\tau) = \sum_{k=0}^{N} \Psi_k(x_k) \approx \int_0^T \ell(x(t))\,dt + m(x(T)) \tag{6.28}$$

$$\text{w.r.t.} \qquad \mathbf{F}\left(\{t_k\}_{k=0}^N, \tau, \{x_k\}_{k=0}^N, x^*\right) = 0, \tag{6.29}$$

a system of algebraic equations resulting from the discretization of Equation (6.24) by an integration scheme, e.g. discrete Euler-Lagrange equations, with x^* denoting the approximated state at switching time τ.

The discretized trajectory $\{x_k\}_{k=0}^N$ is an approximation of the exact solution, i.e. $x_k \approx x(t_k)$ for $k = 0, \dots, N$, and it also depends on the switching time τ. Note that τ is allowed to vary continuously in $(0, T)$. If $\tau \in (t_i, t_{i+1})$ for some $i = 1, \dots, N-1$, τ is taken as an additional grid point in the integration[10], which leads to the approximated state $x^* \approx x(\tau)$.

If it exists, the derivative of Equation (6.28) can be computed via the chain rule,

[10] This is exactly the same approach as for the discrete variational approach in Section 6.2.2.

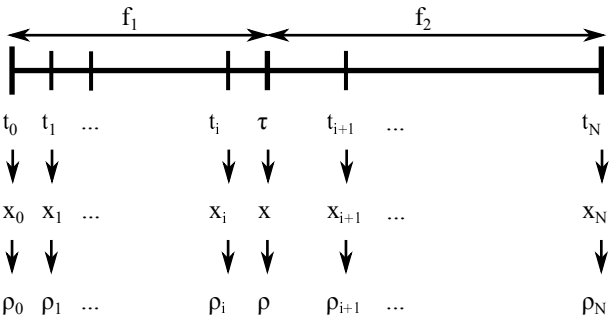

Figure 6.10: Notation for discretization as used in the explicit and implicit integration schemes and for the definition of discrete adjoints.

i.e.

$$J_d'(\tau) = \frac{d}{d\tau} J_d(\tau) = \sum_{k=0}^{N} D\Psi_k(x_k) \cdot \frac{d}{d\tau} x_k \,. \tag{6.30}$$

We assume the Ψ_k for $k = 0, \ldots, N$ to be continuously differentiable functions, which is generally the case if quadrature rules are used to approximate the cost function in Equation (6.28). Then, the crucial part which could cause nondifferentiability is the derivative of the discrete trajectory. We study the differentiability of $\frac{d}{d\tau} x_k$ for explicit one-step integration schemes first and later generalize our results to implicit one-step integration schemes.

Explicit One-Step Integration Schemes We discretize Equation (6.24) by an explicit one-step scheme. Let $i \in \{0, \ldots, N-1\}$ denote the index of the left boundary of the interval in which τ lies, i.e. $\tau \in [t_i, t_{i+1}]$. Then, Equation (6.29) has the following form

$$\mathbf{F} = \begin{cases} x_{k+1} - F_1(x_k, t_k, t_{k+1}) = 0 & \text{for } k = 0, \ldots, i-1, \\ x^* - F_1(x_i, t_i, \tau) = 0 & \text{and} \\ x_{i+1} - F_2(x^*, \tau, t_{i+1}) = 0 & \text{for } k = i, \\ x_{k+1} - F_2(x_k, t_k, t_{k+1}) = 0 & \text{for } k = i+1, \ldots, N-1. \end{cases} \tag{6.31}$$

F_1 and F_2 denote the integration scheme that approximates the vector field f_1 and f_2, respectively. The switch between the schemes happens at τ (cf. Figure 6.10), leading to the approximated switching point $x^* = F_1(x_i, t_i, \tau)$. It can be seen from Equation (6.31) that $\{x_k\}_{k=0}^N$ is continuous w.r.t. τ.

Lemma 6.37: For the derivative of the discrete trajectory $\{x_k\}_{k=0}^N$ w.r.t. $\tau \in$

(t_i, t_{i+1}), the following holds

$$\frac{d}{d\tau}x_{k+1} \tag{6.32}$$
$$= \begin{cases} 0, & k = 0, \dots, i-1, \\ D_1F_2(x^*, \tau, t_{i+1}) \cdot D_3F_1(x_i, t_i, \tau) + D_2F_2(x^*, \tau, t_{i+1}) & k = i, \\ D_1F_2(x_k, t_k, t_{k+1}) \cdot \frac{d}{d\tau}x_k & k = i+1, \dots, N-1. \end{cases}$$

Proof. For $k = 0, \dots, i-1$, $\frac{d}{d\tau}x_{k+1} = 0$, since the states prior to the switch do not depend on τ. Taking the derivative of $x^* = F_1(x_i, t_i, \tau)$ yields $\frac{d}{d\tau}x^* = D_3F_1(x_i, t_i, \tau)$. This can be used to compute

$$\frac{d}{d\tau}x_{i+1} = D_1F_2(x^*, \tau, t_{i+1}) \cdot D_3F_1(x_i, t_i, \tau) + D_2F_2(x^*, \tau, t_{i+1}),$$

where the chain rule is applied. Analogously, one obtains the recursive formula $\frac{d}{d\tau}x_{k+1} = D_1F_2(x_k, t_k, t_{k+1}) \cdot \frac{d}{d\tau}x_k$ for $k = i+1, \dots, N-1$. □

Remark 6.38: The iterative relation of the derivatives at neighboring trajectory points gives rise to a discrete transition operator

$$\mathbf{\Phi}(k+1, k) := D_1F_2(x_k, t_k, t_{k+1}) \tag{6.33}$$

for $k \in \{i+1, \dots, N-1\}$. We define $\mathbf{\Phi}(k, k) := 1$ and for $l > k+1$, $\mathbf{\Phi}(l, k) := \mathbf{\Phi}(l, l-1) \cdot \ldots \cdot \mathbf{\Phi}(k+2, k+1) \cdot \mathbf{\Phi}(k+1, k)$. Thus, for $k \in \{i+1, \dots, N-1\}$ one gets the propagation scheme

$$\frac{d}{d\tau}x_{k+1} = \mathbf{\Phi}(k+1, i+1) \cdot \frac{d}{d\tau}x_{i+1},$$

which is the discrete-time version of Equation (6.25) in the continuous time setting.

In general, the discrete derivative is not differentiable w.r.t. τ, if the switching time coincides with a time grid point. This is due to the fact that the left and right hand side limits of the differential quotients generally do not coincide. As it is formally shown in the following, only if there was equality in Equations (6.34) and (6.35) of Assumption 6.39, differentiability of the continuous time system would be inherited by the discretized system at all switching points.

Assumption 6.39: Given a switched system as in Equation (6.31), the vector fields f_1 and f_2 together with the chosen integration scheme define F_1 and F_2 such that

the following two non-equalities hold for any triple (t_i, t_{i+1}, t_{i+2}) and any states x_i, x^* and x_{i+1}:

$$\begin{aligned}&\mathbf{\Phi}(i+2,i+1)\cdot(D_1F_2(x_{i+1},t_{i+1},t_{i+1})\cdot D_3F_1(x_i,t_i,\ t_{i+1})+D_2F_2(x_{i+1},t_{i+1},t_{i+1}))\\&\neq \mathbf{\Phi}(i+2,i+1)\cdot D_3F_1(x_{i+1},t_{i+1},t_{i+1})+D_2F_2(x_{i+1},t_{i+1},t_{i+2}),\end{aligned} \tag{6.34}$$

and

$$D_1F_2(x_{i+1},t_{i+1},t_{i+1})\cdot D_3F_1(x_i,t_i,t_{i+1})+D_2F_2(x_{i+1},t_{i+1},t_{i+1})\neq 0. \tag{6.35}$$

To see that these non-equalities do hold in general, we refer to Example 6.41, in which the inequality is shown for an arbitrary switched system discretized with the explicit Euler scheme.

Theorem 6.40 (Differentiability of $\{x_k\}_{k=0}^N$)**:** Consider a switched system as defined in Equation (6.31) and assume F_1 and F_2 to be continuously differentiable. Then, $\{x_k\}_{k=0}^N$ is differentiable w.r.t. τ if $\tau \in (t_i, t_{i+1})$. Additionally, if and only if Assumption 6.39 is in effect, $\{x_k\}_{k=0}^N$ is nondifferentiable for $\tau \in \{t_1, \dots, t_{N-1}\}$.

Proof. From Equation (6.32) in Lemma 6.37, it follows that $\tau \in (t_i, t_{i+1})$, $\frac{d}{d\tau}x_{k+1}$ for $k = 0, \dots, N-1$ is continuous, since F_1 and F_2 are continuously differentiable. To study the case when τ coincides with a grid point, without loss of generality, $\tau = t_{i+1}$ can be assumed and we compare left and right limits of the derivative. For $\tau \to t_{i+1}$ with $\tau > t_{i+1}$, $\frac{d}{d\tau}x_{i+1} = 0$ is zero, because it is prior to the switch. The right hand side limit is

$$\begin{aligned}\lim_{\substack{\tau\to t_{i+1}\\ \tau<t_{i+1}}}\frac{d}{d\tau}x_{i+1} &= \lim_{\substack{\tau\to t_{i+1}\\ \tau<t_{i+1}}} D_1F_2(x^*,\tau,t_{i+1})\cdot D_3F_1(x_i,t_i,\tau)+D_2F_2(x^*,\tau,t_{i+1})\\ &= D_1F_2(x_{i+1},t_{i+1},t_{i+1})\cdot D_3F_1(x_i,t_i,t_{i+1})+D_2F_2(x_{i+1},t_{i+1},t_{i+1})\neq\ 0\end{aligned}$$

with $\lim_{\tau\to t_{i+1}} x^* = x_{i+1}$ and because of Assumption 6.39. For the derivative of x_{i+2} we have

$$\begin{aligned}&\lim_{\substack{\tau\to t_{i+1}\\ \tau<t_{i+1}}}\frac{d}{d\tau}x_{i+2} = \mathbf{\Phi}(i+2,i+1)\cdot(D_1F_2(x_{i+1},t_{i+1},t_{i+1})\cdot D_3F_1(x_i,t_i,t_{i+1})\\&+D_2F_2(x_{i+1},t_{i+1},t_{i+1}))\\ \neq &\lim_{\substack{\tau\to t_{i+1}\\ \tau>t_{i+1}}}\frac{d}{d\tau}x_{i+2}\neq \mathbf{\Phi}(i+2,i+1)\cdot D_3F_1(x_{i+1},t_{i+1},t_{i+1})+D_2F_2(x_{i+1},t_{i+1},t_{i+2}).\end{aligned}$$

Thus, $\frac{d}{d\tau}x_{i+2}$ and recursively all $\frac{d}{d\tau}x_{k+1}$ $(k > i)$ are nonexistent for $\tau = t_{i+1}$. □

Although Assumption 6.39 has to be checked for each integration scheme and each system individually, generally the nondifferentiability of x_k, $(k = i+1, \ldots, N)$ at time points is present for a system with arbitrary switching vector fields. As we have seen in Equation (6.30), $\frac{d}{d\tau}x_k$ is part of the discrete cost function derivative and thus, nondifferentiability of the discrete trajectory generally leads to nondifferentiability of the discrete cost function J_d.

Example 6.41 (Explicit Euler)**:** We specify the integration scheme to be an explicit Euler integrator to illustrate the differences in the left and right hand side derivatives and additionally show that the differentiability vanishes for decreasing step sizes in the limit. The explicit Euler scheme for a switched system for $k \in \{0, \ldots, N-1\}$ is given by $F_j(x_k, t_k, t_{k+1}) = x_k + (t_{k+1} - t_k) \cdot f_j(x_k)$, $j = \{1, 2\}$ and on the switching interval with x^* and τ in the appropriate arguments. For $\tau \in (t_i, t_{i+1})$ we get

$$\frac{d}{d\tau}x_{i+1} = f_1(x_i) + \frac{\partial}{\partial x}f_2(x^*) \cdot (t_{i+1} - \tau) \cdot f_1(x_i) - f_2(x^*)$$

with $x^* = x_i + f_1(x_i) \cdot (\tau - t_i)$. Thus, at $\tau = t_{i+1}$, $\frac{d}{d\tau}x_{i+1}$ switches from zero to $f_1(x_i) - f_2(x_{i+1})$. Then, the effect on the next node, x_{i+2} can be studied. From Equation (6.32) we know that $\frac{d}{d\tau}x_{i+2} = (1 + (t_{i+2} - t_{i+1})\frac{\partial}{\partial x}f_2(x_{i+1}))\frac{d}{d\tau}x_{i+1}$ and hence,

$$\lim_{\substack{\tau \to t_{i+1} \\ \tau < t_{i+1}}} \frac{d}{d\tau}x_{i+2} = \left(1 + (t_{i+2} - t_{i+1})\frac{\partial}{\partial x}f_2(x_{i+1})\right) \cdot \left[f_1(x_i) - f_2(x_{i+1})\right],$$

but for the limit from the right we receive by shifting the index in Equation (6.31)

$$\lim_{\substack{\tau \to t_{i+1} \\ \tau > t_{i+1}}} \frac{d}{d\tau}x_{i+2} = \left(1 + (t_{i+2} - t_{i+1})\frac{\partial}{\partial x}f_2(x_{i+1})\right) \cdot f_1(x_{i+1}) - f_2(x_{i+1}).$$

Generally, these two limits do not coincide. Thus, $\{x_k\}_{k=0}^N$ is nondifferentiable at $\tau = t_{i+1}$. However, when reducing the time steps, i.e. in particular $|t_{i+1} - t_i| \to 0$, $\frac{d}{d\tau}x_{i+1}$ matches the continuous case in the limit, $\lim_{\substack{t \to \tau \\ t > \tau}} \frac{d}{d\tau}x(\tau) = f_1(x(\tau)) - f_2(x(\tau))$.

Implicit One-step Integration Schemes When using an implicit scheme instead of an explicit integration scheme, Equation (6.29) of Problem 6.36 becomes

$$\mathbf{G} = \begin{cases} G_1(x_k, x_{k+1}, t_k, t_{k+1}) = 0 & \text{for } k = 0, \dots, i-1, \\ G_1(x_k, x^*, t_k, \tau) = 0 & \text{and} \\ G_2(x^*, x_{k+1}, \tau, t_{k+1}) = 0 & \text{for } k = i, \\ G_2(x_k, x_{k+1}, t_k, t_{k+1}) = 0 & \text{for } k = i+1, \dots, N-1, \end{cases} \tag{6.36}$$

which implicitly defines the discrete trajectory $\{x_k\}_{k=0}^N$ and the switching point x^*. By computations similar to those for explicit schemes, we derive for $\tau \in (t_i, t_{i+1})$

$$\begin{aligned} \frac{d}{d\tau} x_{i+1} = &- D_2 G_2(x^*, x_{i+1}, \tau, t_{i+1})^{-1} \cdot (D_1 G_2(x^*, x_{i+1}, \tau, t_{i+1}) \cdot \frac{d}{d\tau} x^* \\ &+ D_3 G_2(x^*, x_{i+1}, \tau, t_{i+1})) \end{aligned}$$

with $\frac{d}{d\tau} x^* = -D_2 G_1(x_i, x^*, t_i, \tau)^{-1} D_4 G_1(x_i, x^*, t_i, \tau)$. Here and in the following, it is assumed that the derivatives of the schemes w.r.t. their second arguments are non-singular. For general one-step schemes, this is reasonable to assume. Defining the discrete transition operator for $k \in \{i+1, \dots, N-1\}$ as

$$\mathbf{\Phi}(k+1, k) := -D_2 G_2(x_k, x_{k+1}, t_k, t_{k+1})^{-1} \cdot D_1 G_2(x_k, x_{k+1}, t_k, t_{k+1}),$$

the propagation rule can again be written as

$$\frac{d}{d\tau} x_{k+1} = \mathbf{\Phi}(k+1, i+1) \cdot \frac{d}{d\tau} x_{i+1} \text{ for } k = i+1, \dots, N-1.$$

Example 6.42 (Implicit Euler)**:** Let x_0 be the initial value, then the implicit Euler scheme is given by

$$\begin{aligned} x_k - x_{k+1} + f_1(x_{k+1})(t_{k+1} - t_k) = 0, &\quad \text{for } k = 1, \dots, i-1, \\ x_k - x^* + f_1(x^*)(\tau - t_k) = 0 &\quad \text{and} \\ x^* - x_{k+1} + f_2(x_{k+1})(t_{k+1} - \tau) = 0, &\quad \text{for } k = i, \\ x_k - x_{k+1} + f_2(x_{k+1})(t_{k+1} - t_k) = 0, &\quad \text{for } k = i+1, \dots, N-1. \end{aligned}$$

With $G_1(x_k, x^*, t_k, \tau) = x_k - x^* + f_1(x^*)(\tau - t_k)$ and $G_2(x^*, x_{k+1}, \tau, t_{k+1}) = x^* -$

$x_{k+1} + f_2(x_{k+1})(t_{k+1} - \tau)$ and the corresponding partial derivatives we receive

$$\frac{d}{d\tau}x^* = \left(-1 + \frac{d}{dx}f_1(x^*)(\tau - t_k)\right)^{-1} \cdot f_1(x^*),$$
$$\frac{d}{d\tau}x_{i+1} = \left(-1 + \frac{d}{dx}f_2(x_{k+1})(t_{k+1} - \tau)\right)^{-1} \cdot \left(\frac{d}{d\tau}x^* - f_2(x_{k+1})\right).$$

Comparing the left and right hand side limits of the derivatives $\frac{d}{d\tau}x_k$ $(k \geq i+1)$ for $\tau \to t_{i+1}$ shows that the implicit schemes lead to structurally the same nonsmoothness of the discrete problem as explicit schemes.

Again, we have that the nonsmoothness of the discrete trajectory's derivative, in general, leads to nondifferentiability of J_d (cf. Equation (6.30)). Alternatively, this result can be obtained by interpreting the discrete switching time problem as a continuous switching time problem with multiple switches between constant vector fields.

Interpretation as Coinciding Switchings of Constant Vector Fields An alternative proof of the nondifferentiability of $J(\tau)$ for τ lying on the time grid is based on a related continuous time STO problem. Observe that, for instance, the points of the approximated trajectory $\{x_k\}_{k=0}^N$ of the explicit Euler scheme lie on the exact, piecewise linear solution of the following multiple switched system

$$\dot{x}(t) = \begin{cases} f_1(x_k), & \text{if } t_k \leq t \leq t_{k+1}, \quad 0 \leq k < i, \\ f_1(x_i), & \text{if } t_i \leq t \leq \tau, \quad k = i, \\ f_2(x^*), & \text{if } \tau \leq t \leq t_{i+1}, \quad k = i, \\ f_2(x_k), & \text{if } t_k \leq t \leq t_{k+1}, \quad i < k \leq N-1. \end{cases} \tag{6.37}$$

In this interpretation, the switching points $\mathcal{T} = (t_0, \ldots, t_i, \tau, t_{i+1}, \ldots, t_N)$ are guaranteed to be disjoint for $t_i < \tau < t_{i+1}$ with some $i \in \{0, \ldots, N-1\}$. Thus, $J(\tau)$ is differentiable everywhere according to Section 6.4.1 and can be computed by the formulas given there. However, if τ moves onto a time grid point, e.g. $\tau = t_{i+1}$, two switching points coincide and $J'(\tau)$ is not well defined in this case, as shown in [EWA06].

Analogously, multiple switched systems as in Equation (6.37) can be specified for any one-step Runge-Kutta scheme, regardless of their explicit or implicit nature. Extending the notation of [HLW06], we define a general s-stage Runge-Kutta method (with coefficients b_l, $a_{lj} \in \mathbb{R}$ $(l, j = 1, \ldots, s)$) for a switched system by

$$
\begin{aligned}
&x_1 = x_0 + (t_1 - t_0)\sum_{l=1}^{s} b_l d_l^{(0)} && \text{with} \quad d_l^{(0)} = f_1\left(x_0 + (t_1 - t_0)\sum_{j=1}^{s} a_{lj} d_j^{(0)}\right),\\
&\vdots\\
&x^* = x_i + (\tau - t_i)\sum_{l=1}^{s} b_l d_l^{(i)} && \text{with} \quad d_l^{(i)} = f_1\left(x_i + (\tau - t_i)\sum_{j=1}^{s} a_{lj} d_j^{(i)}\right),\\
&x_{i+1} = x^* + (t_{i+1} - \tau)\sum_{l=1}^{s} b_l d_l^{(*)} && \text{with} \quad d_l^{(*)} = f_2\left(x^* + (t_{i+1} - \tau)\sum_{j=1}^{s} a_{lj} d_j^{(*)}\right),\\
&\vdots\\
&x_N = x_{N-1} + (t_N - t_{N-1})\sum_{l=1}^{s} b_l d_l^{(N-1)}\\
&\qquad\qquad \text{with} \quad d_l^{(N-1)} = f_2\left(x_{N-1} + (t_N - t_{N-1})\sum_{j=1}^{s} a_{lj} d_j^{(N-1)}\right).
\end{aligned}
$$

Thus, the resulting discrete trajectory $\{x_k\}_{k=0}^{N}$ can be interpreted as the exact solution of the multiple switched system given by the $N+1$ constant vector fields

$$\sum_{l=1}^{s} b_l d_l^{(0)}, \ldots, \sum_{l=1}^{s} b_l d_l^{(i)}, \sum_{l=1}^{s} b_l d_l^{(*)}, \sum_{l=1}^{s} b_l d_l^{(i+1)}, \ldots, \sum_{l=1}^{s} b_l d_l^{(N-1)},$$

where $b_l\,(l = 1, \ldots, s)$ are constant coefficients, but the $d_l^{(k)}\,(k = 0, \ldots, N-1)$ and $d_l^{(*)}\ (l = 1, \ldots, s)$ depend on the time steps and the current mode. Therefore, the (approximated) cost function of a smooth switching time problem that is discretized with a Runge-Kutta scheme is guaranteed to be differentiable w.r.t. τ at $\tau \in (t_i, t_{i+1})$, but, in general, not if τ matches one of the grid points.

6.4.3 Discrete Adjoint Equations

For classical optimal control problems, the Pontryagin maximum principle states first-order optimality conditions in terms of state and adjoint equations, cf. Section 3.1.2. The adjoint equations for continuous-time STO problems have been introduced in Lemma 6.35. In the discrete case, optimal control problems and STO problems can both be transformed into nonlinear constrained optimization problems. For such problems, necessary optimality conditions are given by the *Karush-Kuhn-Tucker (KKT) equations*, cf. Theorem 3.6. In the following, we derive the adjoint multipliers from the KKT equations for discretized STO problems, based on the *discrete Lagrangian for the optimization problem.*

Discrete Adjoints for Explicit Schemes

Definition 6.43 (Discrete Lagrangian)**:** The discrete Lagrangian of Problem 6.36

is given by

$$\begin{aligned}\mathcal{L}_d(\{x_k\}_{k=0}^N,&\{\rho\}_{k=0}^N,\tau,x^*,\rho^*)\\ &= \sum_{k=0}^{N}\Psi_k(x_k) - \sum_{k=0}^{i-1}\rho_{k+1}\cdot(x_{k+1}-F_1(x_k,t_k,t_{k+1})) - \rho^*\cdot(x^*-F_1(x_i,t_i,\tau))\\ &\quad - \rho_{i+1}\cdot(x_{i+1}-F_2(x^*,\tau,t_{i+1})) - \sum_{k=i+1}^{N-1}\rho_{k+1}\cdot(x_{k+1}-F_2(x_k,t_k,t_{k+1}))\\ &\quad - \rho_0\cdot(x_0-x^0),\end{aligned}$$

with the discrete adjoints $\{\rho\}_{k=0}^N$ and ρ^* (cf. Figure 6.10)[11].

Theorem 6.44 (Discrete Adjoints)**:** The backwards difference equations defining the discrete adjoints for an explicit integration scheme are given by

$$\begin{aligned}\rho_N &= D\Psi_N(x_N),\\ \rho_k &= D\Psi_k(x_k) + \rho_{k+1}\cdot D_1F_2(x_k,t_k,t_{k+1}), \quad \text{for } k = N-1,\dots,i+2,\\ \rho_{i+1} &= D\Psi_{i+1}(x_{i+1}) + \rho_{i+2}D_1F_2(x_{i+1},t_{i+1},t_{i+2}),\\ \rho^* &= \rho_{i+1}\cdot D_1F_2(x^*,\tau,t_{i+1}),\\ \rho_i &= D\Psi_i(x_i) + \rho^*D_1F_1(x_i,t_i,\tau), \text{ and}\\ \rho_k &= D\Psi_k(x_k) + \rho_{k+1}\cdot D_1F_1(x_k,t_k,t_{k+1}), \quad \text{for } k = i-1,\dots,0.\end{aligned}$$

Proof. Taking variations w.r.t. x_k, ρ_k, x^*, ρ^* and τ leads to the necessary optimality conditions, i.e. the discrete equations of motions, the boundary condition $x_0 = x(0) = x^0$ and also the discrete adjoint equations as given above. □

The discrete adjoint equations form an implicit one-step integration scheme in forward time for the continuous time adjoint differential equation (6.26). Starting with a Runge-Kutta scheme for the state system, the state-adjoint scheme together forms a *symplectic partitioned Runge-Kutta scheme* ([BL06]), e.g. a symplectic Euler scheme as shown in Example 6.46. This is analogous to the discrete state-adjoint system that is introduced by Hager et al., e.g. in [Hag00], for classical optimal control problems.

Using the operator $\mathbf{\Phi}(k+1,k)$ from Equation (6.33), the difference equation of the discrete adjoints can be written as

$$\rho_k = D\Psi_k(x_k) + \rho_{k+1}\cdot\mathbf{\Phi}(k+1,k)$$

[11] Note that the discrete adjoints are treated as row vectors here, in contrast to the continuous formulation in Section 6.4.1.

for $k = N, \dots, i+1$, with boundary value $\rho_N = D\Psi_N(x_N)$, or alternatively, $\rho_k = \sum_{j=k}^{N} D\Psi_j(x_j) \cdot \mathbf{\Phi}(j,k)$, where ρ_{i+1} is the last adjoint before switching (looking backwards in time). Thus, the adjoints are continuous w.r.t. τ, since $D\Psi_k$ and the transition operator are continuous.

Lemma 6.45 (Derivative of J_d)**:** If the discrete cost function J_d is differentiable at some switching point τ, the derivative is $J_d{}'(\tau) = \rho_{i+1} \cdot \frac{d}{d\tau} x_{i+1}$.

Proof. Using the recursive relation of the derivatives of x_k (cf. Equation (6.32)) and the discrete adjoints from Theorem 6.44, we obtain $J_d{}'(\tau) = \sum_{k=0}^{N} D\Psi_k(x_k) \frac{d}{d\tau} x_k = \sum_{k=i+1}^{N} D\Psi_k(x_k) \cdot \mathbf{\Phi}(k, i+1) \cdot \frac{d}{d\tau} x_{i+1} = \rho_{i+1} \cdot \frac{d}{d\tau} x_{i+1}$. □

Although the adjoint itself is continuous, the term $\frac{d}{d\tau} x_{i+1}$ leads to nondifferentiability of J_d. In the following, at the isolated nondifferentiable points of x_{i+1}, one-sided derivatives for the cost function derivative are taken.

Example 6.46 (Adjoints for explicit Euler)**:** Recall that in the explicit Euler scheme (cf. Example 6.41), it holds $\mathbf{\Phi}(k+1,k) = D_1 F_2(x_k, t_k, t_{k+1}) = 1 + (t_{k+1} - t_k) \frac{\partial}{\partial x} f_2(x_k)$ for $k = i+1, \dots, N-1$ with f_2 being the active vector field after the switch. If we plug this into the adjoint equation, we receive

$$\begin{aligned} \rho_k &= D\Psi_k(x_k) + \rho_{k+1} \left(1 + (t_{k+1} - t_k) \frac{\partial}{\partial x} f_2(x_k) \right) \\ &= \rho_{k+1} + \left(\frac{D\Psi_k(x_k)}{t_{k+1} - t_k} + \rho_{k+1} \frac{\partial}{\partial x} f_2(x_k) \right) \cdot (t_{k+1} - t_k). \end{aligned} \tag{6.38}$$

For choosing $\Psi(x_k) = (t_{k+1} - t_k) \cdot \ell(x_k)$, Equation (6.38) is a direct discretization of the continuous formulation in Equation (6.26). The resulting adjoint scheme itself is explicit, if we went backwards in time. Thus, the discrete scheme for the system of equations given by Equation (6.24) and Equation (6.26) is a symplectic or semi-implicit Euler scheme (in forward time).

Discrete Adjoints for Implicit Schemes For an implicit integration method as in Equation (6.36), a Lagrangian can be defined and adjoints can be derived analogously

to the explicit case, leading to the following scheme

$$\begin{aligned}
\rho_N &= D\Psi_N(x_N) \cdot D_2G_2(x_{N-1}, x_N, t_{N-1}, t_N)^{-1}, \\
\rho_k &= (D\Psi_k(x_k) - \rho_{k+1} \cdot D_1G_2(x_k, x_{k+1}, t_k, t_{k+1})) \cdot D_2G_2(x_{k-1}, x_k, t_{k-1}, t_k)^{-1} \\
&\qquad\qquad \text{for } k = N-1, \dots, i+2, \\
\rho_{i+1} &= (D\Psi_{i+1}(x_{i+1}) - \rho_{i+2} \cdot D_1G_2(x_{i+1}, x_{i+2}, t_{i+1}, t_{i+2}))D_2G_2(x^*, x_{i+1}, \tau, t_{i+1})^{-1}, \\
\rho^* &= \rho_{i+1} \cdot D_1G_2(x^*, x_{i+1}, \tau, t_{i+1})D_2G_1(x_i, x^*, t_i, \tau)^{-1}, \\
\rho_i &= (D\Psi_i(x_i) - \rho^* D_1G_1(x_i, x^*, t_i, \tau)) \cdot D_2G_1(x_{i-1}, x_i, t_{i-1}, t_i)^{-1}, \\
\rho_k &= (D\Psi_k(x_k) - \rho_{k+1} \cdot D_1G_1(x_k, x_{k+1}, t_k, t_{k+1})) \cdot D_2G_1(x_{k-1}, x_k, t_{k-1}, t_k)^{-1} \\
&\qquad\qquad \text{for } k = i-1, \dots, 0.
\end{aligned}$$

Although the adjoints are continuous under normal smoothness conditions on the implicit scheme and the vector fields, $\frac{d}{d\tau}x_{i+1}$ may not be well defined on time grid points, as it is the case for explicit integration schemes. Thus, for the cost function, the same problem of nondifferentiability occurs.

6.4.4 Analysis of Nonsmoothness

Applying the discrete formulae to numerical examples, e.g. the switched double pendulum (cf. Section 6.4.6 below) for which the optimal switching time coincides with a time grid point, one observes the following: Although the cost function is nondifferentiable at all other time grid points, its derivative smoothly crosses zero at the optimal switching time. This effect is explained theoretically in this section. Furthermore, this analysis also provides useful hints how to design counter examples such as Example 6.52, in which the optimal switching time is at a nondifferentiable point. Here, the use of nonsmooth optimization algorithms (cf. Section 6.4.5) becomes highly important.

Let us first consider a one-dimensional switched system.

Lemma 6.47: Let f be at least $C^1(\mathbb{R})$ and convex, while g is a $C(\mathbb{R})$ function with isolated non-differentiable points. We assume that at such points – one of them being x_0 – a left hand side and a right hand side limit of the difference quotient exist but they do not coincide. Then, $f \circ g$ is differentiable in $x_0 \in \mathbb{R}$ if and only if f has an extremum in $g(x_0)$ with $f'(g(x_0)) = 0$.

Proof. Assume first that f is extremal in $y_0 := g(x_0)$, i.e. $f'(g(x_0)) = 0$. Then we consider the one sided difference quotient of $f \circ g$ to which we are allowed to apply

the chain rule, since one sided limits of both functions exists

$$\begin{aligned}&\lim_{x\uparrow x_0}\frac{(f\circ g)(x)-(f\circ g)(x_0)}{x-x_0}\\ =&f'(g(x_0))\cdot\lim_{x\uparrow x_0}\frac{g(x)-g(x_0)}{x-x_0}=0.\end{aligned}$$

Analogously, this holds for the limit from the right, denoted by $x\downarrow x_0$. Thus both directional derivatives coincide and so they define the derivative of $f\circ g$ at x_0 to be zero. If we now assume that $f\circ g$ is differentiable in $x_0\in\mathbb{R}$, while assuming the one sided difference quotients of g are different, the only solution of this one dimensional equation

$$f'(g(x_0))\lim_{x\uparrow x_0}\frac{g(x)-g(x_0)}{x-x_0}=f'(g(x_0))\lim_{x\downarrow x_0}\frac{g(x)-g(x_0)}{x-x_0}$$

is $f'(g(x_0))=0$. So $g(x_0)$ is a critical point of f and because f is assumed to be convex, it is an extremum. □

Back to discretized STO problems, we see that the interplay of the discretized cost functions Ψ_k with the discrete trajectory as a C^0-function of τ may or may not cause nondifferentiable optimal points. Whenever there is an admissible $\tau\in[0,T]$ that generates a discrete trajectory which minimizes $\Psi(x_d)=\sum_{k=0}^{N}\Psi_k(x_k)$, $D\Psi(x_d)=0$, this will be the minimizer of $J_d=\Psi(x_d(\tau))$ as well and it will be smooth regardless of a possible nonsmoothness of $x_d(\tau)$ at that point.

Remark 6.48: In higher dimensions (but the same situation as in Lemma 6.47), it still holds that if $g(x_0)\in\mathbb{R}^n$ is an unconstrained extremum of $f:\mathbb{R}^n\to\mathbb{R}$ on $\mathbb{R}^n$, then $f\circ g$ is differentiable in x_0 with $D(f\circ g)(x_0)=0$. In addition, there are further chances of differentiability in x_0 despite nondifferentiability of g in this point since $D(f\circ g)(x_0)=Df(g(x_0))\cdot Dg(x_0)=0$ may be also achieved if the derivatives are orthogonal to each other. However, this does not, of course, generally exclude the existence of nonsmooth optima in higher dimensional switched systems.

6.4.5 Optimization Algorithm

To solve an STO problem as Problem 6.34, two different approaches can be used. In most works (cf. e.g. [EWD03], [EWA06], [CM11], and [JM11]), the necessary optimality conditions for continuous switching time problems (cf. Section 6.4.1) are formulated at first. Then, during the optimization process, the state-adjoint system is solved repeatedly by numerical integration. In contrast to that, we directly start with a time-discretization of the problem, cf. Problem 6.36. As it has been shown

in Section 6.4.3, the necessary optimality conditions of the discretized problem give rise to discrete adjoint equations, which can be used for the computation of optimal switching times. This can be called a *direct switching time optimization method* in contrast to the common approach, which first states the necessary optimality conditions and then discretizes for a numerical treatment.

However, due to the nondifferentiable points of the cost function, we cannot apply ordinary methods for nonlinear optimization since those are known to fail for nonsmooth problems. It is reported in [Lem89], for instance, that convergence to wrong points, failure of the stopping criteria or extremely inaccurate gradient approximations may occur.

A simple method of *nonsmooth optimization* is the subgradient method. Here, the classical method of gradient descent (cf. e.g. [Pol97]) is modified, by replacing the gradient, which does not exist everywhere for nonsmooth functions, by *subgradients*. In the following we assume that the cost function is convex, such that we can use the theory of ordinary subgradients. In case of nonconvex discretized STO problems, generalized subgradients as proposed e.g. in [Cla83] can be used.

Definition 6.49 (Subgradient, cf. [Lem89])**:** Let $f : X \to \mathbb{R}$ be a convex function on the convex open set $X \subset \mathbb{R}^n$. A vector $g \in \mathbb{R}^n$ is called a *subgradient* of f in $x \in X$, if

$$f(y) - f(x) \geq g^T \cdot (y - x) \quad \forall y \in X.$$

The set $\partial f(x) \subset \mathbb{R}^n$,

$$\partial f(x) = \{g \in \mathbb{R}^n \,|\, g^T \cdot (y - x) \leq f(y) - f(x) \;\; \forall y \in X\}$$

is called the *subdifferential* of f in $x \in X$.

The necessary and sufficient optimality condition for convex nonsmooth functions is: $x^* \in X$ is a minimum of f if and only if $0 \in \partial f$. For the directional derivative $f'(x;d) = \lim_{t \to 0, t>0} \frac{f(x+td)-f(x)}{t}$ with direction $d \in \mathbb{R}^n$ it holds that $f'(x;d) = \max_{g \in \partial f(x)} g^T d$ for all $d \in \mathbb{R}^n$. If f is differentiable in x, the subdifferential reduces to $\nabla f(x)$ (cf. [Cla83]).

In our numerical examples, we use the following algorithm, similar to subgradient methods proposed in [Lem89], [GK02] or [Alt04], to the discretized STO problem with cost function $J_d : [0,T] \subset \mathbb{R} \to \mathbb{R}$, $J_d(\tau) = \sum_{k=0}^{N} \Psi_k(x_k(\tau))$. For notational simplicity, we give the formula for one-dimensional optimization problems only, although the algorithm is analogously applicable to higher dimensional problems, i.e. several switching times.

Algorithm 6.50 (Subgradient descent with projections)**:** Take an initial point $\tau^{(0)}$,

choose small values $\text{tol}_g, \text{tol}_\tau$ and set $k := 0$.

1. Compute a subgradient $g^{(k)} \in \partial J_d(\tau^{(k)})$
2. Stopping criteria: if $\|g^{(k)}\| \leq \text{tol}_g$ or $\|\tau^{(k-1)} - \tau^{(k)}\| \leq \text{tol}_\tau \rightarrow$ stop!
3. Let $d^{(k)} = -g^{(k)}/\|g^{(k)}\|$. Choose some appropriate step size $s_k \geq 0$ and define $\tau^{(k+1)} = P_{[0,T]}(\tau^{(k)} + s_k d^{(k)})$.
4. Set $k := k + 1$ and return to 1.

Since the nondifferentiable points of the cost function have been identified to be the time grid points, J_d is known to be "piecewise-C^1" (cf. [Lem89]), i.e. a gradient exists almost everywhere (and a directional derivative can be always given). Thus, the probability that we have to compute a real subgradient in step 1 of Algorithm 6.50 is zero, otherwise we would take a directional derivative. However, in step 2, the first stopping criterion ($\|g^{(k)}\| \leq \text{tol}_g$), which is common in smooth optimization, does not take effect if the minimum is a kink as e.g. in Example 6.52. Therefore, we add the second, very simple stopping criterion (cf. [Alt04]). Advanced nonsmooth optimization techniques such as bundle methods (cf. [Lem89] for an early reference; much research on these methods followed since then) allow more sophisticated stopping criteria. In step 3, $P_{[0,T]}$ denotes a projection onto the feasible (convex) set (cf. [GK02]), i.e. the interval $[0, T]$ in our case.

It is shown in [Lem89] that classical line search techniques cannot be applied to nonsmooth optimization problems. However, convergence of the algorithm even though with a very low rate is assured if the step sizes fulfill $\lim_{k\to\infty} s_k = 0$ and $\sum_{k=0}^{\infty} s_k = \infty$ ([Lem89], [GK02]). A simple choice of step sizes that meet this conditions is $s_k = 1/(k+1)$. In case the optimal value J_d^* is known (e.g. if the distance to a reference trajectory has to be minimized, which is admissible for some $\tau \in [0, T]$) an optimal choice of step sizes is given by

$$s_k = \|g^{(k)}\|^{-1} \cdot (J_d(\tau^{(k)}) - J_d^*), \tag{6.39}$$

see e.g. [Lem89] for a proof. For recent works on line searches for nonsmooth optimization methods, cf. [LO12].

6.4.6 Numerical Examples

In this section, we illustrate the nonsmoothness of the discretized cost function in several examples. For the switched linear system in Example 6.51, the solutions from the discretized problem can be compared with the analytical solutions of the state and adjoint system of the original problem formulation. In Example 6.52, a

discretized system is given for which the optimal switching time is at a nonsmooth point. Thus, the modified stopping criterion of Algorithm 6.50 becomes relevant here. Finally, we study the example of a switched mechanical system, namely a locked double pendulum, in Example 6.53.

Example 6.51 (Switched Linear System)**:** We compare the analytic solutions of the commonly used continuous setting to the results we received for the discrete time setting. Therefore, consider the following simple one-dimensional linear switched system

$$\dot{x} = \begin{cases} x & t \leq \tau \\ 2x & t > \tau \end{cases}$$

with linear vector fields $f_1(x) = x$, $f_2 = 2x$ and initial value $x(0) = 10$. The corresponding flow, i.e. the solution of the switched differential equation is hence given by

$$x(t) = \begin{cases} x_0 \exp(t) & t \leq \tau \\ x(\tau)\ \exp(2(t-\tau)) & t > \tau. \end{cases}$$

The cost function to be minimized is chosen as $J(\tau) = \int_0^T x(t)^2\,dt$. The derivative of $x(t)$ w.r.t. τ equals $\frac{d}{d\tau}x(t) = -x_0 \cdot \exp(2t-\tau)$ for $t \geq \tau$ with $f_1(x(\tau)) - f_2(x(\tau)) = -x_0 \exp(\tau)$ and $\mathbf{\Phi}(t,\tau) = \exp(2(t-\tau))$ (cf. Section 6.4.1). Further, the analytic solution of the adjoint equation is given by $\rho(t) = -\frac{1}{2}x(\tau)\exp(2t - 2\tau) + \frac{1}{2}x(\tau)\exp(4T - 2\tau - 2t)$. Thus, $J'(\tau)$ can be exactly determined by Equation (6.27). For comparison, we approximate $x(t)$ by an explicit Euler scheme (cf. Example 6.41) and choose the trapezoidal rule for a quadrature of the cost function, i.e. $J(\tau) \approx \sum_{k=0}^{N} \Psi(x_k) = \sum_{k=1}^{N-1} \ell(x_k) \cdot \frac{t_{k+1}-t_{k-1}}{2} + \ell(x_0) \cdot \frac{t_1-t_0}{2} + \ell(x_N) \cdot \frac{t_N-t_{N-1}}{2}$.

In Figure 6.11a, the approximated trajectory's last point, $x_N = x_d(t_N)$ as a function of the switching time τ is shown. The resulting derivative of x_N w.r.t. τ is given in Figure 6.11b. One can see that $x_N(\tau)$ is only piecewise differentiable. Whenever the switching time coincides with one of the grid points, the left hand side and ride hand side derivative do not coincide.

This causes nondifferentiable points in $J_d(\tau)$. Its graph is given in Figure 6.12. The jumps occur at the points $\tau \in \{t_k\}_{k=0}^{N}$. However, the nondifferentiability becomes less severe, i.e. the jumps become smaller, when the grid width tends to zero as Figure 6.12b illustrates. Here, the step size is reduced from $h = 0.2$ to $h = 0.04$ which leads to a better approximation of the exact derivative and indicates that the nondifferentiability would totally vanish in the limit.

Example 6.52 (Discretized STO Problem with Nonsmooth Optimum)**:** The aim of this example is to show a worst case characteristic of nonsmooth optimization

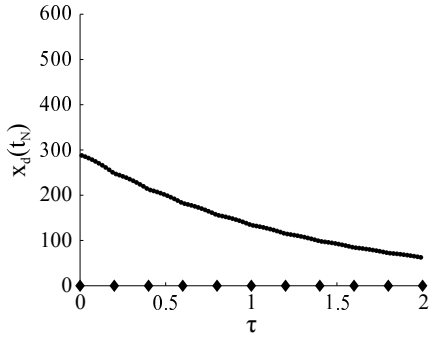

(a) The discrete trajectory's last point $x_N = x_d(t_N)$ as a function of the switching time τ. Black diamonds on the τ-axis mark the grid used for the integration.

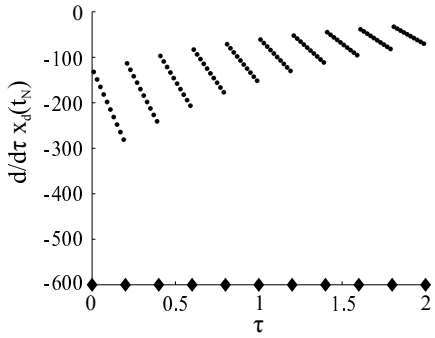

(b) The derivative of $x_N = x_d(t_N)$ shows jumps whenever the switching time τ coincides with one of the time grid points.

Figure 6.11: The last point of the discrete switched trajectory of Example 6.51 and its derivative w.r.t. the switching time τ.

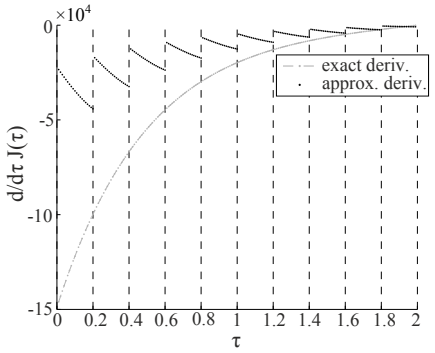

(a) The discrete cost function derivative, the dashed lines illustrate the discrete time grid ($h = 0.2$).

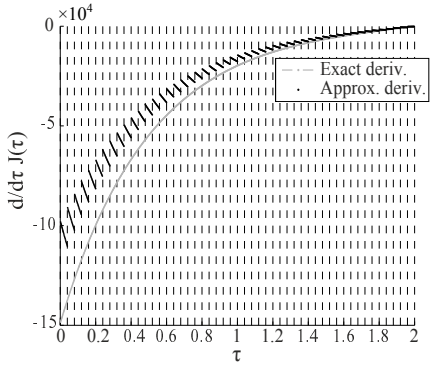

(b) Reducing the grid width, such that $t_k = k \cdot 0.04$, the jumps at the nonsmooth points of the discrete derivative $J_d{}'(\tau)$ get smaller and the discrete derivative approaches the exact derivative.

Figure 6.12: The discrete cost function derivative (black) of Example 6.51 shows nondifferentiability at discrete time points.

problems: the optimum lies on a nonsmooth point and thus, the (smooth) necessary optimality condition $J'(\tau^*) = 0$ does not hold. We consider the switched linear

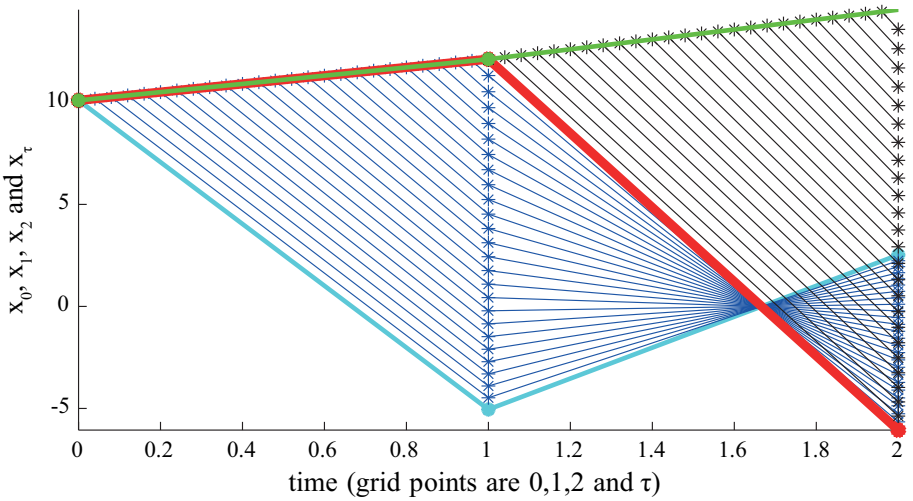

Figure 6.13: Trajectories for varying $\tau \in [0, 2]$ for Example 6.52. The first trajectory for $\tau = 0$ is plotted in cyan, the following ones in blue, the trajectory corresponding to $\tau = 1$ in red (note that this one gives the minimal value for x_{N+1}). Trajectories for $\tau > 1$ are plotted in black except for the last one ($\tau = 2$) which is green.

system

$$\dot{x} = \begin{cases} Ax & t \leq \tau \\ Bx & t > \tau \end{cases}$$

with $A = 0.2$ and $B = -1.5$ and initial point $x_0 = 10.1$. A rough discretization of the time interval $[0, 2]$ is taken by $\Delta t = \{0, 1, 2\}$. For the cost function, only a final point cost is considered, such that Equation (6.28) reduces to $J_d(\tau) = \Psi_N(x_N(\tau))$.

The discrete trajectory $x_d = \{x_0, x_1, x_2\}$ together with x_τ at the switching point is generated by an explicit Euler scheme, cf. Figure 6.13 for exemplary trajectories. In Figure 6.14, only the final point of the trajectory $x_N(\tau)$ is shown as a function of τ. Its minimum is at $\tau = t_1 = 1$.

Now, we choose the final cost function $\Psi_N(x) = (x + 10)^2$ which is smooth and convex, but its extremum at $x = -10$ is not in the image of $x_N(\tau)$ for $\tau \in [0, 2]$ (see Figure 6.14). The resulting $J_d(\tau)$ is given in Figure 6.15. Obviously, it has a minimum in $\tau^* = 1$ but this is also a kink in the graph, so $J_d'(\tau^*) = 0$ does not hold. Thus, in this example, the requirements of Lemma 6.47 do not hold. However, the nonsmooth optimality condition does hold: zero (interpreted as a horizontal straight line supporting the graph of $J_d(\tau)$ in $\tau = \tau^*$) is in the subgradient of $J_d(1.0)$.

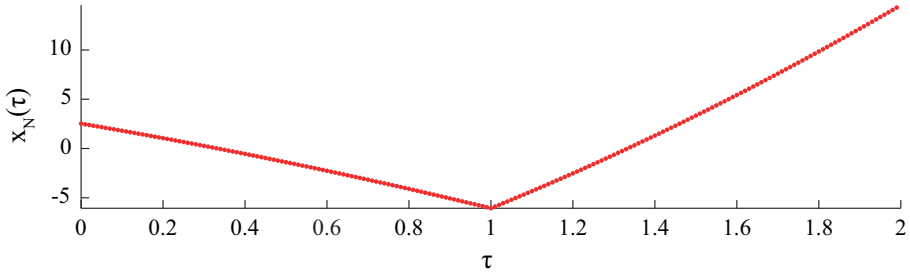

Figure 6.14: The final point of the discrete trajectory, x_N, plotted as a function of τ for $\tau \in [0, 2]$, is nonsmooth at the grid point $\tau = 1$.

We apply Algorithm 6.50 with the simple choice of step sizes, $s_k = 1/(k+1)$ and choose tolerances $\text{tol}_g = \text{tol}_\tau = 5 \cdot 10^{-4}$. Starting with $\tau^{(0)} = 1.7$, the algorithm terminates after almost 2000 steps because the change in $\tau^{(k)}$ is less than tol_τ. The best, i.e. minimal $J_d^{(k)}$ has already occurred at step 981. This example shows the bad convergence of this simple algorithm (also cf. Figure 6.15) and the need for improvement, especially in step size control. Assuming we knew the optimal value of J, the optimal step size strategy (Equation (6.39)) needs only six steps to find the optimal switching time.

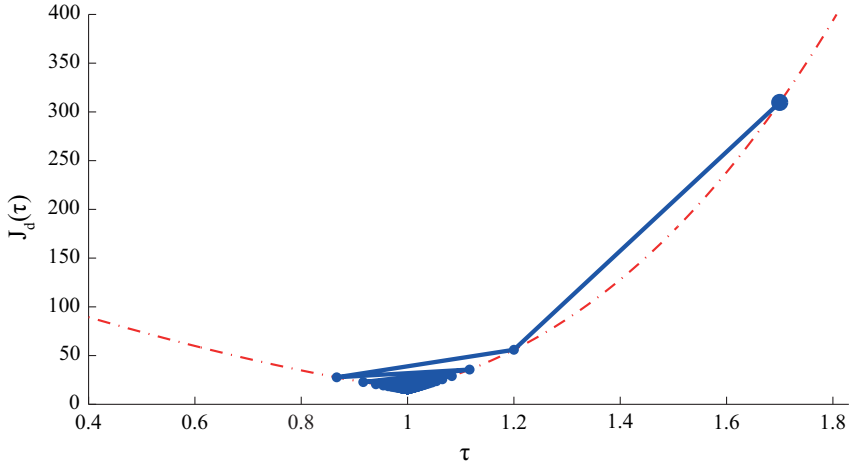

Figure 6.15: $J_d = \Psi(x_N(\tau))$ (dashed red) has a nonsmooth point at the optimum. Algorithm 6.50 converges to the optimum but shows, as expected, a slow convergence with $\tau^{(0)} = 1.7$ and $\text{tol}_\tau = 5 \cdot 10^{-4}$.

Example 6.53 (Switched Double Pendulum)**:** The model of the double pendulum consists of two mass points m_1, m_2 on massless rods of length l_1, l_2. The motion of the pendulum's arms are described by the two angles φ_1 and φ_2 (cf. Figure 6.16). The standard double pendulum is turned into a hybrid system by introducing two different modes:

M1: The outer pendulum is locked w.r.t. the inner pendulum with a fixed relative angle θ (cf. Figure 6.16), i.e. the system behaves like a single pendulum with a special shape dependent inertia tensor.

M2: Both arms can move freely, thus we have the normal two-degree-of-freedom double pendulum system.

The continuous time dynamics of the double pendulum can be derived by the Euler-Lagrange equations for *Lagrangian* $L_i(q,\dot{q}) = K_i(q,\dot{q}) - V_i(q,\dot{q})$ $(i = 1, 2)$. In M1, the following energy terms for the kinetic energy K_1 and potential energy V_1 are valid:

$$K_1(\varphi_1, \dot{\varphi}_1) = \frac{1}{2}(m_1 l_1^2 + m_2 r^2) \cdot \dot{\varphi}_1^2,$$
$$V_1(\varphi_1) = (m_1 + m_2) g l_1 \cos(\varphi_1) + m_2 g l_2 \cos(\varphi_1 + \theta - \pi)$$

with distance r of the outer mass to the origin $r^2 = l_1^2 + l_2^2 - 2 l_1 l_2 \cos(\theta)$. The position of the outer mass can be updated according to $\varphi_2 = \varphi_1 + \theta - \pi$ and it naturally follows that $\dot{\varphi}_1 = \dot{\varphi}_2$.

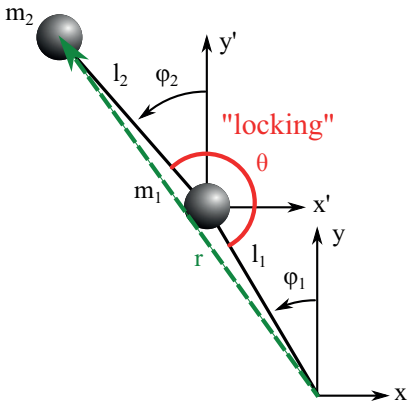

Figure 6.16: Sketch of the locked double pendulum. In the locked mode, the outer joint at mass point m_1 is locked to a fixed angle θ, such that the double pendulum is constrained to a one-degree-of-freedom system.

In M2, the system is defined by the Lagrangian $L_2 = K_2 - V_2$ where

$$K_2(\varphi_1, \varphi_2, \dot{\varphi}_1, \dot{\varphi}_2) = \frac{1}{2} \begin{pmatrix} \dot{\varphi}_1 \\ \dot{\varphi}_2 \end{pmatrix}^T M(\varphi_1, \varphi_2) \begin{pmatrix} \dot{\varphi}_1 \\ \dot{\varphi}_2 \end{pmatrix} \text{ with}$$

$$M(\varphi_1, \varphi_2) = \begin{pmatrix} (m_1 + m_2) l_1^2 & m_2 l_1 l_2 \cos(\varphi_1 - \varphi_2) \\ m_2 l_1 l_2 \cos(\varphi_1 - \varphi_2) & m_2 l_2^2 \end{pmatrix},$$

$$V_2(\varphi_1, \varphi_2) = m_1 g l_1 \cos(\varphi_1) + m_2 g (l_1 \cos(\varphi_1) + l_2 \cos(\varphi_2)).$$

We focus on the scenario that the system switches a single time from M1 to M2[12]. The velocities directly before and after the switch are the same then, $\dot{\varphi}_1^- = \dot{\varphi}_1^+ = \dot{\varphi}_2^+$, such that we have continuous state trajectories.

The cost function to be minimized is

$$J(\tau) = m(x(T)) = \left\| (\varphi_1(T),\, \varphi_2(T))^T - q_{\text{final}} \right\|^2,$$

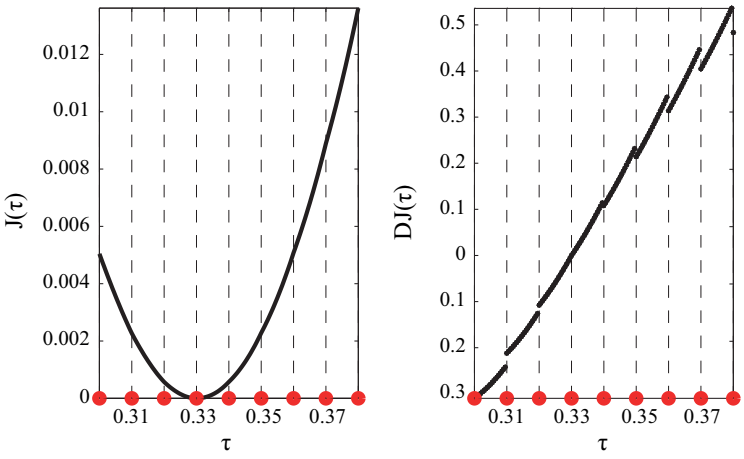

Figure 6.17: Cost function evaluations and its derivative for a switched trajectory of the pendulum: nondifferentiable points of J occur when τ coincides with a node of the discrete time grid (red dots). This is caused by the approximated trajectory, which is nondifferentiable w.r.t. τ at those points.

[12]Switching from the unconstrained mode M2 to the constrained case M1 would be modeled by jumps in the velocities (cf. Section 6.2) and thus, the system would not fall in the category of switched systems as introduced in the beginning. Contrarily, when switching from M1 to M2, one can check that for trivial resets of the velocity even the energies of M1 and M2 coincide in a switching point $x_\tau = (\varphi_1, \varphi_1 + \theta - \pi, \dot{\varphi}_1, \dot{\varphi}_1)$ and thus we have that the energy is conserved along the entire hybrid trajectory.

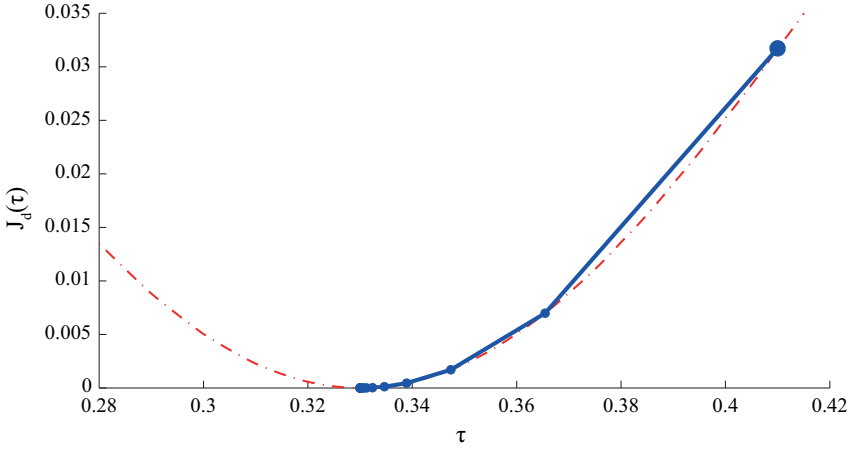

Figure 6.18: Steps of the subgradient algorithm applied to Example 6.53 with the optimal choice of step sizes and starting point $\tau^{(0)} = 0.41$.

with given final point $q_{\text{final}} = (-1.5487, -1.9733)$, which has been generated by the discretized trajectory for $\tau^* = 0.33$. Thus, this is the optimal switching time, as it can be also seen in Figure 6.17. First, we approximate the switching time derivative $J_d{}'(\tau)$ by evaluating the corresponding formula for $\frac{d}{d\tau}x_{i+1}$ and the appropriate discrete adjoints for varying τ. At grid points (except for the optimal τ), the left hand and right hand side derivatives do not coincide.

Due to the design of the cost function, we know that there is an attainable optimal solution and therefore, the optimal costs are known to be $J_d^* = 0$. Then, Algorithm 6.50 is applied with optimal step sizes, initial value $\tau^{(0)} = 0.41$, and tolerances $\text{tol}_\tau = 10^{-12}$, $\text{tol}_g = 10^{-8}$. The algorithm terminates after 27 steps with $\|DJ_d\| = 6.01 \cdot 10^{-9}$ and the optimal solution $\tau^* = 0.33$ up to machine precision (cf. Figure 6.18).

CHAPTER 7

Motion Planning and Hybrid Systems

In this chapter we study two links between the motion planning approach and the control framework for hybrid systems. Firstly, it is shown that the maneuver automaton can be transformed into a hybrid automaton and that the motion planning procedure is then similar to a two layer optimization (Section 7.1). Secondly, we extend the concept of trim primitives to hybrid mechanical systems and illustrate our definition with several spherical pendulum examples in Section 7.2. Finally, in Section 7.3, we extend one of the examples to a motion planning scenario and, by that, give an outlook to motion planning for arbitrary hybrid mechanical systems.

7.1 Motion Planning with Motion Primitives as a Hybrid System

The following proposition shows the ingredients of the hybrid automaton generated from a motion planning graph. Afterwards, some special properties of this automaton are presented.

Proposition 7.1: The maneuver automaton for a library of motion primitives for a mechanical system with controlled potential (cf. Section 5.2 and Section 5.3) can be transformed into a hybrid automaton.

Proof. Let TQ denote the mechanical system's state space, G be a symmetry group of the system and X_L^u be the controlled Lagrangian vector field corresponding to the Lagrangian L and a force $f : U \to T^*Q$ which can be summed up in a controlled Lagrangian with controlled potential V^u (cf. Section 5.3). The hybrid automaton for a given library of motion primitives can then be defined in the following way:

- $\Gamma = \Gamma_T \cup \Gamma_M$ denotes the finite number of motion primitives, where Γ_T indicates the trim primitives and Γ_M the maneuvers.

- $\mathcal{E} \subset (\Gamma_T \times \Gamma_M) \cup (\Gamma_M \times \Gamma_T)$ are the edges modeling the transitions (cf. Corollary 7.2(i)).

- Dropping the discrete component $\{i\}$ and defining the state space of the *clock state* by $\mathbb{T} = \mathbb{R}$, the domains are

$$D_i = \begin{cases} \{(q,v) \in TQ \,|\, (q,v,u_i) \text{ is a trim for fixed } u_i \in U\} \times \mathbb{T} & \text{for } i \in \Gamma_T, \\ TQ \times \mathbb{T} & \text{for } i \in \Gamma_M. \end{cases}$$

  Let $\xi_i \in \mathfrak{g}$ denote the generator for the trim (cf. Definition 5.6) for $i \in \Gamma_T$.

- The collection of vector fields is $(X_i, 1)$, with

$$X_i = \begin{cases} \xi_{TQ,i} : D_i \subset TQ \to T(TQ) & \text{for } i \in \Gamma_T, \\ X_L^u : TQ \to T(TQ) \text{ with } u : [0, t_{f,i}] \to U & \text{for } i \in \Gamma_M, \end{cases}$$

  where $\xi_{TQ,i}$ is the vector field of the infinitesimal generator ξ_i (cf. Definition A.18), which generates a solution of the mechanical subsystem with controlled Lagrangian L^{u_i}, i.e. controlled potential V^{u_i} (cf. Section 5.3).

- The guards are $G_i = D_i$ for $i \in \Gamma_T$ (i.e. switching is allowed in any point and at any time in trim states) and $G_i = \{(q,v,\tau) \in D_i \,|\, \tau = t_{f,i}\}$ for $i \in \Gamma_M$. (Recall that $t_{f,i}$ denoted the final time of a maneuver starting at time zero, e.g. in Definition 5.2.)

- The reset maps for all transitions $(i,j) \in \mathcal{E}$ are $R_{(i,j)} : D_i \to D_j$, $R_{(i,j)} = (\mathrm{id}_{TQ}, 0)$, i.e. the resets are trivial on the configurations and velocities but reset the clocks. By this, the clocks measure the duration which the system spends in one of the domains.

□

Here, we do not have to consider primitives on (un)stable manifolds separately, since it was shown in Section 5.5.1 that they form extended maneuvers which share the same properties as regular maneuvers. Thus, any maneuver state in the designed hybrid automaton may indeed be an extended maneuver which partly moves along a manifold orbit.

Automata which are constructed according to Proposition 7.1 are hybrid automata with special characteristics, as it is pointed out in the following.

Remark 7.2: The hybrid automaton generated from a motion primitives library has the following properties

(i) *Alternating modes:* For all discrete transitions $(i, j) \in \Gamma \times \Gamma$, it holds that either $i \in \Gamma_T$, $j \in \Gamma_M$ or $i \in \Gamma_M$, $j \in \Gamma_T$, thus, $\mathcal{E} \subset (\Gamma_T \times \Gamma_M) \cup (\Gamma_M \times \Gamma_T)$, i.e. the system switches alternately between trim and maneuver states. The system cannot switch continuously between trim primitives for disjoint Lie algebra elements. In principle, a concatenation of controlled maneuvers would be possible, but this contradicts the typical generation of a motion planning library.

(ii) *Input/output sets:* For a disjoint set of trims, a maneuver state has exactly one incoming edge and one outgoing edge connecting it to its preceding and its following trim. A trim state, contrarily, may have several incoming and outgoing edges, namely to all maneuvers which can be used alternatively.

(iii) *Dynamics in trim modes:* The dynamics in the trim modes are defined by the constant control value u_i and the infinitesimal generator ξ_i (cf. Section 5.3). Therefore, the state space is constrained to the trim primitives orbit. Since we assume the collection of maneuvers and trims to be a valid maneuver automaton, it is guaranteed that the transition from a maneuver into the trim state is possible.

(iv) *Dynamics in maneuver modes:* For all executions which visit a certain maneuver mode, the corresponding pieces of the execution always look the same up to a symmetry shift and a time shift, i.e. these parts of the executions are equivalent (cf. Definition 2.4). When generating an execution, the clock state of a maneuver mode can be used to obtain the correct time parametrization of the control trajectory.

(v) *Families of executions:* Let $(x, u) = (q, v, u) : [0, T] \to TQ \times U$ be an execution of the hybrid automaton for final time T with initial and final points in trim states. Let $\mathcal{T} = \{\tau_0 = 0, \tau_1, \tau_2, \ldots, \tau_{N-1}, \tau_N, \tau_{N+1} = T\}$ denote the switching times. Then, there exist valid executions of the hybrid automaton for switching times

$$\mathcal{T} = \{0 = \tau_0, \tau_1 + \beta_1, \tau_2, \tau_3 + \beta_3, \ldots, \tau_{N-1} + \beta_{N-1}, \tau_N, \tau_{N+1} + \beta_{N+1}\}$$

with any $\beta_{2i+1} \geq 0$, $i = 0, \ldots, N/2$, i.e. the durations of the trims may vary. Again, this is due to the symmetry of the system and the trim property. The sequence of visited discrete states remains valid if the times spent in the trim states are varied, because maneuvers are designed such that they can be started at any point on the trim orbit.

Note that, strictly speaking, the hybrid automaton for a motion primitives library cannot be categorized as a hybrid Lagrangian control system according to Definition 6.2, because of the restrictions on the domains and also due to the clock states. However, a corresponding Lagrangian for the system restricted to uncontrolled trim primitives, i.e. relative equilibria can be specified: This is the Routhian, introduced for a general setting by Marsden and Scheurle in [MS93] (cf. Sections 2.3.2 and 2.3.3).

As a part of this thesis, the motion planning library has been extended by motions on (un)stable manifolds to invariant objects of the uncontrolled dynamics (cf. Section 5.4). By the definition of extended maneuvers (Definition 5.12), which consists of a sequence "maneuver – piece of a manifold orbit – maneuver", they can be represented in the hybrid automaton, as well.

While in the maneuver automaton the maneuvers are modeled by edges and only the trim primitives form the vertices of the graph, in the hybrid automaton, both types of motion primitives form edges of the corresponding hybrid automaton's graph.

The interpretation of a maneuver automaton as a hybrid automaton is studied by Frazzoli as well, see [FDF00] and [Fra01]. However, the hybrid automaton definition substantially differs from the one we use. Most importantly, in [Fra01], the maneuvers are modeled as edges and not as vertices. For us, it is necessary to adjust the definition of the maneuver automaton and consider the maneuvers as vertices since in our definition of hybrid time (Definition 6.2), transitions in state space are assumed to happen in zero physical time. In contrast, in [FDF00] and [Fra01], an interpretation of hybrid time is assumed that allows transitions to consume physical time, in this case, the fixed duration of a controlled maneuver.

Motion Planning as a Two Layer Optimal Control Problem Now, we study the relation between the motion planning approach, which has been developed in Chapter 5 and the two layer optimal control problem for hybrid systems. It is shown that a motion planning problem based on a motion primitives library with trims and optimally controlled maneuvers is a special kind of a two layer optimal control problem. However, there are differences in the optimization procedure, as we point out below.

To begin with, we reconsider the design of a motion planning library. Therefore, assume a set Γ_T of trim primitives to be given. Let c_i denote the unit costs corresponding to trim state $i \in \Gamma_T$ and define $\mathcal{E}$ by choosing for which trim states there should be an incoming and/or an outgoing transition to a maneuver state. This also defines the number of maneuver states labeled by Γ_M. Then a cost function $C(q(t), v(t), u(t))$ for the maneuvers has to be chosen.

For each $i \in \Gamma_M$, for which there should be transitions (j, i) and (i, k) with trim states i and k, define the control trajectories $u : [0, t_{f,i}] \to U$ for all $i \in \Gamma_M$ to be

the solution of the optimal control problem

$$\min_{q,u,(t_{f,i})} J_i(q,u) = \int_0^{t_{f,i}} C(q(t),\dot{q}(t),u(t))\,dt \tag{7.1}$$

$$\text{w.r.t. } \frac{d}{dt}\frac{\partial L}{\partial \dot{q}} - \frac{\partial L}{\partial q} = f(q,\dot{q},u) \tag{7.2}$$

$$(q(0),\dot{q}(0)) = a_i,\ (q(0),\dot{q}(0)) = b_i, \tag{7.3}$$

with $a_i \in D_j$, and $b_i \in D_k$ fixed. This is an ordinary optimal control problem as considered in the lower layer of the two layer formulation in Problem 6.30 and it is equivalent to the optimal control problem defined for optimal maneuvers in Section 5.5.2 with fixed boundary values on trims. Because of the symmetry, if a maneuver connecting a_λ and b_λ is computed, the same control trajectory can be used for a maneuver connecting $\Phi_g^{TQ}(a_\lambda)$ and $\Phi_g^{TQ}(b_\lambda)$ for any $g \in G$ (cf. the definition of equivalent trajectories in Definition 2.4).

Together with the maneuver states, the motion planning library and the corresponding hybrid automaton for the motion planning problem are complete. Now, fix initial and final states $x^0 = (q^0, \dot{q}^0)$, $x^T = (q^T, \dot{q}^T)$ on trim primitives. We search for the optimal solution of the motion planning problem for a fixed number of motion primitives, N ($\Lambda = \{0,\dots,N\}$), and a fixed sequence γ connecting the initial and final trim. This gives a fixed finite path in the hybrid automaton's graph. Let $\mathcal{I} = \{I_\lambda\}_{\lambda\in\Lambda}$, $I_\lambda = [\tau_\lambda, \tau_{\lambda+1}]$, $\tau_0 = 0$, $\tau_{N+1} = T$ denote the hybrid interval.

Then, the original[1] motion planning problem 5.5 simplifies to

Problem 7.3:

$$\min_{\mathcal{T},(\mathcal{A},\mathcal{B})} J = \sum_{\lambda\in\{1,3,\dots,N-1\}} J_{\gamma(\lambda)} + \sum_{\lambda\in\{0,2,\dots,N\}} c_{\gamma(\lambda)}(\tau_{\lambda+1} - \tau_\lambda)$$

$$\text{w.r.t. } \tau_0 = 0,\ \tau_{N+1} = T,$$

$$\tau_{\lambda+1} - \tau_\lambda \geq 0,\ \forall\lambda = 0,\dots,N,$$

$$a_0 = x^0,\ b_{N+1} = x^T,$$

$$a_\lambda \in D_{\gamma(\lambda-1)},\ b_\lambda \in D_{\gamma(\lambda+1)},\ \text{for } \lambda \in \{1,3,\dots,N-1\} \text{ (maneuvers)}, \tag{7.4}$$

$$b_\lambda = \exp(\tau_\lambda \xi_{\gamma(\lambda)}, a_\lambda),\ \text{for } \lambda \in \{0,2,\dots,N\} \text{ (trims)}, \tag{7.5}$$

$$a_{\lambda+1} = b_\lambda,\ \text{for } \lambda \in \{0,1,\dots,N-1\}, \tag{7.6}$$

[1] We adjust the notation to match the hybrid system setting, e.g. the coasting times of the trim trajectories are given by the difference of the switching times, $\tau_{\lambda+1} - \tau_\lambda$, and we replaced the independent labeling of maneuvers and trims by one global labeling by means of the switching sequence.

where for $\lambda \in \{1, 3, \ldots, N-1\}$, $J_{\gamma(\lambda)}$ are the costs of a maneuver from a_λ to b_λ.

Because of the auxiliary variables $\mathcal{A}, \mathcal{B}$, the condition for the group displacements (Equation (5.5)) in the original Problem 5.5 are implicitly satisfied since the final point of the hybrid trajectory $x(\tau_{N+1})$ can only meet the desired final state if, in particular, the product of all group displacements (cf. Section 5.2, p. 94) matches the group displacement defined by x^0 and x^T, which was denoted by $g_0^{-1} g_f$.

Problem 7.3 resembles the two layer problem (Problem 6.31), when interpreting Equations (7.4) and (7.5) as the guard conditions and Equation (7.6) as the (trivial) reset condition. In fact, the motion planning problem for a fixed sequence of modes is a simplified upper layer problem since for all trim parts of the hybrid trajectory ($\lambda \in \{0, 2, \ldots, N\}$), the final point b_λ automatically results from the initial point a_λ and time τ_λ. Together with the trivial reset conditions and the fixed maneuvers, only the switching times remain as free optimization variables. From the point of view of the hybrid automaton, in the trim states, only the duration (i.e. the clock state) can be controlled.

Thus, the motion planning with primitives approach has, in principle, the same two layers of optimization problems as our approach for hybrid optimal control. However, a fundamental difference lies in the optimization procedure. While the two layer optimization for hybrid control alternately switches between solving the upper and the lower layer problems, in the motion planning procedure, there is a strict hierarchy: to generate the maneuvers, the corresponding optimal control problems are solved only once and from then on, they are considered to be fixed in the sequence optimization. Another difference is the applicability: while the hybrid two layer formulation is designed to solve one specific hybrid optimal control problem, the motion planning approach in general (for a not predefined mode sequence) provides a bigger library of motion primitives which can be used for any planning problem between trim states in the automaton.

7.2 Hybrid Trim Primitives

In the previous section, we considered the maneuver automaton as a hybrid system that has been derived from an underlying ordinary continuous-time system. In contrast to that, we can also ask if the motion planning with primitives approach is extendable to a dynamical systems with inherent hybrid dynamics. Hybrid optimal control maneuvers can be computed by means of the two layer formulation from Section 6.3.1. Thus, we now study the existence of trim primitives in hybrid dynamics under specified assumptions on the symmetry of a hybrid system.

Definition 7.4 (Joint Symmetry)**:** Let $\mathcal{H}$ be a hybrid Lagrangian control system

with Lagrangian $L_1, \ldots, L_N$ for the N discrete states, $\Gamma = \{1, \ldots, N\}$. Then, G is called a *joint symmetry* of $\mathcal{H}$, if $L_1, \ldots, L_N$ are all invariant w.r.t. the lift of the left action, Φ_g^{TQ}, for all $g \in G$, i.e. G is a symmetry for all subsystems.

For simplicity, we restrict to a hybrid Lagrangian control system $\mathcal{H}$ (cf. Definition 6.6) with only two discrete states, labeled by $\Gamma = \{1, 2\}$ in the following. We further assume that there are guards $G_{(1,2)}$ and $G_{(2,1)}$ that *enforce* switching between the discrete states. The corresponding reset maps are assumed to act trivially on $x = (q, v) \in TQ$. Without loss of generality, all executions are supposed to start in subsystem 1.

Definition 7.5 (Hybrid Trim)**:** Let $\mathcal{H}$ be a hybrid Lagrangian control system with two discrete states and let G be a joint symmetry. (x_1, u_1), $x_1 = (q_1, v_1) \in D_1$, $u_1 \in U$ is called a *hybrid trim*, if the following holds

- (x_1, u_1) is a trim for subsystem 1 according to the ordinary Definition 5.6, i.e. $X_{L_1}^{u_1}(x_1) = T_{x_1}(G \cdot x_1)$. The corresponding Lie algebra element is denoted by $\xi_1 \in \mathfrak{g}$.
- In case there exists a parameter $t_1 \geq 0$ such that

  $$x_2 := \Phi^{TQ}(\exp(t_1\xi_1), (q_1, v_1)) \in G_{(1,2)},$$

  then there also exists a control $u_2 \in U$, such that (x_2, u_2) is a trim for subsystem 2. The corresponding Lie algebra element is denoted by ξ_2.
- If, additionally, there is a parameter $t_2 \geq t_1$ such that

  $$x_{21} := \Phi^{TQ}(\exp((t_2 - t_1)\xi_2), (q_2, v_2)) \in G_{(2,1)},$$

  then there exists some $t_{21} \geq t_2$ such that $\Phi^{TQ}(\exp((t_{21} - t_2)\xi_1), (q_{21}, v_{21})) = x_1$. In this case, (x_{21}, u_1) and (x_1, u_1) define the same trim in subsystem 1.

Corollary 7.6: Thus, we have defined a hybrid trim trajectory to be of one of the following types:

(1) The orbit which is generated by ξ_1 and u_1 and which starts in x_1 stays in D_1 for all times, i.e. $x_1(t) \notin G_{(1,2)} \, \forall t > 0$.

(2) The system switches once from mode 1 to mode 2 and stays in D_2 until the end of observation, i.e. the switching sequence is $\gamma = (1, 2)$. Thus, we have $x(t_1) \in G_{(1,2)}$, but $x(t) \notin G_{(2,1)} \, \forall t > t_1$.

(3) The system switches periodically, i.e. the switching sequence is $\gamma = \{1, 2, 1, 2, ...\}$. Thus, we have $x(t_1) \in G_{(1,2)}$, $x(t_2) \in G_{(2,1)}$, and for all $n \in \mathbb{N}$:

$$x(t_1 + n \cdot t_{21}) \in G_{(1,2)},\ x(t_2 + n \cdot t_{21}) \in G_{(2,1)}.$$

Definition 7.5 is quite restrictive in the sense that for discrete switching sequences with more than two switches, hybrid trims have to be periodic solutions. There might be reasonable extensions of the definition of hybrid trims, in particular when removing the trivial reset assumption as well. However, in this thesis we restrict to Definition 7.5 with trivial resets, since we want to preserve the typical trim property of constant (body fixed) velocities in the hybrid setting. The following lemma directly follows from the construction of the hybrid trim.

Lemma 7.7 (Characterization of Hybrid Trims of Type (3))**:** The tuple (x_1, u_1) with $x_1 \in D_1$ and the tuple (x_2, u_2) with $x_2 \in D_2$ belongs to the same hybrid trim of type (3), if

- (x_1, u_1) and (x_2, u_2) are ordinary trims for subsystems 1 and 2,
- $\exists\, t_1 \geq 0$, s.t. $\Phi^{TQ}(\exp(t_1\xi_1), (q_1, v_1)) \in G_{(1,2)}$ and $\exists\, \tilde{t}_2 \geq 0$, s.t. $\Phi^{TQ}(\exp(\tilde{t}_2\xi_2), (q_2, v_2)) \in G_{(2,1)}$, i.e. starting from either x_1 or x_2 on the corresponding trims, one reaches the guard after finite time[2],
- $\exists\, t_{12}, \tilde{t}_{21} \geq 0$ such that x_1 and x_2 are connected via the concatenation of the left actions with the two Lie algebra elements ξ_1 and ξ_2,

$$\Phi^{TQ}(\exp(t_{12}\xi_2), \Phi^{TQ}(\exp(t_1\xi_1), (q_1, v_1)) = x_2,$$
$$\Phi^{TQ}(\exp(\tilde{t}_{21}\xi_1), \Phi^{TQ}(\exp(\tilde{t}_2\xi_2), (q_2, v_2)) = x_1.$$

"Pick and Place" Scenario of a Simple Robot In the following examples, we study variants of the spherical pendulum system as highly simplified models of open chain jointed robots as used in production facilities, for instance and show that an idealized "pick and place" scenario of a robot is a hybrid trim. By a "pick and place" scenario we refer to a periodic motion of the robot, in which objects are picked up and put down at certain places. When these objects are of considerable weight compared to the robot's mass, they influence the system's dynamics. Thus, we have a hybrid mechanical system with two discrete modes, the unloaded and the loaded spherical pendulum.

[2]Note that $\tilde{t}_2$ here might not be the same as t_2 in Definition 7.5. Correspondingly, x_2 might differ from the x_2 from Definition 7.5 which corresponds to the switching time.

Example 7.8 (Hybrid Spherical Pendulum)**:** First, consider the classical spherical pendulum as introduced in Examples 2.6 and 2.10 with Lagrangian $L(\varphi, \dot{\theta}, \dot{\varphi}) = \frac{1}{2}mr^2(\dot{\varphi}^2 + \dot{\theta}^2 \sin^2(\varphi)) - mgr(\cos(\varphi)+1)$ (on state space TS^2) and relative equilibria, i.e. uncontrolled trims, given by solutions of

$$\dot{\theta}^2 = -\frac{g}{r\cos(\varphi)}. \tag{7.7}$$

Let subsystem 1 be the unloaded pendulum, given by the Lagrangian above, and subsystem 2 the loaded pendulum with an added mass $\tilde{m}$, such that the dynamics are given by the same Lagrangian with mass parameter $m + \tilde{m}$. The area, in which the pendulum picks up the load, namely the guard $G_{(1,2)}$ is given by $G_{(1,2)} = \{(\theta, \varphi) \in S^2 \,|\theta = \pi\}$ and the area in which the load is put down is chosen to be $G_{(2,1)} = \{(\theta, \varphi) \in S^2 \,|\theta = 0\}$. We idealize the pick up and put down actions as instantaneous effects in which the configurations and the velocities are continuous, that is we have trivial resets. Consider an arbitrary point $x_1 = (\theta_1, \varphi_1, \dot{\theta}_1, \dot{\varphi}_1)$ for mode 1 with $0 < \theta_1 \leq \pi$, $\pi/2 < \varphi_1 < \pi$, $\dot{\theta}_1 = \sqrt{-\frac{g}{r\cos(\varphi_1)}}$ and $\dot{\varphi}_1 = 0$, i.e. a relative equilibrium in the lower half sphere. A corresponding motion is constant in $(\varphi, \dot{\varphi})$ and has constant rotational velocity $\dot{\theta}$. A hybrid trajectory starting in $x_1 \in D_1$ reaches the guard $G_{(1,2)}$ at some time and then the Lagrangian is changed by the loaded mass. Since Equation (7.7), the constraint for uncontrolled trims, is independent of the mass parameter, the switching point x_2 gives an uncontrolled trim in subsystem 2, too. (However, the value of the conserved momentum $J = p_\theta = mr^2 \sin^2(\varphi)\dot{\theta}$ (cf. Example 2.6) is changed when switching from m to $m + \tilde{m}$.) To sum up, $(x_1, 0)$ is a hybrid trim of type (3), i.e. a horizontal rotation with periodical switches between loaded and unloaded phases.

Example 7.9 (Hybrid Locked Double Spherical Pendulum I)**:** The previous example becomes more interesting if we replace the pendulum which has its total mass concentrated at the end of the massless rod by a more complex structure. To this aim, we consider the double spherical pendulum, for which the outer joint has been locked in an outstretched position, cf. Figure 7.1.

This gives a single spherical pendulum with two degrees of freedom, but with the new Lagrangian

$$L(\varphi, \dot{\theta}, \dot{\varphi}) = \frac{1}{2}\Theta(\dot{\varphi}^2 + \dot{\theta}^2 \sin^2(\varphi)) - (m_1 l_1 + m_2(l_1 + l_2))g(\cos(\varphi) + 1),$$

with inertia $\Theta = m_1 l_1^2 + m_2(l_1 + l_2)^2$. Computing uncontrolled trims by finding the

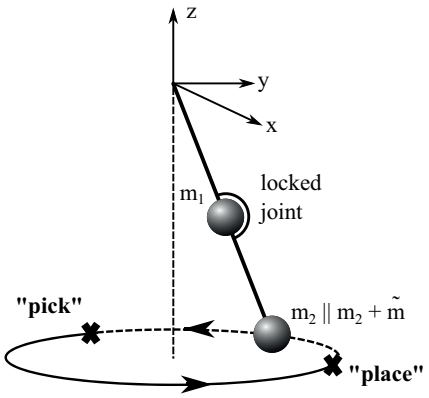

Figure 7.1: Sketch of the pick and place scenario for the locked stretched out double spherical pendulum.

zeros of the amended potential (cf. Section 2.3.3) leads to the condition

$$\dot{\theta}^2 = -\frac{(m_1 l_1 + m_2(l_1 + l_2))g}{\Theta \cos(\varphi)}. \tag{7.8}$$

Let the hybrid setting from the "pick and place" scenario be as before and the picked up load is modeled by increasing m_2. Now, if x_1 is a trim in the subsystem 1, $\dot{\theta}_1$ is *not* a solution to Equation (7.8), when m_2 is replaced by $m_2 + \tilde{m}$ with $\tilde{m} > 0$. However, when replacing the potential by a controlled potential, $V^u = V(\varphi) - \varphi \cdot u$ (cf. Section 5.3), $(x_1, 0)$ (zero control) is a hybrid trim, since u for subsystem 2 can be chosen as

$$\begin{aligned} u_2 = &- (m_1 l_1 + [m_2 + \tilde{m}]\,(l_1 + l_2))g \sin(\varphi_1) \\ &- (m_1 l_1^2 + [m_2 + \tilde{m}]\,(l_1 + l_2)^2) \sin(\varphi_1)\cos(\varphi_1)\dot{\theta}_1^2. \end{aligned}$$

Then, (x_2, u_2) (with arbitrary $\pi < \theta_2 < 2\pi$, $(\varphi_2, \dot{\theta}_2, \dot{\varphi}_2) = (\varphi_1, \dot{\theta}_1, \dot{\varphi}_1)$) is a trim in subsystem 2 and thus (cf. Lemma 7.7), $(x_1, 0, x_2, u_2)$ defines a hybrid trim of type (3). An example is depicted in Figure 7.2, for which the hybrid system (with $m_1 = 20\,\mathrm{kg}$, $m_2 = 8\,\mathrm{kg}$, $\tilde{m} = 4\,\mathrm{kg}$, $l_1 = 1\,\mathrm{m}$, $l_2 = 0.5\,\mathrm{m}$, $g = 9.81\,\mathrm{m/s^2}$) has been simulated with $\varphi_1 = \frac{3}{4}\pi$ and $\dot{\theta}_1 = 3.1416$. It can be observed that by the switching of the control $u(t)$, it is possible to keep the system in horizontal rotations with constant rotational velocity. However, the corresponding horizontal momentum, $p_\theta = \frac{\partial L}{\partial \dot{\theta}} = \Theta \sin^2(\varphi)\dot{\theta}$, which is the conserved quantity in each subsystem, inevitably switches its value at each discrete event.

Example 7.10 (Hybrid Locked Double Spherical Pendulum II)**:** To give an illus-

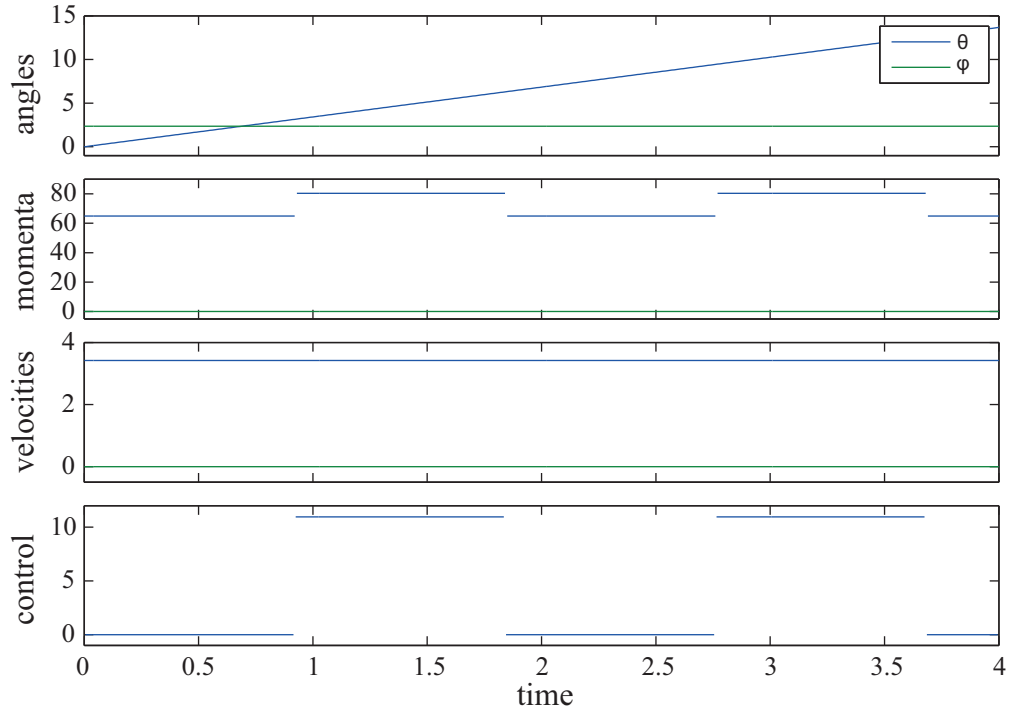

Figure 7.2: Example of a hybrid trim for the pick and place scenario for the locked stretched out double spherical pendulum.

tration of hybrid trims of type (1) and (2) as well, we replace the guards used in the previous examples by single points on the sphere. That is,

$$G_{(1,2)} = \left\{(\theta, \varphi) \in S^2 \,\middle|\, (\theta, \varphi) = \mathbf{a}_{12} \in S^2\right\}$$

with "pick up location" $\mathbf{a}_{12}$ and $G_{(2,1)}$ analogously with "put down location" $\mathbf{a}_{21} \in S^2$. If (x_1, u_1) is a trim for subsystem 1 (the unloaded locked double spherical pendulum), but for a hybrid trajectory starting in x_1, we have $x(t) \neq a_{12}$ for all $t > 0$, then (x_1, u_1) is a hybrid trim of type (1). If there exists a point $x_2 = x(t_2) = a_{12}$ on the hybrid trim trajectory starting in x_1, but no $t > t_2$ such that $x(t) = a_{21}$, the system switches once from mode 1 to mode 2 and, then, stays there until the end of observation. This is a hybrid trim of type (2). Hybrid trims of type (3) for this hybrid system can only exist if for $x_1 = (\theta_1, \varphi_1)$ it holds $\varphi_1 = a_{12,\varphi} = a_{21,\varphi}$, i.e. the guard points are at the same height and fit to the height of the specific trim in subsystem 1.

7.3 Hybrid Sequences of Motion Primitives

To conclude this chapter, the hybrid trim example for the locked outstretched double pendulum (cf. Section 7.2 and Example 7.9, in particular) is integrated into a sequence of motion primitives for the hybrid system of a two-link manipulator. By this, we also give an outlook how a fully hybrid motion planning software could be alike.

As in the classical setting presented in Chapter 5, the first step is the design of the motion primitives library. Here, only choosing trim primitives for each continuous subsystem individually does not exploit the full structure of a hybrid mechanical system. For example, hybrid trim primitives which switch between two discrete modes have been introduced in Section 7.2. It can be searched for such hybrid trim primitives in any admissible switching sequence of the hybrid automaton.

In the next step, controlled maneuvers have to be computed. To connect trim primitives of different discrete modes, these have to be hybrid maneuvers. As in the non-hybrid setting, extended maneuvers which partly follow an (un)stable manifold orbit can be designed; an example is shown below.

Then, the third step is to find an optimal sequence of motion primitives with respect to a specific planning problem for the hybrid system at hand. Practically, this means to formulate a large mixed-integer optimization problem, including the discrete variables originating from the choice of motion primitives and the graph structure of the hybrid automaton as well as the switching times as continuous variables. Also, the hybrid domains, the guard sets and the reset maps have to be considered as constraints in the hybrid planning problem. A concrete implementation and validation by appropriate mixed-integer nonlinear optimization methods is out of the scope of this thesis and left for future work. In a final example, we illustrate a hybrid sequence of motion primitives for an exemplary motion planning scenario.

Example 7.11 (Motion Planning Scenario for a Two-Link Robot)**:** On the grounds of the ordinary model of a double spherical pendulum, we consider a two-link robot with the following four discrete modes:

M1: fully actuated, unconstrained double spherical pendulum (4 degrees of freedom),

M2: folded, locked double pendulum (2 degrees of freedom),

M3: stretched out, locked double pendulum (2 degrees of freedom), and

M4: stretched out, locked double pendulum with additional load (2 degrees of freedom).

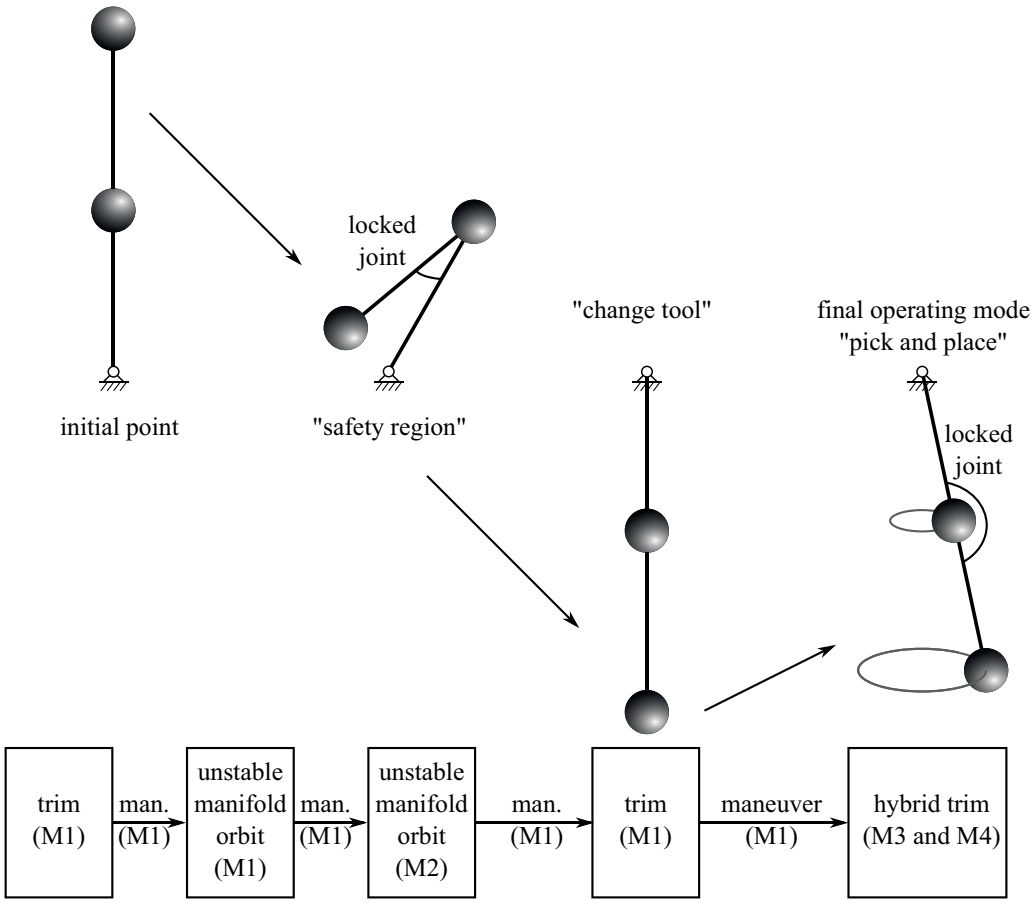

Figure 7.3: Sketch of the hybrid sequence for the motion planning scenario for a two-link robot.

Some of the modes are sketched in Figure 7.3. This example has also been shortly described in [FO12], the parameter values are chosen as listed in Example 7.9 above. For switches between the modes, the reset maps are trivial, i.e. a transition is continuous. Thus, a direct transition from mode 2 to mode 3, for instance, is not possible, the sequence has to visit mode 1 in between. The chosen planning scenario imposes further constraints on the switching sequence. It is depicted in Figure 7.3: the initial point is the up-up equilibrium, an intermediate point constraint is the down-down-equilibrium (motivated by a change of the robot's tool, for instance), and the final operating mode is a pick and place scenario, as illustrated in Example 7.9. Furthermore, for $\varphi_1 \in [\pi/4, \pi/2] \cup [-\pi/4, -\pi/2]$ a folding of the outer arm is required (e.g. to restrict the robot's operating range for safety reasons), i.e. the system has to transit this area while being in mode 2.

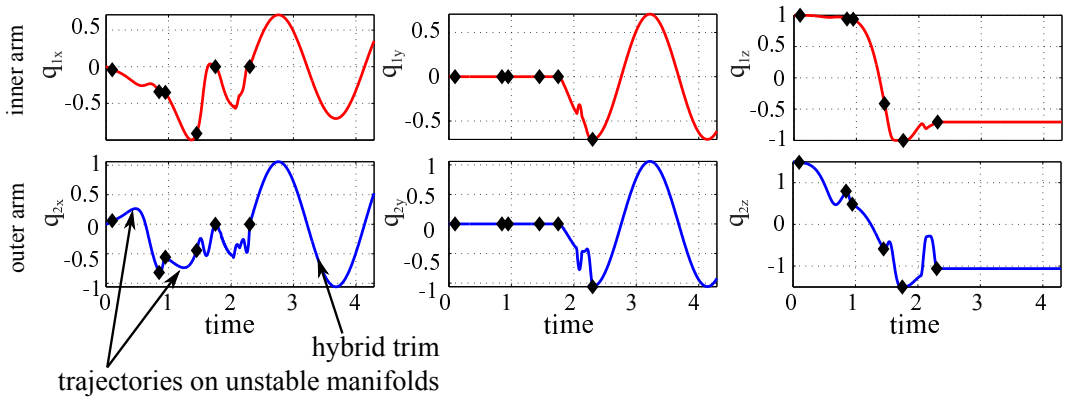

Figure 7.4: Results for the hybrid sequence as sketched in Figure 7.3: the motion of the two pendulum arms are shown in cartesian coordinates, switches between motion primitives are marked by black diamonds.

To exploit the natural dynamics of the continuous subsystems, two kinds of manifold orbits are chosen. One is along the two-dimensional unstable manifold of the up-up equilibrium of the double spherical pendulum (mode 1) restricted to planar motions (cf. Section 5.6.2) and the other one is along the one-dimensional unstable manifold of the upper equilibrium of the locked pendulum (mode 2), which resembles the unstable manifold of a classical planar mathematical pendulum (cf. Example 4.4).

The chosen approach for a solution sequence is also depicted in Figure 7.3 and a numerical result is shown[3] in Figure 7.4. Four controlled maneuvers are needed to connect the trims and the manifold orbits. They have been computed as energy optimal maneuvers in mode 1 while taking into account the constraints given by the "safety region" and the locking requirements of the outer joints in the optimal control problem. At this stage in the motion planning procedure, there opens up a number of different approaches to design alternative hybrid solution sequences, maybe even better ones with respect to energy efficiency or other objectives of interest. In Figure 7.4, it can be seen that for our choice of a sequence, only quite short maneuvers are needed to push the pendulum from its initial point onto the manifold orbit and to switch from the manifold orbit in mode 1 to the manifold orbit in mode 2. At $t = 2.3$, the robot has reached the final operating mode and starts the horizontal rotations with locked outer joint and with a periodic switching. In future

[3] Again, we show the configurations of the two pendulum arms in cartesian coordinates for an easier interpretation. As in Section 5.6.2, in the controlled maneuvers computed from an optimal control problem by the DMOC method, we observed a highly oscillatory behavior of the horizontal angles near the equilibrium points due to the singularities. Again, in future work, an alternative modeling as a DAE system should be taken into account.

work, a mixed-integer optimization problem could be formulated and solved in order to find the optimal sequence from a higher number of possible hybrid sequences.

CHAPTER 8

Conclusion and Outlook

In this thesis, we focus on methods for solving optimal control problems of mechanical systems. In the first part, a method has been developed that is based on hybrid control strategies for classical mechanical systems and in the second part, established ordinary optimal control methods have been extended to include hybrid dynamics of mechanical systems. It can be resumed that hybrid controls provide a control strategy that is beneficial for several reasons, in particular for exploiting inherent system properties, on which we comment in the following. Hybrid dynamics enrich the optimal control problem and require appropriate extensions of classical numerical methods. The methodologies of hybrid control strategies for ordinary mechanical systems on the one hand, and for optimal control of hybrid mechanical systems on the other hand show close relations, as it has been pointed out in the concluding comparison at the end of Chapter 7.

8.1 Optimal Control of Mechanical Systems

The optimal control of nonlinear dynamical systems such as mechanical systems is still a challenging task, even for modern numerical methods. The developments of this thesis are based on the optimal control method DMOC (cf. [OJM11]), which is a direct optimal control method based on discrete variational principles and nonlinear constraint optimization, and they have contributed to several recent improvements and extensions of the DMOC method and its implementation. The underlying idea for the first part of this thesis was to address some of the challenges of direct optimal control methods, in general, by the concept of hybrid control strategies. The term "hybrid control strategy" refers to a combination of several approaches, concepts, and techniques for the computation of controls which outperform solutions that result from the application of one method only. The motion planning with motion

primitives approach (cf. [FDF05]) provides a basic framework for this. Namely, contributions to the following aspects have been made by means of the extended motion planning methodology developed within this thesis.

Providing Initial Guesses Direct optimal control methods strongly rely on good initial guesses for the computation of globally relevant local optima. The motion planning method based on a library of motion primitives addresses this shortcoming in two respects. Searching for the optimal motion primitives sequence is a global (mainly combinatorial) optimization – in our simple search tree implementation as well as in the advanced graph based search algorithms proposed in [Fra01] and [Kob08]. Furthermore, the designed sequences of motion primitives can serve as sophisticated initial guesses, since they are even admissible solutions to the control problem. In particular, the uncontrolled pieces of the sequence (i.e. manifold orbits or uncontrolled trims) indicate the existence of energy optimal solutions nearby. By means of the post optimization, suboptimal transitions from one motion primitive to the next, which are caused by the finite representation of primitives in the library, can be smoothed out. Compared to an application of DMOC with a simple, e.g. linearly interpolated, initial guess, the post optimized sequences are often considerably cheaper solutions. This has been shown numerically for the simple spherical and the double spherical pendulum as well as for the double pendulum on a cart, which is based on a real test rig.

Exploiting Inherent System Properties for Energy Efficiency In control design, energy efficiency is an objective of primary importance. Thus, in space mission design, a straight-forward but very successful idea has been followed for several years now: whenever possible, the inherent, i.e. uncontrolled, dynamics of the system should be used to reduce the number of fuel-consuming control maneuvers. We brought this concept to general mechanical systems and modeled the concatenation of uncontrolled and controlled phases by sequences of motion primitives. Stable and unstable manifolds of invariant objects, equilibrium points, in particular, have been used to represent the systems' natural motions. It has been shown in this thesis that invariant manifold orbits can be formally included in the motion planning framework by defining so called extended maneuvers. Therefore, all properties of the maneuver automaton, e.g. controllability, takes over to the extended case. The numerical tests for the spherical pendula examples have revealed the benefit of manifold orbits in the computation of energy efficient maneuvers.

Exploiting Inherent Symmetry Properties The underlying idea of the motion primitives concept, namely symmetry, is a second crucial possibility of exploitation of inherent properties. Symmetry gives rise to the existence of relative equilibria, called

trim primitives. In this thesis, the trim primitives are formally integrated into the theoretical concept of symmetry in mechanical systems by introducing relative equilibria for Lagrangian with controlled potentials. Thereby, it has been possible to show that the Lagrangian symmetry reduction method can be used to compute trim primitives.

Reusability, Multiple Objectives, and Self-Optimization Symmetry is equivalent to invariances of dynamical systems and thus, it allows the reusability of control maneuvers. This property is the underlying idea of Frazzoli's maneuver automaton (cf. [FDF05]), which can be used to efficiently solve arbitrary planning problems once the automaton is designed. In this thesis, the maneuver automaton has been further extended by Pareto optimal maneuvers, which can be computed by multi-objective optimization techniques. It has then been shown that this is a suitable framework for the optimal control of so called self-optimizing systems (cf. [GRS09]). The generation of the maneuver automaton with the Pareto optimal maneuvers, which is computationally expensive, can be performed during the design phase of a mechanical or, more generally, a mechatronical system. During operation, when a control problem arises, one can then efficiently determine a solution sequence that is optimal w.r.t. the currently prioritized objectives.

8.2 Hybrid Optimal Control and Hybrid Systems

In the second part of this thesis, optimal control problems for mechanical systems with mixed continuous-time and discrete-time behavior are addressed. The following results have been achieved.

Hybrid Variational Principle In order to extend the DMOC principle to hybrid systems, we developed a hybrid variational principle for continuous and for discrete Lagrangian systems. Therefor, the Euler-Lagrange equations and the reset conditions had to be derived on an extended, infinite dimensional path space.

Optimal Control of Hybrid Systems An optimal control problem for a hybrid system consists of three types of optimization variables: the sequence of discrete modes, the switching times, and the continuous control inputs. For the continuous variables, we proposed to split up the problem into two layers. In the lower layer, there remain uncoupled ordinary optimal control problems, which can be solved by the DMOC method, i.e. transformed via the discrete variational principle and then addressed by sequential quadratic programming methods. In the upper layer, an optimization of the switching times and the transition values is required. We have

shown that for multiple objectives this can be performed by the set-oriented multiobjective optimization methods of GAIO and used a hybrid single-mass oscillator as an illustrating example.

Switching Time Problem In order to speed up the optimization, it is beneficial to use gradient-based techniques for the optimization of the switching time, as well. However, this requires differentiability not only of the continuous-time problem, but also of the time-discretized problem which results from applying integration schemes to the state equations. In this thesis, we studied the isolated switching time optimization problem for arbitrary integration schemes on fixed time grids. It was shown that, in general, the discrete problem becomes nondifferentiable, although in a very structured way, independent of the chosen integration scheme. As an alternative proof, this result was related to the well-studied situation of coinciding switching times. By means of discrete adjoint equations and a sub-gradient-based descent method a (nonsmooth) optimization method has been developed and applied to various academic examples.

Finally, the motion planning with primitives and the proposed hybrid optimal control framework have been compared. This revealed several equivalences of the approaches; the reason for that is the same underlying idea of hybrid behavior in terms of piecewise continuous motions interrupted by discrete events – for the controls only in the first approach and also for the states in the second approach.

Both methodologies could be combined for motion planning of hybrid systems by our definition of hybrid trim primitives. This leads over to interesting open problems, which have to be considered in future work.

8.3 Future Work

Interesting directions of future work, which would further extend the developments of this thesis, can be subsumed under the heading "discrete variations and optimal control for mechatronic systems". In the second part, we comment in particular on the challenges given by the hybrid nature of the corresponding mechanical subsystems.

Discrete Variations and Optimal Control for Mechatronic Systems The DMOC method has been exemplarily extended for the mechatronic system of a switched reluctance drive in this thesis and variational integrators for linear and nonlinear electric circuits have been studied in [OTC+13] and [Lin12]. However, for a holistic optimal control framework for arbitrary mechatronic systems, at least the following problems have to be fully resolved in future work. Because of logic devices, for instance, models of mechatronic systems have to include discrete switching behavior,

which has to be considered in a hybrid optimal control problem (cf. the following paragraph on this aspect). For complex mechanic subsystems, as well as for electrical circuits of mechatronic systems, it is often much simpler to derive *differential algebraic equations (DAE)* than a set of purely differential equations. DMOCC is an extension of DMOC for mechanical systems with holonomic constraints, e.g. multibody systems (cf. [LOMO10]). The idea of the DMOCC principle is to locally transform the constrained dynamics into ordinary differential or discrete, respectively, equations of motions by means of a projection matrix. As an alternative approach, the discrete variational calculus could be applied to the original DAE system. This leads to a higher dimensional optimization problem with more constraints, but the projection to a minimal set of coordinates can be omitted. The alternative procedure resembles a direct optimal control method for DAE systems as proposed by Gerdts, for instance (cf. [Ger12]). Interesting questions encompass analytical studies of the stability of the method as well as numerical tests and comparisons for application examples. First numerical experiments with our DMOC implementation showed, for instance, that imposing additional constraints on the discrete momenta improve the convergence of the optimization. Additional constraints of this type are known in the literature as stabilization constraints. A theoretical analysis of the DMOC discretization of DAE systems and the resulting optimization problem has not been done yet. It would also be interesting to analyze if system properties such as symplecticity, momentum conservation and a good long term energy behavior are preserved during discretization and optimization of the full DAE.

From the class of mechatronic systems, it is one step further to consider *multiphysics systems* or *cyber-physical systems*. There are numerous challenges in this field, so we focus on only one to which this thesis leads over, namely a discrete variational approach for the discretization of partial differential equations (PDE) in order to solve *PDE constrained optimal control problems*. PDE models arise e.g. for airflow and fluid dynamics as well as for flexible parts of multibody systems. Discretizations of models from different physical principles certainly require different time scales for an acceptable approximation, e.g. rigid body dynamics can be simulated on a much coarser time grid than highly flexible mechanical structures or electrical circuits. This results in a multirate integration scheme, for which a variational approach has been developed in [LO13]. A so called asynchronous variational integrator (as introduced in [LMOW03]) has been recently developed in [DGL$^+$13] for beam dynamics using different time steps for different beam elements. Thus, it would be quite interesting to examine a corresponding transformed optimal control problem of a multiphysics system, e.g. PDE constrained optimal control problem, and to search for efficient numerical solution methods.

A Holistic Discrete Variational Framework for Hybrid Mechanical Systems We see many interesting directions of future research given by the hybrid nature of many complex dynamical systems: cyber-physical systems in general and hybrid mechanical systems, in particular. Variational Integrators have shown a great applicability for various problems in the simulation and optimization of mechanical systems such that a development of a holistic framework for hybrid mechanical systems is very desirable and quite promising thanks to a number of recent results. For variational integrator simulations of conservative mechanical systems with constant step size, the modified energy (cf. e.g. [HLW06]) is a conserved quantity. Recent works for mechanical systems with impacts therefore replace the continuous-time energy constraint used in [FMOW03] by a constraint on the modified energy, cf. [BL07a, PM11]. A similar question arises in switching time optimization for mechanical systems: Can we construct a variational integration scheme that preserves the modified energy at the switch (or switches to the correct new value of the modified energy in case of energy changes) and does this approach approximate the true, continuous-time behavior over long time intervals of the switched system correctly? Applications for switching time optimization problems, in which the long-term energy behavior may become quite important, can be found in astrodynamics or dynamics of molecular systems.

Symmetry and induced momentum maps are not only properties that should be conserved in integration schemes, they can also be exploited to design efficient optimal control methods such as in the motion planning with primitives technique. At the end of this thesis, we extended the notion of trim primitives to hybrid mechanical systems with a joint symmetry. However, a hybrid system typically exhibits further discrete or mixed discrete-continuous symmetries (cf. e.g. [Hag12]), which are induced, for instance, by the non-static network topology of a coupled system. To design a planning method that combines local optimization methods for hybrid systems with global methods, it would be interesting to generalize the idea of motion primitives to discrete and mixed discrete-continuous symmetries.

Besides efficient, but accurate and even structure preserving optimal control methods for the continuous parts of a hybrid system, there is the combinatorial optimization problem given by the mode sequence or a sequence of motion primitives. A method for computing the optimal sequence of modes and switching times at the same time is the mode-insertion technique (cf. [CM12], also called single mode variation technique in [GVK$^+$10]). In [CM12] a projection-based variant of this method has been developed for the switching time optimization problem with continuous-time dynamics. It would be quite interesting to study the discrete-time analogue of this method in our framework for discretized switched systems, in particular w.r.t. differentiability.

In conclusion, in the simulation and optimal control of hybrid mechanical or mecha-

tronical systems, there are a number of open problems and interesting questions from the theoretical perspective as well as for numerical experiments which can be addressed based on the results of this thesis.

APPENDIX A

Differential Geometry

The following definitions and basic properties are mainly based on [MR99] if not stated otherwise.

Definition A.1 (Differentiable Manifold)**:** Let M be a set. A *chart* on M is a subset $U \subset M$ together with a bijective map $\phi : U \to \phi(U) \subset \mathbb{R}^n$. We call M a *differentiable n-manifold* if the following holds:

(i) The set M is covered by a collection of charts, i.e. every point is represented in at least one chart.

(ii) M has an *atlas*, i.e. it can be written as a union of *compatible* charts. Any two charts (U_1, ϕ_1) and (U_2, ϕ_2) such that $U_1 \cap U_2 \neq \emptyset$ are called compatible if $\phi_1(U_1 \cap U_2)$ and $\phi_2(U_1 \cap U_2)$ are open subsets of $\mathbb{R}^n$ and the overlap map $\phi_{12} := \phi_1 \circ (\phi_2)^{-1}|_{\phi_2(U_1 \cap U_2)} : \phi_2(U_1 \cap U_2) \to \phi_1(U_1 \cap U_2)$ is a C^∞ diffeomorphism.

Two atlases are called equivalent if their union is an atlas. The differentiable structure on M is given by the equivalence class of atlases on M ([AM87]). Denote $\phi(m) \in \mathbb{R}^n$ for some chart ϕ on $U \subset \mathbb{R}^n$ with $m \in U$ by $(x^1, \ldots, x^n)$, then the x^i are called the (local) coordinates of $m \in M$.

A *submanifold* of a manifold M is a subset $S \subset M$ with the property that for each $s \in S$ there is a chart (U, ϕ) in M which satisfies the submanifold property, i.e. $\phi : U \to \mathbb{R}^k \times \mathbb{R}^{n-k}$ and $\phi(U \cap S) = \phi(U) \cap (\mathbb{R}^k \times \{0\})$, where k is the dimension of the submanifold.

Two curves $t \mapsto c_1(t)$ and $t \mapsto c_2(t)$ in an n-manifold M are called equivalent at a point m if $c_1(0) = c_2(0) = m$ and $(\phi \circ c_1)'(0) = (\phi \circ c_2)'(0)$ in some chart ϕ. This definition is chart independent and defines an equivalence relation on the curves.

A *tangent vector* v to a manifold M at a point $m \in M$ is an equivalence class of curves at m.

It can be shown that the set of tangent vectors to M at m, denoted by T_mM and called the *tangent space* to M at m, is indeed a vector space.

Definition A.2 (Tangent Bundle)**:** The *tangent bundle* of M, denoted by TM, is the disjoint union of tangent spaces to M at the points $m \in M$, i.e.

$$TM = \bigcup_{m \in M} T_mM.$$

Thus, points of TM are tangent vectors to M at some point $m \in M$. If M is an n-manifold, i.e. every chart takes values in $\mathbb{R}^n$, then TM is a $2n$-manifold. Local coordinates on TM can be constructed in the following way. Assume $x^1, \ldots, x^n$ are local coordinates of $m \in M$ for some chart $\phi : U \subset M \to \mathbb{R}^n$. Let $v \in T_mM$ be a tangent vector with representative curve c. The components of v are given by $v^i = \frac{d}{dt}(\phi \circ c)^i|_{t=0}$, $i = 1, \ldots, n$. Then, $x^1, \ldots, x^n, v^1, \ldots, v^n$ give a local coordinate system on TM.

The *natural projection* is the map $\tau_m : TM \to M$ that takes a tangent vector $v \in T_mM$ to the point $m \in M$ at which the vector v is attached. The inverse image $\tau_m^{-1}(m)$, i.e. the tangent space T_mM, is called the *fiber* of the tanged bundle over the point $m \in M$.

Definition A.3 (Derivative)**:** Let $f : M \to N$ be a map of a manifold M to a manifold N. f is called *differentiable* (C^k, respectively), if in local coordinates on M and N, the map f is represented by differentiable (C^k, resp.) functions. The *derivative* at a point $m \in M$ is then defined to be the linear map

$$T_mf : T_mM \to T_mN.$$

That is for $v \in T_mM$,

$$T_mf \cdot v = \frac{d}{dt} f(c(t))|_{t=0},$$

i.e. the vector $T_mf \cdot v$ is the velocity vector at $t = 0$ of $f \circ c : \mathbb{R} \to N$ where for the curve c in M it holds that c is defined on an open neighborhood of 0, $c(0) = m$ and $dc/dt|_{t=0} = v$.

Definition A.4 (Vector Field, Integral Curve, Flow)**:** A *vector field* X on a manifold M is a map $X : M \to TM$ that assigns a vector $X(m)$ at $m \in M$. An *integral*

curve of X with initial condition m_0 at $t = 0$ is a differentiable map $c : (a, b) \to M$, such that the open interval (a, b) contains 0, $c(0) = m_0$ and $c'(t) = X(c(t))$ for all $t \in (a, b)$. The *flow* of X is the collection of maps $\phi_t : M \to M$ such that $t \mapsto \phi_t(m)$ is the integral curve of X with initial condition m.

If $f : M \to \mathbb{R}$ is a smooth function, by differentiating it at any point $m \in M$ we obtain the map $T_m f : T_m M \to T_{f(m)}\mathbb{R}$. The tangent space $T_{f(m)}\mathbb{R}$ can be identified by $\mathbb{R}$ itself. Thus, the map is an element of $T_m^* M$, the dual of the vector space $T_m M$.

Definition A.5 (Differential, Cotangent Bundle)**:** Let $f : M \to \mathbb{R}$ be a smooth function on a manifold M. The *differential* of f, denoted $\mathbf{d}f$, is given for any $m \in M$ by the linear map

$$\mathbf{d}f(m) : T_m M \to \mathbb{R},$$

so $\mathbf{d}f(m) \in T_m^* M$. For $v \in T_m M$, we call $\mathbf{d}f(m) \cdot v$ the *directional derivative*. In coordinates, that is (ϕ being a chart at m)

$$\mathbf{d}f(m) \cdot v = \sum_{i=1}^{n} \frac{\partial(f \circ \phi^{-1})}{\partial x^i} v^i.$$

The *cotangent bundle* $T^* M$ is obtained by replacing each vector space $T_m M$ by its dual $T_m^* M$.

The operators $\partial/\partial x^i$, $i = 1, \ldots, n$ form a basis of $T_m M$. Denoting the dual basis by dx^i, for this choice of local coordinates we get

$$\mathbf{d}f(x) = \frac{\partial f}{\partial x^i} dx^i.$$

Here and in the following, we will make use of the *summation convention*, i.e. we will drop the summation sign when there are repeated indices.

The linear maps of $T^* M$ are also called *one-forms*, since they map one single argument to $\mathbb{R}$. A *two-form* Ω on a manifold M is a function $\Omega(m) : T_m M \times T_m M \to \mathbb{R}$ that assigns to each point $m \in M$ a skew-symmetric bilinear form on $T_m M$. More generally we define a k-form as follows.

Definition A.6 (k-Form)**:** A *k-form* α (also called differential form) on a manifold M is a function $\alpha(m) : T_m M \times \cdots \times T_m M \to \mathbb{R}$ (there are k factors of $T_m M$) that assigns to each point $m \in M$ a skew-symmetric k-multilinear map on the tangent space $T_m M$.

Definition A.7 (Pull Back)**:** Let $\phi : M \to N$ be a C^∞ map from the manifold M to the manifold N and α be a k-form on N. The *pull-back* $\phi^*\alpha$ of α by ϕ is defined to be the k-form on M given by

$$(\phi^*\alpha)_m(v_1, \ldots, v_k) = \alpha_{\phi(m)}(T_m\phi \cdot v_1, \ldots, T_m\phi \cdot v_k).$$

If Y is a vector field on a manifold N and $\phi : M \to N$ is a diffeomorphism, the *pull-back* ϕ^*Y is a vector field on M defined by

$$(\phi^*Y)(m) = (T_m\phi^{-1} \circ Y \circ \phi)(m).$$

Definition A.8 (Interior Product)**:** Let α be a k-form on a manifold M and X a vector field. The *interior product* $\mathbf{i}_X\alpha$ (sometimes called the contraction of X and α) is the $(k-1)$-form defined by

$$(\mathbf{i}_X\alpha)_m(v_2, \ldots, v_k) = \alpha_m(X(m), v_2, \ldots, v_k).$$

Definition A.9 (Exterior Derivative)**:** The *exterior derivative* $\mathbf{d}\alpha$ of a k-form α on a manifold M is the $(k+1)$-form on M uniquely defined by the following properties

(i) If α is a 0-form, that is, $\alpha = f \in C^\infty(M)$, then $\mathbf{d}f$ is the differential of f (a one-form).

(ii) $\mathbf{d}\alpha$ is linear in α.

(iii) $\mathbf{d}\alpha$ satisfies the product rule, i.e. $\mathbf{d}(\alpha \wedge \beta) = \mathbf{d}\alpha \wedge \beta + (-1)^k\alpha \wedge \mathbf{d}\beta$, where α is a k-form, β an l-form and $\wedge$ denotes the wedge product (cf. [MR99] for details).

(iv) $\mathbf{d}^2 = 0$, that is, $\mathbf{d}(\mathbf{d}\alpha) = 0$ for any k-form α.

(v) $\mathbf{d}$ is a local operator, that is $\mathbf{d}\alpha(m)$ depends only on α restricted to any open neighborhood of m. If U is open in M, then $\mathbf{d}(\alpha|U) = (\mathbf{d}\alpha)|U$.

Definition A.10 (Cotangent Lift)**:** Given two manifolds M and N and a diffeomorphism $f : M \to N$, the *cotangent lift* $T^*f : T^*N \to T^*M$ of f is defined by

$$\langle T^*f(\alpha_s), v\rangle = \langle \alpha_s, (Tf \cdot v)\rangle,$$

where $\alpha_s \in T_s^*S$, $v \in T_qQ$, and $s = f(q)$.

Definition A.11 (Fiber-preserving Map)**:** A diffeomorphism $\phi : T^*S \to T^*M$ is a *fiber preserving map* if and only if $f \circ \pi_M = \pi_S \circ \phi^{-1}$ with $\pi_M : T^*M \to M$ and $\pi_S : T^*S \to S$ the canonical projections and where $f : M \to S$ is defined by $f = \phi^{-1}|M$.

For $\phi : T^*M \to T^*M$ being a fiber-preserving map over the identity, it holds $\mathrm{id} \circ \pi_M = \pi_M \circ \phi^{-1}$ and therefore $\pi_M \circ \phi = \pi_M$ ([Obe08]).

Definition A.12 (Lie Group)**:** A *Lie group* is a smooth manifold G that has a group structure consistent with the manifold structure in the sense that the group operations of multiplication, $\cdot : G \times G \to G$, $(g, h) \mapsto gh$, and inversion $^{-1} : G \to G$, $g \mapsto g^{-1}$ are C^∞ maps.

A group is *Abelian* if the group operation is commutative, i.e. if $gh = hg$ for all $g, h \in G$ ([BL04]). The *left translation map* of a group G is given by the map $L_g : G \to G$, $h \mapsto gh$.

Definition A.13 (Jacobi-Lie Bracket)**:** Let M be a smooth manifold, X, Y vector fields on M and f a real-valued smooth function. Then the derivation $f \mapsto X[Y[f]] - Y[X[f]]$, where $X[f] = \mathbf{d}f \cdot X$ determines a unique vector field, denoted by $[X, Y]$ and called the *Jacobi-Lie bracket* of X and Y.

$X[f] = \mathbf{d}f \cdot X$ is the *Lie derivative* of f along X, also denoted by $\mathcal{L}_X f$ and in coordinates given by $\mathcal{L}_X f = X^i \frac{\partial f}{\partial x^i}$.

Definition A.14 (Left Invariant Vector Field)**:** A vector field X on G is called *left invariant* if for every $g \in G$, $L_g^* X = X$, that is, if

$$(T_h L_g) X(h) = X(gh).$$

Recall that $L_g^* X$ is the pullback of the vector field X by the diffeomorphism L_g. For each $\xi \in T_e G$ (e denotes the identity element of G), a vector field X_ξ on G can be defined by $X_\xi(g) = T_e L_g(\xi)$. Then, X_ξ is left-invariant.

Definition A.15 (Lie Bracket, Lie Algebra of a Lie Group)**:** Define the *Lie bracket* in $T_e G$ by

$$[\xi, \eta] := [X_\xi, X_\eta](e),$$

where $\xi, \eta \in T_e G$ and where $[X_\xi, X_\eta]$ is the Jacobi-Lie bracket of vector fields. The vector space $T_e G$ with this Lie algebra structure is called the *Lie algebra* of G and

is denoted by $\mathfrak{g}$ or $Lie(G)$.

It can be shown that the vector space T_eG is isomorphic to the vector space of left-invariant vector fields on G. Thus, $(T_eG, [\cdot,\cdot])$ really defines a Lie algebra, i.e. the bracket is bilinear, antisymmetric and satisfies Jacobi's identity:

$$[[\xi,\eta],\zeta] + [[\zeta,\xi],\eta] + [[\eta,\zeta],\xi] = 0 \quad \text{for } \xi,\eta,\zeta \in T_eG.$$

If X_ξ is the left-invariant vector field corresponding to $\xi \in \mathfrak{g}$, there is a unique integral curve $\gamma_\xi : \mathbb{R} \to G$ of X_ξ, the *one-parameter subgroup*, starting at e, $\gamma_\xi(0) = e$ and $\gamma'_\xi(t) = X_\xi(\gamma_\xi(t))$.

Definition A.16 (Exponential Map)**:** The *exponential map* $\exp : \mathfrak{g} \to G$ is defined by $\exp(\xi) = \gamma_\xi(1)$.

Then, $\exp(s\xi) = \gamma_\xi(s)$, i.e. the exponential mapping maps the line $s\xi$ in $\mathfrak{g}$ onto the one-parameter subgroup $\gamma_\xi(s)$ of G, which is tangent to ξ at e. Further, all smooth one-parameter subgroups of G are of the form $\exp(t\xi)$ for some $\xi \in \mathfrak{g}$.

Definition A.17 (Action of a Lie Group)**:** Let M be a manifold and G a Lie group. A *(left) action* of G on M is a smooth mapping $\Phi : G \times M \to M$ such that

(i) $\Phi(e,x) = x$ for all $x \in M$,

(ii) $\Phi(g,\Phi(h,x)) = \Phi(gh,x)$ for all $g,h \in G$ and $x \in M$.

An action is said to be

- *effective* (or *faithful*) if $\Phi_g = \mathrm{id}_M$ implies $g = e$; i.e. $g \mapsto \Phi_g$ is one-to-one,
- *free* if it has no fixed points, that is, $\Phi_g(x) = x$ implies $g = e$ or, equivalently, if for each $x \in M$, $g \mapsto \Phi_g(x)$ is one-to-one, and
- *proper* if the map from $G \times M$ to $M \times M$ defined by $(g,q) \mapsto (q,\Phi_g(q))$ is proper (i.e. the inverse image of any compact set is compact).

For every $g \in G$, let $\Phi_g : M \to M$ be given by $x \mapsto \Phi(g,x)$. The *orbit* of x is defined by

$$\mathrm{Orb}(x) = \{\Phi_g(x) | g \in G\} \subset M.$$

For $x \in M$, the *isotropy group* of Φ at x is given by

$$G_x := \{g \in G | \Phi_g(x) = x\} \subset G.$$

An action is free, if and only if $G_x = \{e\}$ for all $x \in M$. Every free action is faithful.

Definition A.18 (Infinitesimal Generator)**:** Suppose $\Phi : G \times M \to M$ is an action on M. Let $\Phi^\xi : \mathbb{R} \times M \to M$ be the $\mathbb{R}$-action given by $\Phi^\xi(t, x) = \Phi(\exp(t\xi), x)$. Thus, $\Phi_{\exp(t\xi)} : M \to M$ is a flow on M. The *infinitesimal generator* defined as

$$\xi_M(x) = \frac{d}{dt} |_{t=0} \; \Phi_{\exp(t\xi)}(x)$$

is a vector field on M of the action corresponding to ξ.

It can be shown that the tangent space at x to an orbit $\mathrm{Orb}(x_0)$ is given by $T_x\mathrm{Orb}(x_0) = \{ \; \xi_M(x) | \xi \in \mathfrak{g}\}$. The Lie algebra of the isotropy group G_x for $x \in M$, called the isotropy algebra at x equals $\mathfrak{g}_x = \{\xi \in \mathfrak{g} | \xi_M(x) = 0\}$.

Definition A.19 (Symplectic Manifold)**:** A *symplectic manifold* is a pair (P, Ω) where P is a manifold and Ω is a closed, i.e. $\mathbf{d}\Omega = 0$, and (weakly) nondegenerate two-form on P. Ω is strongly nondegenerate, we speak of a strong symplectic manifold. This means, at each $z \in P$, the bilinear form $\Omega_z : T_zP \times T_zP \to \mathbb{R}$ is nondegenerate, i.e. Ω_z defines an isomorphism $\Omega_z^\flat : T_zP \to T_z^*P$, $\Omega^\flat(z_1)(z_2) = \Omega(z_1, z_2)$. In case of a weakly nondegenerate form, $\Omega^\flat$ is injective only.

Given a manifold M, the cotangent bundle T^*M (cf. Def. A.5) has a natural symplectic structure. For local coordinates $(x^1, \ldots, x^n)$ on M, $(dx^1, \ldots, dx^n)$ is a basis of T_x^*M, so any $\alpha \in T_x^*M$ can be written as $\alpha = p_i dx^i$. Thus, $(x^1, \ldots, x^n, p_1, \ldots, p_n)$ are local coordinates of T^*M and induce the canonical two-form $\Omega = dx^i \wedge dp_i$ which is symplectic.

A smooth left action Φ of G induces an equivalence relation on M whereby $x_1 \sim x_2$ if $x_1 = \Phi(g, x_2)$ for some $g \in G$. The orbit $\mathrm{Orb}(x)$ is the equivalence class $\{x_1 \in M | x_1 \sim x\}$. By M/G we denote the set of all orbits, i.e. the quotient space defined by this equivalence relation.

Definition A.20 (Principal Fiber Bundle, cf. [BL04])**:** A *C^∞-principal fiber bundle* is a quadruple (M, G, Φ, B) where M and B are manifolds, G is a Lie group, Φ is a smooth, free and proper left action of G on M, and $B = M/G$. We call M the *total space*, and B the *base space*.

Sometimes, the projection map $\pi : M \to M/G$ on a manifold M with (free and proper) Lie group G and corresponding Lie algebra $\mathfrak{g}$ is called the principal bundle [Blo03].

Definition A.21 (Principal Connection, cf. [Blo03])**:** A *principal connection* on the principal bundle $\pi : M \to M/G$ with G being a free and proper acting Lie group is a map (referred to as the *connection form*) $\mathcal{A} : TM \to \mathfrak{g}$ that is linear on each tangent space (i.e. $\mathcal{A}$ is a $\mathfrak{g}$-valued one-form) and it holds

(i) $\mathcal{A}(\xi_M(x)) = \xi$ for all $\xi \in \mathfrak{g}$ and $x \in M$, and

(ii) $\mathcal{A}$ is equivariant:
$$\mathcal{A}(T_x\Phi_g(v_x)) = \mathrm{Ad}_g\mathcal{A}(v_x)$$
for all $v_x \in T_xM$ and $g \in G$, where Φ_g denotes the given action of G on M and where Ad denotes the *adjoint action* of G on $\mathfrak{g}$, i.e. $\mathrm{Ad} : G \times \mathfrak{g} \to \mathfrak{g}$, $\mathrm{Ad}_g(\xi) = T_e(R_{g^{-1}} \circ L_g)\xi$.

The kernel $\ker T_x\pi$ of the derivative of π, that is the tangent space to the group orbit through $x \in M$ is called the *vertical space* of the bundle at the point m and is denoted by ver_x. The *horizontal space* of the connection at $x \in M$ is the linear space
$$\mathrm{hor}_x = \{v_x \in T_xM | \mathcal{A}(v_x) = 0\}.$$
Thus, at any point x the vector space T_xM can be decomposed: $T_xM = \mathrm{hor}_x \oplus \mathrm{ver}_x$. The same notation is used for the projections onto the vertical and horizontal space, i.e. for $v_x = \mathrm{hor}_x v_x + \mathrm{ver}_x v_x$. The projection onto the vertical part is defined by
$$\mathrm{ver}_x v_x = (\mathcal{A}(v_x))_M(x)$$
and the projection on the horizontal part is
$$\mathrm{hor}_x v_x = v_x - (\mathcal{A}(v_x))_M(x).$$

Definition A.22 (Variation, cf. [BL04])**:** Let $\gamma : [a, b] \to M$ be a C^2-curve. A *variation* of γ is a C^2-map $\sigma : I \times [a, b] \to M$ with the properties

(i) $I \subset \mathbb{R}$ is an interval for which $0 \in \mathrm{int}(I)$,

(ii) $\sigma(0, t) = \gamma(t)$,

(iii) $\sigma(s, a) = \gamma(a)$, and

(iv) $\sigma(s, b) = \gamma(b)$.

The *infinitesimal variation* associated with a variation σ is the vector field along γ given by
$$\delta\sigma(t) = \left.\frac{d}{ds}\right|_{s=0} \sigma(s, t) \in T_{\gamma(t)}M.$$

Sets of mappings between (finite dimensional) manifolds, e.g. path spaces on configuration manifolds Q of the form

$$\mathcal{C}([0,T],Q) = \{q : [0,T] \to Q \,|\, q \text{ is a } C^2 \text{ curve}\}$$

(cf. Section 2.1 or Lemma 6.10 in which the following result is applied) may form infinite dimensional manifolds modeled on Banach spaces. We refer to [Eel66, Mar74] for manifolds of C^k mappings ($k < \infty$) on Banach spaces or to the more recent reference [KM97] on smooth mappings on Fréchet spaces. These Banach spaces are constructed via so called *sections*.

Definition A.23 (Section)**:** Let Q be a finite dimensional manifold, $[0,T] \subset \mathbb{R}$ ($T > 0$) an interval and $c \in C^k([0,T],Q)$ ($k < \infty$) a C^k map from $[0,T]$ to Q. A *section of pullback bundles along* $c : [0,T] \to Q$ *over* Q, denoted by σ, is a map $\sigma : [0,T] \to c^*TQ$ satisfying $c^*\pi_Q \circ \sigma = \mathrm{id}_{[0,T]}$. The pullback vector bundle, denoted by c^*TQ, is defined by

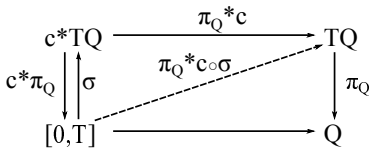

The sections can be identified with maps $[0,T] \to TQ$ via $\sigma \mapsto \pi_Q^* c \circ \sigma$ and they are therefore written as maps $\sigma : [0,T] \to TQ$ which satisfy $\pi_Q \circ \sigma = c$. The Banach space of sections of pullback bundles along c is denoted by $C^k([0,\tau] \leftarrow c^*TQ)$.

APPENDIX B

Further Numerical Methods

While the central numerical methods for this thesis are explained in the main part, this chapter is dedicated to further computational methods which were applied to the various applications throughout this work. These methods were available for the computations in this thesis ready-to-use or with minor modifications only. References are given in the corresponding sections.

B.1 Analysis of Invariant Objects in Dynamical Systems

Nonlinear dynamical systems typically exhibit a complex dynamical behavior, but important organizing structures of the global dynamics can be revealed by numerical techniques only. In this thesis, we focus on stable and unstable manifolds of hyperbolic critical objects, in particular, hyperbolic fixed points. In the last years, a number of different numerical approaches for the computation of (un)stable manifolds have been developed; for a good overview, we refer to [KOD+05]. In our numerical examples, we use the software package GAIO[1] (Global Analysis of Invariant Objects, cf. [DFJ01, DJ02]). GAIO provides a number of algorithms for the computation of invariant sets, such as global relative attractors, invariant manifolds and invariant measures. The basic idea is a quantization of the state space into small boxes. The invariant objects can then be approximated by box coverings with a prescribed accuracy. However, GAIO's performance does not depend on the dimension of the state space but only on the (often quite lower) dimension of the invariant object to approximate. In the following, we give a rough overview of the *continuation method*, namely the "gum" algorithm, for the computation of invariant (un)stable manifolds of fixed points.

[1] http://www2.math.uni-paderborn.de/ags/ag-dellnitz/software.html

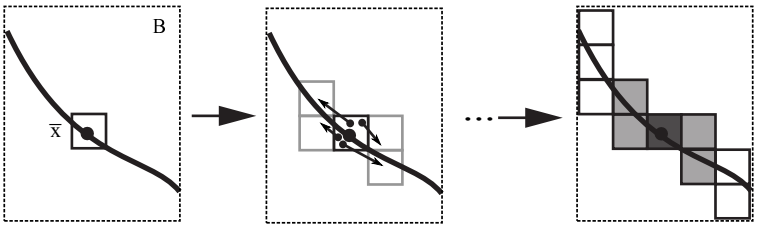

Figure B.1: Sketch of GAIO's continuation method for the computation of unstable manifolds.

B.1.1 Continuation Method

Recall the local stable manifold definition, $W^s_{loc}(\bar{x}) = \{x \in U \,|\, \Phi(x,t) \to \bar{x} \text{ for } t \to \infty \text{ and } \Phi(x,t) \in U \,\forall t \geq 0\}$ and that the global stable manifold can be governed by $W^s(\bar{x}) = \cup_{t \leq 0} \Phi(W^s_{loc}(\bar{x}), t)$. For the unstable manifold, analogous definitions exist for backward time ($t \leq 0$ and $t \to -\infty$). The (un)stable manifolds are invariant w.r.t. the system's flow (cf. e.g. [GH83]).

GAIO, as well as several other numerical tools for the computation of (un)stable manifolds, successively grow the manifold object from a local neighborhood of the equilibrium within a prescribed box B. Since the unstable manifold is the global attractor relative to B (cf. e.g. [DJ02]), convergence of the approximation to the part of the real unstable manifold is guaranteed. The stable manifold is equal to the unstable manifold of the time-reversed system. Therefore, it can be computed in the same way with integrations in backward time.

Figure B.1 roughly sketches the idea of the algorithm "gum" (cf. [DFJ01]). The algorithm starts with an initial box containing the fixed point. Test points of this box are mapped forward by a short time integration of the system's dynamics. Then, all boxes that are hit by one or more test points are filled with new test points for the next step of this continuation method. The algorithm terminates if the part of the unstable manifold in B is fully covered, i.e. no new boxes are hit by mapped test points, or if a finite number of continuation steps have been performed. The size of the boxes has to be chosen as a trade-off between accuracy of the box covering and computational effort. In the integrator, a higher order Runge-Kutta scheme can be used, for instance. Since only short-term integrations are performed during the algorithm, the method is highly robust w.r.t. numerical inaccuracies (e.g. drifts) that could be caused by long-term integrations.

Strong (un)stable manifolds can be computed with GAIO, as well. We shortly sketch the idea for the computation of strong stable manifolds. As a prerequisite, the original dynamical system has to be transformed. The aim is to shift its eigenvalue spectrum at the fixed point zero to the right until λ^{ss} is the last remaining eigenvalue on the left side of the complex plane. Then, GAIO can be applied to the transformed

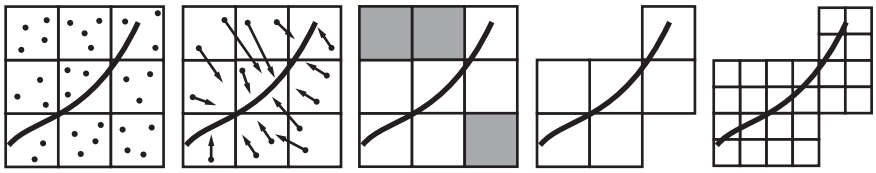

Figure B.2: Sketch of GAIO's subdivision method for the computation of attractors of dynamical systems and also Pareto sets.

system, which is non-autonomous now, and the resulting stable manifold can be transformed back, yielding an approximation of the strong stable manifold of the original system. For a study of invariant manifolds in non-autonomous systems, we refer to [ARS05, ARS06] and for an analysis of the set-oriented methods of GAIO for the computation of strong (un)stable manifolds to [Sch99].

B.1.2 Computation of Pareto Sets

A second method in the GAIO software-package – in fact, the more set-oriented technique in its underlying idea – is the *subdivision method*. Here, the algorithm starts with the prescribed box B and alternately switches between subdivisions of B and selection steps. In a selection step, test points in all active sub-boxes are generated and mapped under the flow. Only boxes which are hit by at least one of the test points are kept for further subdivision, all other are deleted, i.e. become inactive. By the subdivision steps, the box-covering of the manifold grow finer until a satisfying approximation of the invariant object is obtained.

In this thesis, the subdivision technique is used for the computation of a Pareto set. It is shown in [DSH05] that the Pareto set can be considered as the attractor of an artificial dynamical system, defined by the numerical iteration scheme from the necessary conditions for Pareto optimality (cf. also [SWOD13] for a recent overview on these set-oriented multiobjective optimization methods and applications). Then, the mapping in the selection step can be performed by a gradient step or simply, without any gradient information, by comparing the test point's objective values in the sampling algorithm variant (cf. [SWOD13]). For multiobjective optimization problems with a moderate number of optimization parameters, as e.g. the upper-layer problem for the hybrid single-mass oscillator (cf. Section 6.3.3), this subdivision technique has proved to be well applicable.

B.2 Multiobjective Optimal Control Problems

In Section 3.1.3, optimal control problems with multiple objectives have been shortly introduced and in Section 5.5.3, they are discussed in the context of motion planning

by maneuver automata. Here, we give an overview on how DMOC (cf. Section 3.3) can be extended to multiobjective problems as it has been presented in [ORZ12].

Consider a general optimal control problem as defined in Problem 3.1 with a vector valued cost functional. The discretization approach of DMOC transforms the original problem into a multiobjective optimization problem (MOP). We denote the vector of objectives by $J_d = (J_d^1, \dots, J_d^k)$ with the objectives $J_d^l : \mathbb{R}^{(N+1)n_q} \times \mathbb{R}^{Nn_u} \times \mathbb{R} \to \mathbb{R}$, $(q_d, u_d, T) \mapsto J_d^l(q_d, u_d, T)$ for $1 \leq l \leq k$. Here, n_q denotes the dimension of the configurations, n_u the dimensions of the controls, and $N+1$ is the number of grid points used in the DMOC discretization method. Recall that q_d denotes the discrete configuration trajectory, u_d the parametrized control trajectory and T the final time of the OCP, which is an additional optimization variable in free end time problems[2]. Analogous to Definition 3.4, a triple (q_d, u_d, T) is called *admissible* for the MOP, if it satisfies the constraints, i.e. the discrete Euler-Lagrange equations as well as discretized boundary and additional constraints. The triple (q_d, u_d, T) is *dominated* by another triple (q_d^*, u_d^*, T^*) if it holds for all components $l = 1, \dots, k$ of the objective vector that $J_d^l(q_d^*, u_d^*, T^*) \leq J_d^l(q_d, u_d, T)$, while the objective values are not identical, i.e. $J_d(q_d^*, u_d^*, T^*) \neq J_d(q_d, u_d, T)$. Finally, the triple (q_d^*, u_d^*, T^*) is *Pareto optimal* if there does not exist any other admissible solution triple that dominates (q_d^*, u_d^*, T^*). Again, the set of all optimal compromises, i.e. Pareto optimal solutions, is called the *Pareto set* and its image the *Pareto front* (cf. Figure B.3a).

Due to a large number of grid points, discretized multiobjective optimal control problems are typically high dimensional. Therefore, scalarization techniques have to be applied for the approximation of the Pareto front (see also [LHDV10], for instance). More precisely, in [ORZ12], a reference point technique is proposed based on so called target points. In Figure B.3a, the idea of the method is sketched. For a nonadmissible target point R, an auxiliary problem is stated, i.e.

$$
\begin{aligned}
&\min_{(q_d, u_d, T)} \|J_d(q_d, u_d, T) - R\| \\
\text{w.r.t. } & D_1 L_d(q_k, q_{k+1}) + D_2 L_d(q_{k-1}, q_k) + f_k^- + f_{k-1}^+ = 0, \quad k = 1, \dots, N-1, \\
& h_d(q_k, q_{k+1}, u_k) \geq 0, \quad k = 0, \dots, N-1, \\
& r_d((q_0, q_1, u_0), (q_{N-1}, q_N, u_{N-1})) = 0,
\end{aligned}
$$

(for the set of constraints, cf. to the basic optimal control problem 3.8). The auxiliary problem can be solved by any nonlinear constrained optimization technique, we refer to the discussion in Section 3.2.2. The crucial part of the scalarization method is the generation of targets. Here, different approaches exists, which mostly require that

[2] In practical implementations, if the final time T is free, the step size h is used as an optimization variable, instead. The advantage of varying h is that the number of discretization points can be kept constant. It is reasonable to restrict h by some h_{max}, i.e. $0 < h \leq h_{max}$, to not loose accuracy by using to big time steps.

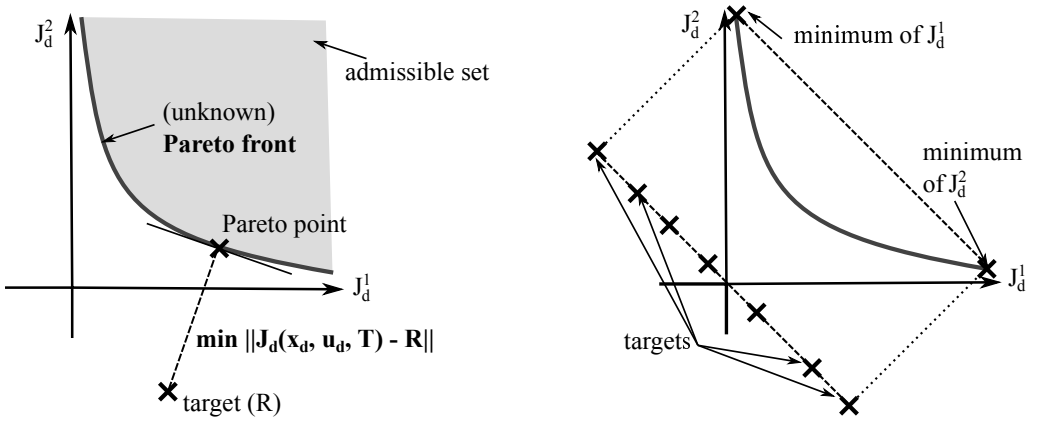

(a) Auxiliary problem for the reference point method.

(b) A heuristic approach for the generation of targets.

Figure B.3: Sketch of the reference point method for multiobjective optimal control problems: an auxiliary problem is stated by a non-admissible target point such that its solution yield a new Pareto point.

some Pareto points, e.g. the minima of the individual objectives, are already known. Then, targets can be generated nearby such that locally nearby Pareto points are computed. For the application in Section 5.6.3, we choose targets as depicted in Figure B.3b. The set of targets on a line is supposed to yield widely spread Pareto points rather than a very fine approximation of (parts of) the Pareto front. However, this cannot be guaranteed by the choice of targets only and depends on the actual problem. In the implementation of the method, as described in [ORZ12], the solution of the previously computed Pareto point is used as an initial guess for the following auxiliary problem with the neighboring target.

APPENDIX C

Modeling Details

C.1 The Planar Double Pendulum Models

Here, the modeling parameters and Euler-Lagrange equations for the double pendula models used in Section 4.3 are given.

C.1.1 Double Pendulum with Torque Control

We consider the two pendulum arms as rigid bodies of length l_1 and l_2 with mass and inertia m_1, J_1 and m_2, J_2, respectively. The inner arm is mounted to the ground by a joint, cf. Figure C.1a. All parameter values are given in Table C.1. The double pendulum exhibits two degrees of freedom and we choose the angles φ_1 and φ_2 as a minimal set of coordinates. The system's Lagrangian is given by

$$\begin{aligned} L(\varphi_1, \varphi_2, \dot{\varphi}_1, \dot{\varphi}_2) = &\begin{pmatrix} \dot{\varphi}_1 \\ \dot{\varphi}_2 \end{pmatrix}^T \cdot \begin{pmatrix} J_1 + a_1^2 m_1 + l_1^2 m_2 & a_2 l_1 m_2 \cos(\varphi_1 - \varphi_2) \\ a_2 l_1 m_2 \cos(\varphi_1 - \varphi_2) & J_2 + a_2^2 m_2 \end{pmatrix} \cdot \begin{pmatrix} \dot{\varphi}_1 \\ \dot{\varphi}_2 \end{pmatrix} \\ &- g \cdot (m_1 a_1 \cos(\varphi_1) + m_2 \cdot (l_1 \cos(\varphi_1) + a_2 \cos(\varphi_2))) \,. \end{aligned}$$

As non-conservative forces, we assume friction torques $F(\dot{\varphi}_1, \dot{\varphi}_2) = (-d_1\dot{\varphi}_1 + d_2(\dot{\varphi}_2 - \dot{\varphi}_1),\, d_2(\dot{\varphi}_1 - \dot{\varphi}_2)))^T$ acting on the joints. External forcing is applied to the system by a torque $u_M(t)$, which acts on the inner joint. Thus, we do not have a fully actuated system. The natural dynamics of the double pendulum, which are used for the stable manifold computations, correspond to $u_M(t) \equiv 0$. The controlled

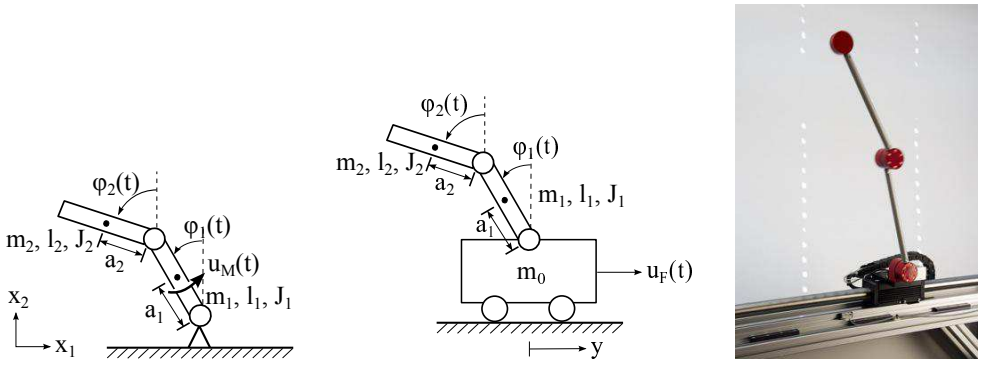

(a) Double pendulum with torque control.

(b) Double pendulum on a controlled cart

(c) Test rig

Figure C.1: Models of double pendula and the test rig.

Parameters	Inner link (i=1)	Outer link (i=2)
Length l_i [m]	0.356	0.356
Distance to center of gravity a_i [m]	0.18	0.148
Mass m_i [kg]	0.775	0.654
Moment of inertia J_i [N m s^2]	0.0224	0.0179
Friction constant d_i [N m s]	0.005	0.005
Mass of the cart m_0: 4 [kg]		

Table C.1: Mechanical parameters of the double pendulum on a cart derived from the real test rig (cf. [TKOT11]).

Euler-Lagrange equations are

$$\begin{aligned}
&\begin{pmatrix} J_1 + a_1^2 m_1 + l_1^2 m_2 & a_2 l_1 m_2 \cos(\varphi_1 - \varphi_2) \\ a_2 l_1 m_2 \cos(\varphi_1 - \varphi_2) & J_2 + a_2^2 m_2 \end{pmatrix} \cdot \begin{pmatrix} \ddot{\varphi}_1 \\ \ddot{\varphi}_2 \end{pmatrix} \\
&+ \begin{pmatrix} -g \sin(\varphi_1)(a_1 m_1 + l_1 m_2) + a_2 l_1 m_2 \sin(\varphi_1 - \varphi_2)\dot{\varphi}_2^2 \\ -a_2 g m_2 \sin(\varphi_2) - a_2 l_1 m_2 \sin(\varphi_1 - \varphi_2)\dot{\varphi}_1^2 \end{pmatrix} \\
&= \begin{pmatrix} -d_1\dot{\varphi}_1 + d_2(\dot{\varphi}_2 - \dot{\varphi}_1) \\ d_2(\dot{\varphi}_1 - \dot{\varphi}_2) \end{pmatrix} + \begin{pmatrix} u_M \\ 0 \end{pmatrix}.
\end{aligned}$$

C.1.2 Double Pendulum on a Cart

In the double pendulum on a cart model (cf. Figure C.1b), the cart leads to a third degree of freedom, i.e. its position $y(t)$. Thus, the state vector is $(\varphi_1, \varphi_2, y, \dot{\varphi}_1, \dot{\varphi}_2, \dot{y})$

and the control input is the force u_F on the cart.

The Lagrangian is still of the form $L(q,\dot{q}) = \dot{q}^T M(q)\,\dot{q} - V(q)$, therefore, the Euler-Lagrange equations can be written as

$$M(q)\ddot{q} + G(q,\dot{q}) = F(q,\dot{q}) \tag{C.1}$$

with

$$M = \begin{pmatrix} J_1 + a_1^2 m_1 + l_1^2 m_2 & a_2 l_1 m_2 \cos(\varphi_1 - \varphi_2) & -(a_1 m_1 + l_1 m_2)\cos(\varphi_1) \\ a_2 l_1 m_2 \cos(\varphi_1 - \varphi_2) & J_2 + a_2^2 m_2 & -a_2 m_2 \cos(\varphi_2) \\ -(a_1 m_1 + l_1 m_2)\cos(\varphi_1) & -a_2 m_2 \cos(\varphi_2) & m_1 + m_2 + m_0 \end{pmatrix} \tag{C.2}$$

$$G = \begin{pmatrix} -g\sin(\varphi_1)(a_1 m_1 + l_1 m_2) + a_2 l_1 m_2 \sin(\varphi_1 - \varphi_2)\dot{\varphi}_2^2 \\ -a_2 g m_2 \sin(\varphi_2) - a_2 l_1 m_2 \sin(\varphi_1 - \varphi_2)\dot{\varphi}_1^2 \\ (a_1 m_1 + l_1 m_2)\dot{\varphi}_1^2 \sin(\varphi_1) + a_2 m_2 \dot{\varphi}_2^2 \sin(\varphi_2) \end{pmatrix} \tag{C.3}$$

$$F = \begin{pmatrix} -d_1\dot{\varphi}_1 + d_2(\dot{\varphi}_2 - \dot{\varphi}_1) \\ d_2(\dot{\varphi}_1 - \dot{\varphi}_2) \\ 0 \end{pmatrix} + \begin{pmatrix} 0 \\ 0 \\ u_F \end{pmatrix}. \tag{C.4}$$

This system with parameters as in Table C.1 models the dynamics of the real test rig of the Chair of Control Engineering and Mechatronics, Heinz Nixdorf Institute, University of Paderborn (cf. Figure C.1c). The test rig has a precise and high-performance linear motor with a maximal driving power of 400 N and a maximal velocity of $6\,\mathrm{m\,s^{-1}}$. The joints with low friction are self-constructed and possess light and compact optical angle encoders with a high resolution. The signals are transmitted via contact rings. The motor of the pendulum on a cart is velocity controlled by a very fast internal controller. For this reason, the modeling of friction in the motor can be neglected.

List of Figures

Bibliography

[AA04] M. Alamir and S. A. Attia. On solving optimal control problems for switched hybrid nonlinear systems by strong variations algorithms. In *Proceedings of 6th IFAC Symposium on Nonlinear Control Systems*, pages 558–563, 2004.

[AAR10] S. Attia, V. Azhmyakov, and J. Raisch. On an Optimization Problem for a Class of Impulsive Hybrid Systems. *Discrete Event Dynamic Systems*, 20:215–231, 2010.

[Alt04] W. Alt. *Numerische Verfahren der konvexen, nichtglatten Optimierung*. Teubner, 2004.

[AM87] R. Abraham and J. E. Marsden. *Foundations of Mechanics*. Addison-Wesley, 1987.

[AMR88] R. Abraham, J. E. Marsden, and T. Ratiu. *Manifolds, Tensor Analysis, and Applications*, volume 75 of *Applied Mathematical Sciences*. Springer, 2nd edition, 1988.

[ARS05] B. Aulbach, M. Rasmussen, and S. Siegmund. Approximation of attractors of nonautonomous dynamical systems. *Discrete and Continuous Dynamical Systems B*, 5(2):215–238, 2005.

[ARS06] B. Aulbach, M. Rasmussen, and S. Siegmund. Invariant manifolds as pullback attractors of nonautonomous differential equations. *Discrete and Continuous Dynamical Systems*, 15(2):579–596, 2006.

[AS06] A. D. Ames and S. Sastry. Hybrid Routhian reduction of Lagrangian hybrid systems. In *Proceedings of the 2006 American Control Conference*, pages 2640–2645, 2006.

[AZGS06] A. D. Ames, H. Zheng, R. D. Gregg, and S. Sastry. Is there life after zeno? Taking executions past the breaking (zeno) point. In *Proceedings of the 2006 American Control Conference*, pages 2652–2657, 2006.

[BBB+01] T. Binder, L. Blank, H. G. Bock, R. Bulirsch, W. Dahmen, M. Diehl, T. Kronseder, W. Marquardt, J. P. Schlöder, and O. von Stryk. Introduction to model based optimization of chemical processes on moving horizons. In M. Grötschel, S. O. Krumke, and J. Rambau, editors, *Online Optimization of Large Scale Systems: State of the Art*, pages 295–340. Springer, 2001.

[Bet98] J. T. Betts. Survey of numerical methods for trajectory optimization. *Journal of Guidance, Control, and Dynamics*, 21(2):193–207, 1998.

[BGH+02] M. Buss, M. Glocker, M. Hardt, O. von Stryk, R. Bulirsch, and G. Schmidt. Nonlinear Hybrid Dynamical Systems: Modeling, Optimal Control, and Applications. In S. Engell, G. Frehse, and E. Schnieder, editors, *Modelling, Analysis, and Design of Hybrid Systems*, volume 279 of *Lecture Notes in Control and Information Sciences*, pages 311–335. Springer, 2002.

[BGR98] A. Barclay, P. E. Gill, and J. B. Rosen. SQP methods and their application to numerical optimal control. In R. Bulirsch, L. Bittner, W. H. Schmidt, and K. Heier, editors, *Variational Calculus, Optimal Control and Applications*, volume 124 of *International Series of Numerical Mathematics*, pages 207–222. Birkhäuser, 1998.

[BL04] F. Bullo and A. D. Lewis. *Geometric Control of Mechanical Systems*, volume 49 of *Texts in Applied Mathematics*. Springer, 2004.

[BL06] J. F. Bonnans and J. Laurent-Varin. Computation of order conditions for symplectic partitioned Runge-Kutta schemes with application to optimal control. *Numerische Mathematik*, 103(1):1–10, 2006.

[BL07a] S. D. Bond and B. J. Leimkuhler. Stabilized integration of Hamiltonian systems with hard-sphere inequality constraints. *SIAM Journal on Scientific Computing*, 30(1):134–147, 2007.

[BL07b] F. Bullo and A. Lewis. Reduction, linearization, and stability of relative equilibria for mechanical systems on Riemannian manifolds. *Acta Applicandae Mathematicae*, 99(1):53–95, 2007.

[Blo03] A. M. Bloch. *Nonholonomic mechanics and control*. Springer, 2003.

[Cla83] F. H. Clarke. *Optimization and nonsmooth analysis*. Wiley, New York, 1983.

[CLH+05] H. Choset, K. M. Lynch, S. Hutchinson, G. A. Kantor, W. Burgard, L. E. Kavraki, and S. Thrun. *Principles of Robot Motion: Theory, Algorithms, and Implementations*. MIT Press, 2005.

[CM11] T. M. Caldwell and T. D. Murphey. Switching mode generation and optimal estimation with application to skid-steering. *Automatica*, 47(1):50–64, 2011.

[CM12] T. M. Caldwell and T. D. Murphey. Projection-based switched system optimization: Absolute continuity of the line search. In *Proceedings of the 51th IEEE Conference on Decision and Control*, pages 699–706, 2012.

[CM13] T. Caldwell and T. D. Murphey. Sufficient descent and backtracking for optimal mode scheduling. Submitted to IEEE Transactions on Automatic Control, 2013.

[Con68] C. Conley. Low energy transit orbits in the restricted three-body problem. *SIAM Journal on Applied Mathematics*, 16(4):732–746, 1968.

[DFJ01] M. Dellnitz, G. Froyland, and O. Junge. The algorithms behind GAIO – set oriented numerical methods for dynamical systems. In B. Fiedler, editor, *Ergodic Theory, Analysis, and Efficient Simulation of Dynamical Systems*, pages 145–174. Springer, 2001.

[DGL+13] F. Demoures, F. Gay-Balmaz, T. Leitz, S. Leyendecker, S. Ober-Blöbaum, and T. S. Ratiu. Asynchronous variational Lie group integration for geometrically exact beam dynamics. to appear in: Proceedings of ECCOMAS 2013, 2013.

[DJ02] M. Dellnitz and O. Junge. Set oriented numerical methods for dynamical systems. In B. Fiedler, editor, *Handbook of Dynamical Systems*, volume 2, pages 221 – 264. Elsevier Science, 2002.

[DJK+06] M. Dellnitz, O. Junge, A. Krishnamurthy, S. Ober-Blöbaum, K. Padberg, and R. Preis. Efficient control of formation flying spacecraft. In F. Meyer auf der Heide and B. Monien, editors, *New Trends in Parallel & Distributed Computing*, volume 181, pages 235–247. Heinz Nixdorf Institut Verlagsschriftreihe, 2006.

[DJPT06] M. Dellnitz, O. Junge, M. Post, and B. Thiere. On target for Venus – set oriented computation of energy efficient low thrust trajectories. *Celestial Mechanics & Dynamical Astronomy*, 95:357–370, 2006.

[DK05] U. Diemar and E. Kallenbach. Die Anwendung des Lagrange-Formalismus zum Entwurf mechatronischer Systeme. In *Mechatronik-Tagung – Innovative Produktentwicklung, VDI-Bericht 1892*, pages 295–314, 2005.

[DOP+09] M. Dellnitz, S. Ober-Blöbaum, M. Post, O. Schütze, and B. Thiere. A multi-objective approach to the design of low thrust space trajectories using optimal control. *Celestial Mechanics & Dynamical Astronomy*, 105:33–59, 2009.

[DSH05] M. Dellnitz, O. Schütze, and T. Hestermeyer. Covering Pareto Sets by Multilevel Subdivision Techniques. *Journal of Optimization Theory and Application*, 124(1):113–136, 2005.

[Eel66] J. Eells. A setting for global analysis. *Bulletin of the American Mathematical Society*, 72:751–807, 1966.

[Ehr05] M. Ehrgott. *Multicriteria Optimization*. Springer, 2nd edition, 2005.

[EWA06] M. Egerstedt, Y. Wardi, and H. Axelsson. Transition-time optimization for switched-mode dynamical systems. *IEEE Transactions on Automatic Control*, 51(1):110–115, 2006.

[EWD03] M. Egerstedt, Y. Wardi, and F. Delmotte. Optimal control of switching times in switched dynamical systems. In *IEEE Conference on Decision and Control*, pages 2138–2143, 2003.

[FB02] E. Frazzoli and F. Bullo. On quantization and optimal control of dynamical systems with symmetries. In *Proceedings of the 41st IEEE Conference on Decision and Control*, pages 817–823, 2002.

[FDF99] E. Frazzoli, M. Dahleh, and E. Feron. A hybrid control architecture for aggressive maneuvering of autonomous helicopters. In *Proceedings of the 38th IEEE Conference on Decision and Control*, pages 2471–2476, 1999.

[FDF00] E. Frazzoli, M. A. Dahleh, and E. Feron. Robust hybrid control for autonomous vehicle motion planning. In *Proceedings of the 39th IEEE Conference on Decision and Control*, pages 821–826, 2000.

[FDF05] E. Frazzoli, M. A. Dahleh, and E. Feron. Maneuver-based motion planning for nonlinear systems with symmetries. *IEEE Transactions on Robotics*, 21(6):1077–1091, 2005.

[FMO12] K. Flaßkamp, T. Murphey, and S. Ober-Blöbaum. Switching time optimization in discretized hybrid dynamical systems. In *Proceedings of the 51th IEEE Conference on Decision and Control*, pages 707 – 712, 2012.

[FMO13a] K. Flaßkamp, T. Murphey, and S. Ober-Blöbaum. Discretized switching time optimization problems. In *Proceedings of the 12th European Control Conference*, pages 3179–3184, 2013.

[FMO13b] K. Flaßkamp, T. D. Murphey, and S. Ober-Blöbaum. Switching time optimization for discretized switched systems. In preparation, June 2013.

[FMOW03] R. C. Fetecau, J. E. Marsden, M. Ortiz, and M. West. Nonsmooth Lagrangian Mechanics and Variational Collision Integrators. *SIAM Journal on Applied Dynamical Systems*, 2(3):381–416, 2003.

[FO11] K. Flaßkamp and S. Ober-Blöbaum. Variational formulation and optimal control of hybrid Lagrangian systems. In *Proceedings of the 14th International Conference on Hybrid Systems: Computation and Control*, pages 241–250, 2011.

[FO12] K. Flaßkamp and S. Ober-Blöbaum. Motion planning for mechanical systems with hybrid dynamics. In *Progress in Industrial Mathematics at ECMI 2012*, Mathematics in Industry (To appear). Springer, 2012.

[FO13] K. Flaßkamp and S. Ober-Blöbaum. Optimale Steuerungsstrategien für selbstoptimierende mechatronische Systeme mit mehreren Zielkriterien. In *9. Paderborner Workshop Entwurf mechatronischer Systeme*, HNI-Verlagsschriftenreihe, pages 65–78, 2013.

[FOK10] K. Flaßkamp, S. Ober-Blöbaum, and M. Kobilarov. Solving optimal control problems by using inherent dynamical properties. *PAMM*, 10(1):577–578, 2010.

[FOK12] K. Flaßkamp, S. Ober-Blöbaum, and M. Kobilarov. Solving optimal control problems by exploiting inherent dynamical systems structures. *Journal of Nonlinear Science*, 22(4):599–629, 2012.

[FOR+11] K. Flaßkamp, S. Ober-Blöbaum, M. Ringkamp, T. Schneider, C. Schulte, and J. Böcker. Berechnung optimaler Stromprofile für einen 6-phasigen, geschalteten Reluktanzantrieb. In J. Gausemeier, F. J. Rammig, W. Schäfer, and A. Trächtler, editors, *8. Paderborner Workshop Entwurf mechatronischer Systeme*, volume 294 of *HNI-Verlagsschriftenreihe*, pages 81–92. Heinz-Nixdorf-Institut, Universität Paderborn, 2011.

[Fra01] E. Frazzoli. *Robust Hybrid Control for Autonomous Vehicle Motion Planning*. PhD thesis, Massachusetts Institute of Technology, 2001.

[Fra03] E. Frazzoli. Explicit solutions for optimal maneuver-based motion planning. In *Proceedings of the 42nd IEEE Conference on Decision and Control*, pages 3372–3377, 2003.

[FTO+12] K. Flaßkamp, J. Timmermann, S. Ober-Blöbaum, M. Dellnitz, and A. Trächtler. Optimal control on stable manifolds for a double pendulum. *PAMM*, 12(1):723–724, 2012.

[FTOT13] K. Flaßkamp, J. Timmermann, S. Ober-Blöbaum, and A. Trächtler. Control strategies on stable manifolds for energy-efficient swing-ups of double pendula. Accepted for International Journal of Control, 2013.

[Ger12] M. Gerdts. *Optimal Control of ODEs and DAEs*. De Gruyter, 2012.

[GH83] J. Guckenheimer and P. Holmes. *Nonlinear Oscillations, Dynamical Systems, and Bifurcations of Vector Fields*, volume 42 of *Applied Mathematical Sciences*. Springer, 1983.

[GJL+00] P. E. Gill, L. O. Jay, M. W. Leonard, L. R. Petzold, and V. Sharma. An SQP method for the optimal control of large-scale dynamical systems. *Journal of Computational and Applied Mathematics*, 120:197–213, 2000.

[GK02] C. Geiger and C. Kanzow. *Theorie und Numerik restringierter Optimierungsaufgaben*. Springer, Berlin, 2002.

[GKL+04] G. Gómez, W. S. Koon, M. W. Lo, J. E. Marsden, J. Masdemont, and S. D. Ross. Connecting orbits and invariant manifolds in the spatial three-body problem. *Nonlinearity*, 17:1571–1606, 2004.

[GMS05] P. E. Gill, W. Murray, and M. A. Saunders. SNOPT: An SQP Algorithm for Large-Scale Constrained Optimization. *SIAM Review*, 47(1):99–131, 2005.

[GRS09] J. Gausemeier, F. J. Rammig, and W. Schäfer, editors. *Selbstoptimierende Systeme des Maschinenbaus*, volume 234 of *HNI-Verlagsschriftenreihe*. Heinz Nixdorf Institute, University of Paderborn, Paderborn, 2009.

[GVK+10] H. Gonzales, R. Vasudevan, M. Kamgarpour, S. Sastry, R. Bajcsy, and C. J. Tomlin. A Descent Algorithm for the Optimal Control of Constrained Nonlinear Switched Dynamical Systems. In *HSCC '10 Proceedings of the 13th ACM international conference on Hybrid systems: computation and control*, pages 51–60, 2010.

[GW08] A. Griewank and A. Walther. *Evaluating Derivatives: Principles and Techniques of Algorithmic Differentiation*. SIAM, 2nd edition, 2008.

[Hag00] W. W. Hager. Runge-Kutta methods in optimal control and the transformed adjoint system. *Numerische Mathematik*, 87:247–282, 2000.

[Hag12] S. Hage-Packhäuser. *Structural Treatment of Time-Varying Dynamical System Networks in the Light of Hybrid Symmetries*. PhD thesis, University of Paderborn, 2012.

[HLW06] E. Hairer, C. Lubich, and G. Wanner. *Geometric Numerical Integration: Structure-Preserving Algorithms for Ordinary Differential Equations*, volume 31 of *Springer Series in Computational Mathematics*. Springer, 2nd edition, 2006.

[HPS77] M. W. Hirsch, C. C. Pugh, and M. Shub. *Invariant Manifolds*. Number 583 in Lecture Notes in Mathematics. Springer, 1977.

[IMDD02] R. B. Inderka, M. Menne, and R. W. A. A. De Doncker. Control of switched reluctance drives for electric vehicle applications. *IEEE Transactions on Industrial Electronics*, 49(1):48–53, 2002.

[JM11] E. R. Johnson and T. D. Murphey. Second-order switching time optimization for nonlinear time-varying dynamic systems. *IEEE Transactions on Automatic Control*, 56(8):1953–1957, 2011.

[JMO05] O. Junge, J. E. Marsden, and S. Ober-Blöbaum. Discrete Mechanics and Optimal Control. In *Proceedings of the 16th IFAC World Congress*, 2005.

[JMO06] O. Junge, J. E. Marsden, and S. Ober-Blöbaum. Optimal Reconfiguration of Formation Flying Spacecraft - a decentralized approach. In *Proceedings of the 45th IEEE Conference on Decision and Control*, pages 5210–5215, 2006.

[Joh12] E. Johnson. *Trajectory Optimization and Regulation for Constrained Discrete Mechanical Systems*. PhD thesis, Northwestern University, 2012.

[Jun00] O. Junge. *Mengenorientierte Methoden zur numerischen Analyse dynamischer Systeme*. PhD thesis, University of Paderborn, Shaker, 2000.

[KH98] A. Katok and B. Hasselblatt. *Introduction to the modern theory of dynamical systems*. Cambridge University Press, 1998.

[Kir70] D. E. Kirk. *Optimal Control Theory*. Prentice-Hall, 1970.

[KKP+08] L. Kolomeitsev, D. Kraynov, S. Pakhomin, F. Rednov, E. Kallenbach, V. Kireev, T. Schneider, and J. Böcker. Control of a linear switched reluctance motor as a propulsion system for autonomous railway vehicles. In *13th International Power Electronics and Motion Control Conference*, pages 1598–1603, 2008.

[KL13] M. W. Koch and S. Leyendecker. Structure preserving simulation of monopedal jumping. *Archive of Mechanical Engineering*, LX(1):127–146, 2013.

[KLMR00] W. S. Koon, M. W. Lo, J. E. Marsden, and S. D. Ross. Shoot the Moon. *Spaceflight Mechanics*, 105(2):1017–1030, 2000.

[KLMR01] W. S. Koon, M. W. Lo, J. E. Marsden, and S. D. Ross. Low energy transfer to the Moon. *Celestial Mechanics & Dynamical Astronomy*, 81(1-2):63–73, 2001.

[KM97] A. Kriegl and P. W. Michor. *The Convenient Setting of Global Analysis*, volume 53 of *Mathematical Surveys and Monographs*. American Mathematical Society, 1997.

[KM05] E. Kanso and J. E. Marsden. Optimal motion of an articulated body in a perfect fluid. In *Proceedings of the 44th IEEE Conference on Decision and Control and the European Control Conference*, pages 2511–2516, 2005.

[Kob08] M. Kobilarov. *Discrete geometric motion control of autonomous vehicles*. PhD thesis, University of Southern California, USA, 2008.

[KOD+05] B. Krauskopf, H. M. Osinga, E. J. Doedel, M. E. Henderson, J. Guckenheimer, A. Vladimirsky, M. Dellnitz, and O. Junge. A survey of methods for computing (un)stable manifolds of vector fields. *International Journal of Bifurcation and Chaos*, 15(3):763–791, 2005.

[Kri01] R. Krishnan. *Switched Reluctance Motor Drives: Modeling, Simulation, Analysis, Design and Application*. CRC Press, 2001.

[KT12] M. Kamgarpour and C. Tomlin. On optimal control of non-autonomous switched systems with a fixed mode sequence. *Automatica*, 48(6):1177 – 1181, 2012.

[LaV06] S. M. LaValle. *Planning Algorithms*. Cambridge University Press, 2006.

[Lem89] C. Lemaréchal. Nondifferentiable optimization. In G. L. Nemhauser, editor, *Handbook in OR & MS*, volume 1, pages 529–572. Elsevier, North-Holland, 1989.

[LHDV10] F. Logist, B. Houska, M. Diehl, and J. Van Impe. Fast Pareto set generation for nonlinear optimal control problems with multiple objectives. *Structural and Multidisciplinary Optimization*, 42:591–603, 2010.

[LHK+12] S. Leyendecker, C. Hartmann, M. W. Koch, G. Johnson, and M. Ortiz. Variational collision integrators in forward dynamics and optimal control. In *Proceedings of the 7th International Conference of the Croatian Society of Mechanics*, 2012.

[Lib12] D. Liberzon. *Calculus of Variations and Optimal Control Theory*. Princeton University Press, 2012.

[Lin12] H. Lindhorst. Variational integrators for nonlinear and hybrid electric circuits. Master's thesis, University of Paderborn, 2012.

[LJS+03] J. Lygeros, K. H. Johansson, S. N. Simić, J. Zhang, and S. Sastry. Dynamical Properties of Hybrid Automata. *IEEE Transactions on Automatic Control*, 48(1):3–17, 2003.

[LL09] J. Lunze and F. Lamnabhi-Lagarrigue, editors. *Handbook of hybrid systems control: theory, tools, applications*. Cambridge University Press, 2009.

[LMOW03] A. Lew, J. E. Marsden, M. Ortiz, and M. West. Asynchronous variational integrators. *Archive for Rational Mechanics and Analysis*, 167:85–146, 2003.

[LO12] A. S. Lewis and M. L. Overton. Nonsmooth optimization via quasi-newton methods. *Mathematical Programming*, pages 1–29, 2012.

[LO13] S. Leyendecker and S. Ober-Blöbaum. A variational approach to multirate integration for constrained systems. In P. Fisette and J.-C. Samin, editors, *Multibody Dynamics: Computational Methods and Applications*, volume 28, pages 97–121. Springer, 2013.

[Loc01] A. Locatelli. *Optimal Control*. Birkhäuser, 2001.

[LOMO07] S. Leyendecker, S. Ober-Blöbaum, J. E. Marsden, and M. Ortiz. Discrete mechanics and optimal control for constrained multibody dynamics. In *6th International Conference on Multibody Systems, Nonlinear Dynamics, and Control, ASME International Design Engineering Technical Conferences*, volume 5, pages 623–632, 2007.

[LOMO10] S. Leyendecker, S. Ober-Blöbaum, J. E. Marsden, and M. Ortiz. Discrete mechanics and optimal control for constrained systems. *Optimal Control, Applications and Methods*, 31(6):505–528, 2010.

[LSE99] H. Ludvigsen, A. Shiriaev, and O. Egeland. Stabilization of stable manifold of upright position of the spherical pendulum. In *Proceedings of the 1999 American Control Conference*, volume 6, pages 4034–4038, 1999.

[Mar74] J. E. Marsden. *Applications of global analysis in mathematical physics*. Publish or Perish, Inc., 1974.

[Mar93] J. E. Marsden. *Lectures on Mechanics*. Number 174 in London Mathematical Society Lecture Note Series. Cambridge University Press, 1993.

[Mar94] J. E. Marsden. Geometric mechanics, stability, and control. In *Trends and perspectives in applied mathematics*, number 100 in Springer Applied Mathematical Sciences Series, pages 265–291. Springer, 1994.

[McG69] R. McGehee. *Some Homoclinic Orbits for the Restricted Three-Body Problem*. PhD thesis, University of Wisconsin, 1969.

[Mie99] K. Miettinen. *Nonlinear Multiobjective Optimization*. Kluwer, 1999.

[ML13] R. Maas and S. Leyendecker. Biomechanical optimal control of human arm motion. *Proceedings of the Institution of Mechanical Engineers, Part K: Journal of Multi-body Dynamics*, 2013.

[MOM12] A. Moore, S. Ober-Blöbaum, and J. E. Marsden. Trajectory design combining invariant manifolds with discrete mechanics and optimal control. *Journal of Guidance, Control, and Dynamics*, 35(5):1507–1525, 2012.

[MPS98] J. E. Marsden, G. W. Patrick, and S. Shkoller. Multisymplectic geometry, variational integrators, and nonlinear PDEs. *Communications in Mathematical Physics*, 199:351–395, 1998.

[MR99] J. E. Marsden and T. S. Ratiu. *Introduction to mechanics and symmetry*, volume 17 of *Texts in Applied Mathematics*. Springer, 2nd edition, 1999.

[MRS00] J. E. Marsden, T. S. Ratiu, and J. Scheurle. Reduction theory and the Lagrange-Routh equations. *Journal of Mathematical Physics*, 41:3379–3429, 2000.

[MS93] J. E. Marsden and J. Scheurle. Lagrangian reduction and the double spherical pendulum. *Zeitschrift für angewandte Mathematik und Physik (ZAMP)*, 44:17–43, 1993.

[MV91] J. Moser and A. P. Veselov. Discrete versions of some classical integrable systems and factorization of matrix polynomials. *Communications in Mathematical Physics*, 139:217–243, 1991.

[MW01] J. E. Marsden and M. West. Discrete mechanics and variational integrators. *Acta Numerica*, 10:357–514, 2001.

[MW07] I. Moson and A. Wilk. Lagrange's energy method based approach for switched reluctance drive systems modelling. In *2007 European Conference on Power Electronics and Applications*, pages 1–10, 2007.

[Obe08] S. Ober-Blöbaum. *Discrete mechanics and optimal control*. PhD thesis, University of Paderborn, 2008.

[OJM11] S. Ober-Blöbaum, O. Junge, and J. E. Marsden. Discrete mechanics and optimal control: an analysis. *Control, Optimisation and Calculus of Variations*, 17(2):322–352, 2011.

[OLT04] H. M. Osinga, G. R. R. Lamooki, and S. Townley. Numerical approximations of strong (un)stable manifolds. *Dynamical Systems*, 19(3):195–215, 2004.

[ORZ12] S. Ober-Blöbaum, M. Ringkamp, and G. Zum Felde. Solving multiobjective optimal control problems in space mission design using discrete mechanics and reference point techniques. In *Proceedings of the 51th IEEE Conference on Decision and Control*, pages 5711–5716, 2012.

[OT09] S. Ober-Blöbaum and J. Timmermann. Optimal control for a pitcher's motion modeled as constrained mechanical system. In *7th International Conference on Multibody Systems, Nonlinear Dynamics, and Control, ASME International Design Engineering Technical Conferences*, volume 4, pages 597–606, 2009.

[OTC+13] S. Ober-Blöbaum, M. Tao, M. Cheng, H. Owhadi, and J. E. Marsden. Variational integrators for electric circuits. *Journal of Computational Physics*, 242:498–530, 2013.

[OW10] S. Ober-Blöbaum and A. Walther. Computation of derivatives for structure preserving optimal control using automatic differentiation. *PAMM*, 10(1):585–586, 2010.

[PAM07] D. Pekarek, A. D. Ames, and J. E. Marsden. Discrete mechanics and optimal control applied to the compass gait biped. In *Proceedings of the 46th IEEE Conference on Decision and Control*, pages 5376–5382, 2007.

[PBGM86] L. S. Pontryagin, V. Boltyanskii, R. V. Gamkrelidze, and E. F. Mishchenko. The Mathematical Theory of Optimal Processes. In *L. S. Pontryagin selected works*, volume 4 of *Classics in Soviet mathematics*. Gordon and Breach, 1986.

[PM11] D. Pekarek and T. D. Murphey. A backwards error analysis approach for simulation and control of nonsmooth mechanical systems. In *Proceedings of the 50th IEEE Conference on Decision and Control and European Control Conference*, pages 6942–6949, 2011.

[Pol97] E. Polak. *Optimization: Algorithms and Consistent Approximations*. Springer, 1997.

[Pow78] M. J. D. Powell. A fast algorithm for nonlinearly constrained optimization calculations. In G. A. Watson, editor, *Numerical Analysis*, volume 630 of *Lecture Notes in Mathematics*, pages 144–157. Springer, 1978.

[RWL02] M. Roberts, C. Wulff, and J. Lamb. Hamiltonian systems near relative equilibria. *Journal of Differential Equations*, 179(2):562–604, 2002.

[SC07] M. Shaikh and P. Caines. On the hybrid optimal control problem: Theory and algorithms. *IEEE Transactions on Automatic Control*, 52(9):1587 –1603, 2007.

[Sch99] M. Schlör. Die Berechnung stark (in-)stabiler Mannigfaltigkeiten. Master's thesis, Fakultät für Mathematik und Physik, Universität Bayreuth, 1999.

[Sch04] O. Schütze. *Set oriented methods for global optimization*. PhD thesis, University of Paderborn, 2004.

[SDEL09] A. Schild, X. C. Ding, M. Egerstedt, and J. Lunze. Design of optimal switching surfaces for switched autonomous systems. In *IEEE Conference on Decision and Control*, pages 5293–5298, 2009.

[SJSL05] S. N. Simić, K. H. Johansson, S. Sastry, and J. Lygeros. Towards a Geometric Theory of Hybrid Systems. *Dynamics of Continuous, Discrete and Impulsive Systems, Series B: Applications & Algorithms*, 12(5-6):649–687, 2005.

[SM12] V. Seghete and T. D. Murphey. Conditions for uniqueness in simultaneous impact with application to mechanical design. In *Proceedings of the IEEE International Conference on Robotics and Automation*, pages 5006–5011, 2012.

[SS00] A. J. v. d. Schaft and H. Schumacher. *An Introduction to Hybrid Dynamical Systems*, volume 251 of *Lecture Notes in Control and Information Sciences*. Springer, 2000.

[ST10] R. G. Sanfelice and A. R. Teel. Dynamical properties of hybrid systems simulators. *Automatica*, 46(2):239–248, 2010.

[Sus99a] H. J. Sussmann. A maximum principle for hybrid optimal control problems. In *Proceedings of the 38th IEEE Conference on Decision and Control*, volume 1, pages 425–430, 1999.

[Sus99b] H. J. Sussmann. A nonsmooth hybrid maximum principle. In D. Aeyels, F. Lamnabhi-Lagarrigue, and A. Schaft, editors, *Stability and Stabilization of Nonlinear Systems*, volume 246 of *Lecture Notes in Control and Information Sciences*, pages 325–354. Springer, 1999.

[SW97] H. J. Sussmann and J. C. Willems. 300 years of optimal control: from the Brachystochrone to the maximum principle. *IEEE Control Systems*, 17(3):32–44, 1997.

[SWOD13] O. Schütze, K. Witting, S. Ober-Blöbaum, and M. Dellnitz. Set oriented methods for the numerical treatment of multi-objective optimization problems. In E. Tantar, A.-A. Tantar, P. Bouvry, P. Del Moral, P. Legrand, C. A. Coello Coello, and O. Schütze, editors, *EVOLVE – A Bridge Between Probability, Set Oriented Numerics, and Evolutionary Computation*, volume 447 of *Studies in Computational Intelligence*, pages 187–219. Springer, 2013.

[TKOT11] J. Timmermann, S. Khatab, S. Ober-Blöbaum, and A. Trächtler. Discrete mechanics and optimal control and its application to a double pendulum on a cart. In *Proceedings of the 18th International Federation of Automatic Control World Congress (IFAC)*, volume 18, 1, pages 10199–10206, 2011.

[Ves88] A. P. Veselov. Integrable discrete-time systems and difference operators. *Functional Analysis and Its Applications*, 22(2):83–93, 1988.

[vNM98] M. J. van Nieuwstadt and R. M. Murray. Real time trajectory generation for differentially flat systems. *International Journal of Robust and Nonlinear Control*, 8(11):995–1020, 1998.

[WB06] A. Wächter and L. T. Biegler. On the implementation of an interior-point filter line-search algorithm for large-scale nonlinear programming. *Mathematical Programming*, 106(1):25–57, 2006.

[WM97] J. M. Wendlandt and J. E. Marsden. Mechanical integrators derived from a discrete variational principle. *Physica D: Nonlinear Phenomena*, 106(3–4):223–246, 1997.

[XA02a] X. Xu and P. J. Antsaklis. Optimal control of switched autonomous systems. In *IEEE Conference on Decision and Control*, pages 4401–4406, 2002.

[XA02b] X. Xu and P. J. Antsaklis. Optimal control of switched systems via nonlinear optimization based on direct differentiations of value functions. *International Journal of Control*, 75(16-17):1406–1426, 2002.

[XA04] X. Xu and P. J. Antsaklis. Optimal control of switched systems based on parameterization of the switching instants. *IEEE Transactions on Automatic Control*, 49(1):2–16, 2004.